RELEASABLE

PHASE I OF THE DEVELOPMENT OF THE DEMODULATOR PORTION OF A JTIDS RECEIVE TERMINAL

FINAL REPORT

VOLUME 1 OF 2

MCS MILLER COMMUNICATIONS SYSTEMS LTD.

PHASE I OF THE DEVELOPMENT OF THE DEMODULATOR PORTION OF A JTIDS RECEIVE TERMINAL

FINAL REPORT

VOLUME 1 OF 2

MCS File No. 8231

SSC Contract No. OST81-00142

SSC File No. 21ST.36001-1-1401

Date: April 21, 1982

Prepared by: S. Crozier B. Mazur

Approved by: R.J. Matyas

SUBMITTED BY

MCS MILLER COMMUNICATIONS SYSTEMS LTD.

300 Legget Drive,
Kanata, Ontario,
Canada K2K 1Y5

Government of Canada   Gouvernement du Canada

Department of Communications

DOC CONTRACTOR REPORT   DOC-CR-SP

DEPARTMENT OF COMMUNICATIONS - OTTAWA - CANADA

SPACE PROGRAM

TITLE: Phase I of the Development of the Demodulator Portion of a JTIDS Terminal (2 Volumes)

AUTHOR(S): S. Crozier
B. Mazur
R. Matyas

ISSUED BY CONTRACTOR AS REPORT NO: MCS 8231

PREPARED BY: Miller Communications Systems Ltd.
300 Legget Drive
Kanata, Ontario
K2K 1Y5

DEPARTMENT OF SUPPLY AND SERVICES CONTRACT NO: OST81-00142

DOC SCIENTIFIC AUTHORITY: B. Bryden

CLASSIFICATION: UNCLASSIFIED (2 Volumes)

DATE:

TABLE OF CONTENTS

VOLUME I

1.0 INTRODUCTION 1

1.1 Background 1

1.2 Statement of The Problem 1

1.3 Terms of Reference 3

1.4 Why DMSK? 3

1.5 Clock Synchronization 7

1.6 Performance Evaluation Approach 6

1.7 Outline of The Report 8

2.0 PRELIMINARY THEORETICAL ANALYSIS 13

2.1 The DMSK Signal And Its Detection 13

2.1.1 Single Error Correction (SEC) 18

2.2 BER Performance 20

2.2.1 Ideal Coherent Detection 20
2.2.2 Ideal Differential Detection 21
2.2.3 No-ISI Degradation Lower Bound 22
2.2.4 Improvement With SEC 28

3.0 SIMULATION MODELS 29

3.1 Overall Model And Implementation Strategy 29

3.2 PN Input Sequence 34

	3.3	Differential Encoder	36
	3.4	MSK Modulator	38
	3.5	Sampling	42
	3.6	Filtering	42
	3.7	Gaussian Noise	44
	3.8	DMSK Demodulator	45
	3.9	Single Error Correction (SEC) Circuit	52
	3.10	Bit Error Counting	54
	3.11	Non-Constant Group Delay	54
	3.12	Hard Limiters	56
	3.13	Multipath	58
	3.14	Jamming	59
	3.15	Eye Patterns	59
4.0	SIMULATION PERFORMANCE RESULTS		60
	4.1	Optimum MSK Demodulator	60
	4.2	DMSK Filter Evaluation	64
	4.2.1	Receive Filter	64
	4.2.2	Post-Demodulation Filter	74
	4.2.3	Transmit Filter	77

4.3	Best BER Performance	77
4.4	Sensitivity Evaluation	80
4.4.1	Bit Timing Errors	80
4.4.2	Threshold Errors	82
4.4.3	Delay Errors	84
4.4.4	Phase Shift Errors	86
4.4.5	Carrier Frequency Offset	88
4.4.6	Non-Constant Group Delay	90
4.4.7	Combination of Errors	91
4.5	Hard Limiters In The Demodulator	95
4.6	Multipath	100
4.7	Jamming	100
4.8	Doppler	103
4.9	Error Rate Monitoring	107
4.10	Eye Patterns	111
4.11	Zero Crossing RMS Jitter	121
5.0	INVESTIGATION OF PERFORMANCE WITH EQUALIZATION	127
5.1	Equalization Strategy	127
5.2	Theoretical And Simulated Performance	131
5.2.1	Calculation of Noise Correlation	138

5.3 Optimum Filters 140

5.4 Realizability 142

6.0 ISI INVESTIGATION AND ADAPTIVE THRESHOLDING 143

6.1 Definitions 143

6.2 ISI And No Noise 149

6.3 ISI And Noise 154

6.4 Optimum Threshold Levels 157

6.5 Performance With Adaptive Thresholding 159

6.6 Realizability 170

7.0 MAXIMUM LIKELIHOOD NONCOHERENT MSK BURST CLOCK SYNCHRONIZATION 172

7.1 Introduction 172

7.2 Overview of The Matched Filter Synchronization Approach 176

7.2.1 Reveiw of Radar Fundamentals 176

7.2.2 Application of Maximum Likelihood Time of Arrival Estimation To Synchronization 179

7.3 Estimate of Performance 184

7.3.1 Time of Arrival Accuracy 186

7.3.2 Probability of Not Correctly Acquiring 189

7.4 Implementation Considerations 190

7.4.1 Bandpass Matched Filtering With SAW's 194
7.4.2 Baseband Matched Filtering With CCD's 194

8.0 SUMMARY AND RECOMMENDATIONS 196

8.1 Demodulator Structure 197

8.2 Distortion and Interfering Factors Investigated 198

8.3 BER Performance 200

8.4 Improving Performance 205

8.4.1 Performance With Equalization 205
8.4.2 Adaptive Thresholding 207

8.5 Bit Timing Recovery 208

8.6 Degradation Budget for Implementation 209

8.7 Conclusions And Recommendations 209

REFERENCES 212

VOLUME II - APPENDICES

APPENDIX A: INTERMEDIATE SIMULATION RESULTS FOR DMSK FILTER EVALUATION A-1

A.1 Receive Filter A-1

A.2 Post-Demodulation Filter A-37

A.3 Transmit Filter A-45

APPENDIX B: INTERMEDIATE SIMULATION RESULTS FOR SENSITIVITY EVALUATION B-1

B.1 Bit Timing Errors B-1

B.2 Threshold Errors B-3

B.3 Delay Errors B-7

B.4 Phase Shift Errors B-11

B.5 Carrier Frequency Offset B-17

B.6 Non-Constant Group Delay B-22

APPENDIX C: ANALYTICAL DETAILS OF ISI INVESTIGATION C-1

APPENDIX D: ANALYTICAL DETAILS OF MAXIMUM LIKELIHOOD SYNCHRONIZATION APPROACH D-1

D.1 Derivation of The MSK Preamble Matched Filter D-1

D.1.1 Conventional Viewpoint D-1

D.1.2 Serial MSK Viewpoint D-4

D.2 Time of Arrival Accuracy D-9

D.3 Probability of Not Correctly Acquiring D-13

D.3.1 False Alarm Rate D-14

D.3.2 Probability of False Alarm D-21

D.3.3 Probability of Detection D-23

D.3.4 Probability of Not Correctly Acquiring D-24

APPENDIX E: PROGRAM DOCUMENTATION E-1

E.1 Usage E-1

E.2 Routine Listings E-8

1.0 INTRODUCTION

1.1 Background

The Joint Tactical Information Distribution System (JTIDS) is a military Integrated Communication, Navigation and Identification system that features spread spectrum, frequency hopping, high performance and secure digital communications. While specific information pertinent to JTIDS is classified, some background information has appeared in the open literature [1 - 3].

JTIDS is a tactical command and control system to be used by all elements of a task force within line-of-sight or relay range of one another. The system evolved from separate development programs initiated independently by the US Air Force and the US Navy. The current development is under the executive leadership of the US Air Force. The variations of JTIDS include TDMA, Distributed TDMA and Advanced TDMA. Common to all of these are the pulse width, carrier modulation, data modulation, symbol encoding and spread spectrum noncoherent frequency hopping.

The purpose of this study is to address the modulation portion of the JTIDS terminal, in a general context.

1.2 Statement of The Problem

MSK has been identified as the modulation required for JTIDS. The modem is required to acquire and detect burst signals and therefore rapid reliable acquisition is required. Differential detection of MSK (DMSK) is a technique that avoids the need of regenerating a local carrier by means of a coherent carrier recovery loop and thereby can greatly improve signal acquisition time.

The purpose of this study is to identify the essential components of a DMSK demodulator and to determine its bit error rate (BER) performance subject to a number of degrading factors. This study will then provide a basis for determining modem specifications for a specific communications application. In a given application the following signal factors impact the performance and consequently the decision as to whether a modulation technique is suitable for implementation:

(a) transmit spectrum filtering and bandwidth occupancy
(b) data rate
(c) channel model
(d) error rate performance and range of E_b/N_o
(e) IF and carrier frequency offset
(f) input level and variation
(g) burst duration
(h) synchronization description including number of bits used for acquisition
(i) maximum acquisition time.

Distortion mechanisms related to the channel include propagation characteristics and accidental or willful interference. Specific examples are:

(a) timing jitter in receive time slots resulting from intentional dither and propagation delay inequalities,

(b) level and phase jitter of the received signal resulting from multipath,

(c) benign noise resulting from other active transmitters,

(d) burst jamming,

(e) frequency uncertainty due to Doppler shift.

Filtering as it relates ultimately to error rate performance is a major concern. Cost factors, while always relevant, are not of primary concern in Phase I.

Distortion mechanisms directly related to the DMSK modem design are described in the outline of the report given in Section 1.7.

1.3 Terms of Reference

This study investigates the effects on demodulator performance for an extensive list of distortion and interfering factors. The terms of reference for this study are to evaluate in a general sense the performance of DMSK technology such that the results can be applied to the JTIDS situation without restricting their usefullness to other applications. The fact that JTIDS employs a sophisticated TDMA/spread spectrum architecture enters into this study only in so far as it necessitates evaluating the channel distortions described in Section 1.2.

The approach taken here is to assess modem performance for ranges of distortion and interference values that include but are not restricted to the JTIDS application. Any performance or operational values (e.g. modem burst rate is 5 Mbps) and in fact any information relating to JTIDS that appears in this report is taken from the open literature. This report does not contain classified material.

1.4 Why DMSK?

Minimum Shift Keying (MSK), which is also known as Fast Frequency Shift Keying (FFSK), is a phase coherent binary FSK modulation with modulation index $h = 0.5$ [4-16]. It has the following significant properties:

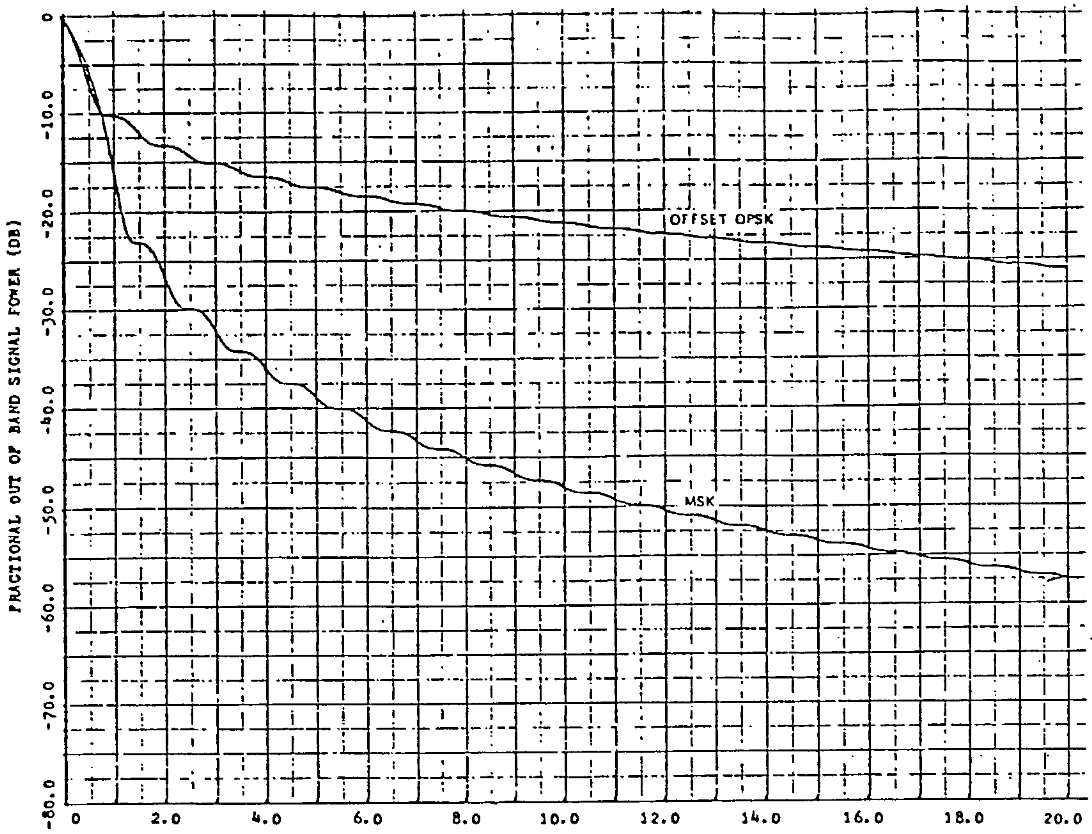

2BT - TWO SIDED NORMALIZED BANDWIDTH
(Hz/BIT/SEC)

Figure 1.1 Fractional Out-Of-Band Power for Offset QPSK and MSK [7]

(a) 99.5% of the signal energy is contained within an IF bandwidth of 1.5 x (data rate),

(b) the signal envelope is essentially constant and therefore MSK is suitable for use in nonlinear channels,

(c) the ideal error rate (coherent detection) is the same as that of 2- and 4-phase PSK.

Figure 1.1 displays the fractional out-of-band power for OQPSK and MSK.

As a result of these properties, MSK has received widespread interest [7-9] because of its potential in band- and power-limited systems. In particular, the Department of Communications has supported over the past few years the development of a single chip LSI version of a nominal 16 kbit/s FFSK modem for use in voice and continuous data applications [10].

During the past few years, MSK modems that have been fabricated have been based upon coherent recovery techniques that is, the demodulator must first regenerate a carrier reference in order to recover the data. In bursty signal environments such as TDMA, DAMA signalling and voice activ~~i~~ated SCPC, the demodulator must re-acquire at the beginning of each burst (assuming that there is no phase coherence from burst to burst). PSK demodulators have been developed that can acquire the signal within 30 symbols. The design of carrier recovery loops for these modems is non-trivial [11]. Furthermore, these designs are usually restricted to applications where the available E_b/N_o is relatively large (>8 dB).

Differential detection can be used in PSK systems to avoid the carrier recovery problem. A differential PSK demodulator (DPSK) compares the phase of adjacent symbol intervals by using a 1 symbol delayed version of the received signal as the local reference signal. The need for a coherent recovery circuit is thereby removed.

It has been shown in [12] that MSK signals can be demodulated by differential detection. While there may be implementation similarity between DMSK and DPSK, DMSK exhibits bandwidth and potentially power efficiency advantages over DPSK that make it a more attractive technique for development. A DMSK modem uses the usual FFSK/MSK modulator but recovers data by differential detection.

The main advantages of a DMSK modem over a coherent MSK modem are:

(a) improved signal acquisition times, and

(b) decreased circuit complexity.

Signal acquisition times for DMSK are primarily based upon clock recovery while joint carrier and clock recovery determine acquisition times for MSK. This is of prime concern in TDMA environments such as JTIDS.

The decreased circuit complexity indicates a potential for improved reliability over coherent MSK modems. The major disadvantage is a theoretical E_b/N_o penalty arising from the use of an essentially noisier reference signal in differential detection and ISI imposed by the received filter. However, it is possible that the advantage of MSK over DMSK may be reduced as a result of increased implementation margins arising from the greater circuit complexity. Furthermore, this penalty can be reduced by observing [12, 13] that phase comparison of alternate symbol intervals provides a parity check for successive symbols. Single errors can be corrected by a simple circuit without the need for the transmission of redundant bits. Such circuitry has been shown to be particularly useful for the correction of errors due to intersymbol interference. For example, in [12] it is shown that for BT = 0.6, a 2.5 dB improvement was measured.

1.5 Clock Synchronization

With carrier recovery occurring essentially immediately for DMSK, the major acquisition problem relates to rapid clock recovery. The problem with phase locked loop recovery techniques is the finite probability of occasionally long acquisition times. This effect is referred to as "hang-up" and is described in [11]. However, once an initial clock phase is established a phase-locked loop-type circuit could be used. Depending on the environment, a digital phase locked loop might be preferable because of narrow tracking bandwidths needed to counteract multipath and other disturbances.

Establishing an initial clock phase can be performed by designing clock regenerator circuits that operate on a suitable preamble at the beginning of the burst. In this case, two approaches can be used

(1) non-linear regeneration with appropriate pre and post filters, and

(2) matched filter detection.

Techniques for non-linear baseband regeneration are reviewed in [11]. Non-linear techniques usually are applied where reasonably large E_b/N_o exists. Matched filter detection may be more appropriate where the chip E_b/N_o is quite low. This approach is based upon detecting an N-bit preamble at the beginning of the burst using a filter whose impulse response is the time inverse of the received signal over the interval of duration NT. The matched filter output would be compared with a suitable threshold to indicate the correlation event and provide an initial timing reference. Maximum likelihood noncoherent MSK burst clock synchronization is the topic of Section 7.0.

1.6 Performance Evaluation Approach

In determining the BER performance of the DMSK demodulator, both theoretical analysis and computer simulation have been used. Theoretical performances usually correspond to simplified system configurations or performance bounds (depending on the assumptions made), and thus tend to be used for benchmarking purposes. Determining the theoretical performance for realistic cases quickly becomes a formidable task, especially when distortion mechanisms (either in the channel or the receiver) or non-linearities such as the single error correction circuit and hard limiters, are introduced. For these reasons the bulk of the BER performance evaluation was performed through computer simulation, where the generation of noise samples is used, as opposed to other techniques which involve a combination of simulation and analysis. Because of the lengthy computation times required by this approach, E_b/N_o degradations are determined for BER's on the order of 10^{-4} or higher. Lower rates would require extremely long computation times. However it is expected that this error rate is in the range of interest.

While it is expected that the best selection of component parameters (e.g. filter) and the corresponding performance will vary to some degree depending upon the error rate, the results produced in this study should identify the preferred class, order, and the approximate BT products required, of filters to be used, as well as the allowable range of values for degrading factors.

1.7 Outline Of The Report

Preliminary theoretical analysis is performed in Section 2.0. The purpose of this section is to describe the MSK signal format, DMSK detection, and to establish the theoretical BER performance bounds which are used as benchmarks for comparison with BER's obtained through simulation and additional theoretical analysis, in the sections which follow.

In Section 3.0 the simulation models are presented. The overall DMSK simulation model and implementation strategy is discussed first, and then a more detailed description of the following modules or aspects of the simulation is given:

(a) PN input sequence

(b) Differential encoder

(c) MSK modulator

(d) Sampling

(e) Filtering

(f) Gaussian noise

(g) DMSK demodulator

(h) Single error correction (SEC) circuit

(i) Bit error counting

(j) Non-constant group delay

(k) Hard limiters

(l) Multipath

(m) Jamming

(n) Eye patterns

Presented in Section 4.0 are the simulation performance results. Section 4.1 presents the simulated BER performance for an optimum coherent MSK demodulator, for which theoretical performance is readily available, and is given in Section 2.0. The purpose for presenting this result is to indicate to the reader that the simulation program is well calibrated and gives expected results. In Section 4.2 the BER performance of various DMSK filters are evaluated. The desired result is a transmit/receive/post-demodulation filter combination which yields the best BER performance. The best BER performance found is presented in Section 4.3. The sensitivity evaluation of Section 4.4. presents the degradations in performance associated with the following:

(a) Bit timing errors,

(b) Threshold errors,

(c) Delay errors,

(d) Phase shift errors,

(e) Carrier frequency offset, and

(f) Non-constant group delay.

Sections 4.5 to 4.8 present the BER performances related to:

(a) Hard limiters in the demodulator,

(b) Multipath (one additional path),

(c) Jamming, and

(d) Doppler.

The capability of certain state variables, available from the single error correction circuit, to monitor or predict the BER performance of the DMSK detector is presented and discussed in Section 4.9. A number of simulated eye patterns are presented in Section 4.10. In Section 4.11 simulated zero crossing RMS jitter results are presented and discussed in the context of bit timing recovery strategies based on zero crossing detection techniques.

In Section 5.0 an investigation of performance with equalization to remove intersymbol interference (ISI) is presented, and includes both theoretical and simulated BER performance results.

In Section 6.0 the intersymbol interference associated with common filter shapes is investigated and a simple adaptive thresholding technique, for the purposes of partial ISI cancellation, is described. Close to optimum threshold levels are determined (in terms of minimizing the probability of bit error) and BER performance with adaptive thresholding is presented.

Presented in Section 7.0 is the maximum likelihood noncoherent approach to MSK burst clock synchronization. An overview of the matched filter bit timing recovery (BTR) approach is presented in Section 7.2. In Section 7.3 an estimate of performance is presented for both time of arrival estimation accuracy and the probability of not correctly acquiring. Matched filter implementation considerations are discussed in Section 7.4 with reference to the state of the art in SAW and CCD devices.

2.0 PRELIMINARY THEORETICAL ANALYSIS

2.1 The DMSK Signal And Its Detection

An MSK signal can be written as

$$s(t) = \sin(\omega_c t + \frac{d_k \pi t}{2T} + \psi_k), \quad kT \leqslant t \leqslant (k+1)T \qquad (2.1)$$

where $f_c = \omega_c/2\pi$ is the carrier frequency, d_k represents the data and is ± 1, ψ_k is a phase constant and T is the bit interval. The phase change over each interval T is determined by the second argument in the sine function and amounts to $\pm\frac{\pi}{2}$. This argument represents a linear phase change over T which is equivalent to a frequency shift of

$$\Delta f = \pm \left(\frac{1}{4T}\right)$$

$$= \pm \frac{\text{bit rate}}{4} \qquad (2.2)$$

The phase function

$$\theta(t) = \frac{d_k \pi t}{2T} + \psi_k \qquad (2.3)$$

is piecewise linear. A plot of the phase trellis for a particular data sequence is shown in Figure 2.1. Note that in Figure 2.1 there is a one-to-one relationship between data bit and the frequency transmitted. This is not necessarily the case for MSK signals generated as a form of offset - QPSK where the frequency transmitted depends upon the relative sign of adjacent data bits [7]. Differential encoding of the modulator input data can be used to yield the one-to-one data/frequency relationship.

A circuit incorporating the differential detector with a single-error correction circuit is shown in Figure 2.2. Note that because differential detection entails a comparison of adjacent symbols, the MSK modulator must include differential encoding. The upper circuit comprising the T second delay line, 90° phase shifter and phase comparator represents the differential detector while the circuit consisting of the 2T delay line and phase comparator is the parity generator. The balance of the circuit consists of the syndrome generator and error correction elements. Signals and signal phases are shown in Figure 2.3 which demonstrates the recovery and correction principle. Note that ideal clock recovery is assumed.

An important relationship exists between carrier frequency, f_c, and bit duration, T. Let the received signal be given by

$$r(t) = \sin[\omega_c t + \theta(t)] \tag{2.4}$$

The differential detector output is then given by

$$r(t)[r(t-T)\measuredangle 90^\circ] = \cos[\omega_c (t-T)+\theta(t-T)]\sin[\omega_c t+\theta(t)] \tag{2.5}$$

Using a standard trigonometric identity and ignoring double frequency terms gives

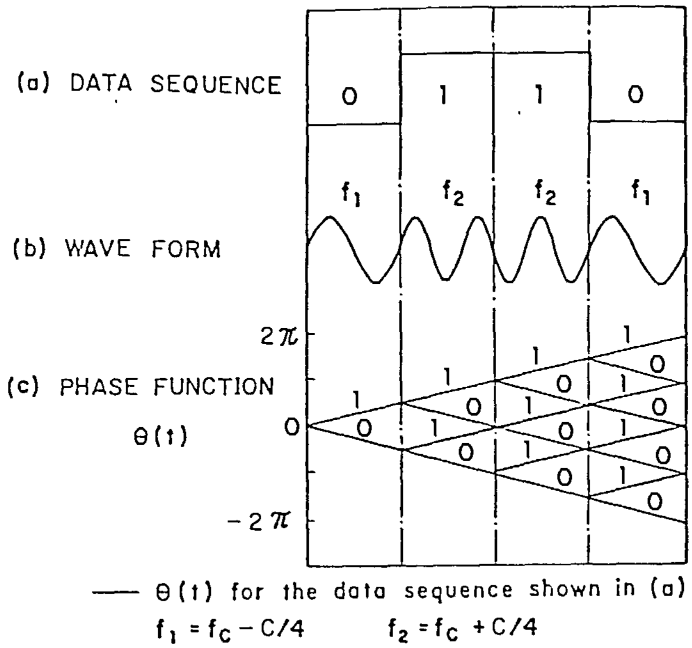

Figure 2.1 MSK Waveform Characteristics [12]

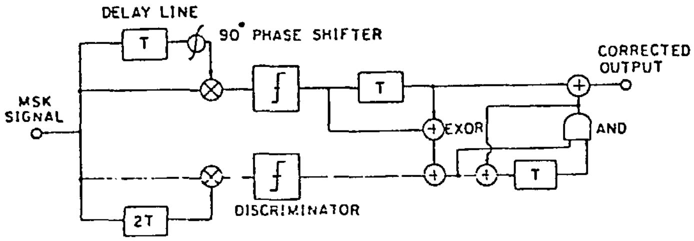

Figure 2.2 Differential Detector and Error Correction Unit [12]

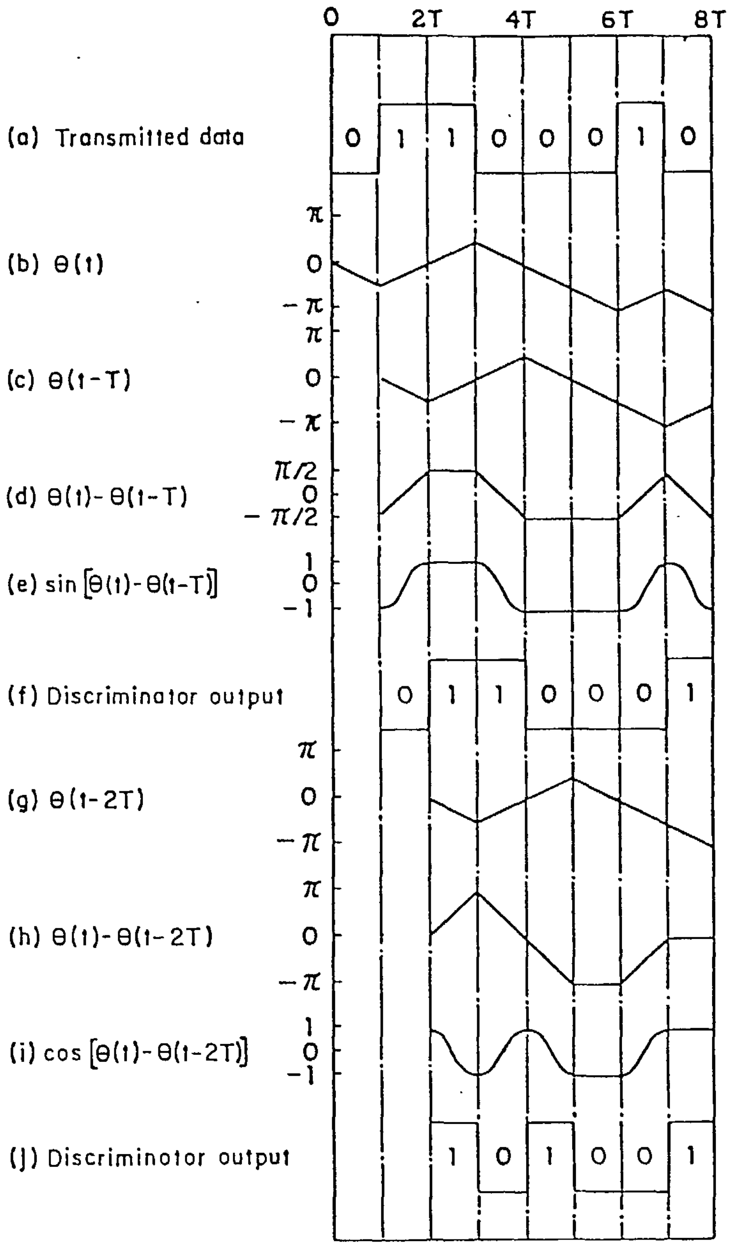

Figure 2.3 Relation Between Differential Detection System Outputs [12]

$$r(t)[r(t-T)\angle 90°] = \tfrac{1}{2}\sin[\omega_c T + \theta(t) - \theta(t-T)]$$

$$= \tfrac{1}{2}\{\sin\omega_c T\cos[\theta(t) - \theta(t-T)]$$

$$+ \cos\omega_c T\cdot\sin[\theta(t)-\theta(t-T)]\} \qquad (2.6)$$

As shown in waveform (d) of Figure 2.3 at t=nT,

$$[\theta(t)-\theta(t-T)] = \pm\frac{\pi}{2} \qquad (2.7)$$

and the detector output is

$$r(t)[r(t-T)\angle 90°] = \pm\cos\omega_c T \qquad (2.8)$$

The desired detector output is maximized with $\omega_c T = 2K\pi\,(K=1,2,3,..)$ and this indicates how carrier frequency and bit duration are related. If there is a carrier frequency offset such that ω_c is replaced by $\omega_c + \Delta\omega_c$ then a phase/frequency compensation may be required.

2.1.1 Single Error Correction (SEC)

The single error correcting mechanism is based on the following [12]. Let $\dot{D}_i$, $\dot{D}_{i-1}$ represent the error free data bits in the i-th and (i-1)-th data intervals. Let

$$\dot{P}_i = \dot{D}_i \oplus \dot{D}_{i-1} \qquad (2.9)$$

where $\oplus$ is the EXOR function.

If e_{D_i} and e_{P_i} represent channel errors in D_i and P_i respectively then at the receiver

$$D_i = \dot{D}_i \oplus e_{D_i} \tag{2.10}$$

$$P_i = \dot{P}_i \oplus e_{P_i} \tag{2.11}$$

The syndrome (error detection variable) is given by

$$S_i = D_i \oplus D_{i-1} \oplus P_i \tag{2.12}$$

and is 0 when no errors occur and equal to 1 when a single error occurs in one of D_i, D_{i-1}, P_i. S_i can be expanded using (2.9) as follows:

$$\begin{aligned} S_i &= D_i \oplus D_{i-1} \oplus P_i \\ &= \dot{D}_i \oplus e_{D_i} \oplus \dot{D}_{i-1} \oplus e_{D_{i-1}} \oplus \dot{D}_i \oplus \dot{D}_{i-1} \oplus e_{P_i} \end{aligned} \tag{2.13}$$

For the previous interval a single error will have been detected and correct and

$$S_{i-1} = e_{D_{i-1}} \oplus e_{P_{i-1}} \tag{2.14}$$

The error bit can be determined by

$$S_i \cdot S_{i-1} = (e_{D_i} \oplus e_{D_{i-1}} \oplus e_{P_i}) \cdot (e_{D_{i-1}} \oplus e_{P_{i-1}}) \tag{2.15}$$

If only one of (e_{D_i}, $e_{D_{i-1}}$, e_{P_i}, $e_{P_{i-1}}$) is in error then $S_i \cdot S_{i-1}$ is always 0 except for

$$S_i \cdot S_{i-1} = e_{D_{i-1}} \tag{2.16}$$

In other words the syndrome circuitry can detect an error in D_{i-1}. Adding $e_{D_{i-1}}$ to the T-delayed data will correct the error.

2.2 BER Performance

2.2.1 Ideal Coherent Detection

For later comparison, the BER performance of coherent minimum shift keying (CMSK) is of interest. We assume an ideal linear, infinite bandwidth channel, corrupted only by additive white Gaussian noise (WGN), and perfect carrier and timing references available at the receiver. With these assumptions, and viewing MSK as orthogonal binary channels with antipodal signalling, the binary error probability is known to be [14]*.

$$P_e = Q(\lambda) = \int_{\lambda}^{\infty} \frac{1}{\sqrt{2\pi}} e^{-x^2/2} \, dx \qquad (2.17)$$

where

$$\lambda = \sqrt{2E_b/N_o} \qquad (2.18)$$

E_b = signal energy per bit

N_o = single-sided spectral density of WGN

and matched filtering has been assumed. With the above assumptions the BER performance of BPSK, QPSK, offset QPSK, or any other orthogonal antipodal signalling scheme, is the same. For the most part this theoretical performance will serve as the benchmark for determining the degradation associated with the suboptimal differential detection scheme.

*Note that in this case the data is not differentially encoded and there is not a one-to-one data/output frequency relationship.

2.2.2 Ideal Differential Detection

Assuming no-ISI, the probability of bit error for the differential or comparison detection of binary FM (including DMSK) is given by [15]

$$P_e = \frac{1}{2} \exp(-SNR) \tag{2.19}$$

where the signal-to-noise power ratio (SNR) is given by

$$SNR = \frac{P_s}{P_n} \tag{2.20}$$

The noise power P_n is given by

$$P_n = N_o B \tag{2.21}$$

where N_o is the single sided power spectral density of the additive white Gaussian noise and B is the IF noise bandwidth of the receive (Rx) filter. The validity of (2.19) also depends on the assumption that the autocorrelation function of the noise, $R_n(\tau)$, is zero at $\tau=T$, where T is the bit period.

The differential detector performs optimally only when the transmitted signal is Nyquist, i.e. when the signal format is such that matched filtering may be used at the receiver and the resultant signal is free of ISI. For this case the instantaneous SNR at the desired comparison points is given by $SNR = E_b/N_o$. Thus the corresponding probability of bit error is given by

$$P_e = \frac{1}{2} \exp(-E_b/N_o) \tag{2.22}$$

This represents a degradation relative to CMSK of about 1 dB at BER = 10^{-4}. The DMSK signal format does not possess the above desired property and thus exhibits inferior performance to that of (2.22).

The main problem with the DMSK signal format is that filters with BT products on the order of 1.0 cause quite severe ISI which results in degraded performance. Thus for the most part, optimizing the performance of the differential detector corresponds to trading off noise bandwidth against ISI.

2.2.3 No-ISI Degradation Lower Bound

As already stated equation (2.19) only holds true for an Rx bandwidth approaching infinity (assuming no attempt is made to equalize for ISI), i.e. any bandwidth constraint causes undesirable ISI. For the most part, the problem of finding the best Rx filter reduces to the problem of trading off noise bandwidth B against imposed intersymbol interference. When comparing detection schemes, an appropriate reference is the ratio of energy per bit to noise power spectral density, E_b/N_o, which is required to give the same bit error rate (BER) performance. In terms of E_b/N_o the signal-to-noise ratio is given by

$$SNR = \frac{E_b}{N_o} \cdot \frac{1}{BT} \tag{2.23}$$

From (2.19) and (2.23) we easily obtain the relationship

$$E_b = -N_o\ BT\ \ln 2P_e \tag{2.24}$$

From (2.17), the optimum performance for CMSK is given by

$$P_e = Q((2E_b'/N_o)^{\frac{1}{2}}) \tag{2.25}$$

Thus from (2.25) the required energy per bit to give the desired probability of error is

$$E_b' = \frac{N_o}{2}\left[Q^{-1}(P_e)\right]^2 \tag{2.26}$$

Of interest is the no-ISI degradation of DMSK from CMSK as a function of the BT product of the Rx filter, and from (2.24) and (2.26) it is given by

$$D = 10\ \log\frac{E_b}{E_b'}\quad (\mathrm{dB})$$

$$= 10\ \log\frac{-2BT\ell n(2P_e)}{\left[Q^{-1}(P_e)\right]^2}\quad (\mathrm{dB}) \tag{2.27}$$

This degradation can be rewritten as

$$D = A + 10\ \log\ BT \quad (\mathrm{dB}) \tag{2.28}$$

where A is the no-ISI degradation for a BT product of unity, and is tabulated in Table 2.1 for $P_e = 10^{-1}$ to 10^{-6}. In Figure 2.4, D is plotted against the BT product for a number of bit error probabilities. The degradation at any error rate approaches infinity as BT increases. Due to ISI, actual degradations are expected to be much worse than the degradations shown for BT products less than 2.0. In fact the degradations are expected to approach plus infinity as BT approaches zero. The curves in Figure 2.4, however, are valuable as lower bounds and tell us the asymptotic performance as BT becomes large.

P_e	A(dB)
10^{-1}	2.933
10^{-2}	1.587
10^{-3}	1.145
10^{-4}	0.902
10^{-5}	0.754
10^{-6}	0.657
0	0

Table 2.1: No-ISI Degradation of DMSK From CMSK For BT = 1.0

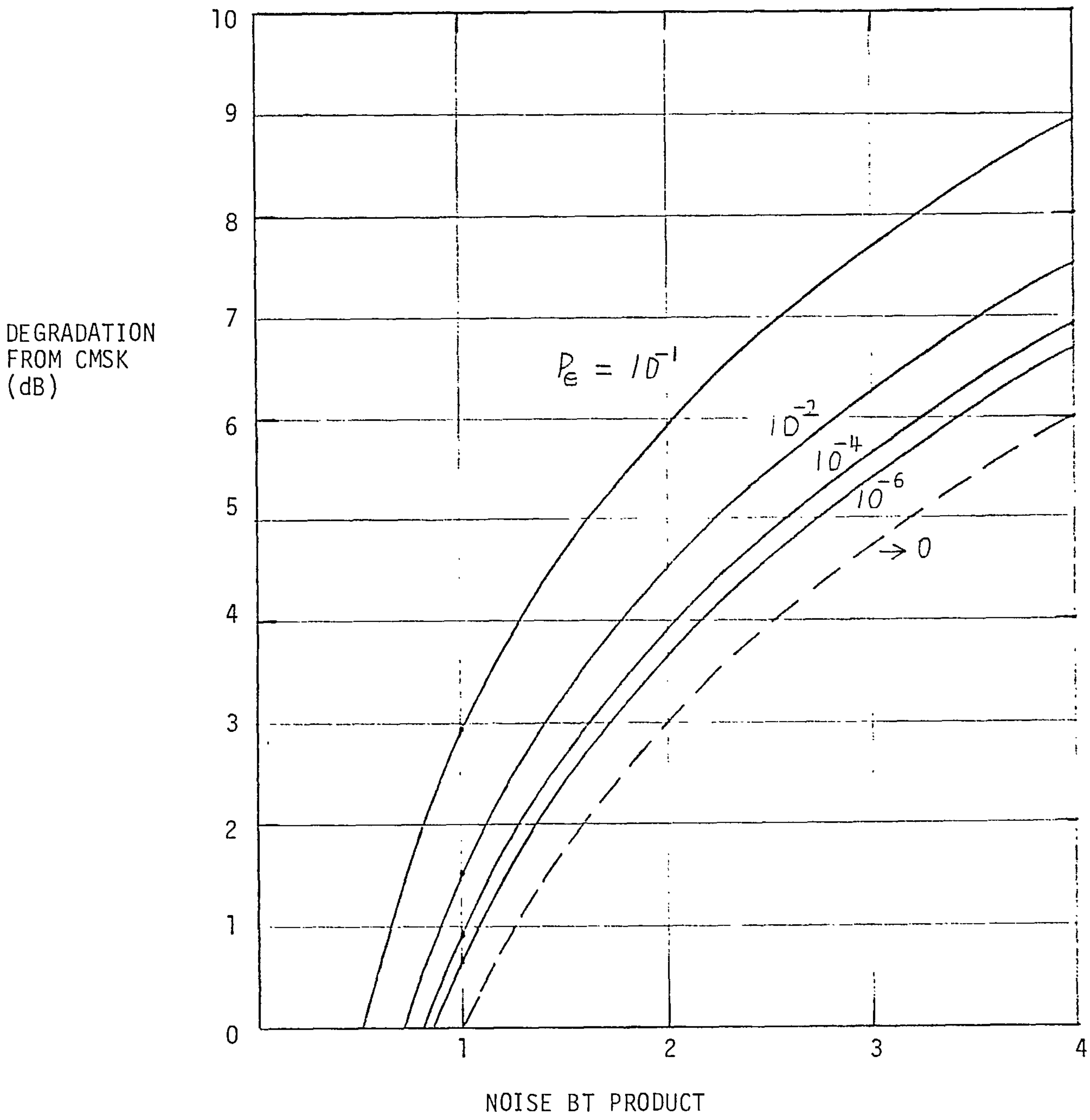

Figure 2.4 No-ISI Degradation For Bandlimited Noise and Unfiltered DMSK Spectrum.

As an example, for $P_e = 10^{-4}$ and BT = 1.25 we obtain a fundamental no-ISI degradation of 2.0 dB for conventional DMSK over CMSK. Thus the actual degradation must be greater than 2.0 dB.

An example [16] of theoretical performance with ISI is presented in Figure 2.5 for a Gaussian Rx filter and $P_e=10^{-6}$. In this Figure, B is the 3 dB bandwidth where the actual noise bandwidth is given by

$$B_n = \frac{1}{2}\left(\frac{\pi}{\ell n 2}\right)^{\frac{1}{2}} B = 1.064B \tag{2.29}$$

Using the bandwidth relationship in (2.29) the appropriate no-ISI lower bound (2.27) was superimposed on this result. Evident is the degrading effect of ISI for BT products less than 2.0 and the asymptotic behaviour for larger BT products. The minimum degradation from CMSK, in terms of E_b/N_o, was found to be 4.02 dB for a BT product of 1.21. For these results single error correction was not considered. Using the same filter type and BT product, Masamura [12] indicates a 3.6 dB degradation for the conventional branch, by means of simulation techniques. The reason for the 0.4 dB discrepancy between these two results is not clear. What is clear, however, is the degrading effect that ISI has on performance. Specifically if no signal distortion were caused (no-ISI) then the corresponding degradation would only be about 1.5 dB for a BT product of 1.21 and BER of 10^{-6} (see Figure 2.4).

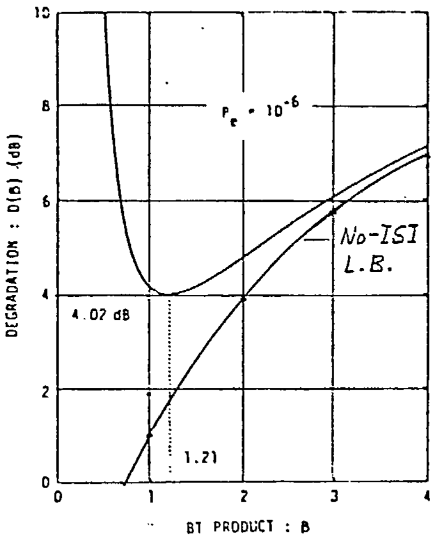

Dependence of degradation $D(\beta)$ upon β.

Figure 2.5 Degradation of DMSK From CMSK For a Gaussian RX Filter [16]. No-ISI Lower Bound (L.B.) Based on Equation (2.27).

2.2.4 Improvement With SEC

Assuming uncorrelated noise samples and no ISI the probability of bit error at the output of the SEC circuit is shown [12] to be given by

$$P_o = 0.89\ P_i^{1.06} \tag{2.30}$$

$$= 0.43\ e^{-1.06\ SNR} \tag{2.31}$$

where P_i is the BER probability at the circuit input.

For an error rate of 10^{-4}, the advantage of this circuit relative to differential detection is given by

$$SNR_i - SNR_o = 9.30 - 8.99$$

$$= 0.31\ \text{dB} \tag{2.32}$$

For DMSK the above result only holds for very large bandwidths. When trying to optimize performance in terms of E_b/N_o, both ISI and noise correlation are introduced. As shown in [12] the improvement with SEC increases dramatically when BT products on the order of 1.0 are used. For BT = 0.6 a 2.5 dB improvement is exhibited at a BER of 10^{-4}.

As can be seen from the preliminary analysis presented, the determination of performance which includes the effects of ISI, noise correlation, and SEC, is not a trivial task. Many assumptions must be made and some factors neglected. Compound the evaluation problem by adding combinations of delay, bit timing, threshold level, frequency errors, etc. and simulation becomes an attractive means of further evaluating system performance.

3.0 SIMULATION MODELS

The following sub-sections describe the DMSK simulation models used and the implementation strategy.

3.1 Overall Model And Implementation Strategy

The DMSK modem simplified simulation model is shown in Figure 3.1. This figure illustrates the fundamental components of the system. With reference to this figure, a differentially encoded PN sequence is supplied to the MSK modulator. The generated MSK signal is filtered by the transmit (Tx) filter and Gaussian noise with double sided power spectral density $N_o/2$ is added. The received noisy MSK signal is then filtered by the receive (Rx) filter and provided to the DMSK demodulator. The conventional DMSK demodulator is shown in the upper branch of the detector, where the signal is delayed by the bit interval T, phase shifted by 90° and multiplied by itself. The resultant signal is then filtered by the post-demodulation (DEM) filter to remove the unwanted harmonics and noise, and the result is then sampled to generate the decoded bit stream. The lower branch is similar, with the reference being the signal delayed by 2T with zero phase shift. This branch generates the parity bits required by the single error correction (SEC) circuit, which generates the second detected data stream. Both of these detected data streams are then compared to the original transmitted data stream for purposes of error detection and counting.

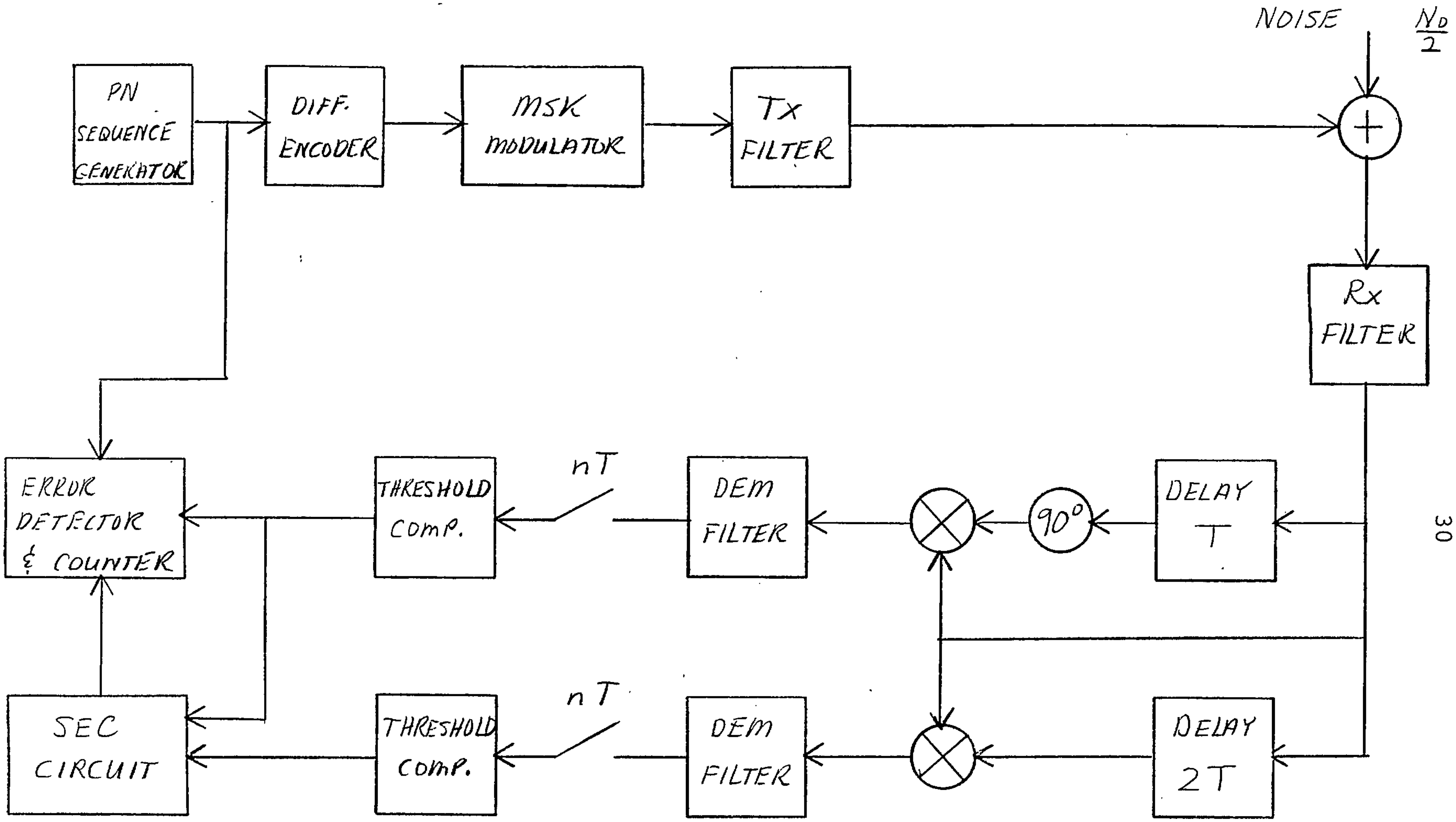

Figure 3.1 DMSK Modem Simulation Model

In the above discussion an ideal DMSK demodulator was assumed. The various system parameters and perturbations from ideal are discussed in more detail below.

The DMSK modem simulation implementation strategy is shown in Figure 3.2. The translation from Figure 3.1 to Figure 3.2 is fairly straightforward. Complex envelope notation is used to represent bandpass signals, and the translation from the time domain to the frequency domain and back again, for the purpose of filtering, is performed by the Fast Fourier Transform (FFT) operator and its inverse. Justification for the above implementation is given in the more detailed mathematical analysis and discussion of the following sub-sections.

The simulation structure (see Figure 3.2) is designed to investigate the effects of the following on BER performance (with and without SEC):

(i) Noise

- white Gaussian
- parameter: E_b/N_o (dB)

(ii) Filtering (T_x, R_x, and DEM)

- for any specified filter shapes
- parameter: BT product

(iii) Bit Timing Error

- assumed constant over each burst
- parameters: bit timing offset ε_3 and ε_4 (fraction of a bit).

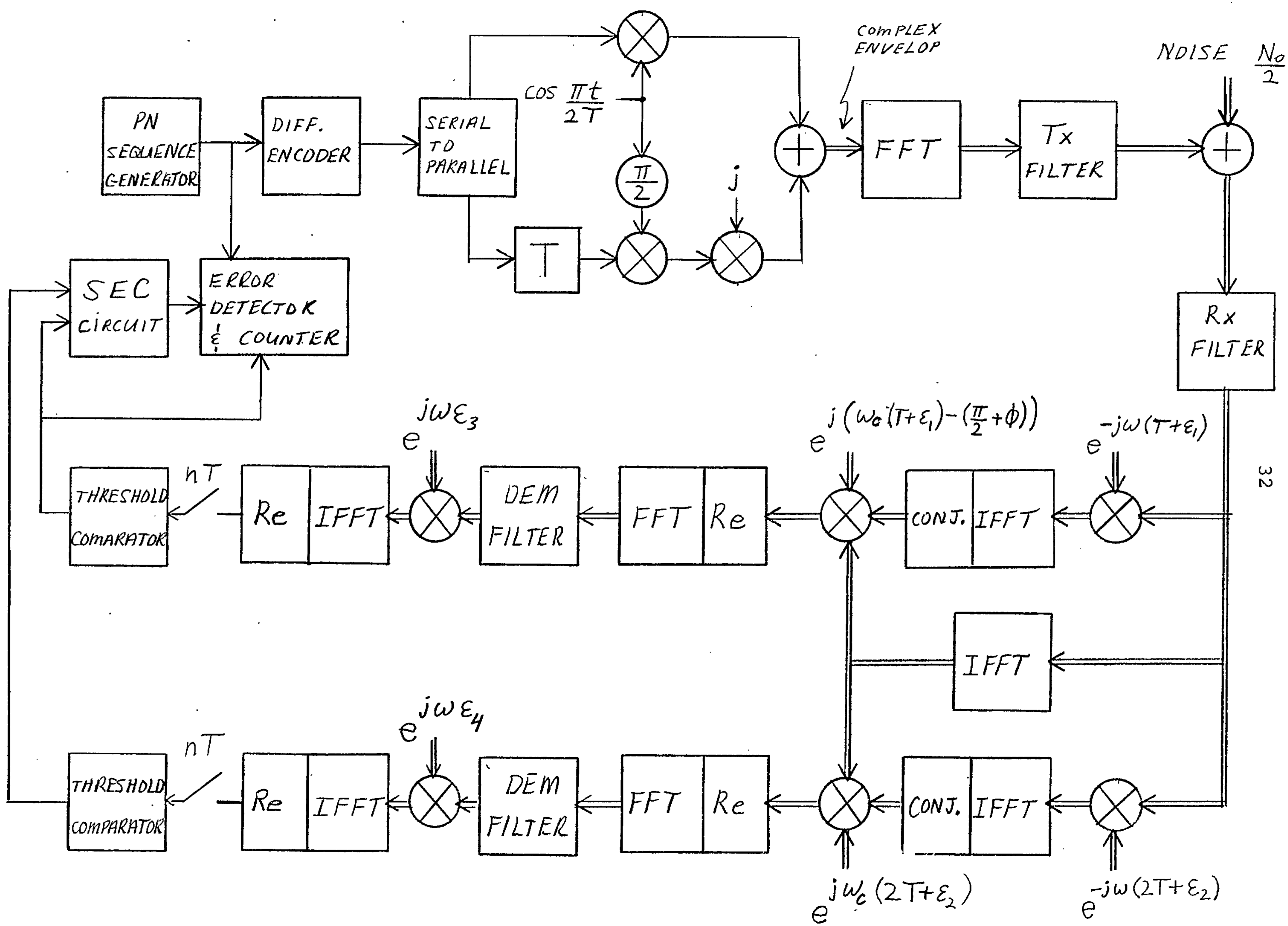

Figure 3.2 DMSK Modem Simulation Implementation Strategy

(iv) Differential Detector Implementation Errors

- delay errors ε_1 and ε_2 in the two branches of the demodulator.
- phase error ϕ in the conventional (upper) branch
- non-constant group delay in delay elements

(v) IF Frequency Offset

- IF frequency ω_c is specified

- also includes the effects of offset Rx filtering

(vi) Doppler Shift

- can be viewed in terms of a frequency offset, and delay errors where $\varepsilon_2 = 2\varepsilon_1$. Thus doppler is covered under a combination of (iv) and (v).

(vii) Threshold Errors

- non-zero thresholds are considered in the threshold comparators.

Although not shown explicitly in Figure 3.2 the simulation also considers the effects of hard limiters, multipath, and jamming. These aspects are discussed in more detail in the following sub-sections.

The simulation also has the capability to generate eye-patterns, which provide a visual quality gauge.

3.2 PN Input Sequence

In the simulation, we consider ISI contributions only from 4 past bits and 4 future bits.* Thus, we need to generate a 9-sequence in order to include the effect of all possible ISI patterns on the BER performance of the modem.

The 9-sequence is generated by using a 9-stage shift register, as shown in Figure 3.3, with feedback taps from stage 5 and stage 9. The shift register is initialized to "100000000". This generator generates a 511-bit PN sequence which is the same as that generated from the following algorithm.

(i) Initialize the first 9 bits of the sequence to "100000000".

$a_i = -1 \quad \text{for } i=1, 8$

$a_9 = +1$

(ii) generate the remaining bits

if $a_{i-9} \neq a_{i-5}$ then $a_i = 1$

else $a_i = -1$, for $i = 10$ to 511

As with any PN sequence the all zero's state is missing. Artificially inserting an additional zero at the start yields all possible 9-bit states and the resulting sequence is 512 bits long, a nice power of 2 in order to facilitate FFT operations.

---

*Based on simulation results, the ISI is indeed negligible four bit periods away from the reference pulse, even for receive filter BT products as small as 0.5.

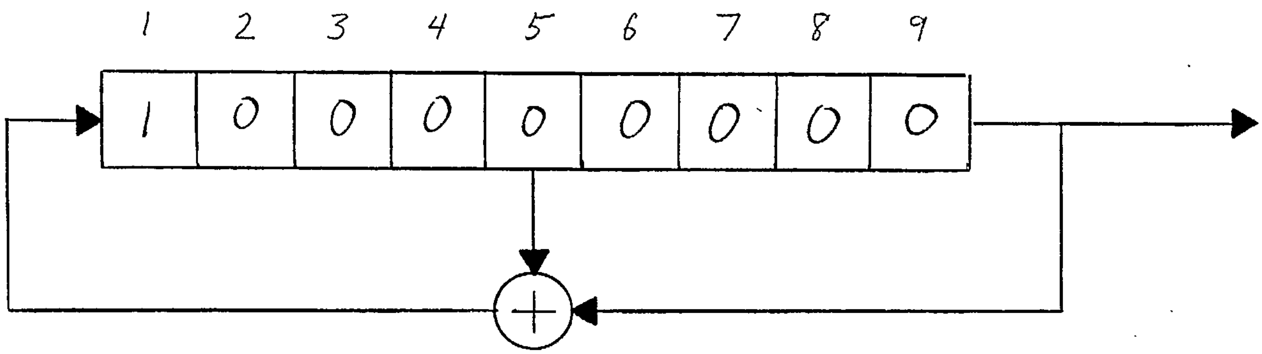

Figure 3.3 9 Stage PN Sequence Generator

3.3 Differential Encoder

The transmitted data sequence $\{a_i\}$, i=1 to 512 is to be differentially encoded, as required when using the differential DMSK demodulator. To generate the differentially encoded sequence $\{b_i\}$, the following rule is followed:

(i) when a_i is a "0" in some bit interval, the coded bit does not change from its previous value in the preceeding interval, but

(ii) when a_i is a "1", the coded bit does change.

The differential encoder is shown in Figure 3.4. The encoder performs the following. When $a_i \neq b_{i-1}$ then $b_i = 1$. When $a_i = b_{i-1}$ then $b_i = 0$.

The differentially encoded sequence requires a reference bit, b_0, from which to start encoding from. Thus it would appear that the encoded sequence might be 1 longer than the original. This can be avoided with the following observation. Since the original 512 bit long sequence has an even number of 1's, then the encoded sequence must have an even number of transitions which implies that $b_{512} = b_0$. Envoking the circular property of PN sequences, b_{512} may be eliminated and the encoded sequence may be thought of as being periodic with period 512 the same as the original sequence. It is important that the differentially encoded sequence have this periodic or circular property so that the FFT's used in the simulation program will not yield unexpected results.

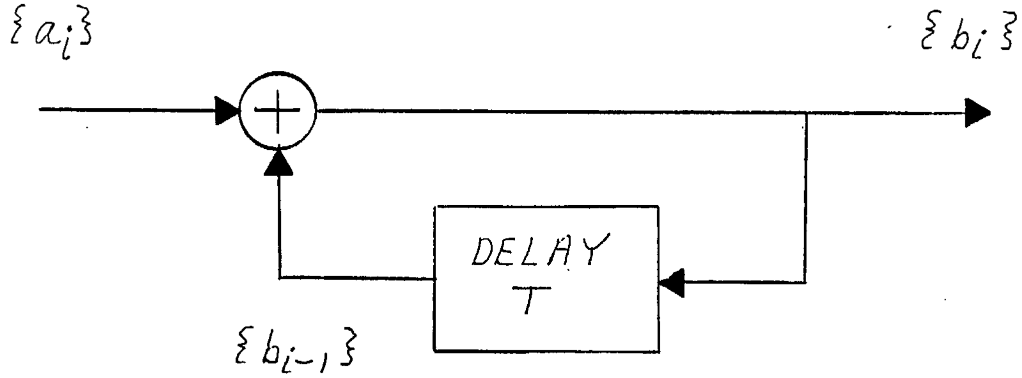

$$b_i = 0, \text{ if } a_i = b_{i-1}$$
$$\quad = 1, \text{ if } a_i \neq b_{i-1}$$

T = Bit Period

Figure 3.4 Differential Encoder

3.4 MSK Modulator

The MSK modulator used in simulating the MSK signal is shown in Figure 3.5. The I and Q data streams are multiplied by

$$\cos \frac{\pi t}{2T} \cos\omega_c t \qquad (3.1)$$

and

$$\sin \frac{\pi t}{2T} \sin\omega_c t \qquad (3.2)$$

respectively. Assuming that the input data stream is $\{b_k = \pm 1\}$ for k=0,..., then the output MSK signal is [7]

$$x(t) = b_{2[\frac{k+1}{2}]} \cos \frac{\pi t}{2T} \cos\omega_c t + b_{2[\frac{k}{2}]+1} \sin\frac{\pi t}{2T} \sin\omega_c t,$$

$$kT \leqslant t \leqslant (k+1)T \qquad (3.3)$$

where $[\cdot]$ denotes the "integer part of". Alternatively x(t) can be written as

$$x(t) = \mathrm{Re}\{[b_{2[\frac{k+1}{2}]} \cos\frac{\pi t}{2T} - jb_{2[\frac{k}{2}]+1} \sin\frac{\pi t}{2T}]e^{j\omega_c t}\},$$

$$kT \leqslant t \leqslant (k+1)T \qquad (3.4)$$

Thus the MSK signal can be represented by the complex envelope notation

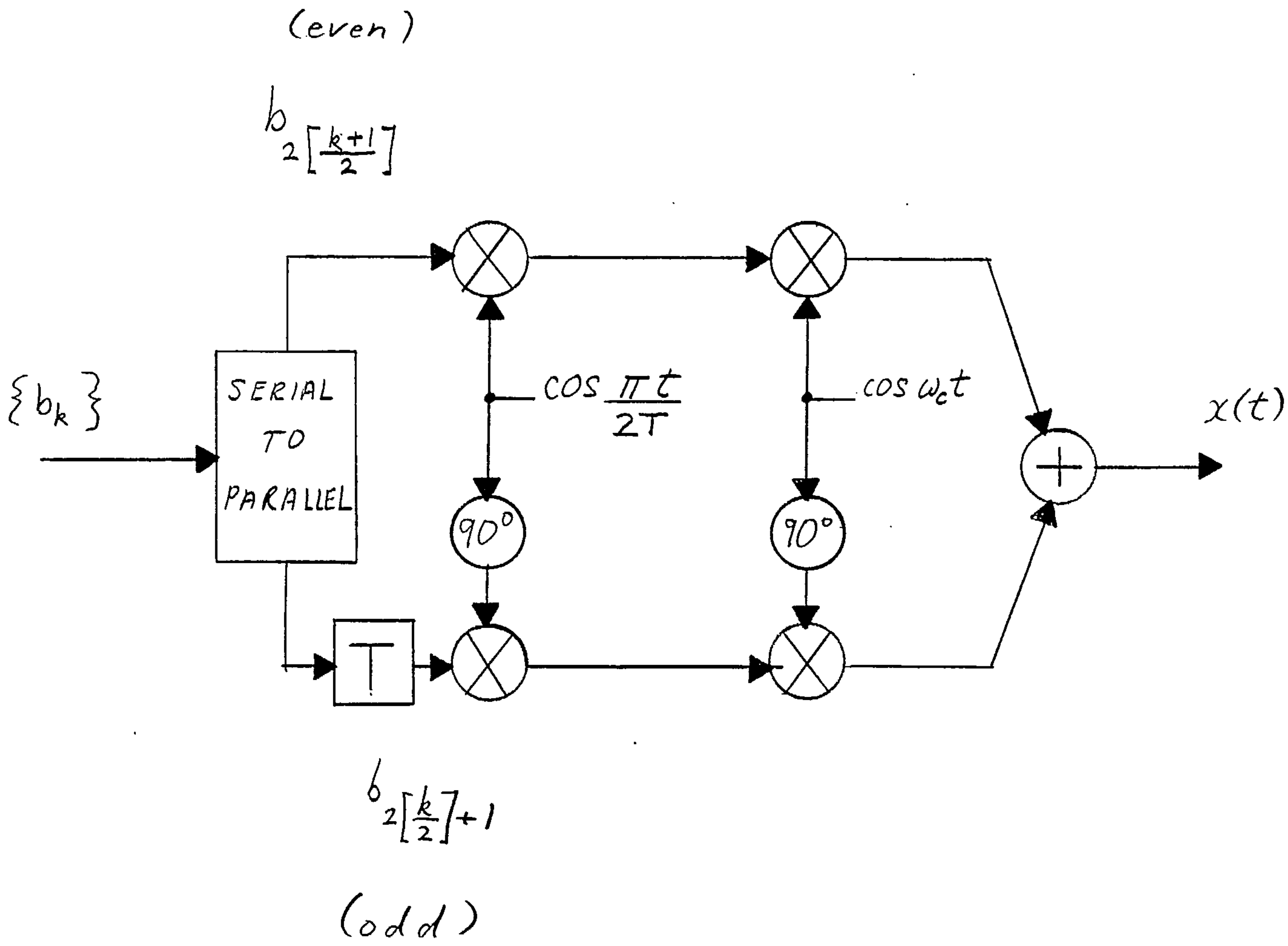

Figure 3.5 MSK Modulator

$$s(t) = b_{2[\frac{k+1}{2}]} \cos \frac{\pi t}{2T} - j b_{2[\frac{k}{2}]+1} \sin \frac{\pi t}{2T},$$

$$kT \leq t \leq (k+1)T \qquad (3.5)$$

The real (inphase or I) and imaginary (quadrature or Q) parts of this waveform are illustrated in Figure 3.6.

In the simulation program, the MSK signal is sampled at the rate of M times the data rate (M samples per bit), that is the sampling interval is $\Delta = T/M$. The complex signal samples are given by

$$s(i\Delta) = b_{2[\frac{k+1}{2}]} \cos \frac{i\pi}{2M} - j b_{2[\frac{k}{2}]+1} \sin \frac{i\pi}{2M},$$

$$kT \leq i\Delta \leq (k+1)T \qquad (3.6)$$

Equation (3.6) is used to generate the complex signal samples. If the data stream $\{b_k\}$ is 512 - bits long, then 512M signal samples will be generated. To use FFT's M should be a power of 2, and M=4 or M=8 should be sufficient to prevent significant aliasing in the frequency domain.

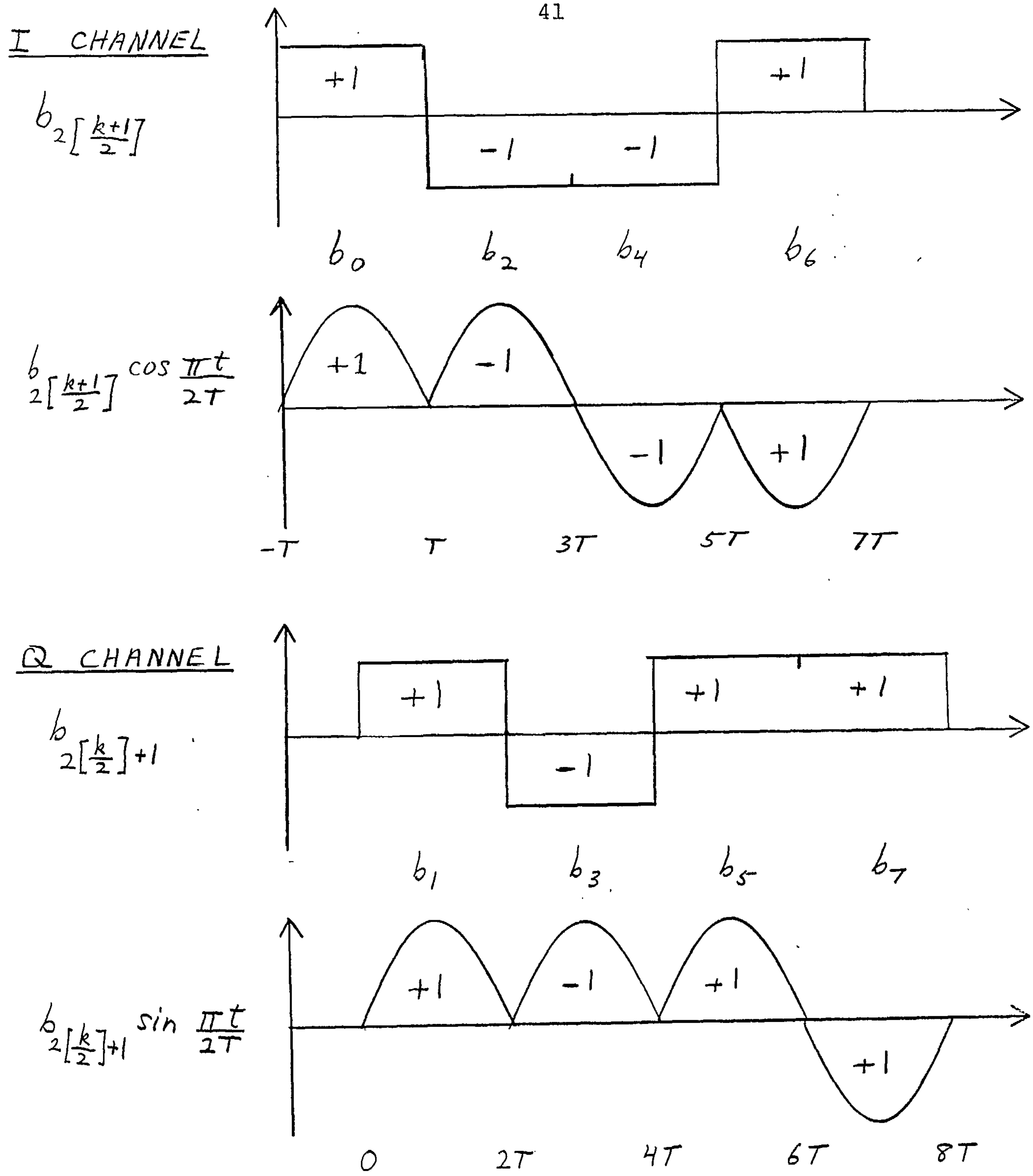

Figure 3.6 MSK Baseband Waveforms

3.5 Sampling

Sampling the MSK generated signal at 8 times the bit rate, R, allows for characterization of the spectrum out as far as the -50 dB point with respect to the main lobe [7]. The power outside this ±4R frequency band is computed to be -45 dB or approximately 3 x 10^{-5} of the total power. For E_b/N_o values of 0 → 20 dB, which is certainly more than the range of interest, this small amount of signal aliasing power will be negligible. Upon filtering the MSK signal by the transmit filter to a maximum of ±2R, as illustrated in Figure 3.7, the remaining digital signal processing may be performed with only 4 samples per bit interval, without further distortion due to digitizing the MSK signal, i.e. Nyquist sampling theorem is properly satisfied. This will reduce the memory requirements by approximately a factor of 2 as most of the storage is required after the transmit filter. In addition the saving in computations will be slightly greater than a factor of 2.

3.6 Filtering

Despite the fact that 99.5% of the MSK signal power is confined within 1.5 times the bit rate [7], filtering is still needed to reduce adjacent channel interference. In the simulation program, all filters are simulated in the frequency domain. The signal samples are transformed to the frequency domain by using a Fast Fourier Transform algorithm, and are then multiplied by the frequency response of the filter to produce the output signal which is also in the frequency domain.

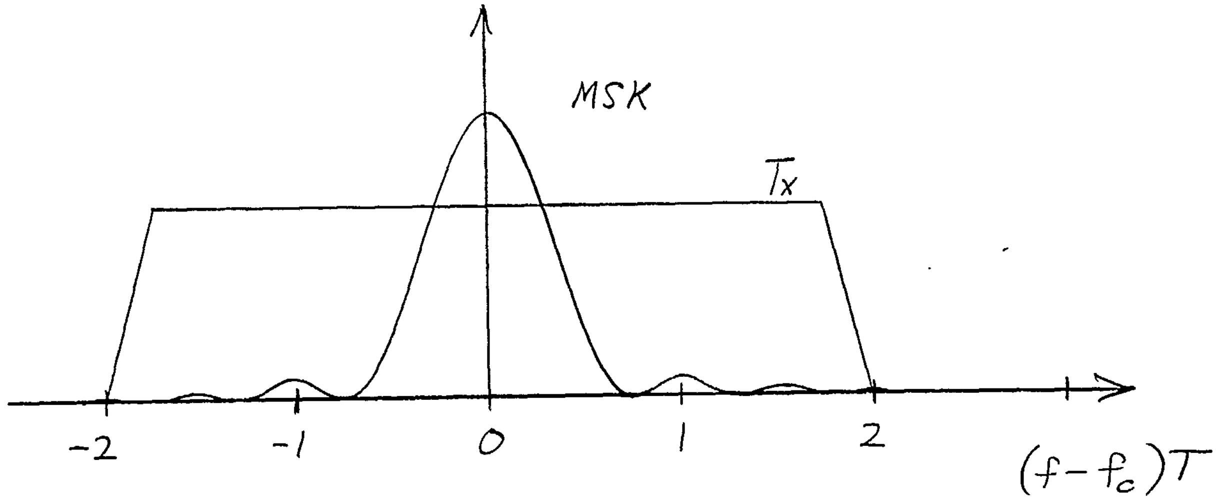

Figure 3.7 MSK Power Spectrum and Tx Filter Requirements to allow only Four Samples per Bit Interval

3.7 Gaussian Noise

Noise is assumed to be Gaussian at the demodulator input in the simulation program. Gaussian noise can be represented in complex envelope notation

$$n(t) = n_c(t) + j\, n_s(t) \tag{3.7}$$

where $n_c(t)$ and $n_s(t)$ are cosine and sine components respectively. Both $n_c(t)$ and $n_s(t)$ are also Gaussian with variance N_oB, where N_o is the single sided power spectral density of n(t) over bandwidth B. The complex noise envelope is added in the time domain.

Since the simulation program must work with sampled signal formats, it is important to have an accurate noise model. Let E_b be the received energy per bit, corresponding to the received baseband symbol pulse, g(t). Then, by Nyquist's theorem,

$$\begin{aligned} E_b &= \int \left|g(t)\right|^2 \, dt \\ &= \tau \sum_k \left|g(k\tau)\right|^2 \\ &\triangleq \tau S \end{aligned} \tag{3.8}$$

where it is assumed that g(t) is effectively bandlimited to $(-\frac{1}{2\tau}, \frac{1}{2\tau})$, and the sampling rate is $1/\tau$. WGN may be modelled as a flat spectrum finite-variance noise, bandlimited to $(-\frac{1}{2\tau}, \frac{1}{2\tau})$. If noise samples are taken with sampling period τ, then each noise sample will have variance

$$\sigma^2 = \frac{N_o}{2} \cdot \frac{1}{\tau} \tag{3.9}$$

and will be independent, as the autocorrelation of this bandlimited noise is given by

$$R(t) = \frac{N_o}{2\tau} \operatorname{sinc} \frac{t}{\tau} \tag{3.10}$$

which is zero for $t = k\tau$ $(k \neq 0)$. Thus with this noise model, $N_o = 2\tau\sigma^2$. A narrower band noise model will introduce correlation between samples, and a wider band noise model, not satifying Nyquist's sampling theorem, will suffer from spectral overlap, as well as introduce slight correlation between noise samples.

Performance is usually determined as a function of E_b/N_o, which is given by

$$\begin{aligned} E_b/N_o &= \frac{\tau S}{2\tau\sigma^2} \\ &= \frac{S}{2\sigma^2} \end{aligned} \tag{3.11}$$

Thus given a desired E_b/N_o we simply generate Gaussianly distributed independent discrete noise samples with variance given by

$$\sigma^2 = \frac{S}{2E_b/N_o} \tag{3.12}$$

where S is computed as defined in (3.8).

3.8 DMSK Demodulator

The received MSK signal with noise is given by

$$r(t) = \operatorname{Re}\{r_c(t)\, e^{j\omega_c t}\} \tag{3.13}$$

where $r_c(t)$ is the complex envelope notation of $r(t)$. The conventional DMSK demodulator is shown in Figure 3.8, and uses a T-delayed, 90° - phase (advanced) shifted version of $r(t)$ as the reference signal which is given by

$$r(t-T)\angle 90° = \mathrm{Re}\{r_c(t-T)e^{j\omega_c(t-T)}\ e^{j\frac{\pi}{2}}\} \tag{3.14}$$

The demodulated signal is

$$y(t) = r(t)\cdot[r(t-T)\angle 90°] \tag{3.15}$$

Equations (3.13) and (3.14) can be written as

$$r(t) = \frac{1}{2}\ [r_c(t)\ e^{j\omega_c t} + r_c^*(t)e^{-j\omega_c t}] \tag{3.16}$$

$$r(t-T)\angle 90° = \frac{1}{2}\ [r_c(t-T)e^{j\omega_c(t-T)}\ e^{j\frac{\pi}{2}} + r_c^*(t-T)e^{-j\omega_c(t-T)}\ e^{-j\frac{\pi}{2}}] \tag{3.17}$$

where $r_c^*(t)$ is the complex conjugate of $r_c(t)$. After some manipulation, ignoring the factor 1/4 and the double frequency terms, we arrive at

$$y(t) = \mathrm{Re}\{r_c(t)r_c^*(t-T)e^{j\omega_c T}\ e^{-j\frac{\pi}{2}}\} \tag{3.18}$$

If there is no filtering, the complex envelope notation of the received signal $r(t)$ is

$$r_c(t) = s(t) + n(t) \tag{3.19}$$

where $s(t)$ and $n(t)$ are the signal and noise and are given in equations (3.5) and (3.7) respectively.

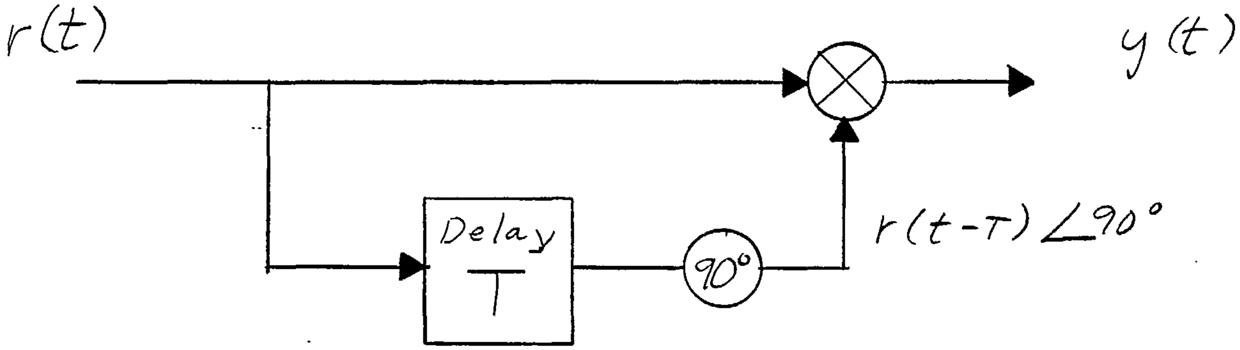

Figure 3.8 DMSK Demodulator

For the ideal case where $\omega_c T = 2k\pi$ (k an integer) and no noise, equation (3.18) becomes (see derivation in Section 3.8.1)

$$y(t) = \mathrm{Re}\{s(t)\cdot s^*(t-T)e^{-j\frac{\pi}{2}}\} \tag{3.20}$$

or

$$y(t) = -b_m b_{m-1}\cos^2\frac{\pi t}{2T} - b_n b_{n-1}\sin^2\frac{\pi t}{2T} \tag{3.21}$$

where

$$m = 2\left[\frac{k+1}{2}\right],\ n = 2\left[\frac{k}{2}\right] + 1,$$

$[\cdot]$ denotes the "integer part of", and the equation is valid for

$$kT < t < (k+1)T$$

As a check, if we sample y(t) at kT, we obtain

$$y(kT) = -b_m b_{m-1}\cos^2\frac{k\pi}{2} - b_n b_{n-1}\sin^2\frac{k\pi}{2} \tag{3.22}$$

$$= -b_k b_{k-1}$$

$$= a_k \text{ (by definition)}$$

Thus we obtain our original data sequence before differential encoding, where $a_k = \pm 1$.

The single error correction circuit requires an additional demodulated waveform, y'(t), similar to that of y(t), and is defined by

$$y'(t) = r(t) \cdot r(t-2T) \tag{3.23}$$

Replacing T with 2T and $\frac{\pi}{2}$ with 0 in the derivation of y(t), and again neglecting double frequency terms, we obtain

$$y'(t) = \text{Re}\{r_c(t) \cdot r_c^*(t-2T)e^{j\omega_c 2T}\} \tag{3.24}$$

For the ideal case y'(t) is given by

$$y'(t) = \text{Re}\{s(t) \cdot s^*(t-2T)\} \tag{3.25}$$

or (see derivation in Section 8.2.2)

$$y'(t) = -b_m b_{m-2} \cos^2 \frac{\pi t}{2T} - b_n b_{n-2} \sin^2 \frac{\pi t}{2T}, \tag{3.26}$$

$$kT \leq t \leq (k+1)T$$

where

$$m = 2\left[\frac{k+1}{2}\right], \quad n = 2\left[\frac{k}{2}\right] + 1$$

As a check if we sample y'(t) at kT, we obtain

$$\begin{aligned} y'(kT) &= -b_k \cdot b_{k-2} \\ &= -(b_k \cdot b_{k-1}) \cdot (b_{k-1} \cdot b_k) \\ &= -a_k \cdot a_{k-1} \quad \text{(by definition)} \end{aligned} \tag{3.27}$$

which is the parity of original data bits a_k and a_{k-1}, where $a_k = \pm 1$.

3.8.1 Derivation of y(t) Given In Equation (3.21)

$$y(t) = \mathrm{Re}\{s(t)\cdot s^*(t-T)e^{-j\frac{\pi}{2}}\} \tag{3.28}$$

where

$$s(t) = b_m \cos\frac{\pi t}{2T} - jb_n \sin\frac{\pi t}{2T}, \tag{3.29}$$

$$kT \leqslant t \leqslant (k+1)T$$

and

$$m = 2[\frac{k+1}{2}],\ n=2[\frac{k}{2}] + 1 \tag{3.30}$$

Thus

$$s^*(t-T) = b_m \sin\frac{\pi t}{2T} \ -jb_n \cos\frac{\pi t}{2T} \tag{3.31}$$

which is valid for $kT \leqslant t-T \leqslant (k+1)T$

$$\text{or } (k+1)T \leqslant t \leqslant (k+2)T$$

If we let $\ell = k+1$ in (3.30) and (3.31) and then replace ℓ with k, (3.31) becomes

$$s^*(t-T) = b_{n-1} \sin\frac{\pi t}{2T} - jb_{m-1} \cos\frac{\pi t}{2T} \tag{3.32}$$

$$kT \leqslant t \leqslant (k+1)T$$

Since $e^{-j\frac{\pi}{2}} = -j$, (3.28) becomes

$$y(t) = -b_m b_{m-1} \cos^2\frac{\pi t}{2T} - b_n b_{n-1} \sin^2\frac{\pi t}{2T}, \tag{3.33}$$

$$kT \leqslant t \leqslant (k+1)T$$

3.8.2 Derivation of y'(t) Given In Equation (3.26)

$$y'(t) = \mathrm{Re}\{s(t) \cdot s^*(t-T)\} \tag{3.34}$$

where

$$s(t) = b_m \cos\frac{\pi t}{2T} - jb_n \sin\frac{\pi t}{2T},\ kT \leqslant t \leqslant (k+1)T \tag{3.35}$$

and

$$m = 2\left[\frac{k+1}{2}\right],\ n=2\left[\frac{k}{2}\right] + 1 \tag{3.36}$$

Thus

$$s^*(t-2T) = -b_m \cos\frac{\pi t}{2T} \ -jb_n \sin\frac{\pi t}{2T} \tag{3.37}$$

which is valid for $kT \leqslant t-2T \leqslant (k+1)T$

$$\text{or } (k+2)T \leqslant t \leqslant (k+3)T$$

If we let $\ell = k+2$ in (3.36) and (3.37) and then replace ℓ with k, (3.37) becomes

$$s^*(t-2T) = -b_{m-2} \cos\frac{\pi t}{2T} - jb_{n-2} \sin\frac{\pi t}{2T} \tag{3.38}$$

$$kT \leqslant t \leqslant (k+1)T$$

Thus (3.34) becomes

$$y'(t) = -b_m b_{m-2} \cos^2\frac{\pi t}{2T} - b_n b_{n-2} \sin^2\frac{\pi t}{2T}, \tag{3.39}$$

$$kT \leqslant t \leqslant (k+1)T$$

3.9 Single Error Correction (SEC) Circuit

The SEC logic circuit is shown in Figure 3.9. The input data streams are the conventional DMSK detected bits, A(k), and the DMSK detected parity bits, B(k). The state variables required to implement this circuit are shown in the figure and the logical equations are also listed. The output, A'(k-1), is the corrected version of A(k) and is delayed by one bit interval.

If all variables take on values of + and -1, then the logical transformation

$$a \leftrightarrow A$$

$$0 \leftrightarrow -1$$

$$1 \leftrightarrow +1$$

allows all XOR gates to be implemented with the rule

$$a+b \leftrightarrow -A \cdot B$$

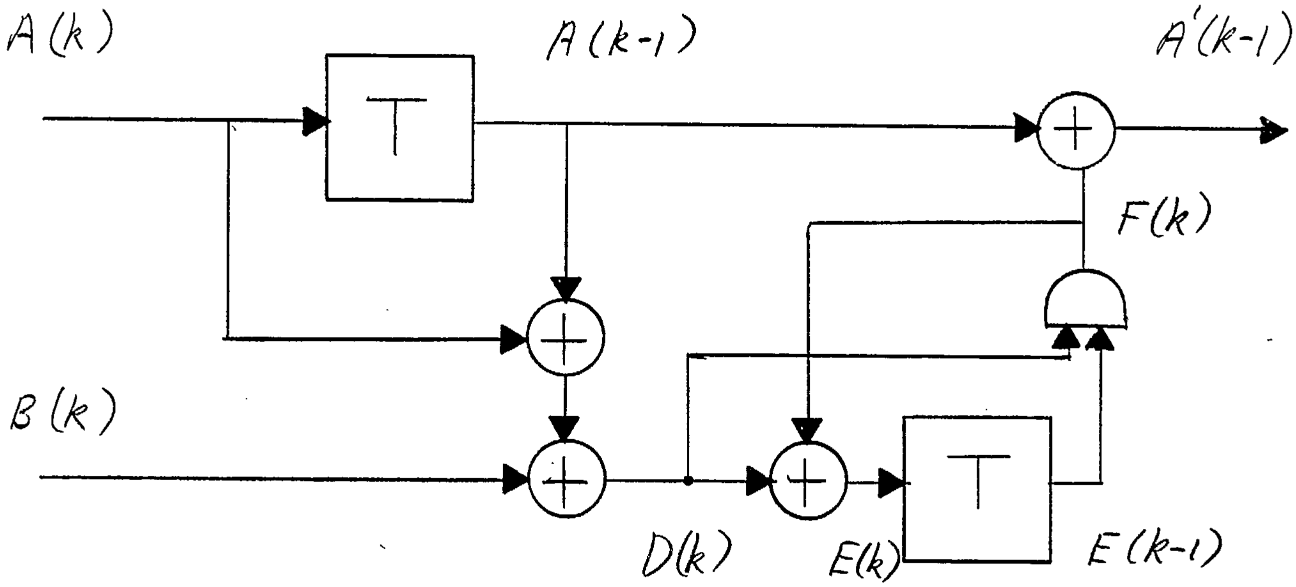

$$D(k) = A(k) \oplus A(k-1) \oplus B(k)$$

$$E(k) = F(k-1) \oplus D(k)$$

$$F(k) = D(k) \cdot E(k-1)$$

$$A'(k-1) = A(k-1) \oplus F(k)$$

Figure 3.9 Single Error Correction (SEC) Logic Circuit

3.10 Bit Error Counting

The bit error rate performance of the modem is estimated by counting the discrepancies between the data stream recovered from a noisy, distorted MSK signal and the data stream used in modulating the MSK signal. If n discrepancies are counted in N bits transmitted, then the estimated value of the true bit error rate p is

$$p' = \frac{n}{N} \tag{3.40}$$

If errors are made independently from bit to bit, then the BER estimation RMS error is given by [17]

$$\sqrt{E\{(p'-p)^2\}} = \sqrt{\frac{p(1-p)}{N}} \tag{3.41}$$

We can only estimate the value of the RMS error since p is not known in equation (3.41). An approximate value of the RMS error can be found by using p' in place of p in (3.41).

3.11 Non-Constant Group Delay

For the DMSK receiver, a delay of one bit period is required for the conventional branch and a delay of 2 bit periods for the parity bit branch. Ideally these delays should be constant throughout the frequency band of interest. In practice the group delay will not be a constant but will be given by

$$D'(f) = T_o + A'f + \text{higher order terms} \tag{3.42}$$

where T_o is the desired constant delay, and A' is the parameter which determines the severity of the linear component. For the purposes of our investigation we have neglected the higher order terms and thus assume the group delay for the conventional branch is given by

$$D_c(f) = T + A'f \tag{3.43}$$

where T is the bit period and is the desired delay for the conventional branch. The group delay for the parity bit branch is assumed to be given by $D_p(f) = 2D_c(f)$, which that 2 identical T-delay elements have been cascaded to obtain the desired 2T-delay. The group delay is defined as the negative derivative of the phase response, i.e.

$$D(f) = \frac{-d\phi(f)}{d\omega} = \frac{-1}{2\pi} \; \frac{d\phi(f)}{df} \tag{3.44}$$

Thus the phase response corresponding to the group delay defined in (3.43) is

$$\phi(f) = -2\pi\left[fT + \frac{A}{2}(fT)^2\right] \tag{3.45}$$

where $A = A'/T^2$ is normalized so that the degradation resulting from a given value of A is not dependent on the data rate.

Of interest is the phase error at f=R which is given by

$$\begin{aligned} \phi_e(f{=}R) &= -\pi A \text{ radians} \\ &= -180A \text{ degrees} \end{aligned} \tag{3.46}$$

Equation (3.45) is used as the simulation model.

3.12 Hard Limiters

The ideal hard limiter voltage transfer function is given by

$$L[x] = V_L, \quad \text{for } x > 0$$

$$= -V_L, \quad \text{for } x < 0$$

$$= V_L \operatorname{sgn}[x] \tag{3.47}$$

If the limiter input is an amplitude and phase modulated carrier given by

$$s_i(t) = A(t)\cos(z(t)) \tag{3.48}$$

where the amplitude, $A(t)$, is assumed always greater than zero and the phase function, $z(t)$, is given by

$$z(t) = 2\pi f_c t + \phi(t) \tag{3.49}$$

then the limiter output, $s_o'(t)$, is given by

$$s_o'(t) = L[s_i(t)]$$

$$= V_L \operatorname{sgn}[s_i(t)]$$

$$= V_L \operatorname{sgn}[\cos(z(t))] \tag{3.50}$$

Note that $s_o'(t)$ is a rectangular wave, periodic in $z(t)$, and thus can be represented by the Fourier series

$$s_o'(t) = \frac{4V_L}{\pi}\left[\cos z - 1/3 \cos 3z + 1/5 \cos 5z - \ldots\right] \tag{3.51}$$

If the carrier frequency, f_c, is sufficiently large and the limiter is followed by a zonal filter, then the remaining harmonic of interest will be

$$s_o(t) = \frac{4V_L}{\pi} \cos(z(t)) \tag{3.52}$$

which has all amplitude variation removed without affecting the phase characteristic.

Using complex notation the input and output waveforms are given by

$$s_i(t) = R_e[c_i(t)e^{j2\pi f_c t}] \tag{3.53}$$

$$s_o(t) = R_e[c_o(t)e^{j2\pi f_c t}] \tag{3.54}$$

where the respective complex envelopes are

$$c_i(t) = A(t)\ e^{j\phi(t)} \tag{3.55}$$

$$c_o(t) = \frac{4V_L}{\pi}\ e^{j\phi(t)} \tag{3.56}$$

Thus the equivalent complex envelope baseband input-output relationship is given by

$$c_o(t) = \frac{4V_L}{\pi} \cdot \frac{c_i(t)}{|c_i(t)|} \tag{3.57}$$

which is the function implemented in the DMSK simulation program.*

*Without loss of generality, $V_L = \pi/4$ in the simulation program, which yields an amplitude of unity.

3.13 Multipath

Only the degradation caused by one additional path is considered here. The first path is assumed to be the line-of-sight (LOS) or dominant path. If the second path has attenuation A, Delay τ, and phase ϕ, with respect to the first or dominant path, then in complex baseband notation the received signal is given by

$$r(t) = s(t) + Ae^{j\phi}\, s(t-\tau) \tag{3.58}$$

where the transmitted signal is s(t). For simulated performance, the attenuation A and differential path delay τ are held fixed for each entire simulation run. However, the phase is assumed to take on a uniform distribution from 0 to 2π, which corresponds to just averaging the probability of bit error for all phases. This is actuated using the formula

$$\phi_n = \frac{n}{N} \cdot 2\pi \tag{3.59}$$

where n=1, 2,...,N is the small run index and N is the number of small runs (typically 200) which constituted an entire simulation run. Each small run consists of one 512 bit long PN sequence. In terms of the above notation, if we assume the second path to be undesired interference, then the carrier to interference ratio (C/I) is given by

$$C/I = -20 \log A \text{ (dB)} \tag{3.60}$$

3.14 Jamming

The jamming signal is assumed to be an in-band tone, and is added to the signal just prior to Rx filtering. Only the worst case jammer is considered, i.e. the in-band tone is assumed to have the same frequency as the carrier frequency of the desired signal, for maximum interference power throughput. If the interfering tone is assumed to have attenuation A, and phase ϕ, with respect to the carrier, then in complex baseband notation the received signal is given by

$$r(t) = s(t) + Ae^{j\phi} \qquad (3.61)$$

where the transmitted signal is s(t). For simulated performance, the attenuation A is held fixed for each entire simulation run. The phase is assumed to be uniformly distributed from 0 to 2π and was actuated using the same relationship described in (3.59). As in the multipath case, the carrier to interference ratio is given by (3.60).

3.15 Eye Patterns

The simulation program generates eye patterns by superimposing a number of bit periods of the demodulated waveform. Linear interpolation is used in the time domain to fill in the gaps between the given sample points. this is quite accurate when 4 or more samples per bit period are used. Eye patterns can be generated for both the conventional and parity bit branches, and with or without noise for a prespecified number of bits.

4.0 SIMULATION PERFORMANCE RESULTS

4.1 Optimum MSK Demodulator

A test of the MSK modulator, the noise model, and the optimum coherent demodulator was performed using the simple configuration shown in Figure 4.1. The optimum coherent detector assumes perfect carrier recovery, coherent inphase and quadrature demodulation, matched filtering, and perfect bit timing recovery. Differential encoding is not used and thus performance is expected to be that of CMSK which is the same as that of ideal coherent OQPSK or BPSK for which theoretical performance is given by

$$P_e = Q(\sqrt{2E_b/N_o}) \tag{4.1}$$

where E_b is the energy per bit and the noise has single sided power spectral density N_o.

The simulated BER performance is plotted in Figure 4.2. Also shown in this figure is the theoretical performance given by (4.1). We see that the Gaussian noise model is well calibrated to $E_b/N_o = 8$ dB. Error bars indicating plus and minus the theoretical RMS error are also shown. It should be noted that with 4 BER samples the probability of all error bars crossing the theoretical curve (assuming Gaussian statistics) is $(.683)^4 \simeq .22$. In other words, the probability of at least one error bar not crossing the theoretical curve is .78, which is quite likely. Thus we conclude that simulated performance is as expected for this simple case.

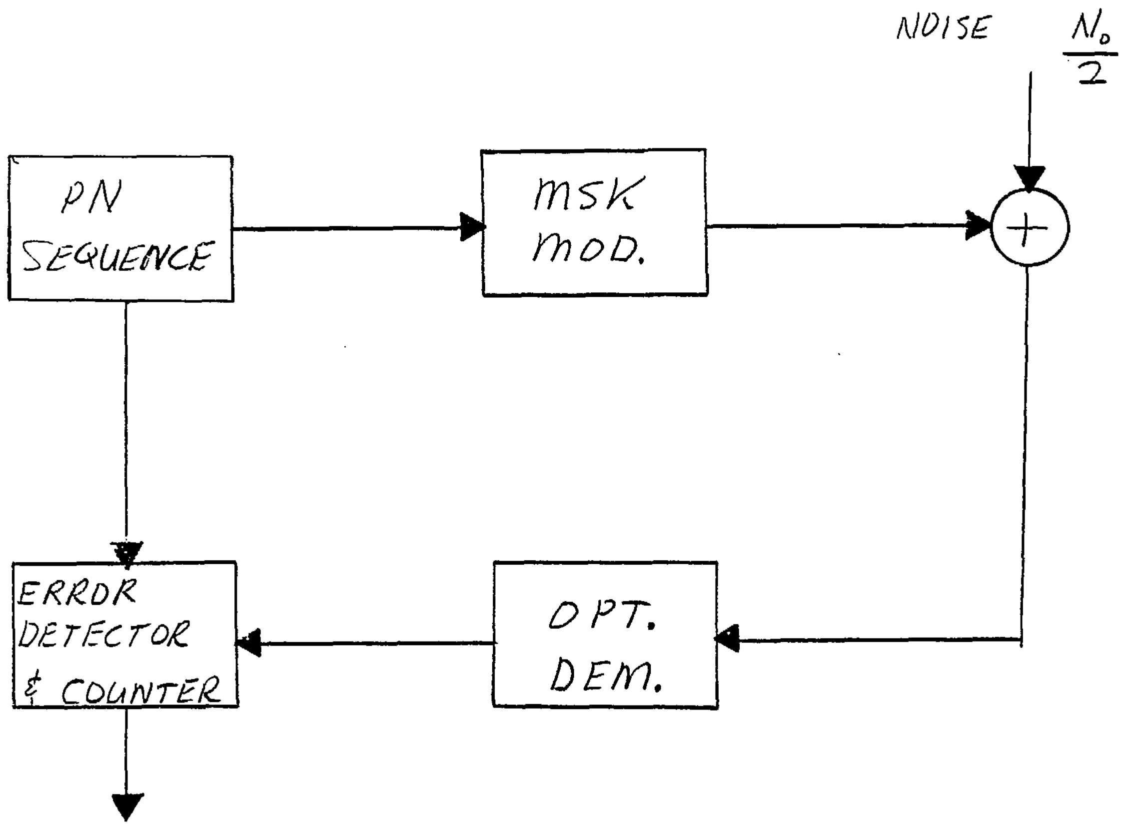

Figure 4.1 Preliminary Test Configuration For Ideal CMSK Demodulator

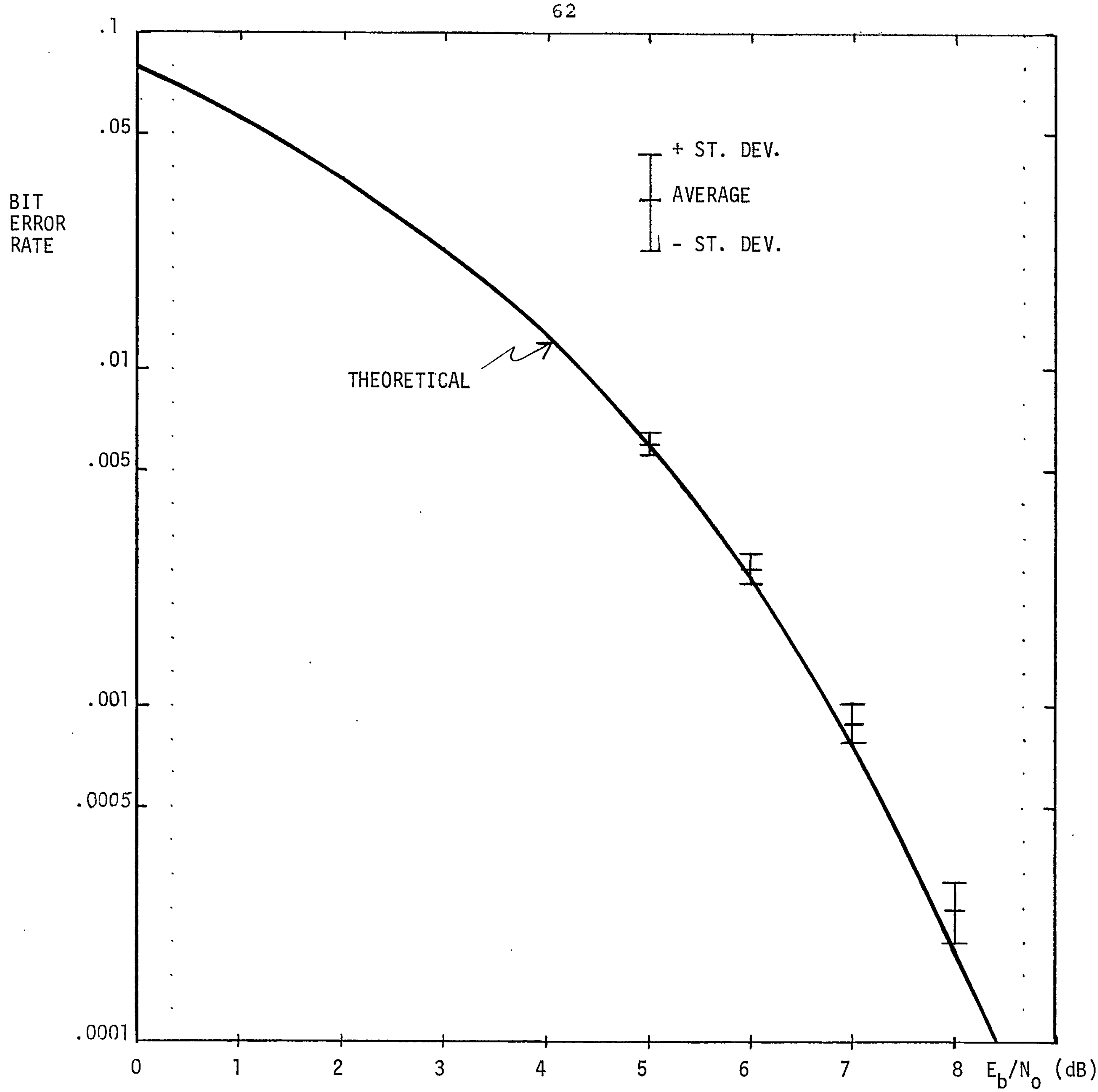

Figure 4.2 Simulated Performance With Ideal CMSK Demodulator

E_b/N_o (dB)	BER	RMS ERROR	LOG of		
			+ST.DEV	AV.	-ST.DEV.
5	.006074	.000343	-2.19	-2.22	-2.24
6	.002578	.000224	-2.55	-2.59	-2.63
7	.000937	.000135	-2.97	-3.03	-3.10
8	.000254	.000050	-3.52	-3.60	-3.69

TABLE 4.1 Simulated Performance of Optimum MSK Demodulator

4.2 DMSK Filter Evaluation

In the following 3 subsections the performance of the DMSK detector, for various transmit, receive, and post-demodulation filters is determined. The primary objective is to find the filter combination which requires the least amount of energy per bit to provide a reasonable BER performance. An assumed constraint, however, is that the transmit filtering is not allowed to degrade the DMSK signal format, i.e. severe filtering at the transmitter would destroy the constant envelope characteristic.

4.2.1 Receive Filter

The DMSK modem simulation model was presented in Figure 3.1. This subsection presents the results obtained in trying to optimize the receive (Rx) filter in the absence of any other filtering, i.e. no transmit (Tx) filter* was used and the post-demodulation (DEM) filter was assumed to remove only unwanted signal harmonics without distorting the baseband spectrum. All delays, phase shifts, and sampling times were set to the correct values for optimum performance. The only variable parameters were:

(i) filter type,

(ii) filter BT product, and

(iii) E_b/N_o

Performance is presented for both conventional DMSK and with single error correction (SEC), in terms of the corresponding degradations (in dB) from optimum coherent minimum shift keying (CMSK).

---

*The transmitted spectrum was characterized out to plus and minus 2 times the bit rate (i.e. BT=4). For receive filter BT products on the order of 1.0, and transmit bandwidth effects can be neglected.

Performance has been obtained for the following 6 filter types:

(i) Ideal Gaussian

(ii) 2-nd Order Butterworth (BW2)

(iii) 2-nd Order Butterworth Equalized (BW2 Equ.)

(iv) 4-th Order Butterworth (BW4)

(v) 4-th Order Butterworth Equalized (BW4 Equ.)

(vi) Ideal rectangular bandpass

The variable parameter was taken to be the BT product, where B stands for the 3-dB double sided bandwidth and T is the bit period, equal to the reciprocal of the data rate. Equalized filters refer to an ideal zero or linear phase response. For each filter type the objective was to obtain the BT product which resulted in the smallest degradation (in dB) from CMSK, for the specified BER.

To obtain the results presented, simulations were performed for E_b/N_o of 9,10, and 11 dB for each of the filter types and BT products. The resulting dB degradations were plotted against the BER's obtained. Interpolation between obtained points was required to estimate the degradation for a BER of $5x10^{-4}$. These intermediate plots are contained in Appendix A, and could be used to obtain similar results for BER's larger than $5x10^{-4}$. Smaller BER's would require much more computer execution time to obtain reasonable confidence intervals.

Figures 4.3 to 4.8 contain the measured degradations for each filter type. The degradation (in dB) for both detection schemes is plotted against the BT product. Also shown is the 0.48 dB degradation associated with ideal coherent detection of differentially encoded MSK (DIFF. CMSK) for the specified BER. Scanning these 6 figures, we see that the smallest degradations tend to be on the order of 3 dB for conventional detection, and 2 dB with SEC included. The degradation appears to be least sensitive to the BT product for the second-order Butterworth filters. Unfortunately these filters correspond to the worst performance.

Note that the optimum BT product with SEC tends to be slightly smaller than that for conventional DMSK. The optimum BT products, and corresponding degradations from ideal, are summarized in Table 4.2 for each filter type.

The fourth order Butterworth filter with ideal linear phase response resulted in the smallest degradation; approximately 2.9 and 1.9 dB for conventional DMSK and with SEC respectively, for a BT product of about 1.1. From Table 4.2 the penalty associated with not having an ideal linear phase (i.e. unequalized fourth-order Butterworth) as seen to be 3.15 - 2.9 = 0.25 dB and 2.0 - 1.9 = 0.1 dB for conventional DMSK and with SEC respectively. For the 5 x 10^{-4} BER considered, this penalty is not severe.

The minimum degradation from CMSK for convention DMSK with a Gaussian receive filter was determined to be 3.35 dB, at the BER of 5×10^{-4}. This degradation is expected to be less than the 4.02 dB degradation, obtained by Suzuki [16], because his theoretical analysis was for a BER of 10^{-6}, where ISI has a greater impact.

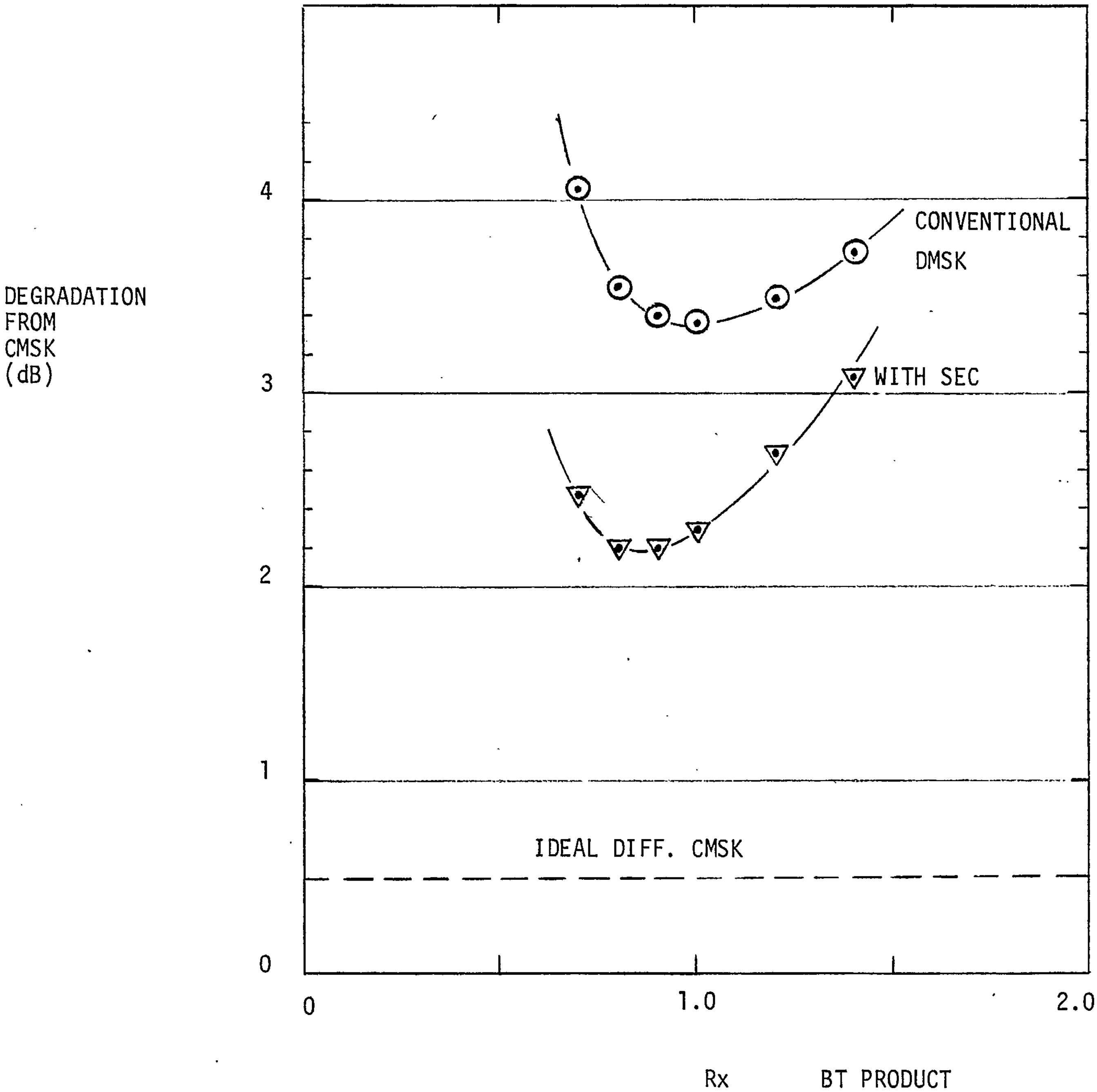

Figure 4.3 Simulated DMSK With:

Rx = Gaussian

Pe = $5x10^{-4}$

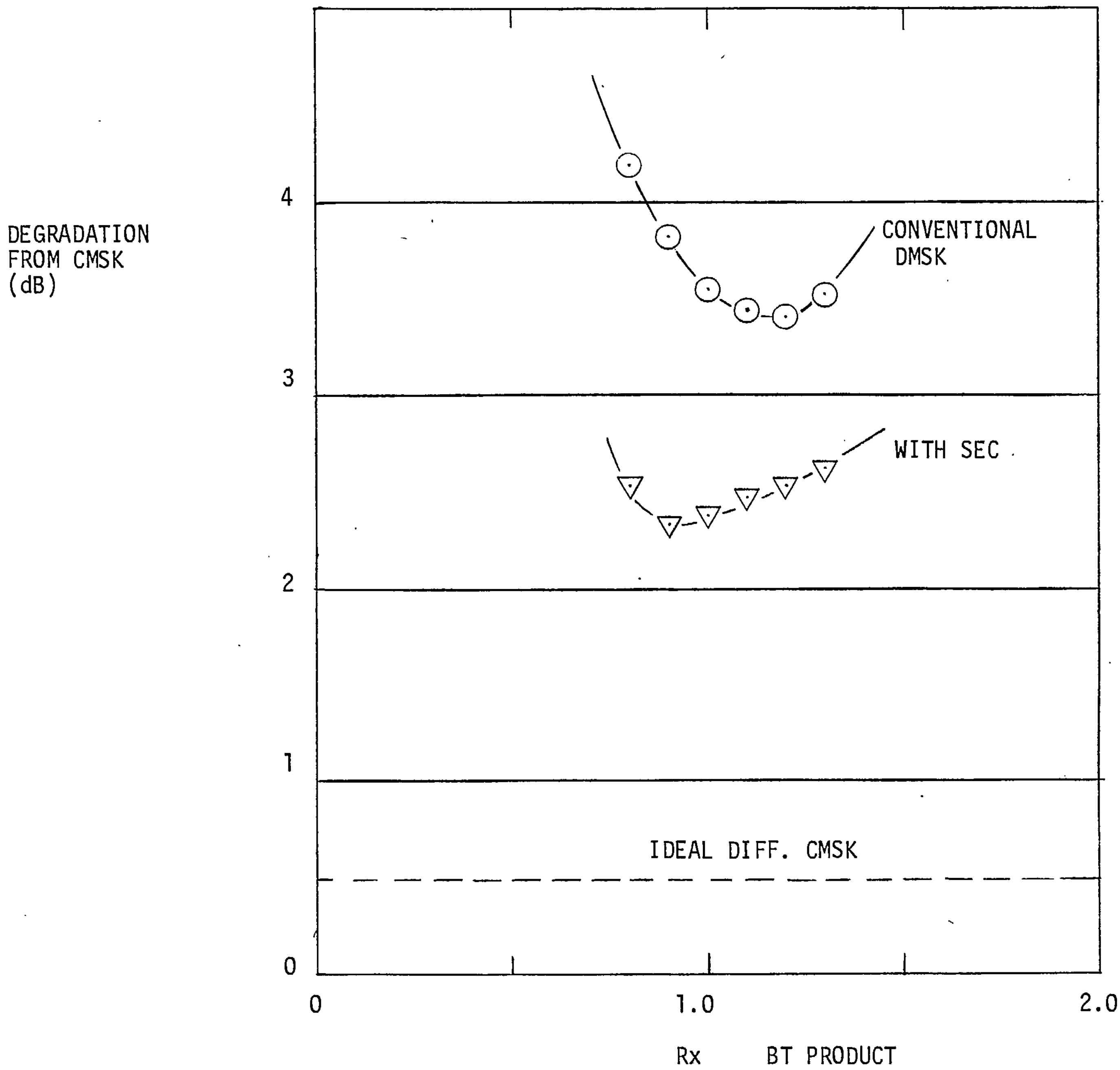

Figure 4.4 Simulated DMSK With:
Rx = 2nd Order Butterworth
$P_e = 5\times10^{-4}$

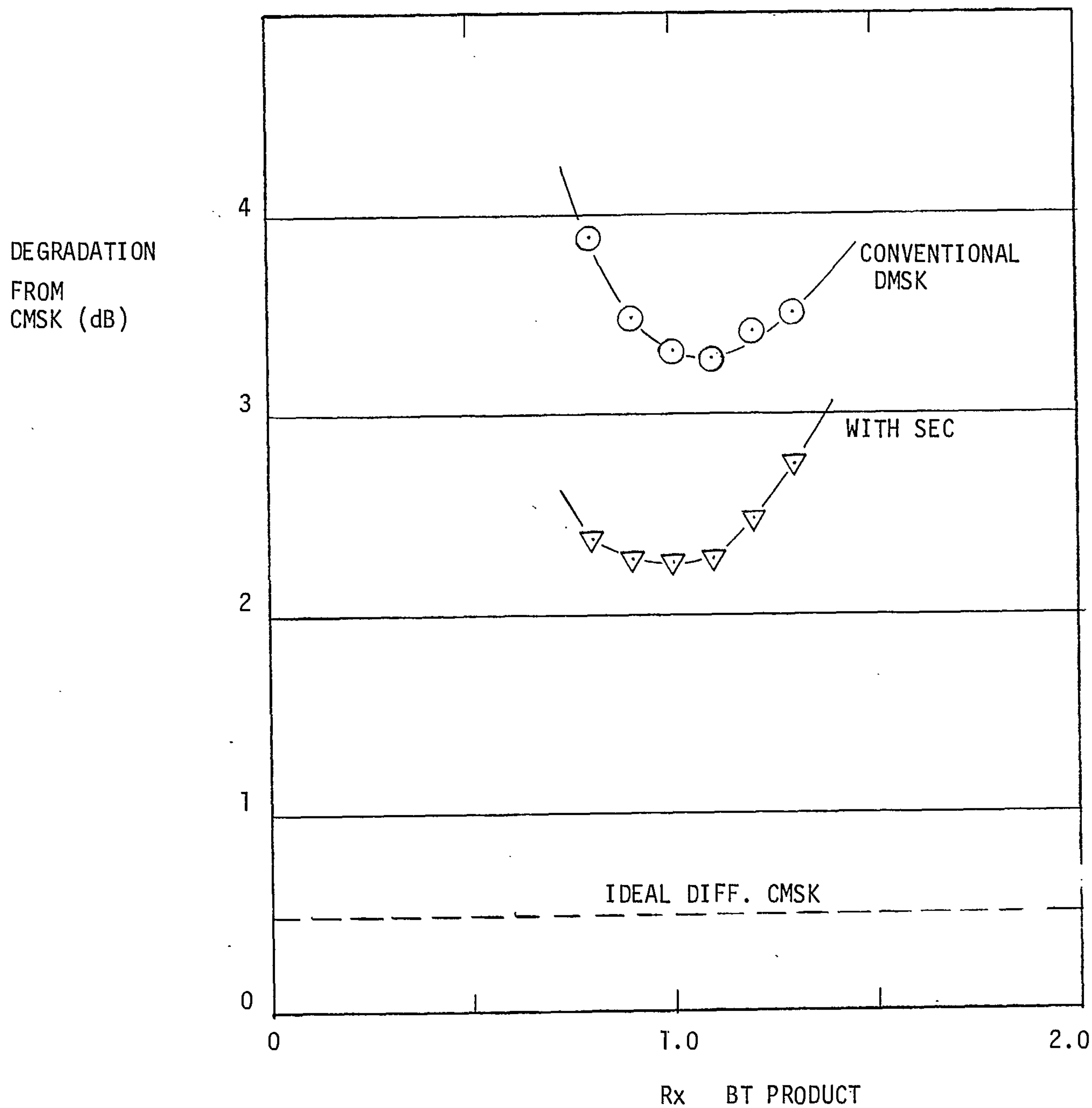

Figure 4.5 Simulated DMSK With:

Rx = 2nd Order Butterworth Equalized
$P_e = 5\times10^{-4}$

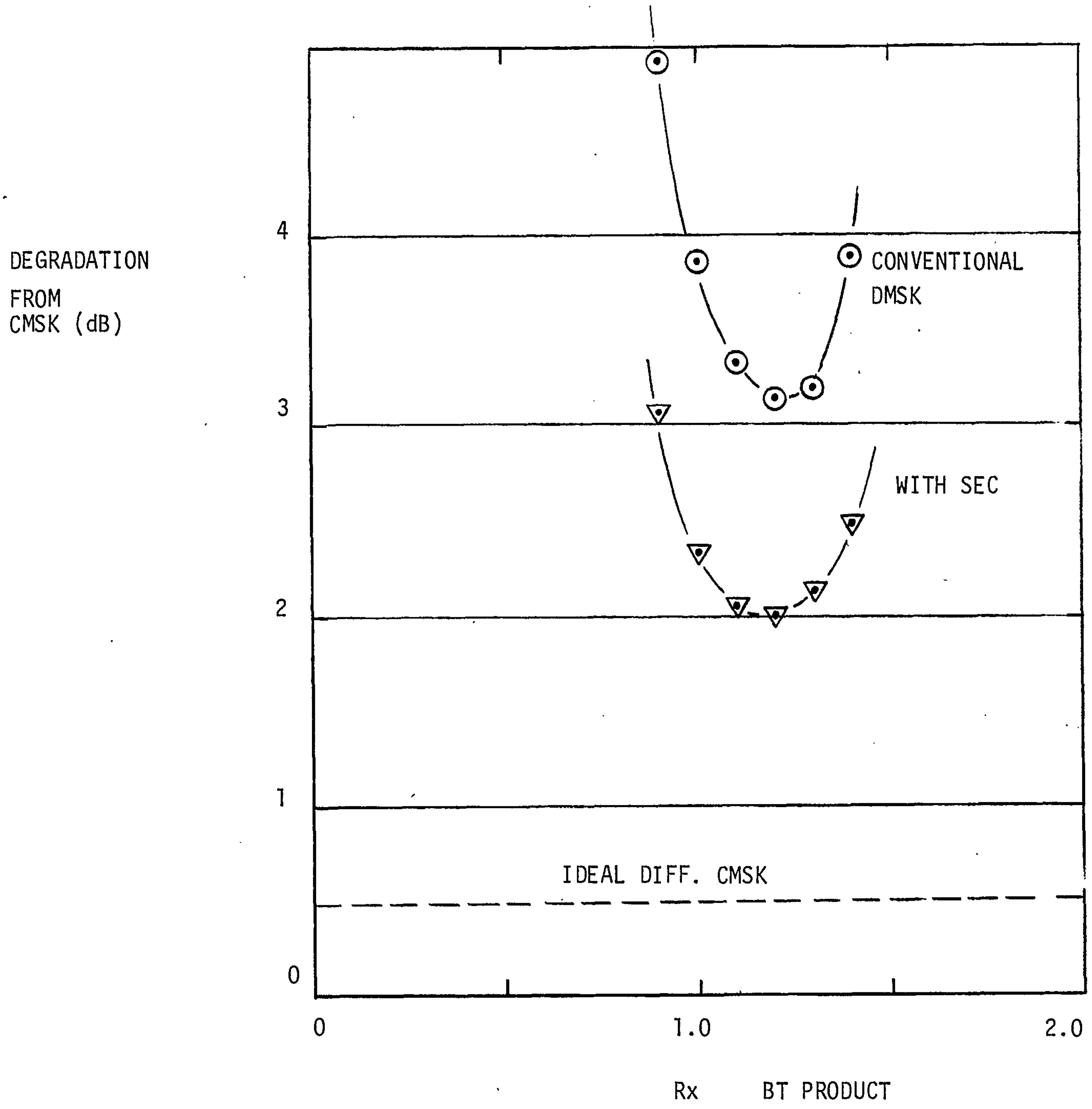

Figure 4.6 Simulated DMSK with:
Rx = 4th Order Butterworth
$P_e = 5x10^{-4}$

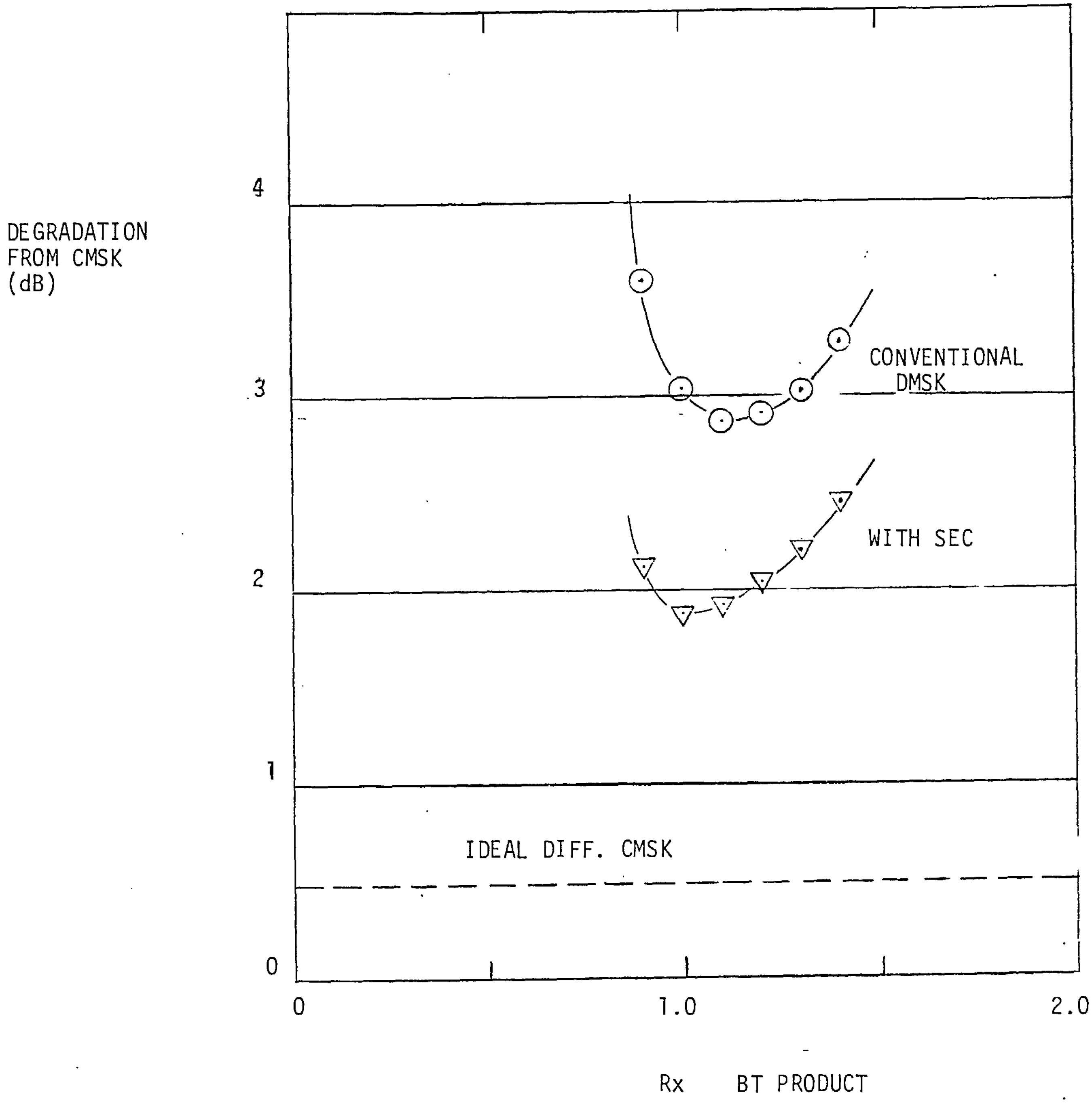

Figure 4.7 Simulated DMSK With:
Rx = 4th Order Butterworth Equalized
$P_e = 5x10^{-4}$

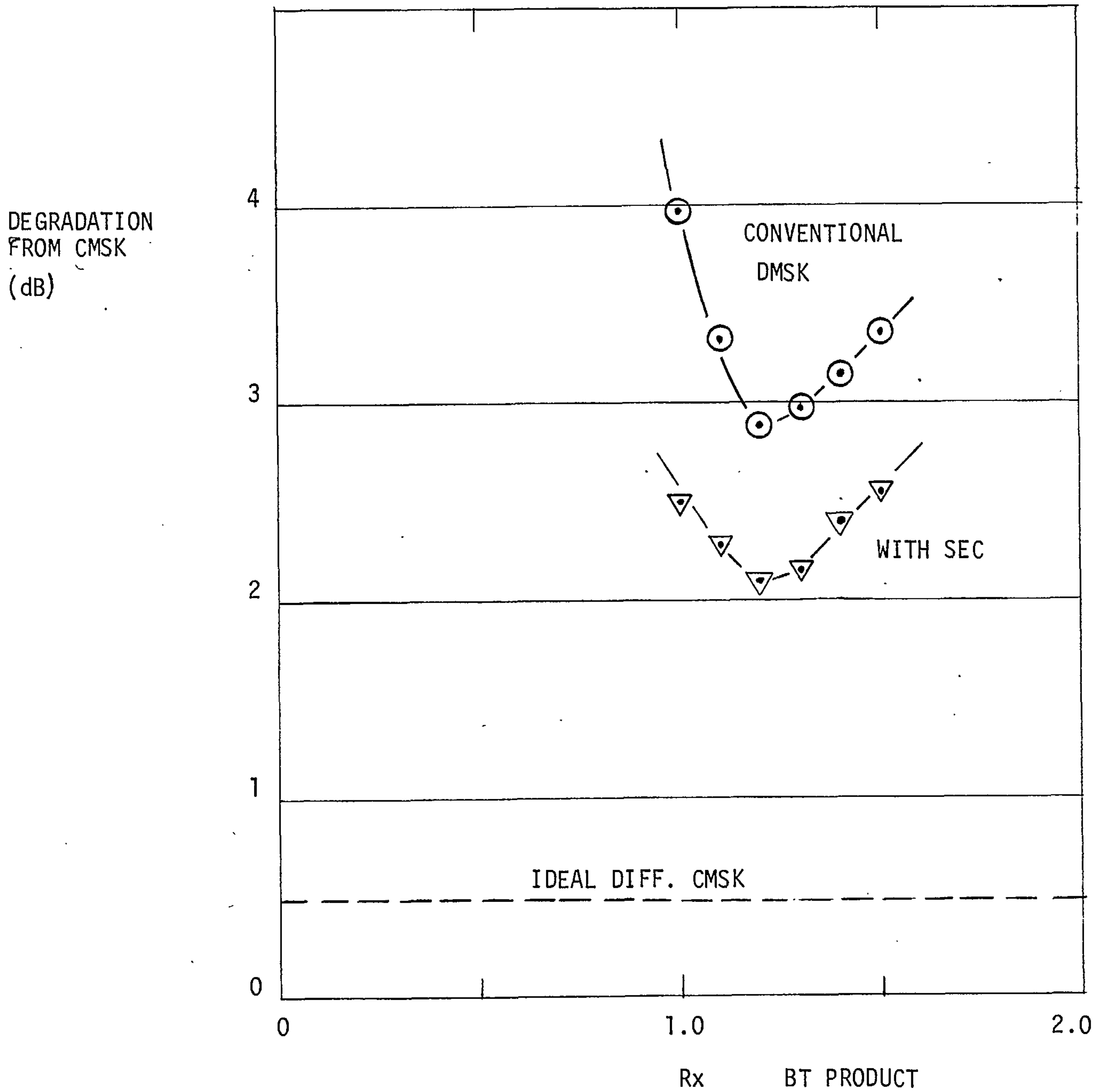

Figure 4.8 Simulated DMSK With:
Rx = Ideal Band-Pass Filter
$P_e = 5x10^{-4}$

FILTER TYPE	CONVENTIONAL DMSK		WITH SEC	
	OPTIMUM BT PROD.	DEG FROM CMSK (dB)	OPTIMUM BT PROD.	DEG. FROM CMSK (dB)
1. GAUSSIAN	1.0	3.35	0.85	2.20
2. BW 2	1.15	3.40	0.90	2.35
3. BW 2 EQU.	1.10	3.30	1.00	2.25
4. BW 4	1.20	3.15	1.20	2.00
5. BW 4 EQU.	1.10	2.90	1.00	1.90
6. IDEAL BANDPASS	1.20	2.90	1.20	2.10

NOTE: The computed theoretical standard deviation on all degradations is approximately 0.15 dB.

Table 4.2 Optimum BT Product and Corresponding Degradations from Ideal coherent MSK (BER = 5×10^{-4})

4.2.2 Post-Demodulation Filter

For the best receive (Rx) filter found in the previous section, an attempt was made to improve performance by adding a post-demodulation (DEM) filter. In the previous analysis a DEM filter was required, but was assumed to remove only unwanted signal harmonics without distorting the baseband spectrum. Of the Rx filters analysed the one exhibiting the best performance was a 4-th order Butterworth with ideal linear phase response (i.e. phase equalized) and having a BT product of approximately 1.1, where B is the 3 dB bandwidth and T is the bit period equal to the reciprocal of the data rate.

The DEM filter type was taken to be the same as the Rx filter, leaving the BT product as the variable parameter to be optimized. Results are presented in Figures 4.9 and 4.10. In Figure 4.9 the degradation (in dB) from CMSK is plotted against the BT product of the DEM filter, for both conventional DMSK and with SEC. For both detection schemes it would appear that the degradation is a decreasing function of the BT product. The best performance is thus given by an ideal low pass filter which is assumed to remove only the unwanted harmonics without further distorting the baseband signal. This was the assumption made for the Rx filter analysis, and results are presented for this case as having a DEM BT product of 4.0.

The results shown in Figure 4.10 are similar, the only change being that the Rx filter BT product was 1.2 instead of 1.1.

Based on the above results, the DEM filter was chosen to be an ideal low pass for the remainder of the analysis.

Intermediate plots of degradation versus BER are presented in Appendix A.

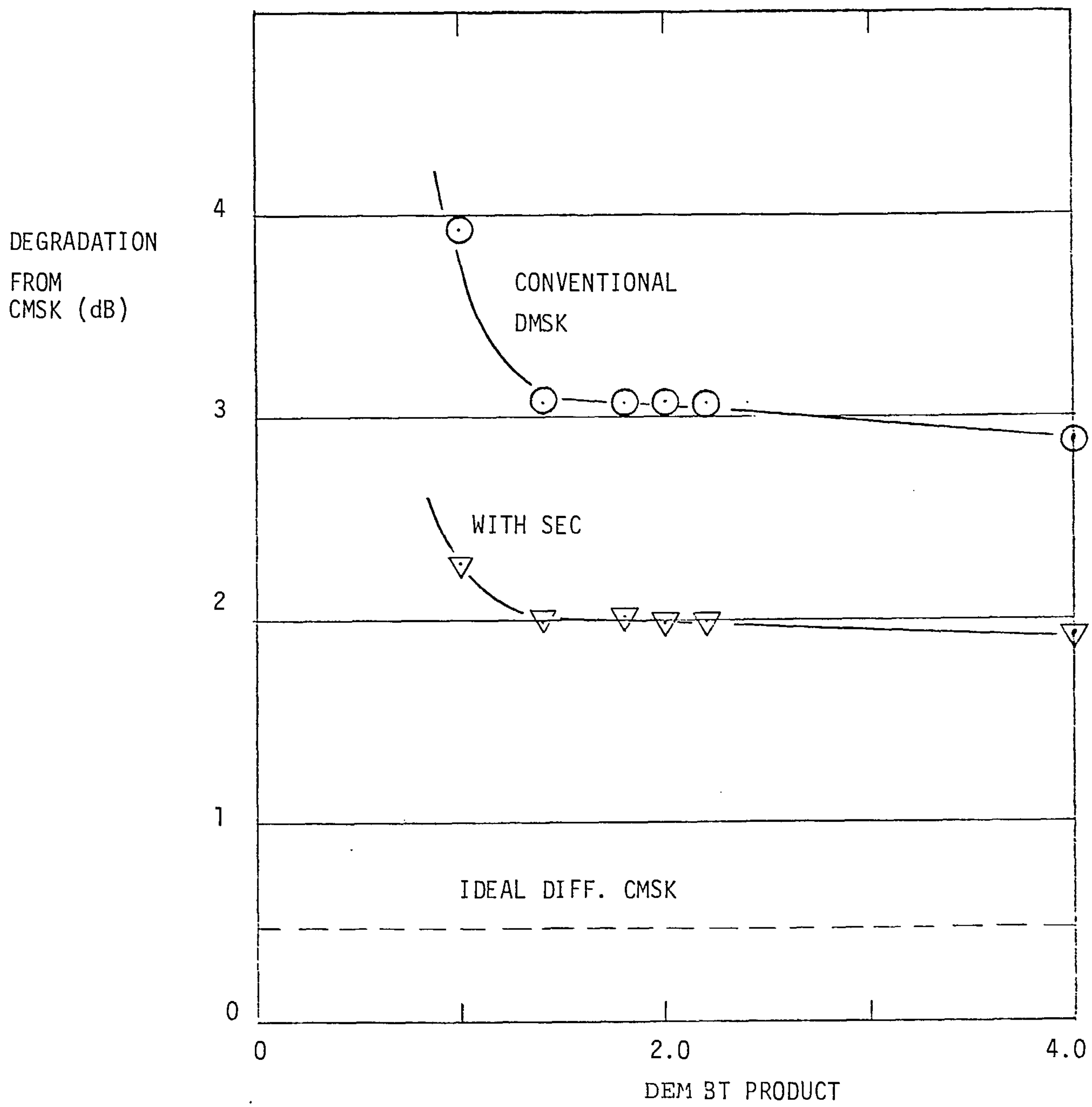

Figure 4.9 Simulated DMSK With:

Rx = 4th Order Butterworth Equ. (BT=1.1)

DEM = 4th Order Butterworth Equ.

$P_e = 5x10^{-4}$

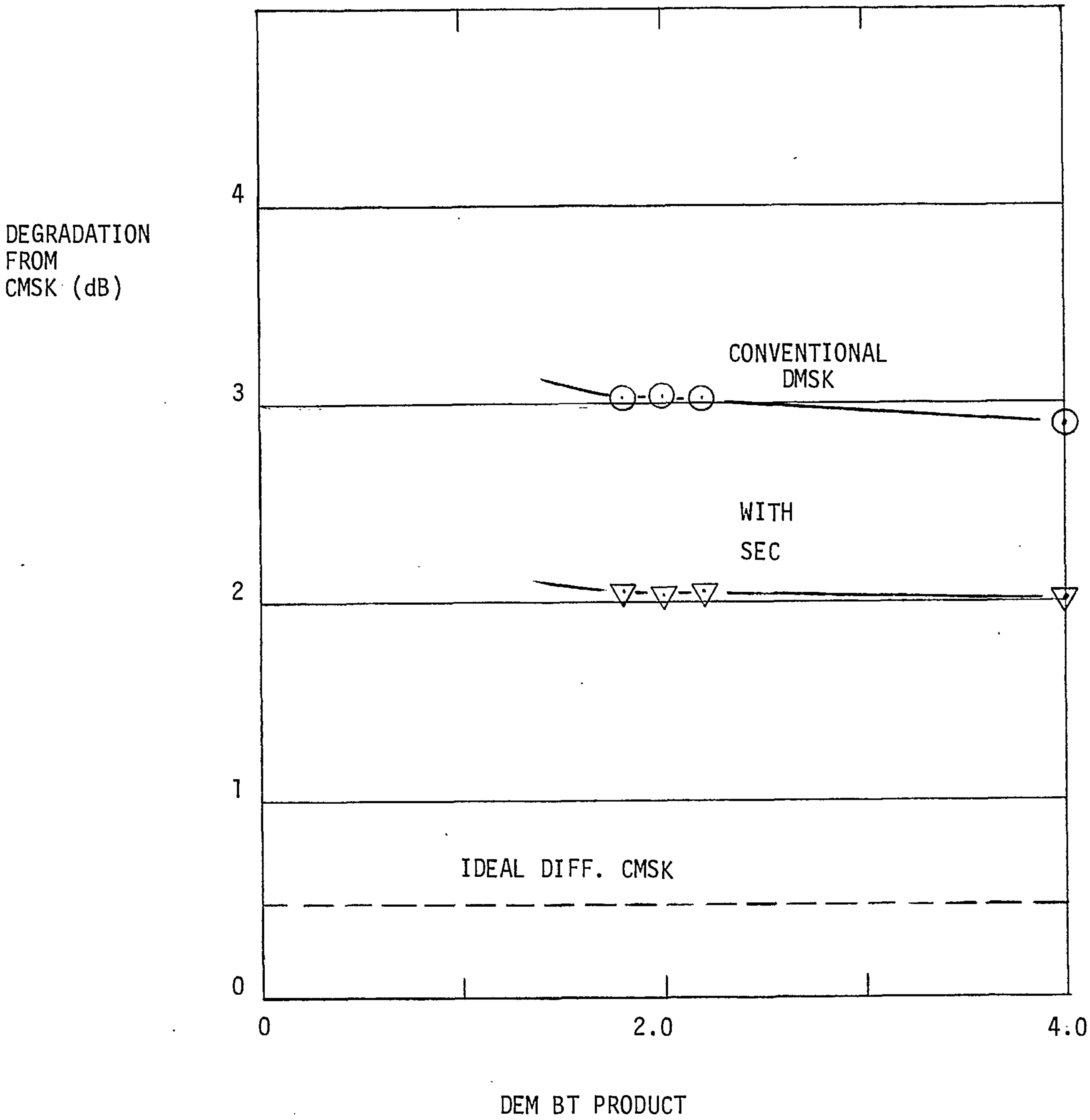

Figure 4.10 Simulated DMSK with:

Rx = 4th Order Butterworth Equ. (BT = 1.2)

DEM =4th Order Butterworth Equ.

$P_e = 5 \times 10^{-4}$

4.2.3 Transmit Filtering

In order to use the available spectrum efficiently, transmit (Tx) filtering must be performed to satisfy transmission bandwidth requirements. Simulated performance is presented in Figure 4.11 for a 4-th order phase-equalized Butterworth Tx filter, which was the same type used at the receiver. In this figure the degradation (in dB) from CMSK is plotted against the BT product of the Tx filter for both conventional DMSK and with SEC, for a bit error rate of 5×10^{-4}. The BT product of the receiver was fixed at 1.1. Performance is expected to be best for an infinite Tx bandwidth as no ISI will be introduced at the transmitter. Of concern then is the additional degradation imposed by a transmit bandwidth constraint. We can see from Figure 4.11 that for a BT product of 1.5 (the width of the signal's mainlobe) the additional degradations are about 0.3 and 0.25 dB for conventional DMSK and with SEC respectively, and for a BT product of 1.0 the respective additional degradations jump to about 2.1 and 1.6 dB. The smaller the BT product the greater the improvement provided by SEC, e.g. the improvement is about 1.0 dB for large BT products but is 1.5 dB for a BT product of 1.0.

Given a transmit bandwidth constraint, no attempt has been made to find the optimum Tx/Rx filter pair.

Intermediate plots of degradation versus BER are presented in Appendix A.

4.3 Best BER Performance

The best BER performance attained with the DMSK simulation is shown in Figure 4.12, and was obtained using a phase-equalized 4-th order Butterworth receive filter and ideal

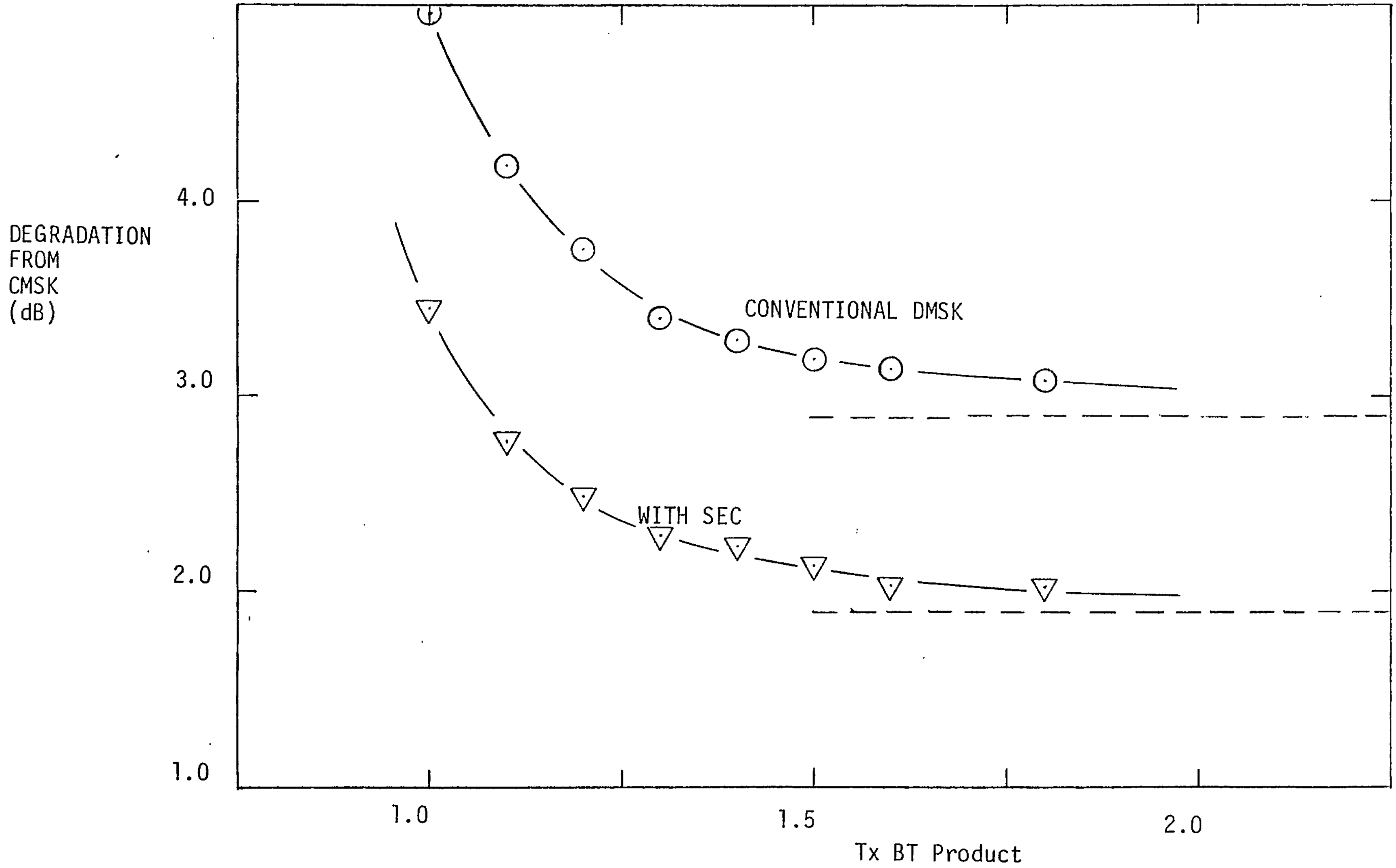

Figure 4.11 Simulated DMSK With:
Rx = 4-th order Butterworth Equ. (BT=1.1)
Tx = 4-th Order Butterworth Equ.
$P_e = 5\times10^{-4}$

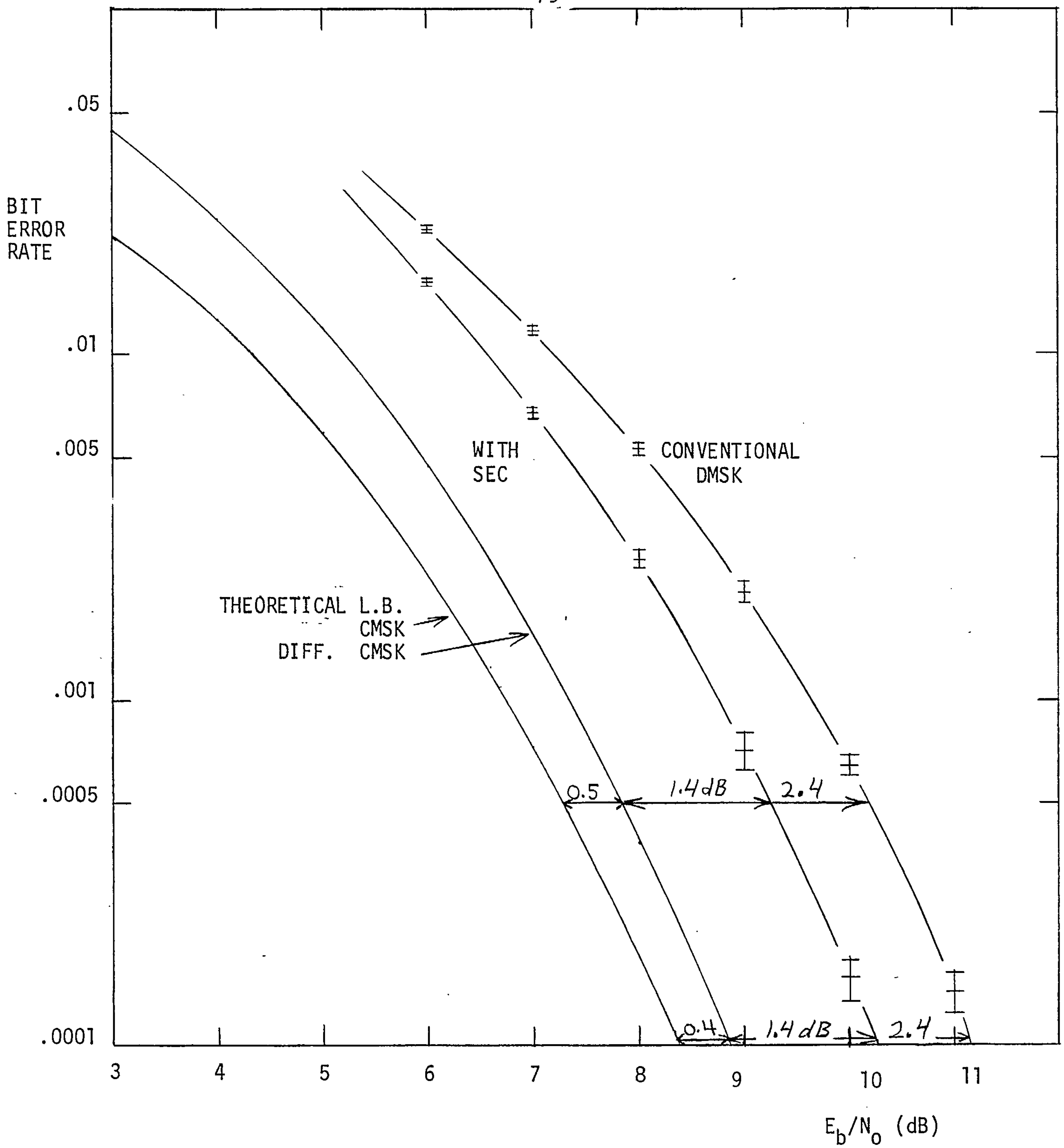

Figure 4.12 Simulated DMSK With:

Tx = Ideal Low Pass Filter (BT = 4.0)
Rx = 4th Order Butterworth Equalized (BT=1.1)
DEM = Ideal Low Pass Filter (BT=4.0)

transmit and post-demod filters. Degradations from differential CMSK of 2.4 dB and 1.4 dB are exhibited for conventional DMSK and with SEC respectively for BER's of $5\text{x}10^{-4}$ and $1\text{x}10^{-4}$. Degradations are expected to steadily increase for smaller BER's, due to the ISI.

4.4 Sensitivity Evaluation

Using the best resulting filter combination, Sections 4.4.1 to 4.4.7 present the sensitivity analysis for the following receiver parameters:

(a) bit timing,

(b) delay elements,

(c) threshold level,

(d) phase shift, and

(e) carrier frequency

(f) non-constant group delay

Appendix B contains intermediate plots of degradation versus BER used in obtaining the results presented.

4.4.1 Bit Timing Errors

Plotted in Figure 4.13 is the degradation (in dB) from CMSK versus bit timing error, for both conventional DMSK and with SEC. The timing error was set to the same value in both branches of the detector when SEC was used. For a timing phase error of 10% the additional degradations from the no-error cases are seen to be approximately 0.7 and 0.5 dB respectively. Additional degradations for a timing

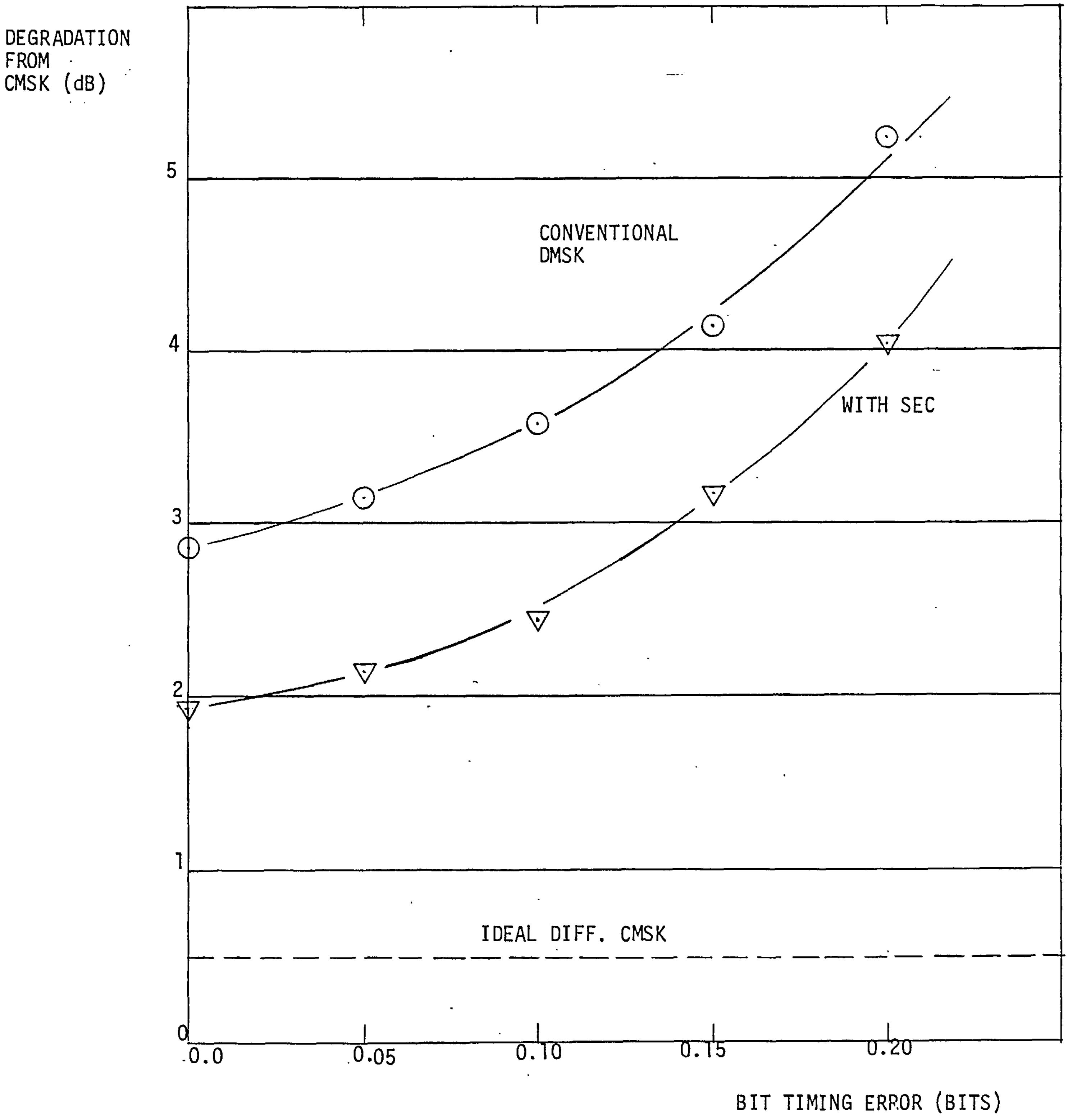

Figure 4.13 Simulated DMSK With Bit Timing Errors:
Rx = 4th Order Butterworth Equalized (BT=1.1)
$P_e = 5x10^{-4}$

error of 20% are greater than 2 dB. The SEC scheme exhibits a fairly consistant 1.0 dB improvement for the range of timing errors analysed.

Applying the same bit timing phase error to both branches is thought to be realistic since typically only one bit timing recovery circuit would be included, from which both branches would draw their timing reference.

4.4.2 Threshold Errors

Decisions are based on the output from the post-demod (DEM) filter using a threshold device. The output of the threshold device is given by

$$\begin{aligned} d &= 1, \quad \text{if input} > \alpha \\ &= -1, \quad \text{if input} < \alpha \end{aligned} \qquad (4.2)$$

where d is the decision and α is the threshold level. If the input signal does not contain a dc offset, then the optimum threshold level is $\alpha=0$ (assuming no attempt is made to compensate for known ISI). The degradation from CMSK for a number of non-zero threshold levels is presented in Figure 4.14. The degradation is in dB and the threshold level is given as a fraction of the no-ISI signal amplitude at the correct sampling time.

The same threshold level is applied to both the conventional and parity bit branches of the detector. For a threshold level of $\alpha = 0.10$, Figure 4.14 shows an additional degradation over the zero threshold case of approximately 0.4 dB and 0.2 dB for the conventional and SEC schemes respectively. For higher thresholds the degradation is seen to increase more rapidly. The

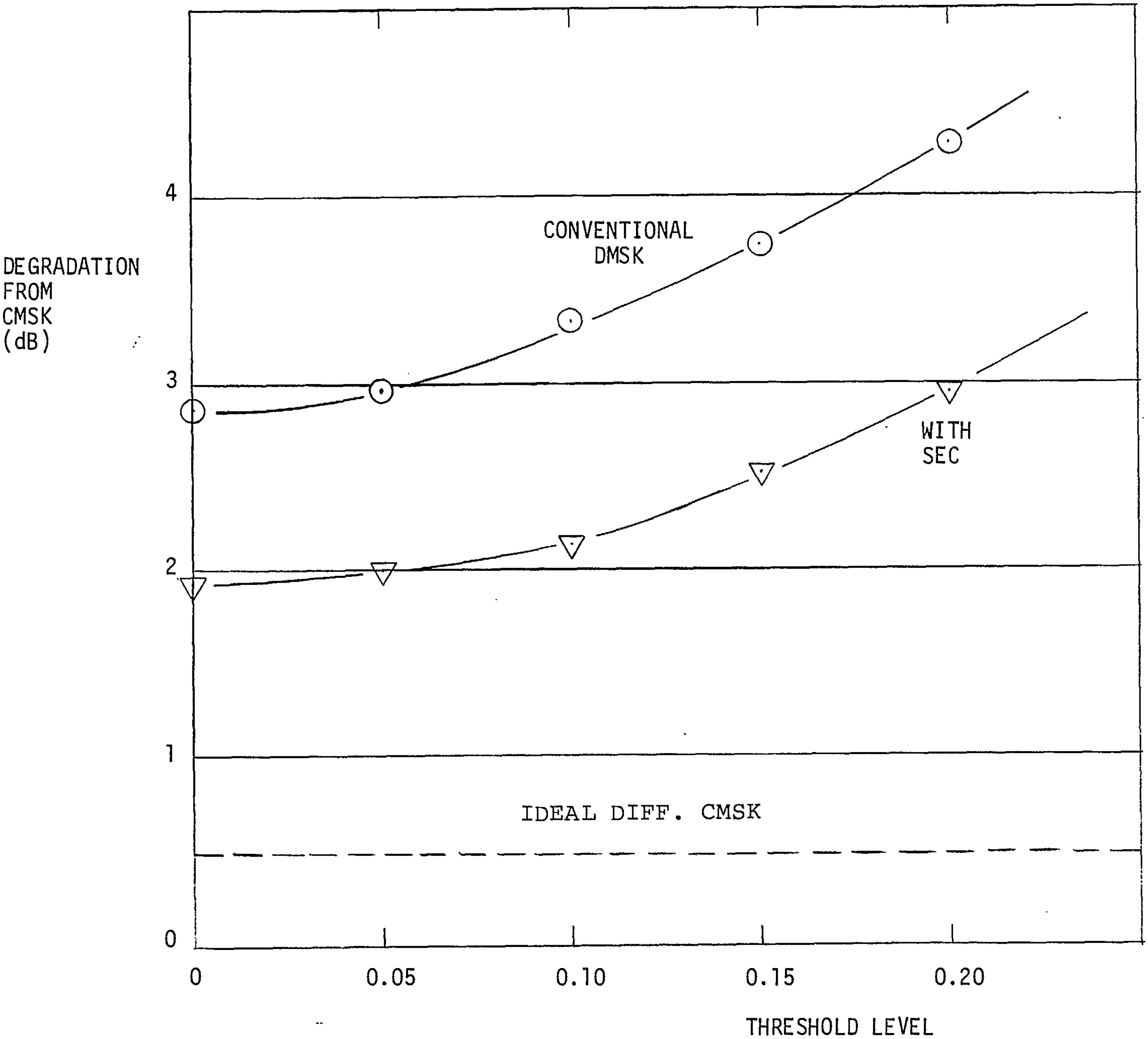

Figure 4.14 Simulated DMSK With Threshold Errors:
Rx = 4th Order Butterworth Equ. (BT = 1.1)
Pe = 5×10^{-4}

improvement exhibited by the SEC scheme over the conventional scheme is also seen to increase slightly as the threshold level increases. The SEC improvement is observed to be approximately 1.3 dB for a threshold of α = 0.20, as compared to the 1.0 dB improvement exhibited for the correct zero threshold level.

4.4.3 Delay Errors

Figure 4.15 displays the degradation (in dB) from CMSK versus errors in the delay elements of the detector. The delay errors are expressed as a percent of the correct delays required, i.e. a 0.1% delay error corresponds to a 0.001 bit period delay error in the delay element of the conventional branch, and a .002 bit period delay error in the delay element of the parity branch used for SEC. This is probably a realistic relationship between the two delay elements if for example the error is a function of device temperature.

Since a bit timing error on the order of 1% introduces a very small degradation, the possible effects due to delay errors of 1% or less on bit timing can be neglected. Thus the major source of degradation is caused by the $\omega_c T$ product not being a multiple of 2π. As in the simulation, for a carrier frequency f_c of 70 MHz and a bit rate R of 5 Mbps, the $\omega_c T$ product modulo 2π is given by

$$\theta = 2\pi \times 14 \times E \qquad (4.3)$$

where E is the error in the delay element in units of bit periods. When E=0 the above product is zero as desired. The sensitivity due to a delay error is easily seen to be a function of the f_c/R ratio which is 14 in this case. As an example, a 0.1% delay error corresponds to a phase error of approximately 5° in the conventional branch and 10° in the

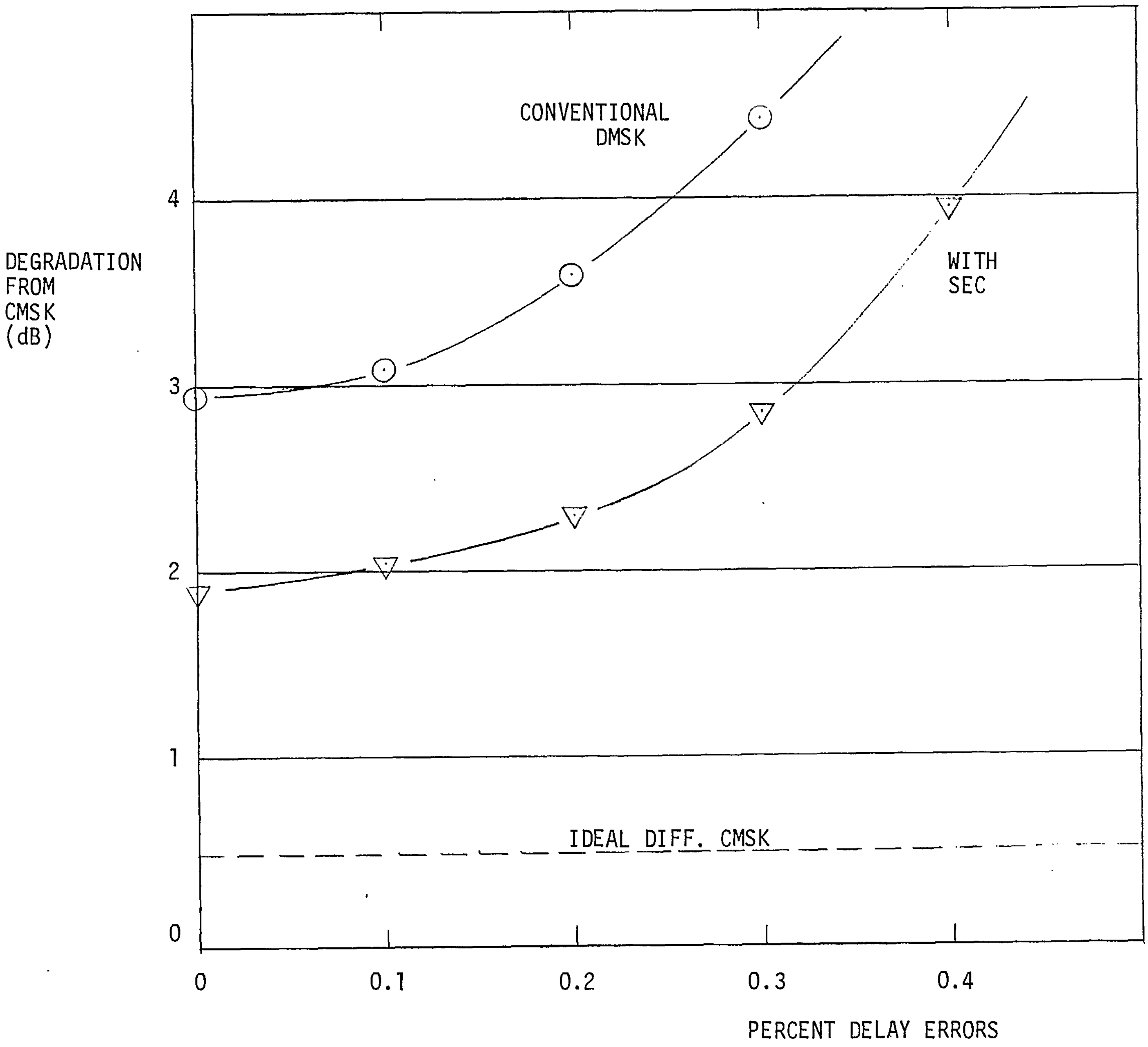

Figure 4.15 Simulated DMSK With Delay Errors:
Rx = 4th Order Butterworth Equalized (B·T = 1.1)
fc = 70 MHz
R = 5 Mbps
Pe = 5×10^{-4}

parity bit branch. The sensitivity of the detector to delay errors could be reduced by reducing the f_c/R ratio.

From Figure 4.15, a 0.2% delay error in both branches yields additional degradations over the no-error case of 0.7 and 0.4 dB for the conventional DMSK and with SEC respectively.

The demodulator should include a constant phase adjust to ensure the resultant phase is zero, thus eliminating the above delay error problem.

4.4.4 Phase Shift Errors

In the conventional DMSK branch of the receiver a 90° phase shifter is required. Figure 4.16 shows the degradation (in dB) from CMSK versus the phase shift error (in degrees). The conventional DMSK branch performs as expected, with performance degrading fairly quickly with increased phase shift error. For a phase shift error of 20° the additional degradation from the no-phase error case is seen to be greater than 2 dB. When SEC is included, performance is seen to be amazingly insensitive to phase errors even as large as 20°. At first glance this result seems counter intuitive, as the SEC must use the conventional decisions as well as the parity bits (which do not suffer from a phase shift error in the conventional branch). It would appear that most additional errors, caused by a moderate phase shift error in the conventional branch, are isolated errors and that the SEC circuit has little difficulty correcting them. The number of single error correction attempts (syndrome error counter) indicated by the program reinforces the above conclusion. It is observed that the SEC circuit exhibits approximately a 3 dB improvement with a 20° phase shift error in the conventional branch, at a BER of 5×10^{-4}.

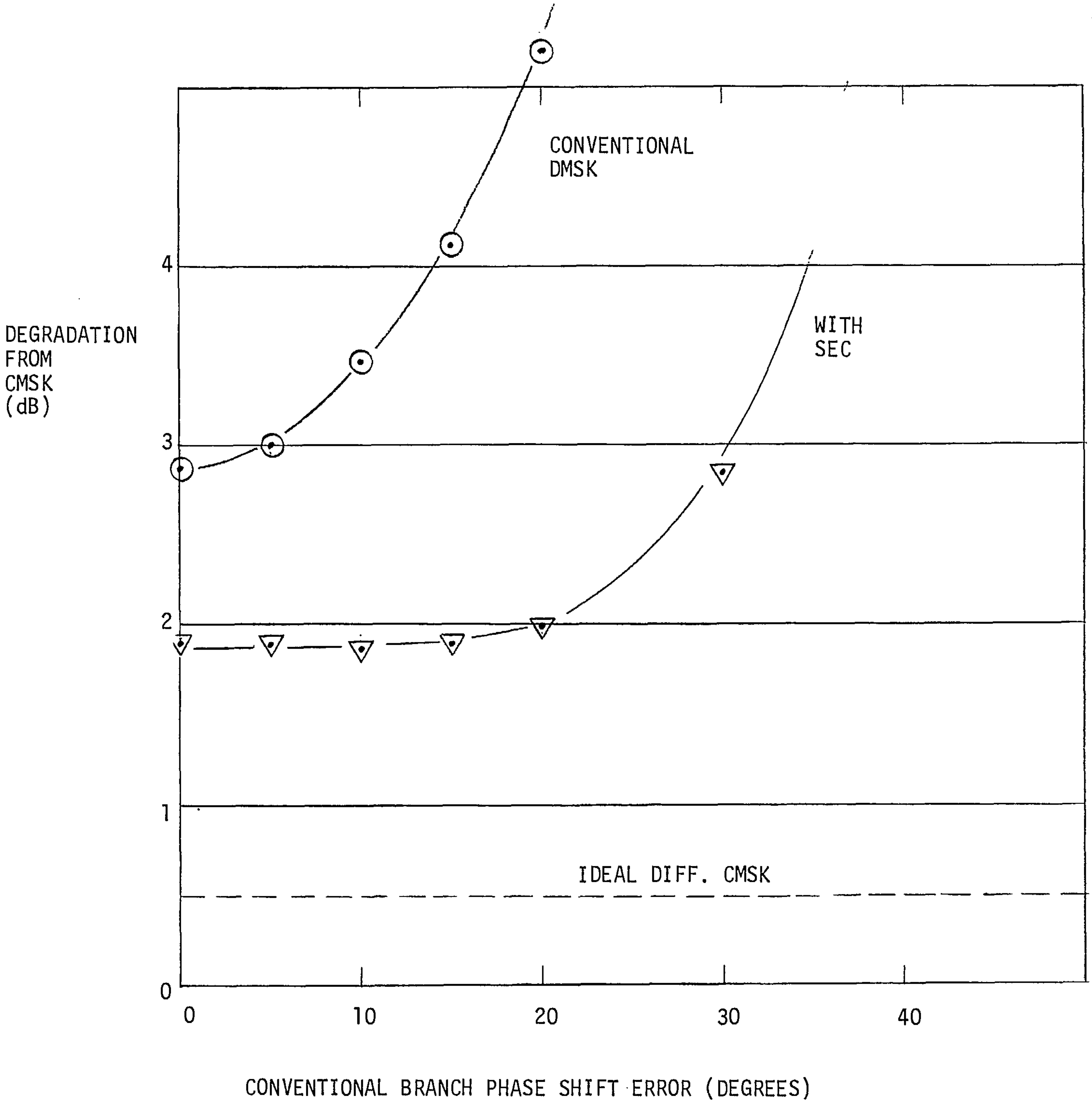

Figure 4.16 Simulated DMSK With Phase Shift Error:
Rx = 4th Order Butterworth Equ. (BT = 1.1)
Pe = 5×10^{-4}

It should be noted that if a 20° phase error did exist in the conventional branch, then the likelihood of no phase error in the parity bit branch is very small. Thus the above situation is not expected to occur often. Figure 4.16 does however give a good illustration of the SEC circuit's ability to correct single errors.

4.4.5 Carrier Frequency Offset

The desired signal amplitude and amount of quadrature interference is a strong function of the $\omega_c T$ product, where $\omega_c = 2\pi f_c$ is the carrier frequency and $T = 1/R$ is the bit period. Optimum values of $\omega_c T$ are integer multiples of 2π (π, if one is not bothered by factors of -1). Equivalently the ratio f_c/R should be an integer. Figure 4.17 shows the degradation (in dB) from CMSK versus the fractional portion of the f_c/R ratio, or equivalently the carrier frequency (in MHz) assuming a bit rate of R = 5 Mbps and a nominal carrier frequency of f_c = 70 MHz. The Rx filter is assumed to be centred at 70 MHz. Thus a carrier frequency offset also causes non-symmetric Rx filtering.

For the fractional portion of $f_c/R = 0.04$ the additional degradations from the no-frequency offset case are seen to be approximately 1.5 and 0.8 dB for conventional DMSK and with SEC respectively. The SEC performance is seen to be much more sensitive to a frequency offset error than to the phase shift errors of the previous section. This is expected, since the parity bit branch of the receiver is twice as sensitive to a frequency error as is the conventional branch, due to the 2T delay element required by the parity bit branch. In fact, if the fractional portion of the f_c/R ratio was 1/8 (corresponding to a 90°

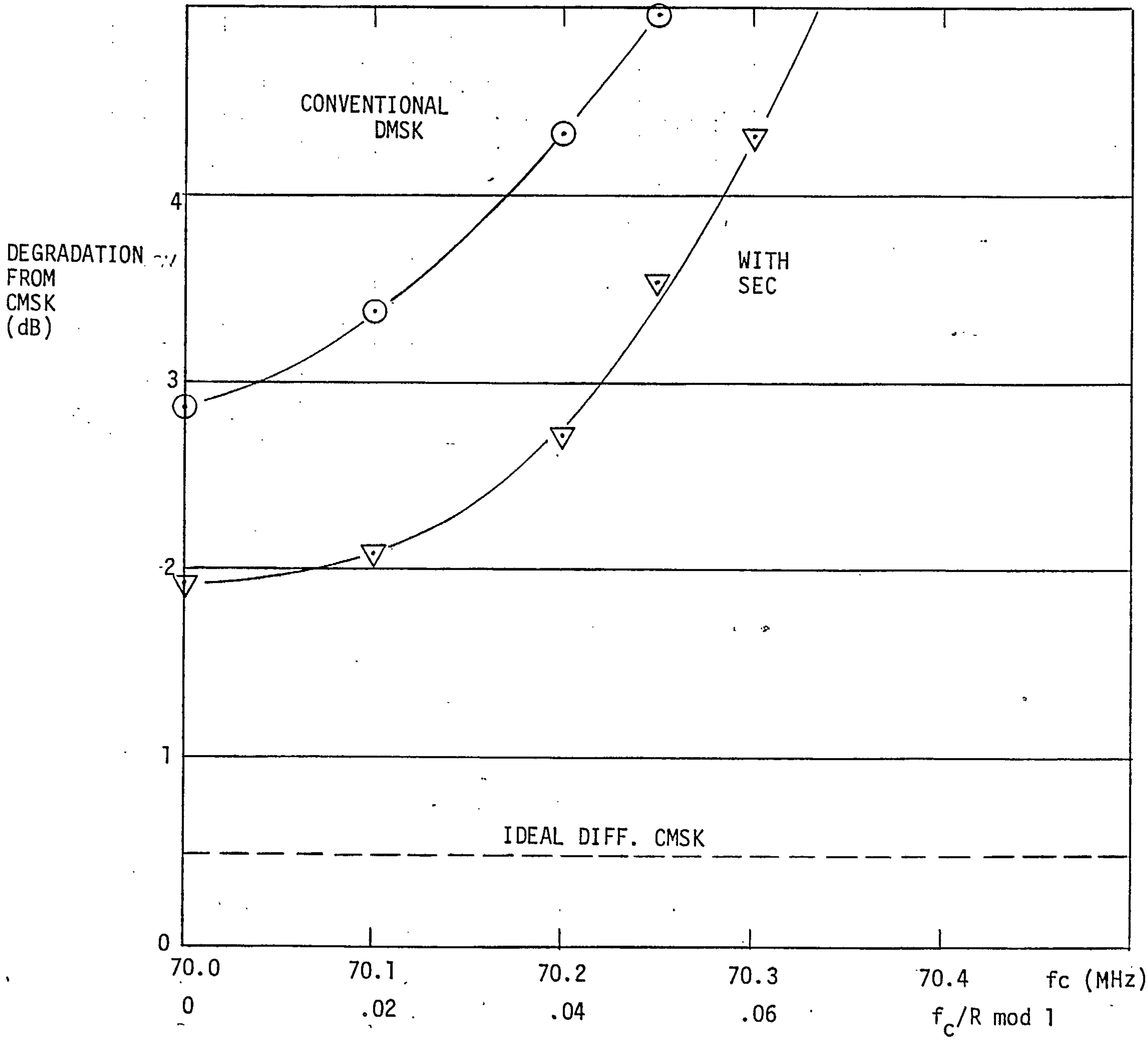

Figure 4.17 Simulated DMSK With Carrier Frequency Offset:
Rx = 4th Order Butterworth Equ. (BT = 1.1)
Pe = 5×10^{-4}

phase shift in the parity bit branch of the receiver) then the generated parity bits would be completely erroneous and likewise the output decisions from the SEC. The conventional DMSK branch does not completely degenerate until a ratio of 1/4 is reached.

For the nominal carrier frequency and bit rate stated above, frequency offsets on the order of 50 kHz (±.07%) will result in degradations on the order of only 0.1 dB

4.4.6 Non-Constant Group Delay

For the purposes of our investigation we have assumed the group delay for the conventional branch to be given by (see Section 3.11)

$$D(f) = T + AfT^2 \tag{4.4}$$

where the frequency, f, and parameter, A, are normalized against the bit rate, $R = 1/T$, so that the degradation resulting from a given value of A is not dependent on the data rate. The group delay is assumed to be 2D(f) for the parity bit branch, i.e. we have assumed the use of 2 cascaded T-delay elements.

Of interest is the phase error at f=R which is given by

$$\begin{aligned} \phi_e(f{=}R) &= -\pi A \text{ radians} \\ &= -180A \text{ degrees} \end{aligned} \tag{4.5}$$

Simulated performance is shown in Figure 4.18. Plotted is the degradation in dB from ideal CMSK versus the group delay parameter A, or the phase error at f=R for the conventional branch. The phase error for the parity bit branch is twice that for the conventional branch. For A=.5 additional degradations of 0.2 and 0.5 dB from the A=0 case are exhibited for conventional DMSK and with SEC respectively. The improvement with SEC is seen to decrease as A gets larger. This is expected because the phase error in the parity branch grows twice as fast as the phase error in the conventional branch with increasing A, under the stated delay relationship between branches.

4.4.7 Combination of Errors

Plotted in Figure 4.19 is the BER versus E_b/N_o (dB) for the following parameter combination:

Rx = 4th order Butterworth equalized (BT = 1.1)

f_c = 70 MHz

R = 5 Mbps

Bit timing errors = 5%

Delay errors (linear phase error) = 0.1%

Threshold levels = 5%

The individual degradations due to the last three error parameters are quite small, and are approximately given by 0.2, 0.15, and 0.1 dB respectively, for both conventional DMSK and with SEC at a BER of 5×10^{-4} (see Figures 4.13, 4.14, and 4.15). Adding these three individual degradations gives an expected total degradation of about 0.45 dB (assuming they are additive).

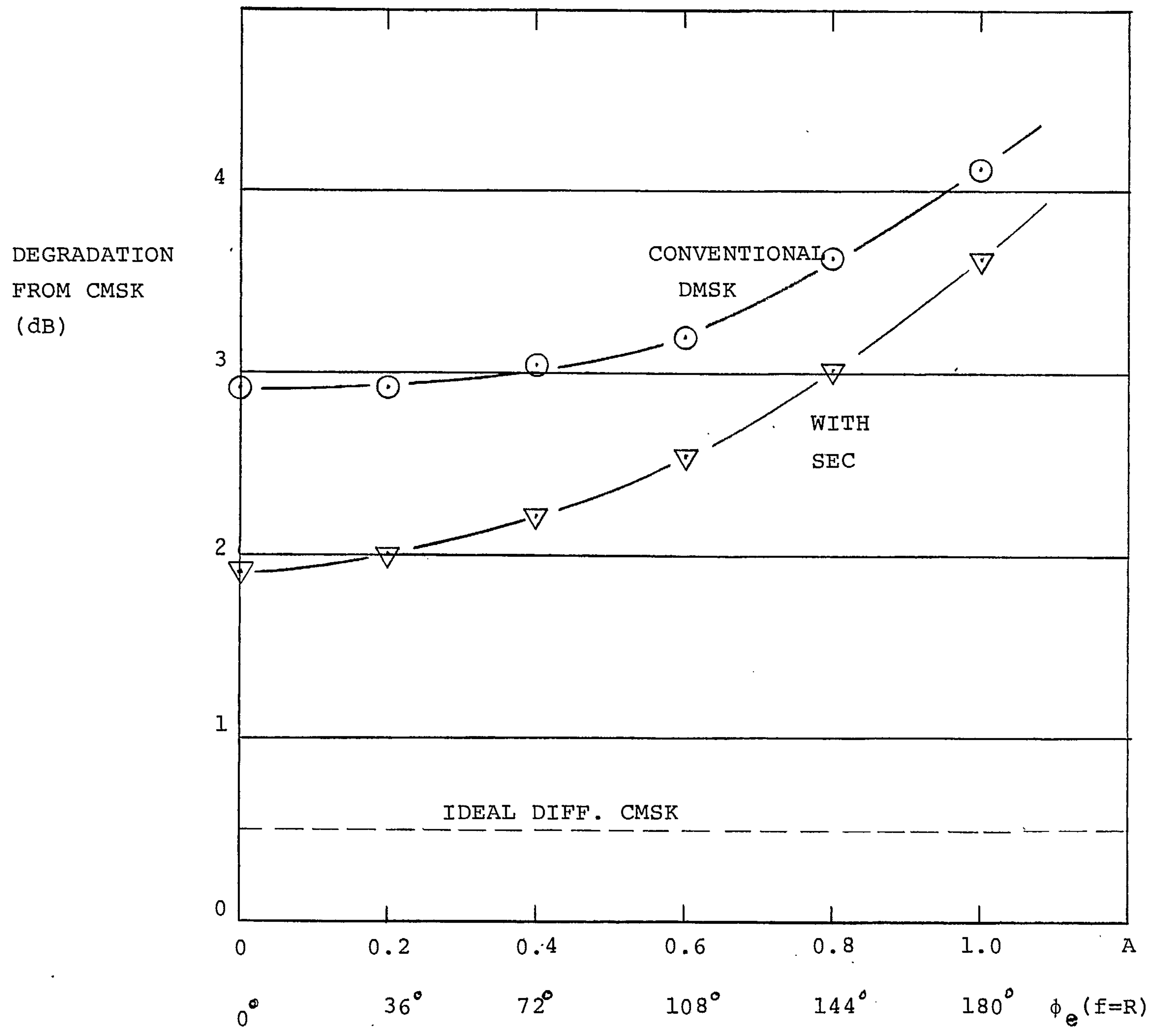

Figure 4.18 Simulated DMSK With Non-Constant Group Delay:

Rx = 4th Order Butterworth Equ. (BT=1.1)
$P_e = 5x10^{-4}$

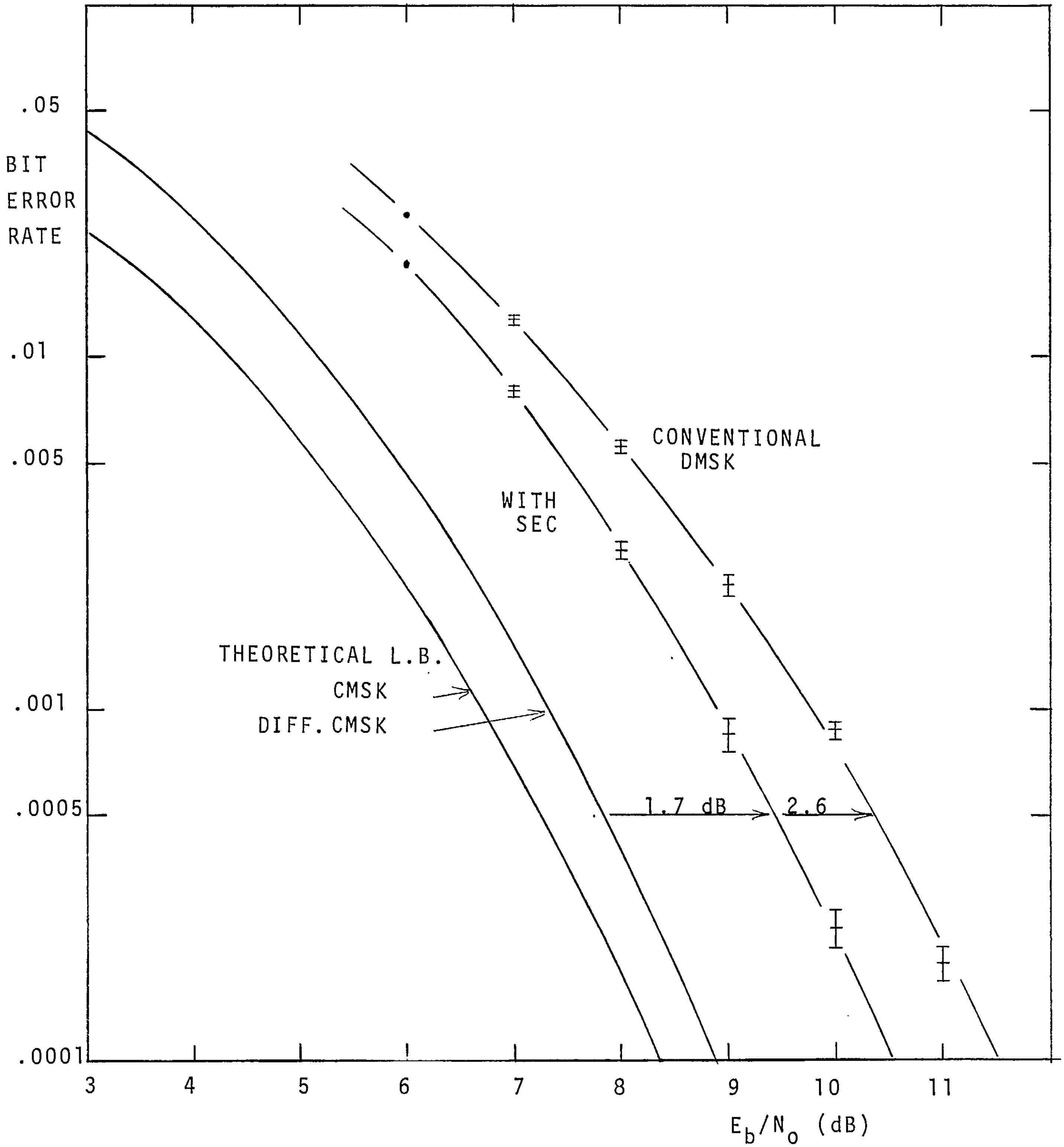

FIGURE 4.19 Simulated DMSK With:
Rx = 4th Order Butterworth Equalized (BT=1.1)
f_c = 70 MHz
Bit Timing Error = 5%
Delay Errors = 0.1%
Threshold Level = 5%

Since degradations from differential CMSK (no ISI) without parameter errors are given by 1.4 and 2.4 dB respectively, we see from Figure 4.19 that the additional degradations, caused by the given combination of error parameters are about 0.3 and 0.2 dB. Thus the performance exhibited for this case is quite good, and indicates that adding individual degradations tends to give pessimistic expectations, which can be used for conservative performance estimation.

4.5 Hard Limiters In The Demodulator

Figure 4.20 shows the possible locations of hard limiters in the receiver structure. A limiter preceding the demodulator performs a form of automatic gain control (AGC). Limiters following the Rx filter could simplify the demodulator. In the results that follow an ideal hard limiter is assumed. Simulated performance has been obtained for the following limiter combinations:

a) #1

b) #3

c) #2, #3, and #4

Obviously combination (c) corresponds to a single hard limiter just after the Rx filter.

The BER performance versus E_b/N_o (dB) is plotted in Figures 4.21, 4.22, and 4.23 for configurations (a), (b), and (c) respectively. In Figure 4.21 we see that for a BER of 5×10^{-4} the degradations from differential CMSK are 3.3 dB and 2.6 dB for conventional DMSK and with SEC respectively. Without any hard limiters the respective degradations are approximately 2.4 dB and 1.4 dB. Thus the resulting degradations due to the hard limiter in front of the receive filter are 0.9 and 1.2 dB respectively.

For configuration (b), Figure 4.22 shows BER performance which is essentially indistinguishable from the best performance obtained without a hard limiter, i.e. degradations of 1.4 dB and 2.4 dB at a BER of 5×10^{-4} are displayed. It is easy to convince oneself that if limiters #2 and #4 were used, instead of #3, that equivalent performance would result. As can be seen from Figure 4.23, using a single hard limiter just after Rx filtering (configuration (c)) did not result in any further degradation.

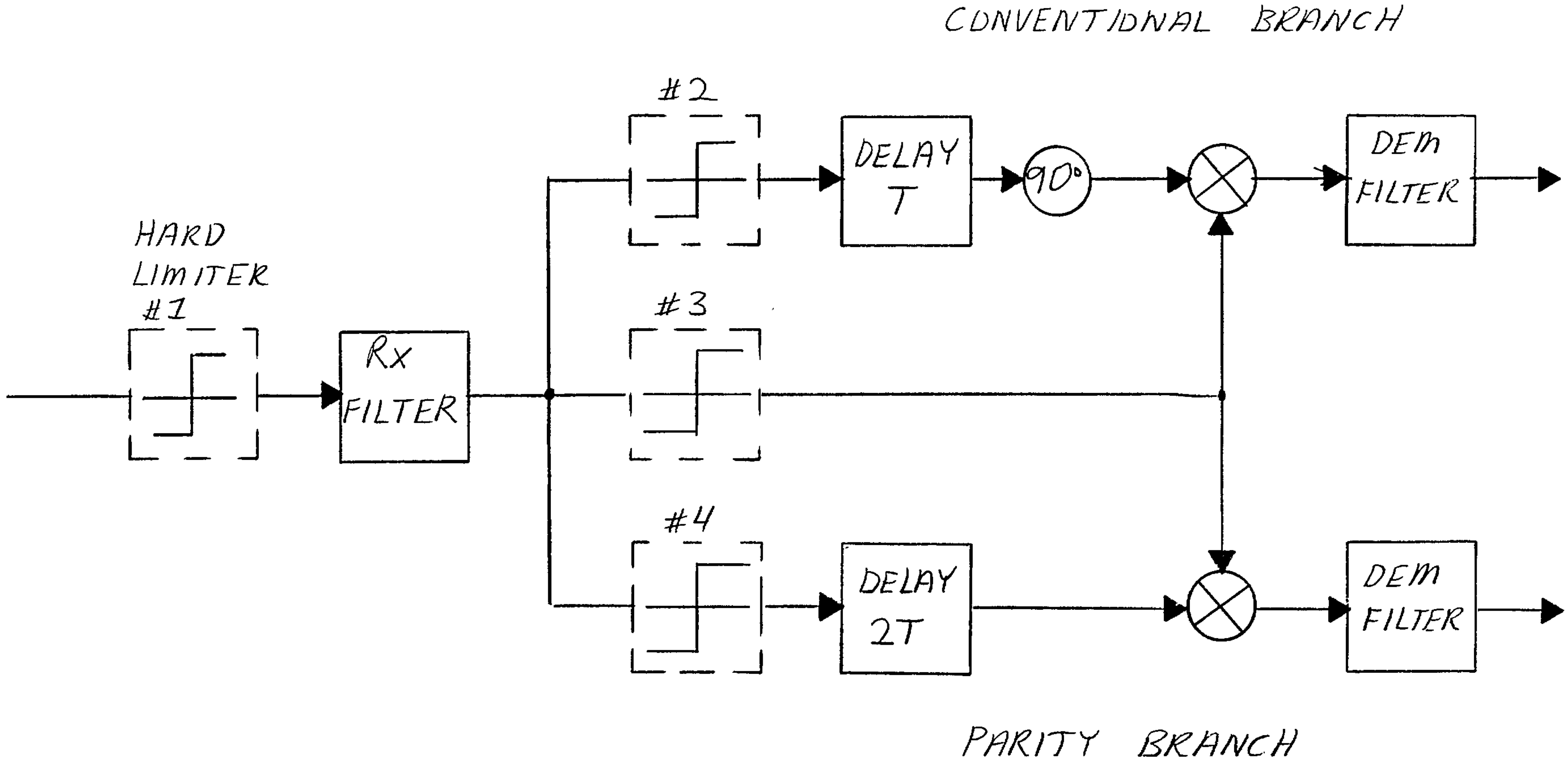

FIGURE 4.20 Possible Location of Hard Limiters In Receiver Structure

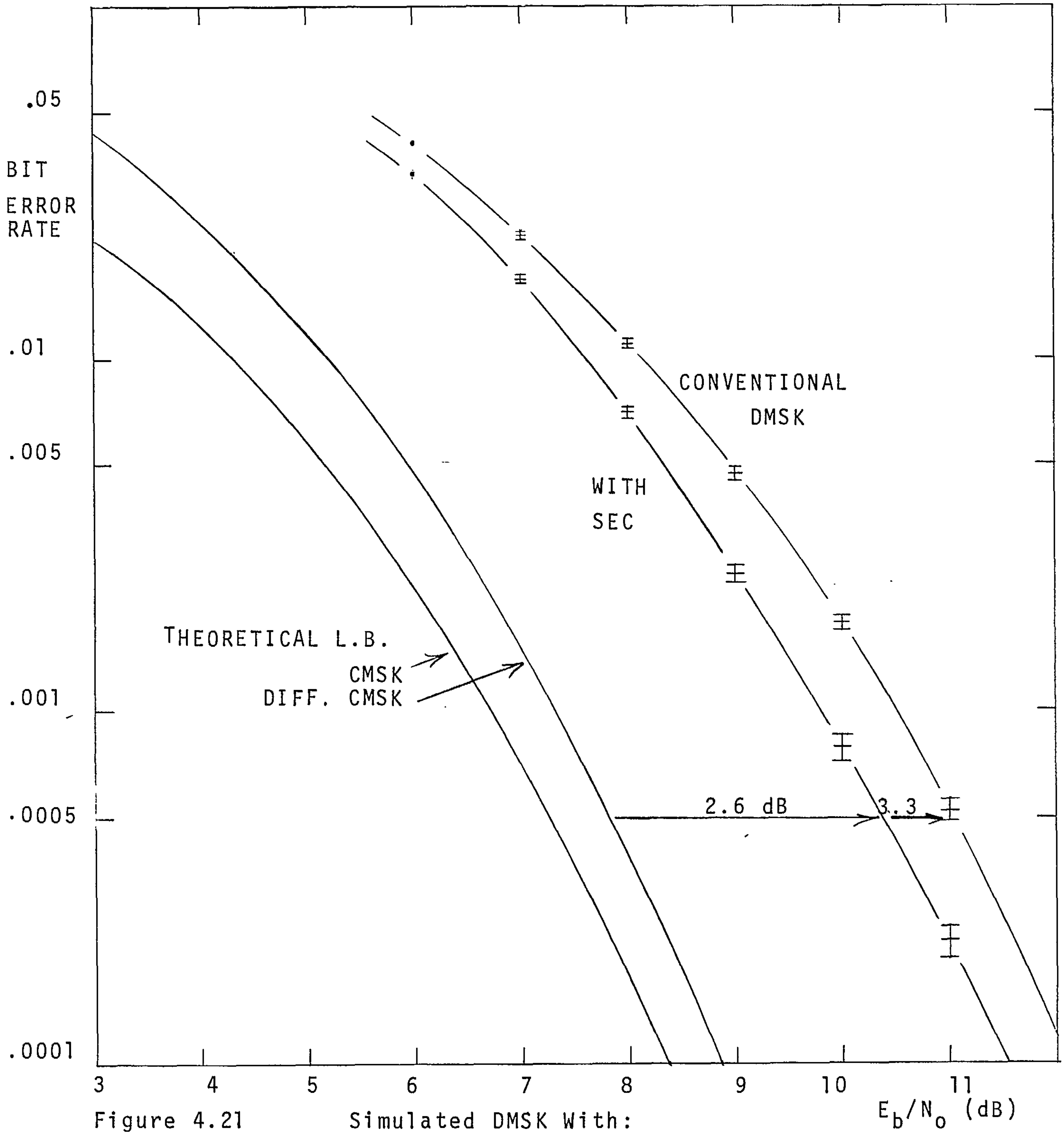

Figure 4.21 Simulated DMSK With:
Rx = 4-th Order Butterworth Equ. (BT =1.1)
Hard Limiter Prior to Rx Filter

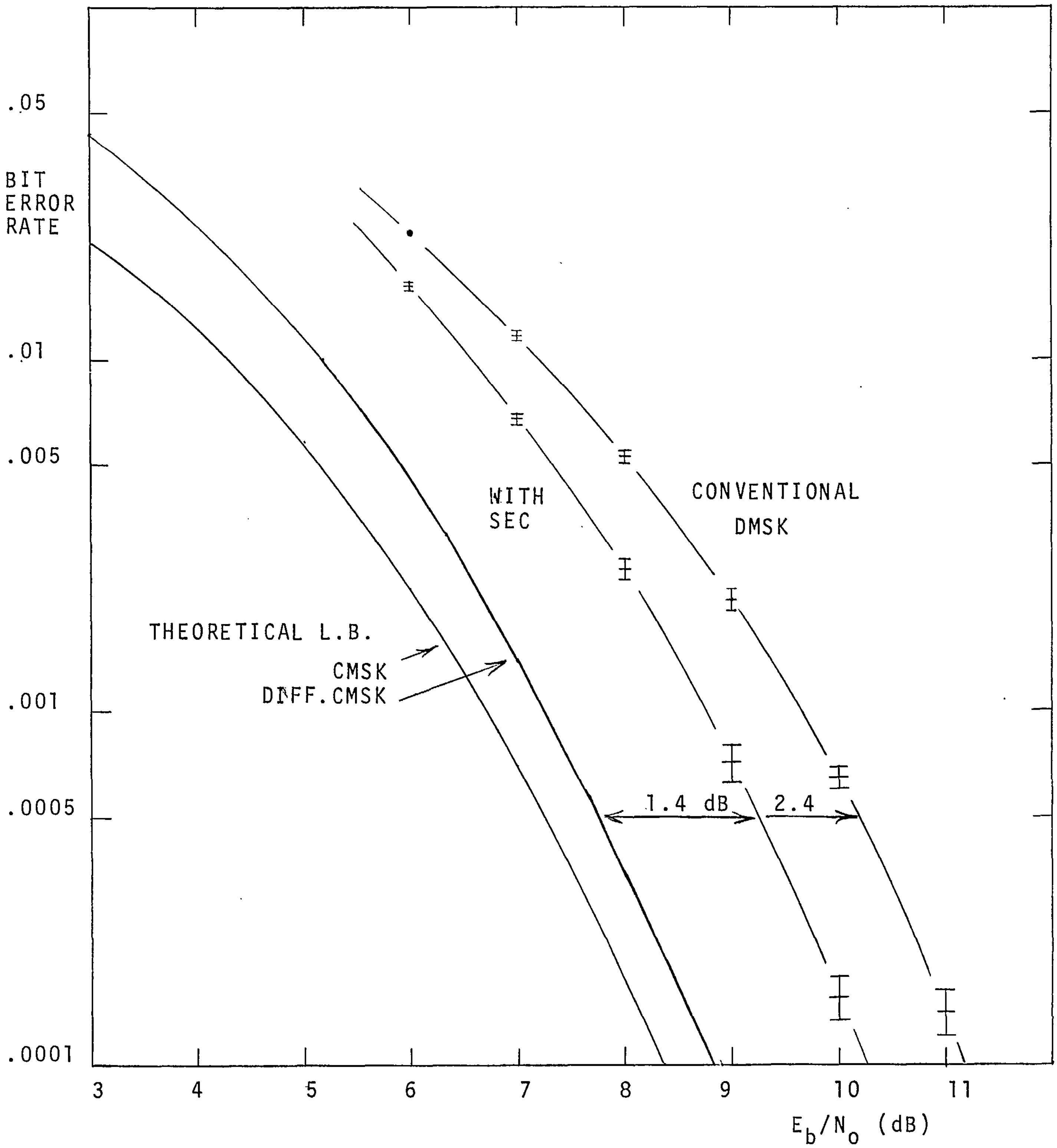

Figure 4.22 Simulated DMSK With:
Rx = 4-th Order Butterworth Equ. (BT=1.1),
Hard Limiter In Non-Delayed Branch of Demodulator

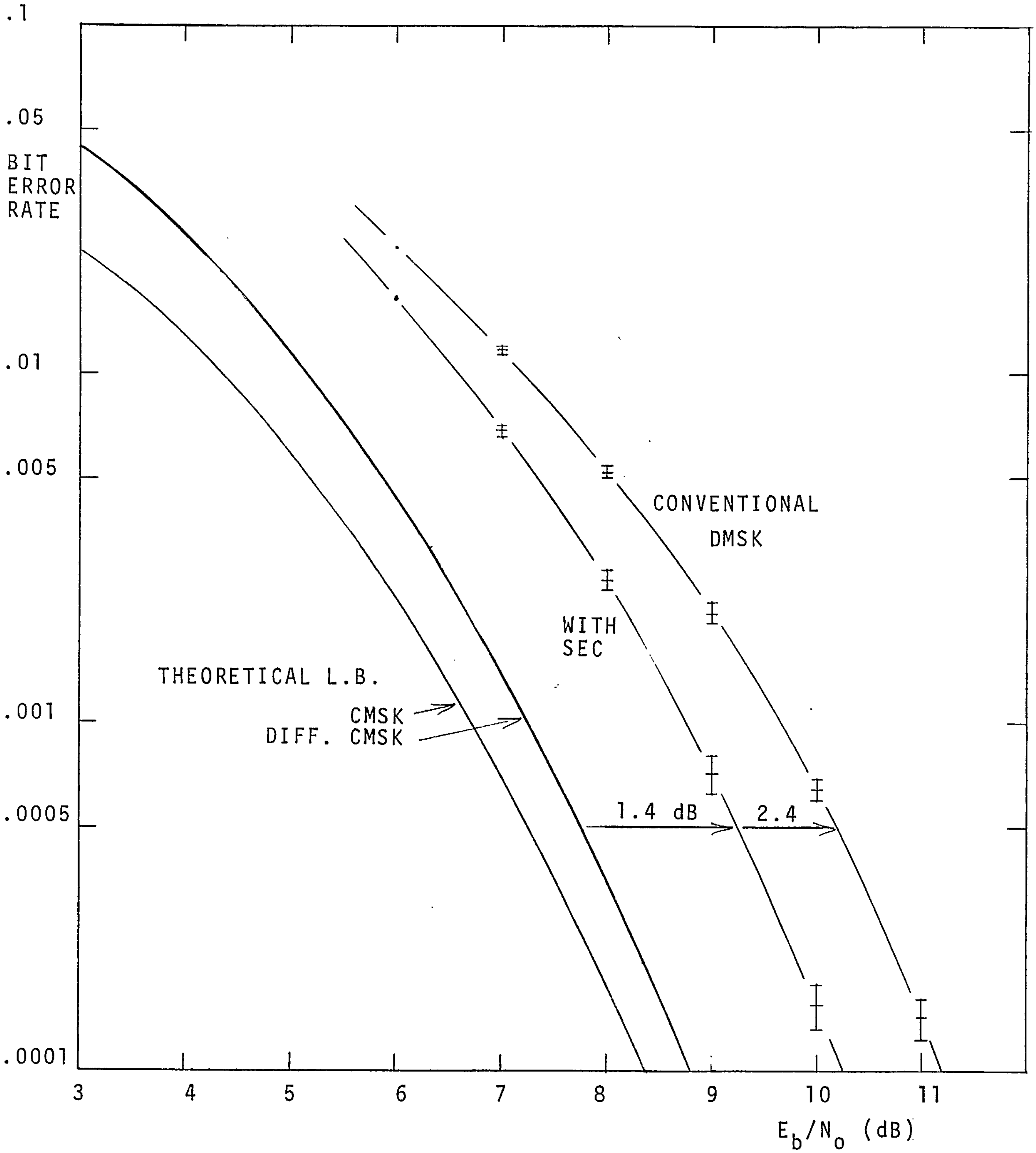

Figure 4.23 Simulated DMSK With:
Rx = 4th Order Butterworth Equ. (BT = 1.1)
Hard Limiters In All Three Branches
Of Demodulator

We conclude then that hard limiting just prior to Rx filtering is not a desired form of automatic gain control (AGC), but hard limiting anywhere after the Rx filtering does not introduce a degradation. Thus the pure product law in the basic system model can be approximated by a simple switched mixer without introducing a further degradation.

4.6 Multipath

Simulated performance for carrier to interference ratios (C/I) of 5, 10, 15, 20, ∞ dB, and E_b/N_o = 9, 10, 11 dB, is presented in Figures 4.24 and 4.25 for conventional DMSK and with SEC respectively. The receive filter used was a 4-th order Butterworth with ideal linear phase response and BT product of 1.1. Ideal bit timing recovery with respect to the dominant path is assumed. A delay of an integral number of bit periods is thought to be a worst case delay as the interference will be a maximum at the desired sampling times.

Since delays of greater than one bit period are required to make the two received signals look independent (selective fading), the differential path delay was chosen to be 2.0 bit periods. Delays of one bit period or less corresponding to flat fading are not considered.

Note that for C/I = 15 dB and BER=10^{-4}, the degradation is approximately 0.7 dB with SEC.

The improvement with SEC is seen to be a fairly consistent 1.0 dB for all C/I ratios considered.

4.7 Jamming

The jamming signal was assumed to be an in-band tone,and was added to the signal just prior to Rx filtering. Only

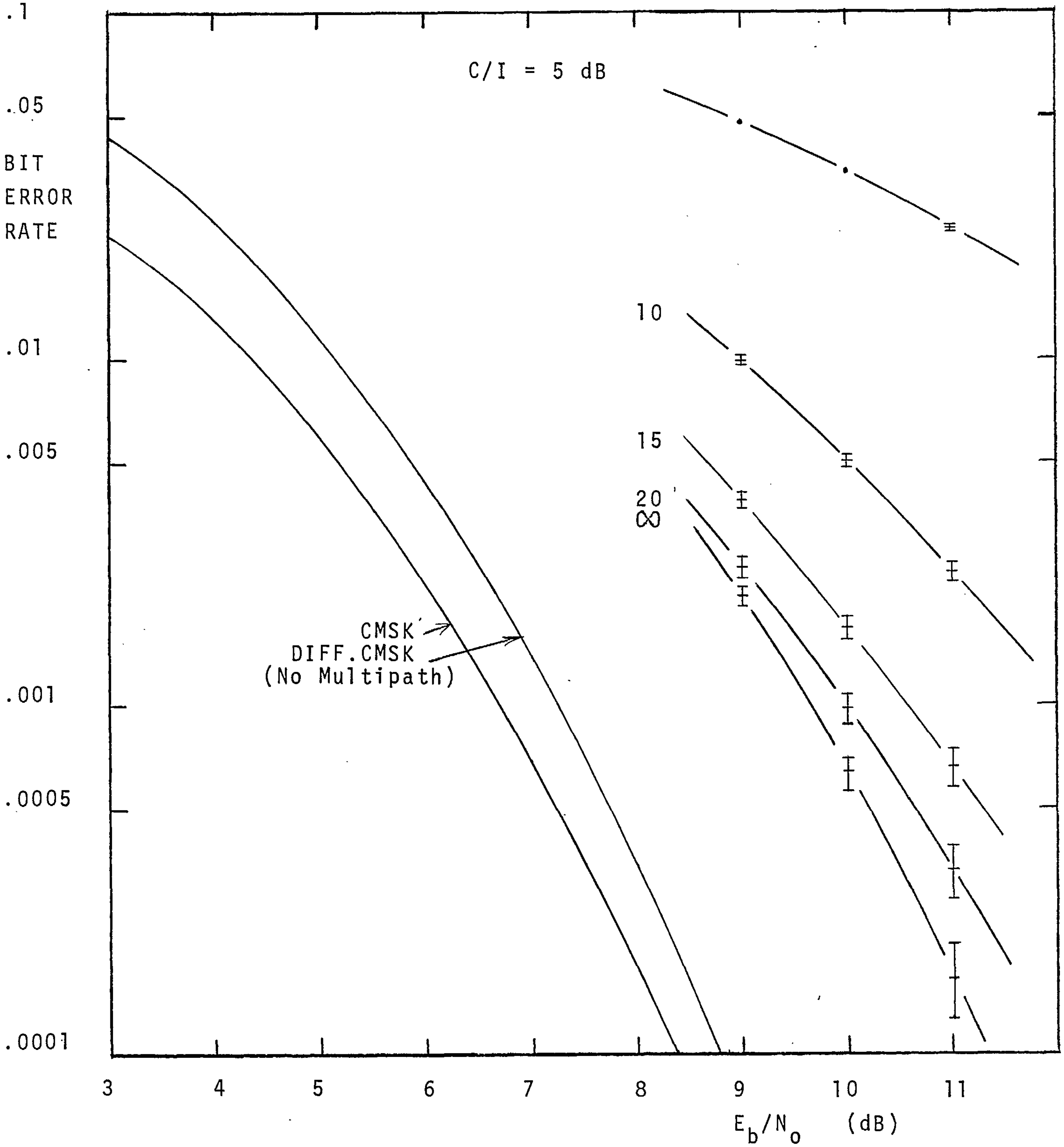

FIGURE 4.24 Simulated DMSK With Multipath:
Rx = 4th Order Butterworth Equ. (BT = 1.1)

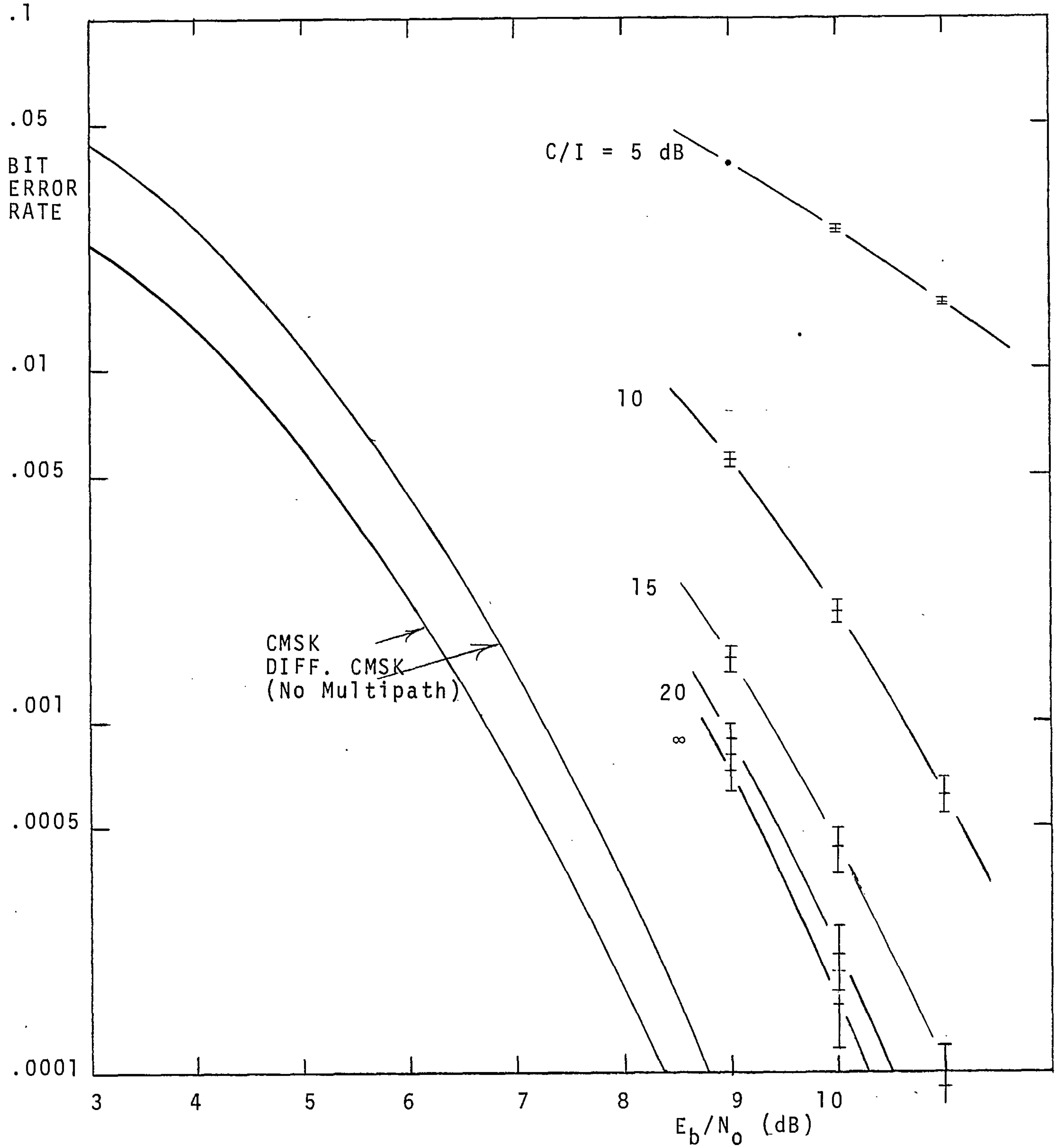

Figure 4.25 Simulated DMSK With Multipath And SEC:
Rx = 4th Order Butterworth Equ. (BT=1.1)

the worst case jammer was considered, i.e. the inband tone was assumed to lie in the centre of the Rx filter for maximum interference power throughput.

Simulated performance for carrier to interference ratios (C/I) of 5, 10, 15, 20, ∞ dB, and E_b/N_o = 9, 10, 11 dB, is presented in Figures 4.26 and 4.27 for conventional DMSK and with SEC respectively. The Rx filter was the same as that used for the multipath case, and ideal bit timing recovery was assumed.

The improvement with SEC is seen to be only about 0.5 dB for C/I ratios of 15 dB or less.

4.8 Doppler

If the approach velocity between transmitter and receiver is v, then the effective received carrier frequency is given by

$$f_d = \left(\frac{c}{c-v}\right) f_c \tag{4.6}$$

where f_c is the nominal carrier frequency, and $v \ll c$ where $c = 3\times10^8$ m/sec is the speed of electromagnetic propagation through free space. The received signal is translated to an IF frequency where differential detection takes place. Without Doppler the IF frequency is given by

$$f'_{IF} = f_c - f_t \tag{4.7}$$

where f_t is the amount of frequency translation. When Doppler is present the actual IF frequency is given by

$$f_{IF} = f_d - f_t \tag{4.8}$$

$$= \left(\frac{c}{c-v}\right) f_c - (f_c - f'_{IF})$$

$$\simeq \frac{v}{c} f_c + f'_{IF} \tag{4.9}$$

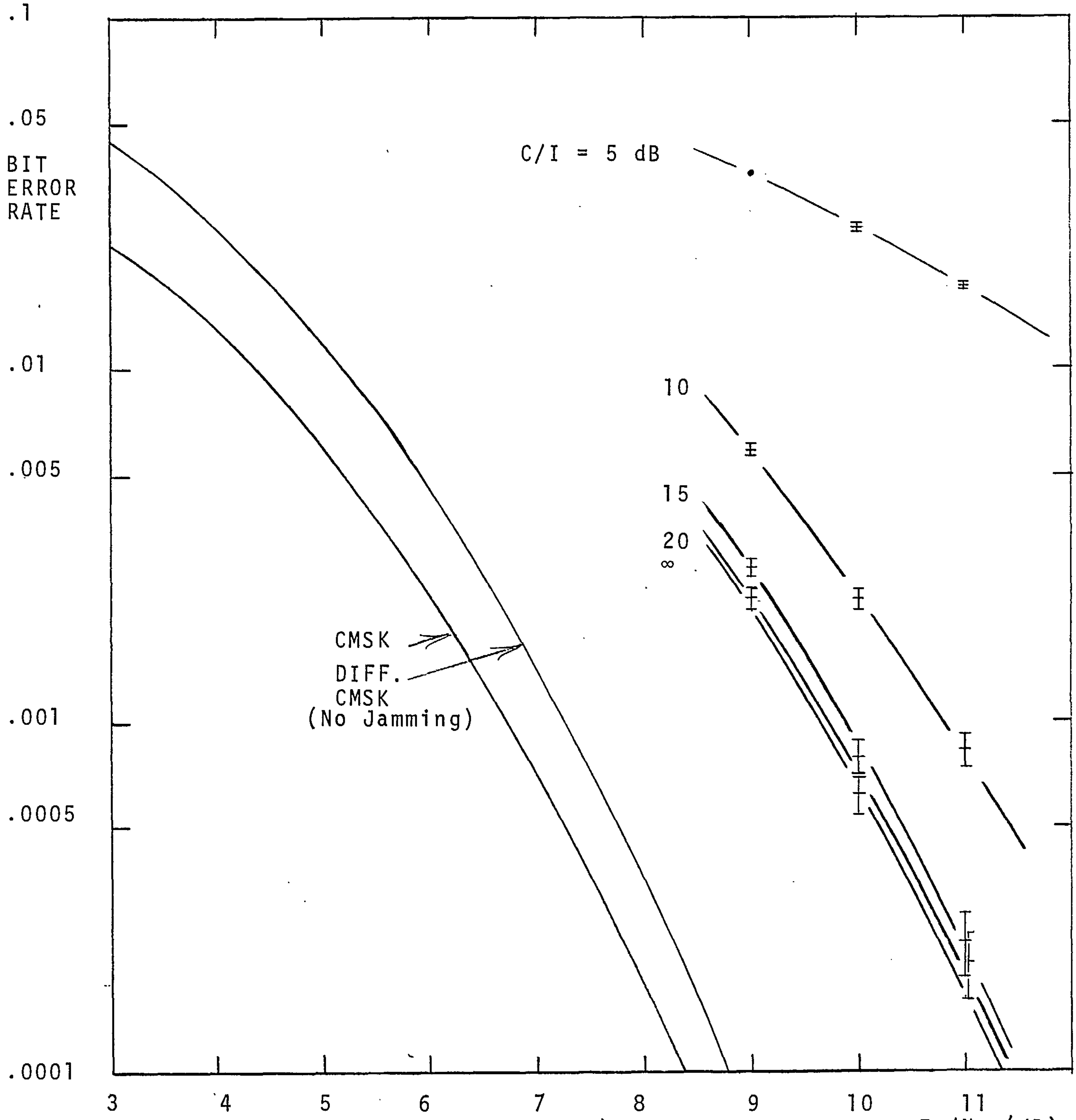

Figure 4.26 Simulated DMSK With Jamming:
Rx = 4th Order Butterworth Equ. (BT=1.1)

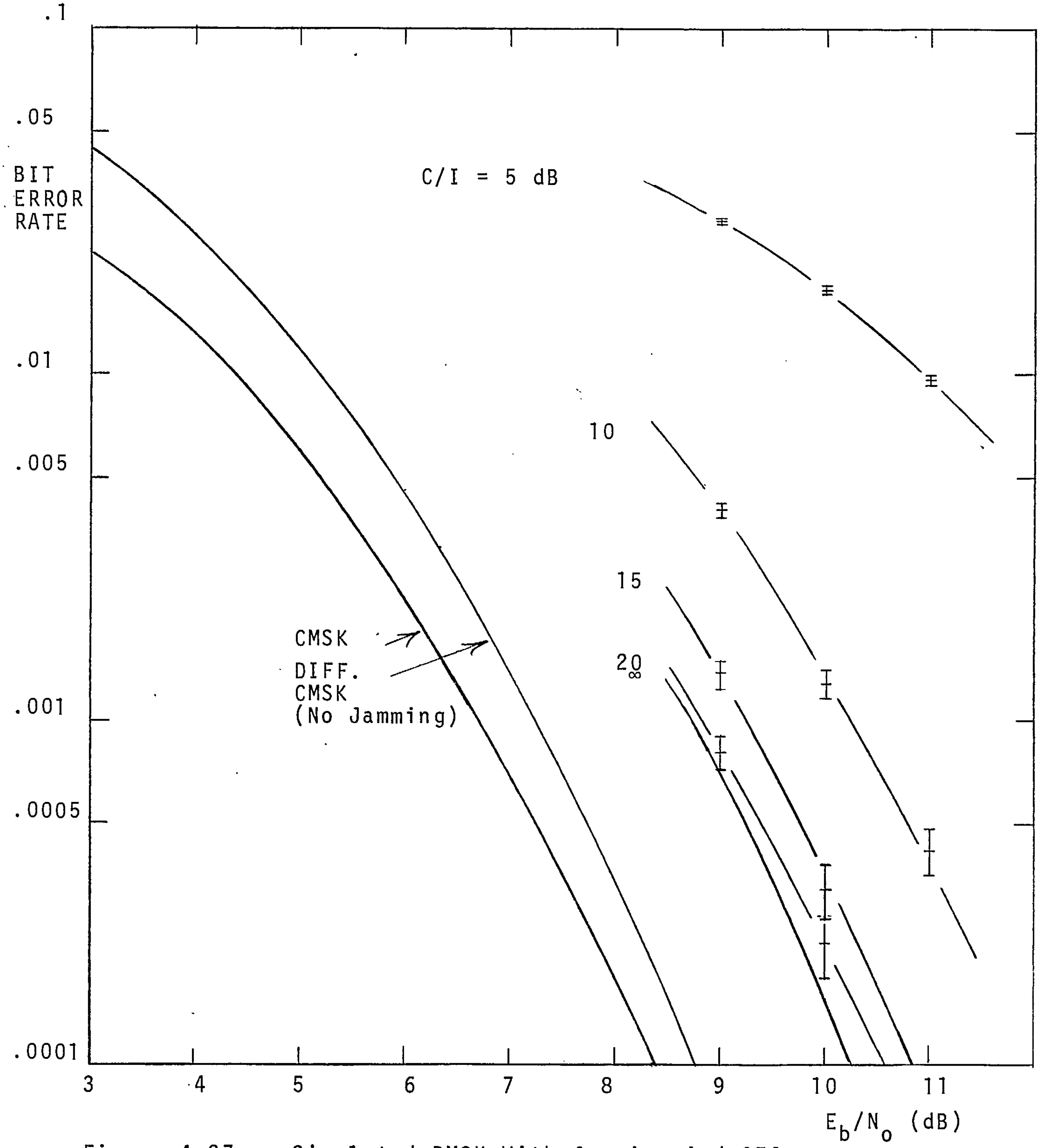

Figure 4.27 Simulated DMSK With Jamming And SEC:
Rx = 4th Order Butterworth Equ. (BT = 1.1)

Thus the phase error, ϕ_c, for the conventional branch is given by $2\pi f_{IF}T \bmod 2\pi$, which is

$$\phi_c = 2\pi \left(\frac{v}{c} f_c + f'_{IF}\right)T, \bmod 2\pi$$

$$= 2\pi \frac{v}{c} f_c T \tag{4.10}$$

where we have assumed that the detector is calibrated correctly when Doppler is not present, i.e. $f'_{IF}T$ is an integer. The phase error, ϕ_p, for the parity bit branch is twice this value. If we now assume a maximum approach speed of MAC 10 (highly unlikely), then $v = 3 \times 10^3$ m/sec, and

$$\phi_c = 2\pi\ 10^{-5}\ f_c T \quad \text{radians.}$$

$$= .0036\ f_c T \quad \text{degrees} \tag{4.11}$$

It is interesting to observe that the phase error is not a function of the IF frequency where differential detection takes place, but depends on the carrier to bit rate ratio. As an example, consider a bit rate of R=5 Mbps and a carrier frequency of f_c=1 GHz, which gives ϕ_c = 0.72 degrees. From the simulated results presented earlier for carrier frequency offset, we observed that a phase shift error of 5 degrees only caused a degradation on the order of 0.1 dB at a BER of 5×10^{-4}. Thus we can conclude for the example given that carrier frequencies on the order of 1 GHz or less present no significant threat to the performance of the DMSK detector. The degradation associated with higher f_c/R ratios can easily be determined from the results of section 4.4.5, which includes the effect of a frequency offset in the Rx filter.

4.9 Error Rate Monitoring

The single error correction (SEC) logic circuit is shown in Figure 3.9 The input data streams are the conventional DMSK detected bits, A(k), and the DMSK detected parity bits, B(k). The state variables required to implement this circuit are shown in the figure and the logical equations are also listed. The output A'(k-1), is the corrected version of A(k) and is delayed by one bit interval.

Two state variables of the SEC circuit are potentially useful for error monitoring purposes. With reference to Figure 3.9, they are the syndrome

$$D(k) = A(k) + A(k-1) + B(k) \qquad (4.12)$$

and the final correction parameter F(k). The syndrome, D(k), counts the number of single errors in one of the detected bits A(k), A(k-1), or the parity bit, B(k). The correction parameter F(k) gives an indication of the number of single error correction attempts.

The simulation program generates statistics for both of these SEC circuit state variables. The F and D rates of occurrence are plotted against the BER with SEC in Figures 4.28 and 4.29. Figure 4.28 is for a 4th order Butterworth receive filter with linear phase and a BT product of 1.1, and Figure 4.29 is for an equalizer filter. The equalizer creates a 50% roll-off raised cosine spectrum and is described in more detail in Section 5.0. For all cases simulated results provide fairly straight lines when plotted on a log-log scale. Thus for the Butterworth filter the BER with SEC is easily predicted by either

$$BER = 9.04\ F^{1.45} \qquad (4.13)$$

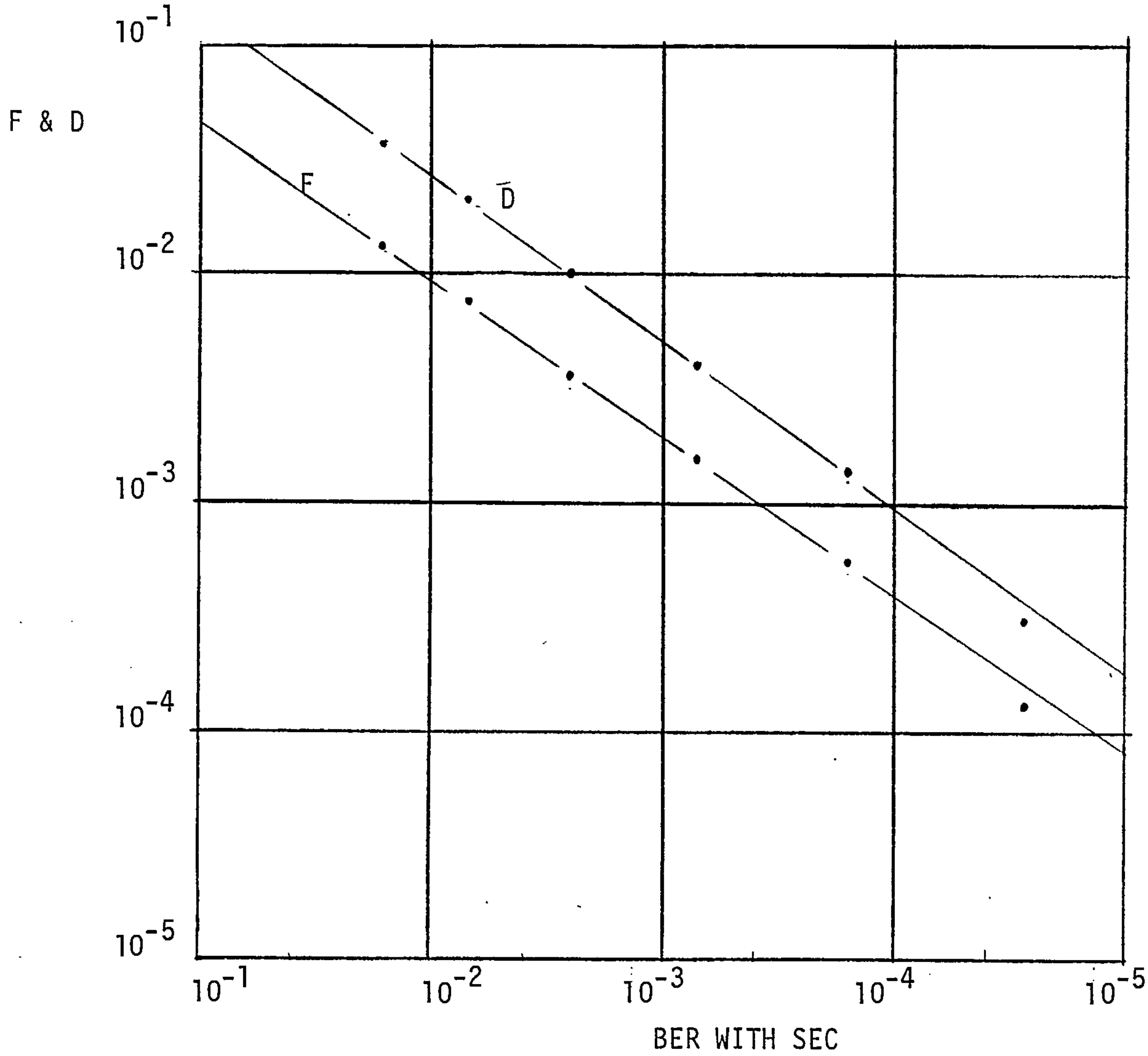

Figure 4.28 Simulated F and D Versus BER with SEC: Rx = 4-th Order Butterworth Equ. (BT=1.1)

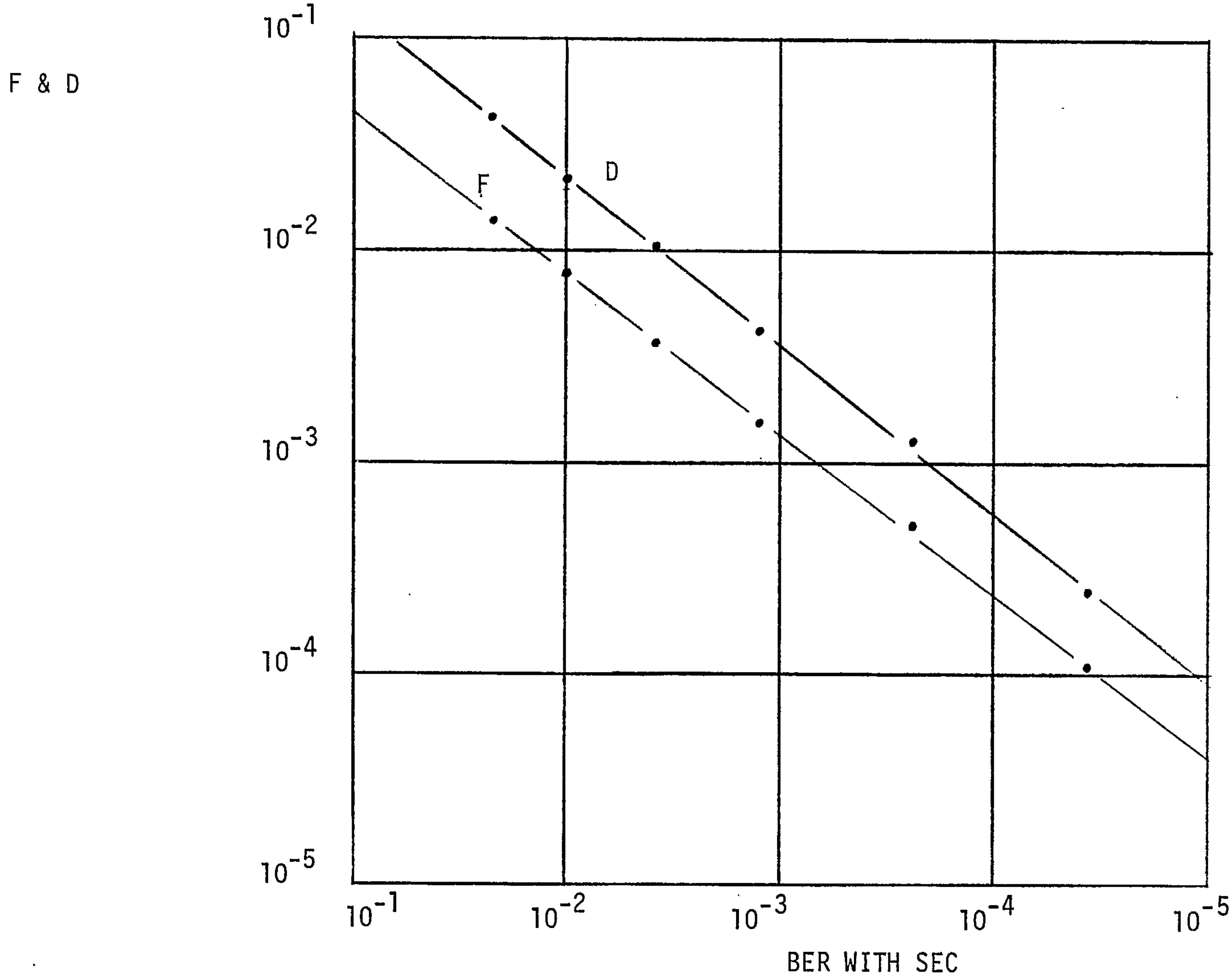

Figure 4.29 Simulated F and D Versus BER With SEC: Rx = Equalizer

or

$$BER = 1.52\ D^{1.39} \tag{4.14}$$

and for the equalizer

$$BER = 5.97\ F^{1.32} \tag{4.15}$$

or

$$BER = 1.15\ D^{1.25} \tag{4.16}$$

Since the D rate is higher than the F rate, the results using the D rate are likely to be more accurate. This is reflected in equations (4.14) and (4.16) by the fact that a smaller exponent and multiplier are required to compute the predicted BER, as compared to equations (4.13) and (4.15) respectively for the F rate. Thus it is recommended that the syndrome rate D be used for BER monitoring or prediction purposes.

As can be seen from the two examples given, the F and D rates depend on the filtering used, and thus the appropriate BER prediction formula is not unique. A different formula must be determined for each possible system configuration.

4.10 Eye Patterns

Presented are a number of eye patterns generated at the output of the demodulator for a number of receive (R_x) filters. All patterns were created using the full duration of a 512 bit PN sequence and no noise. No transmit (T_x) filtering was used, and the post-demodulation (DEM) filter was assumed ideal, i.e. only the unwanted second harmonics were removed without causing any distortion to the baseband waveform.

Figure 4.30 shows the eye pattern for no R_x filtering (ideal signal). As can be seen the eye is very clean and completely open, reaching its full positive and negative peak values . Figures 4.31 through 4.35 show the eye patterns for a phase-equalized 4-th order Butterworth R_x filter and respective BT products of 1.2, 1.1, 1.0 0.9, and 0.8. As the BT product decreases we can see how the eye opening gets smaller due to the increased ISI caused by the narrower bandwidth. Noticeable eye closure appears for $BT<0.9$.

Note that the eye pattern displayed in Figure 4.32, with a BT product of 1.1, corresponds to the R_x filter which resulted in the best performance for a BER of $5x10^{-4}$.

Figure 4.36 displays the eye pattern which results when matched filtering is used, i.e. the R_x filter is matched to the signal spectrum (over a bandwidth equal to the width of the main lobe). Note the severity of the ISI, but also the cleanness of the four possible signal values at the sampling time.

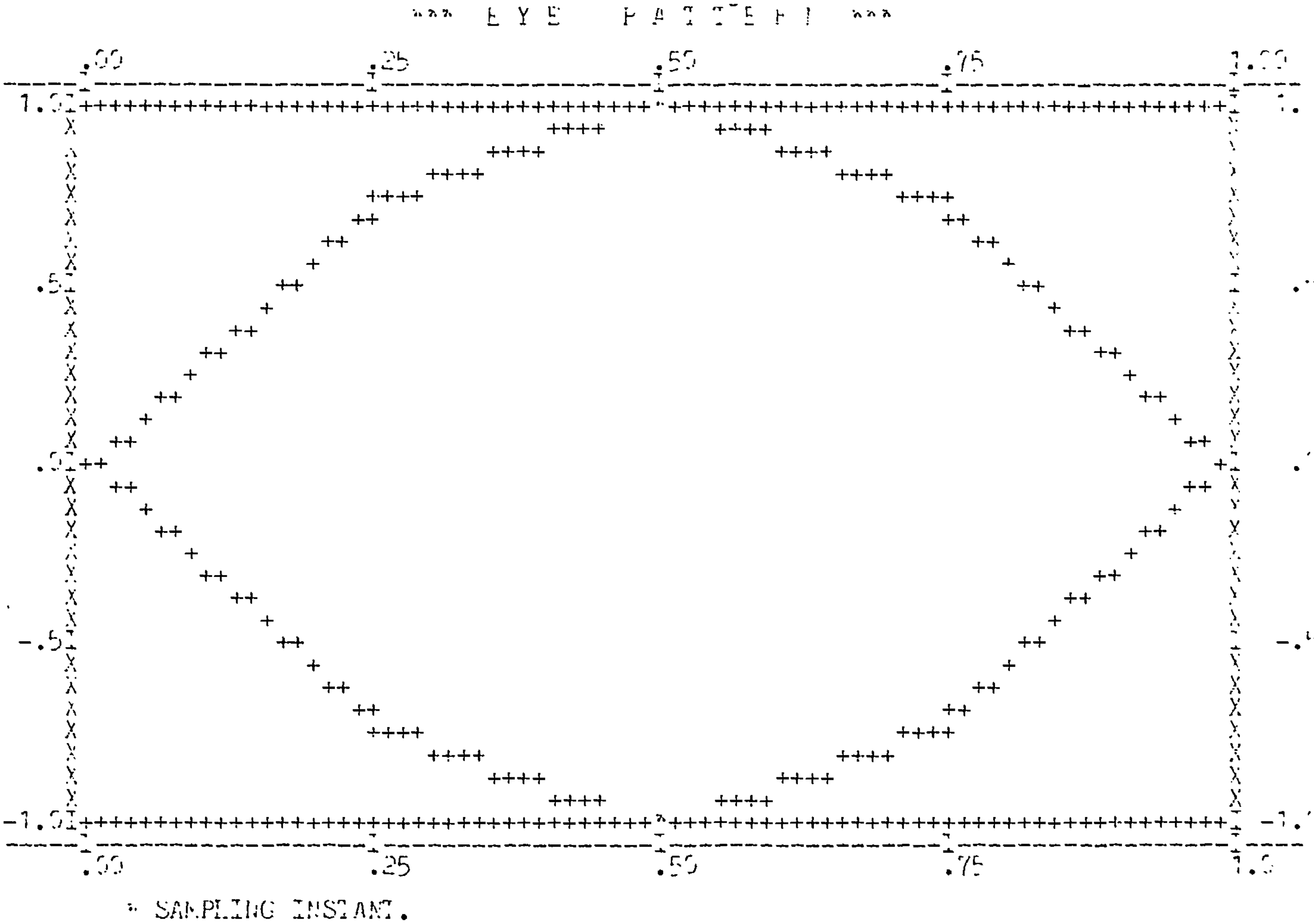

Figure 4.30 Eye Pattern For Negligible Filtering (BT = 4.0)

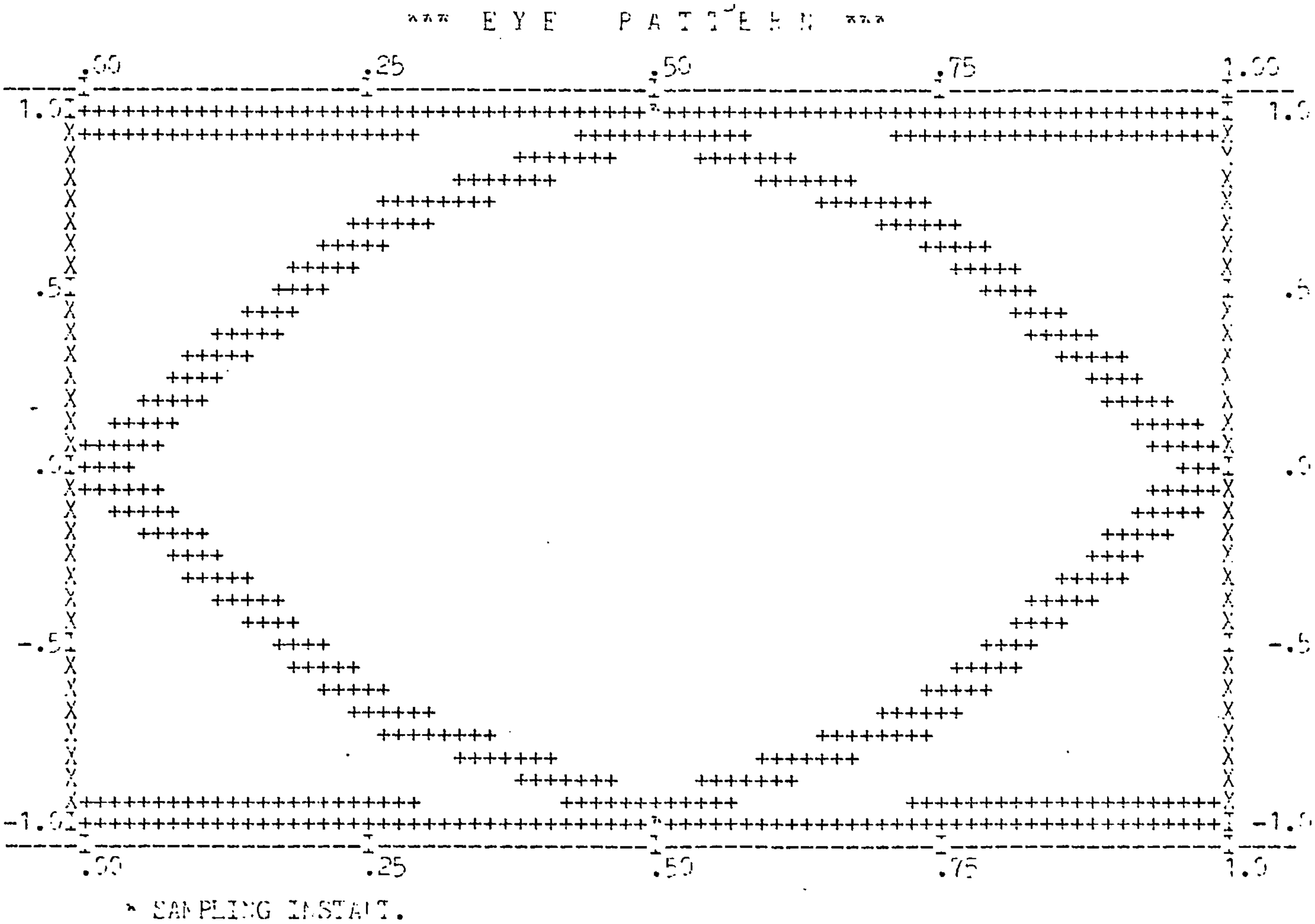

Figure 4.31 Eye Pattern For:

Rx = 4th Order Butterworth Equ. (BT=1.2)

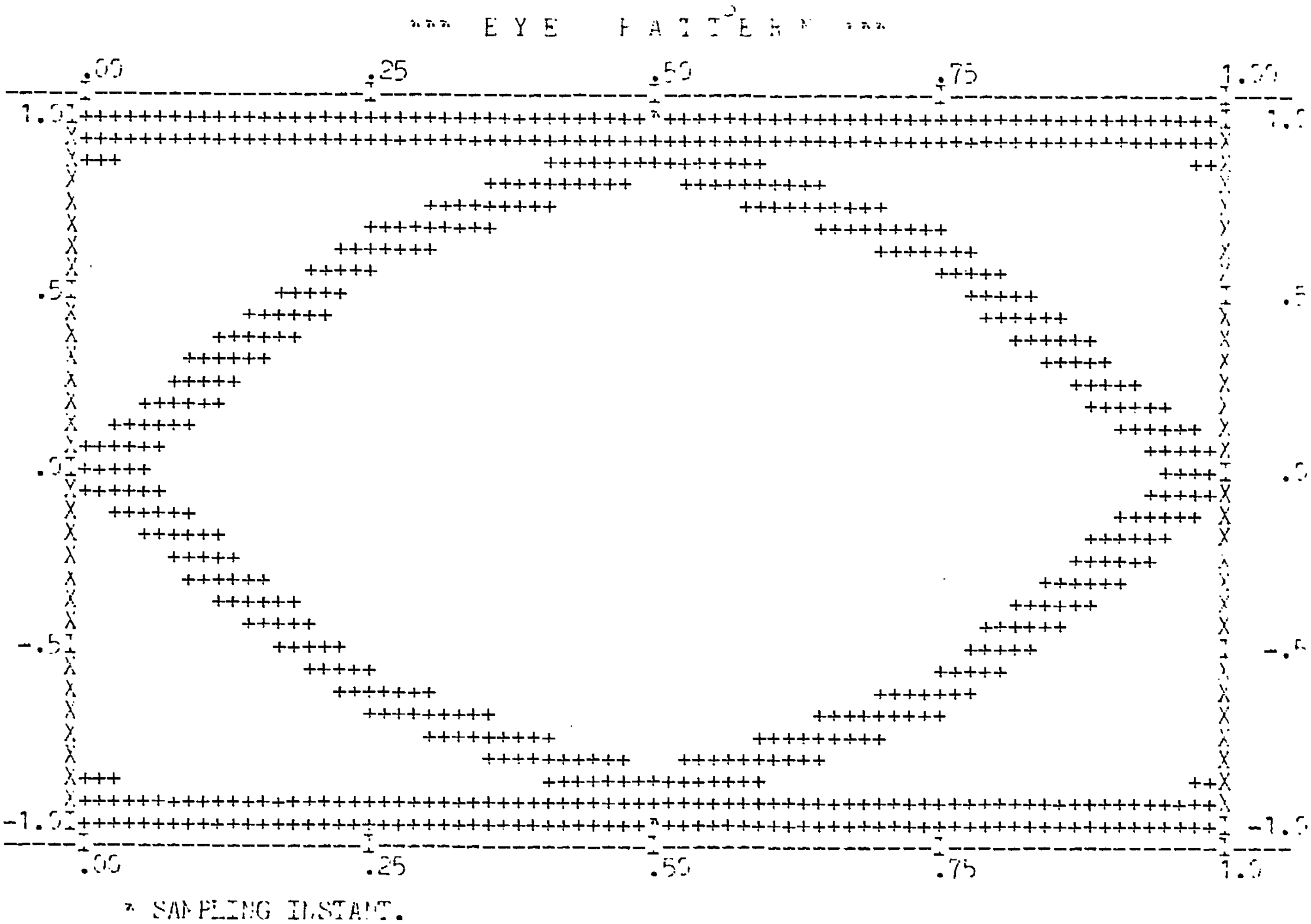

Figure 4.32 Eye Pattern For:

Rx = 4th Order Butterworth Equ. (BT = 1.1)

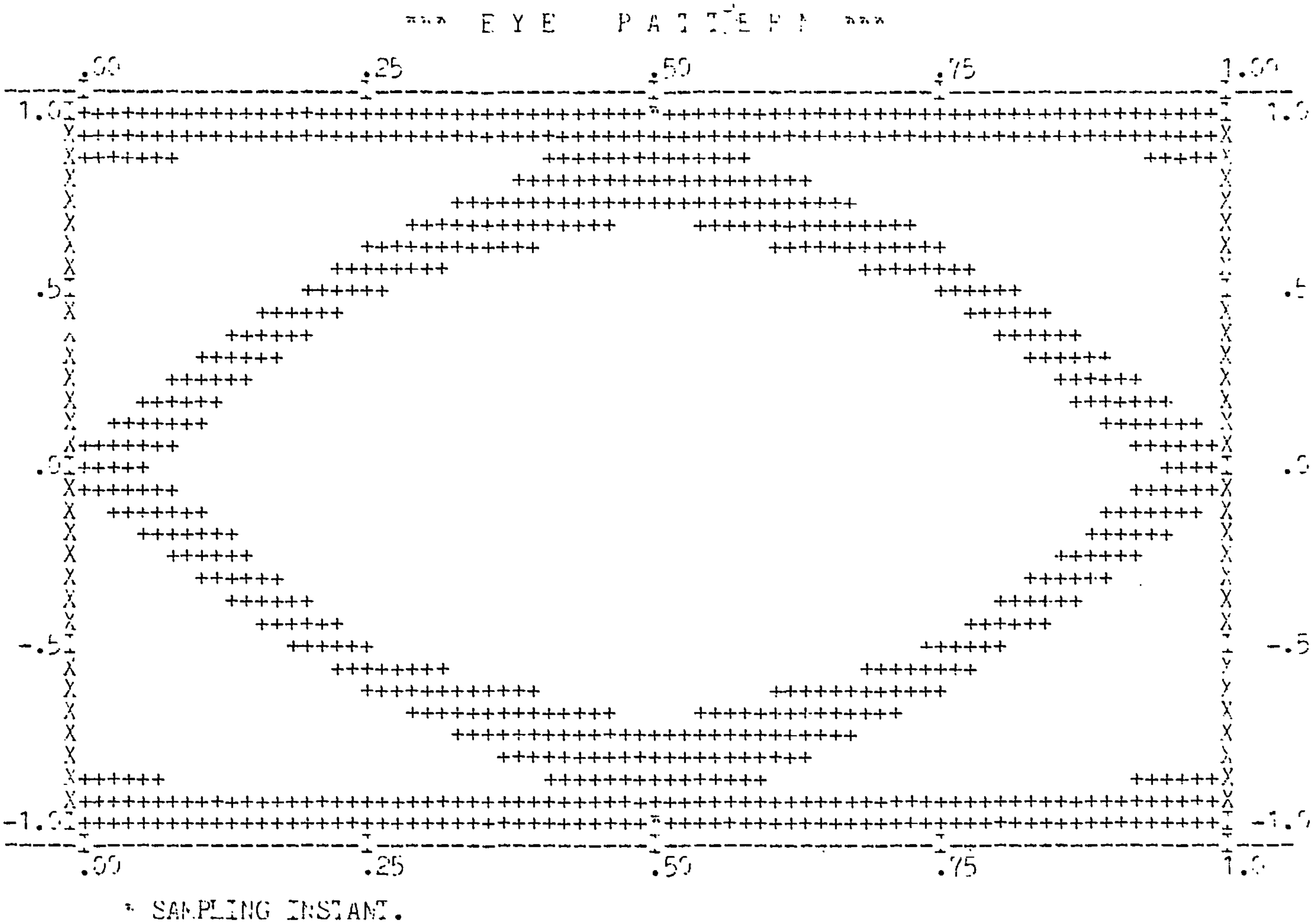

Figure 4.33 Eye Pattern For:

Rx = 4th Order Butterworth Equ. (BT=1.0)

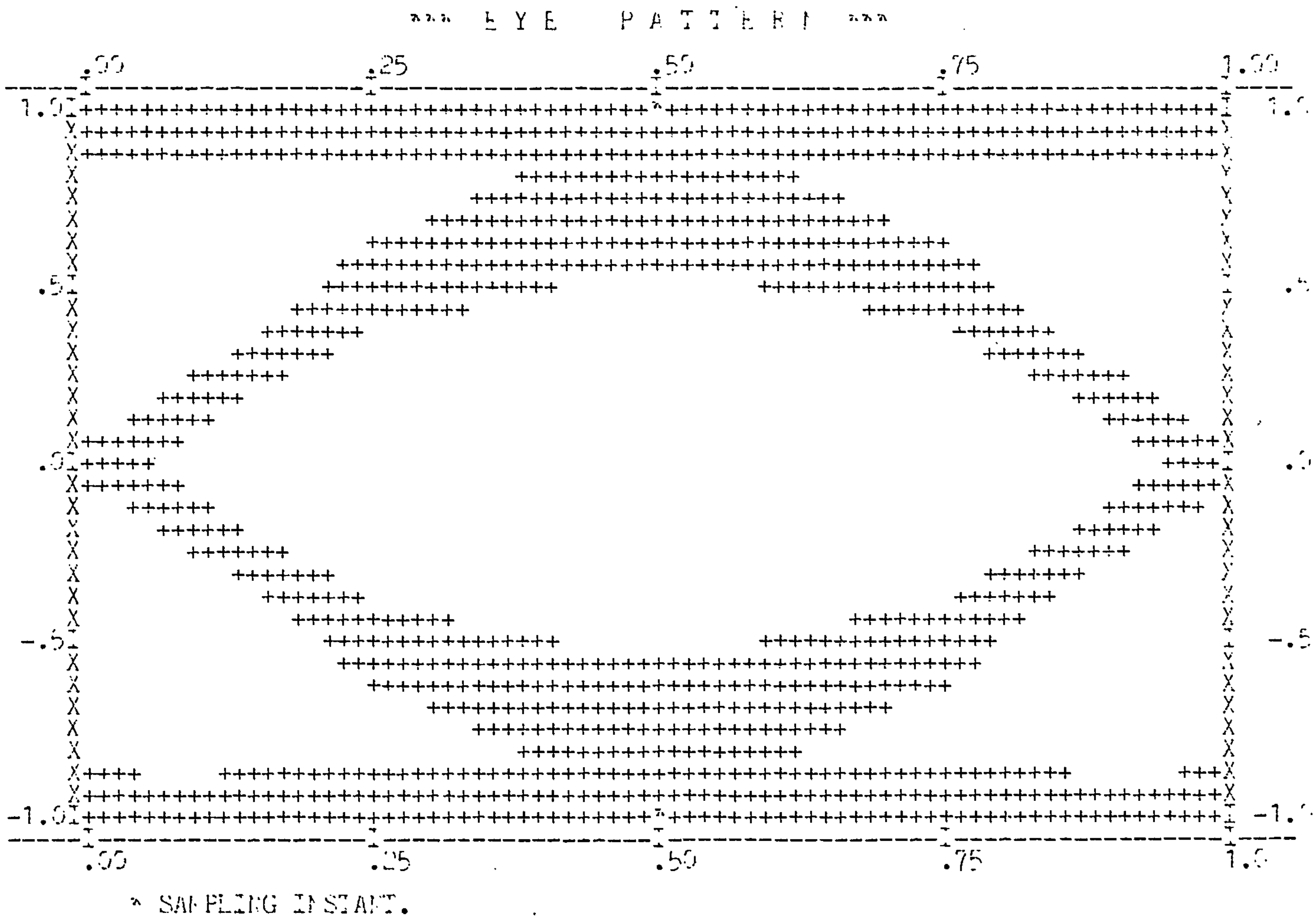

Figure 4.34 Eye Pattern for:

Rx = 4th Order Butterworth Equ. (BT = 0.9)

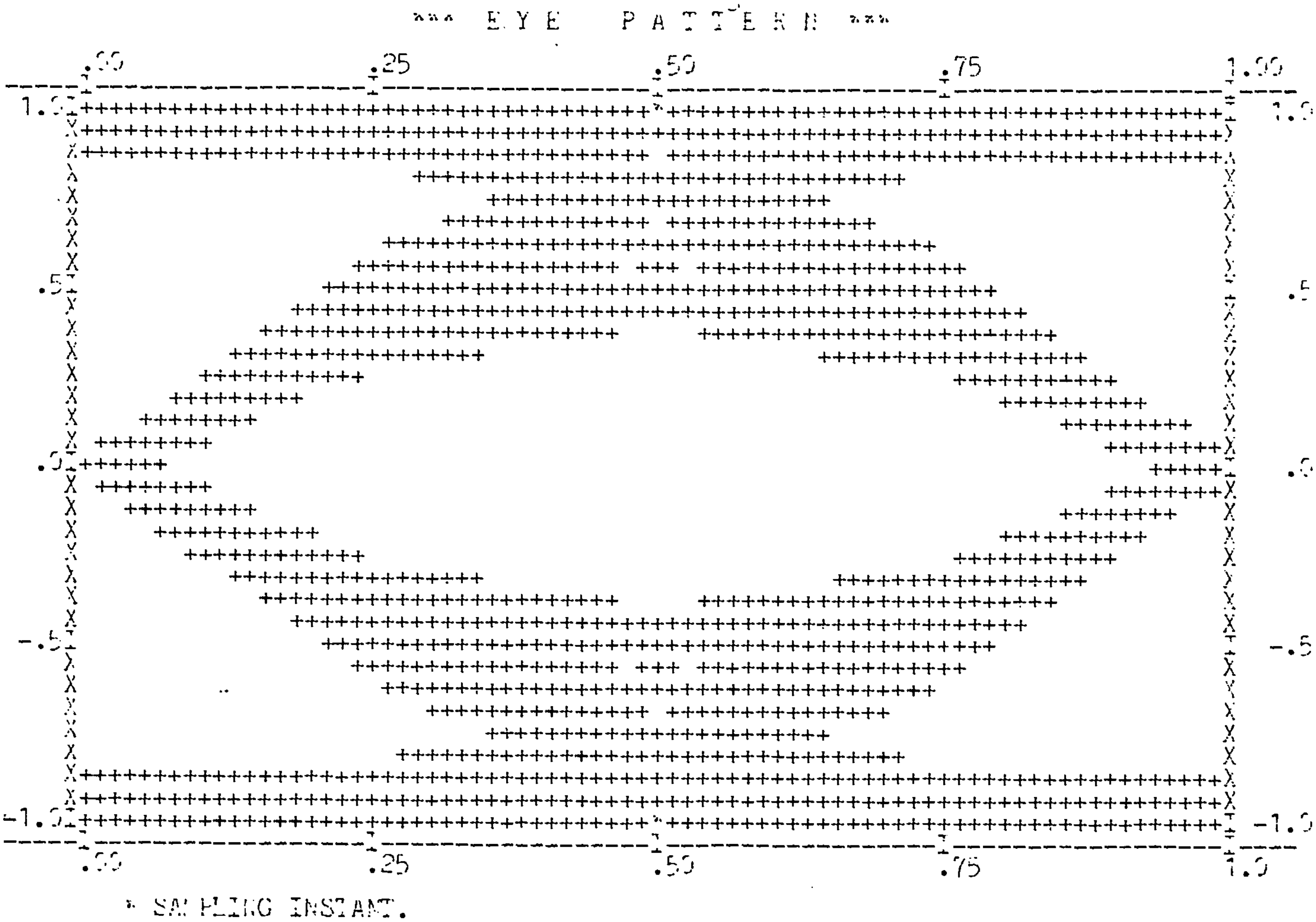

Figure 4.35 Eye Pattern For:
Rx = 4th Order Butterworth Equ. (BT = 0.8)

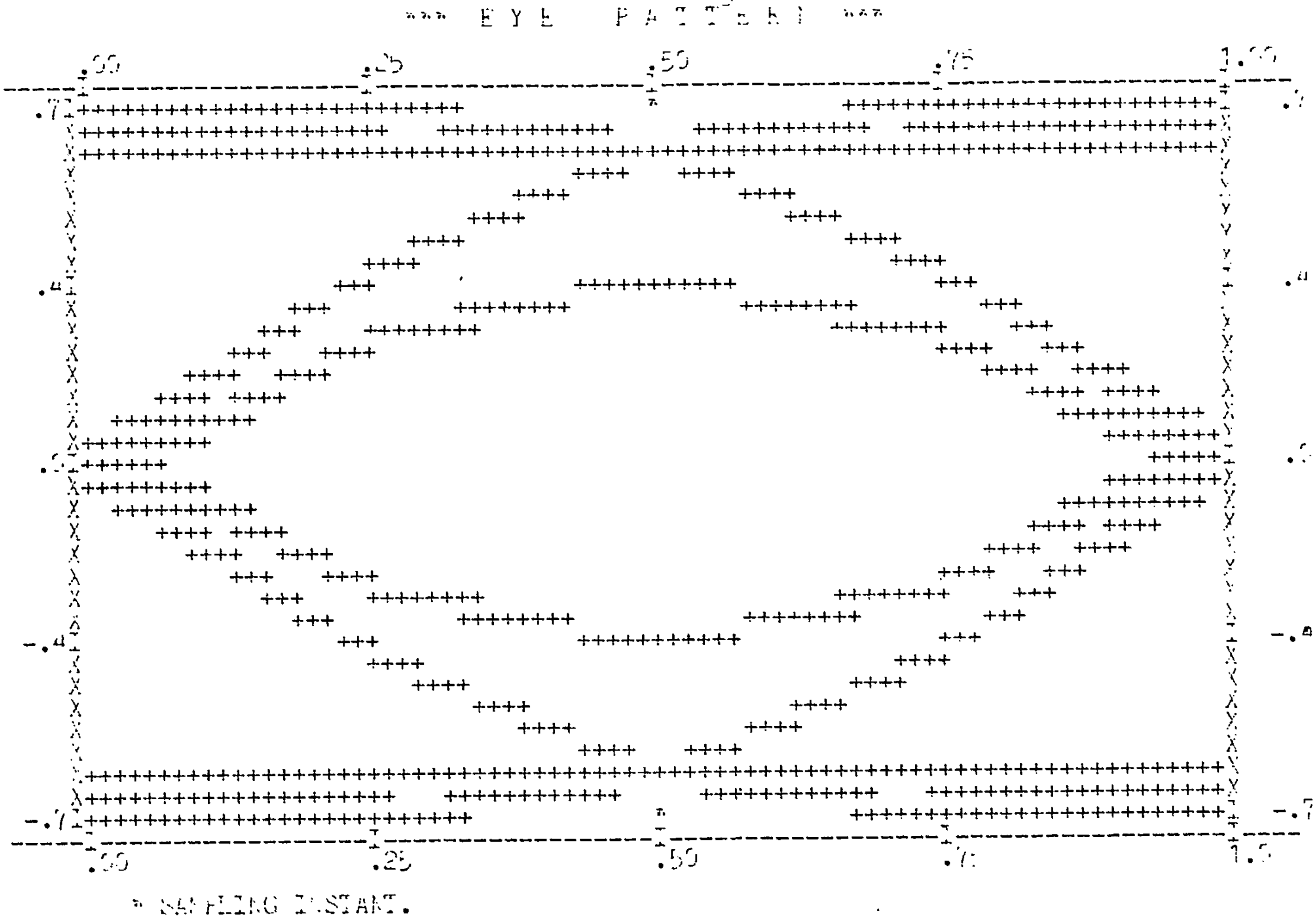

Figure 4.36 Eye Pattern For:
Rx = Matched Filter (BT=0.6)

When ISI is present, the eye patterns for the parity bit branch of the receiver are not the same as those generated for the conventional branch. The reason for this stems from the fact that the signals s(t) and s(t-2T) are not completely independent at any given time instant (due to ISI). Because of this, part of the ISI signal contribution is squared, resulting in a slight positive dc offset. Figure 4.37 displays the result when matched filtering is used. This peculiar ISI phenomenon of the DMSK detector is discussed in more detail in Section 6.0. (Note that there are only four possible signal values in the parity branch output for the matched filter case).

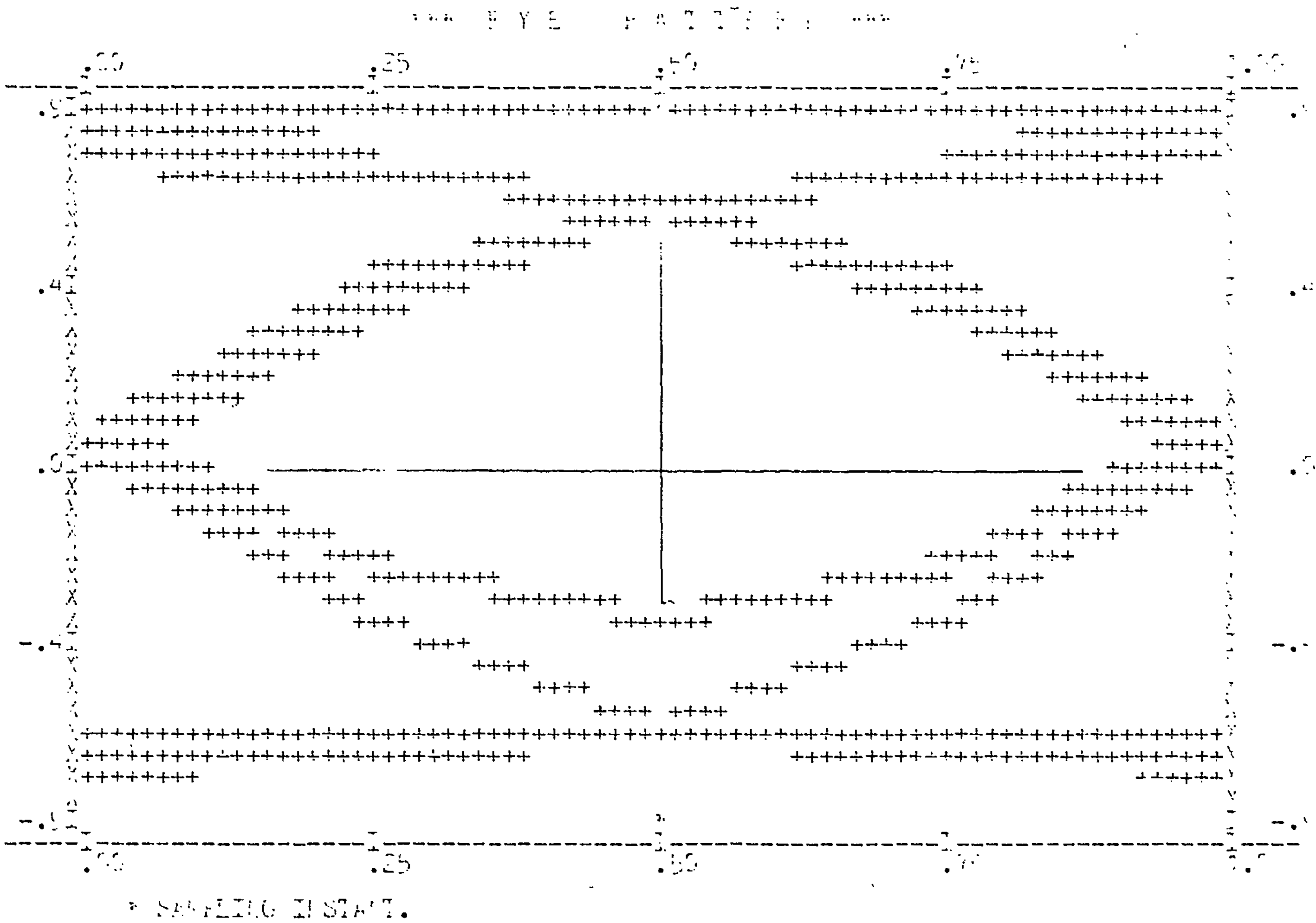

Figure 4.37 Parity Bit Branch Eye Pattern For:

Rx = Matched Filter (BT=0.6)

4.11 Zero Crossing RMS Jitter

While the differential demodulator does not require a carrier recovery loop, clock recovery is still required. Some non-linear BTR schemes use simple zero crossing detection to adjust or reset a local BTR clock. Of interest is the zero crossing root mean square (RMS) jitter of the DMSK detector output waveform. The zero crossing RMS jitter is defined as

$$J_{RMS_k} = E[e_k^2]^{\frac{1}{2}} \tag{4.17}$$

where

$$e_k = C_k - \overline{C}_k \tag{4.18}$$

is the zero crossing error at time k, C_k is the random variable representing the crossing time for the k-th zero crossing, $\overline{C}_k$ is the k-th expected zero crossing time, and the expected value, $E[\cdot]$, is taken with respect to the assumed independent random data and zero-mean noise. With the above assumptions the zero crossing error, e_k, is stationary with respect to crossing time k, and thus the RMS jitter can be computed using the formula:

$$J_{RMS} = \left[\lim_{k\to\infty} \frac{1}{K} \sum_{k=1}^{K} e_k^2\right]^{\frac{1}{2}} \tag{4.19}$$

Simulated RMS jitter values for K=2000 bits are presented in Table 4.3 for alternating and random (PN) sequences, E_b/N_o values of 8, 11, and 14 dB, two Rx filter types, with and without a hard limiter following the Rx filter. The two filters considered are the 4-th order Butterworth with

Rx FILTER	E_b/N_o (dB)	RMS JITTER (bit periods) ALTERNATING SEQ.	RANDOM SEQ.
BW4E (BT=1.1)	8	0.159/0.159*	0.159/0.156
	11	0.108/0.107	0.110/0.108
	14	0.074/0.073	0.078/0.077
EQUALIZER	8	0.137/0.139	0.161/0.160
	11	0.092/0.095	0.109/0.110
	14	0.063/0.069	0.078/0.081

*Note: Without/With a hard limiter at the output of the Rx filter.

Table 4.3 Simulated Zero Crossing RMS Jitter linear phase (BW4E) with BT product of 1.1 and the equalizer used to create a 50% roll -off raised cosine spectrum, which is discussed in Section 5.0. The jitter values presented are normalized to the bit period, T, so that the values given are in bit periods. An interesting observation is that RMS jitter is about the same with and without the hard limiter, for all configurations. The RMS jitter for the random sequence is greater than that for the alternating sequence because of the jitter caused by ISI at the zero crossing points.

Now assume a BTR technique which adjusts or resets a timing clock based on a uniform average of the last N zero crossings. The error at the output of such a device is given by

$$\varepsilon = \frac{1}{N} \sum_{k=1}^{N} e_k \tag{4.20}$$

Since the expected value of ε is zero, the RMS jitter of the output of this averaging device is given by

$$\begin{aligned} J_N &= E[\varepsilon^2]^{\frac{1}{2}} \\ &= \left(\frac{1}{N^2} \sum_{k=1}^{N} E[e_k^2]\right)^{\frac{1}{2}} \\ &= \frac{J_{RMS}}{\sqrt{N}} \end{aligned} \tag{4.21}$$

where we have assumed that e_k and e_i are independent for $i \neq k$*. The RMS jitter as defined by (4.21) is plotted in Figure 4.38 for the 4-th order Butterworth and in Figure 4.39 for the equalizer. Assuming an alternating sequence is used as a preamble for BTR, then the number of zero crossings, N, is the number of bits needed to obtain the desired RMS timing jitter. As an example, for an E_b/N_o of 8 dB and a maximum allowed RMS jitter of 5%, the minimum number of bits required for a BTR preamble is 10 bits for the Butterworth filter and 8 bits for the equalizer. Using twice as many bits reduces the RMS jitter to 3.5% (i.e. a factor of $1/\sqrt{2}$). When operating on random equiprobable data, many more bits are required to obtain the same accuracy, because the number of zero crossings is random and the average number of bits required for N crossings is 2N bits.

---

*This is probably a very good assumption for zero crossings 2 bit periods apart or more, but for adjacent zero crossings one bit period apart ISI and noise correlation may be significant depending on the Rx filter used.

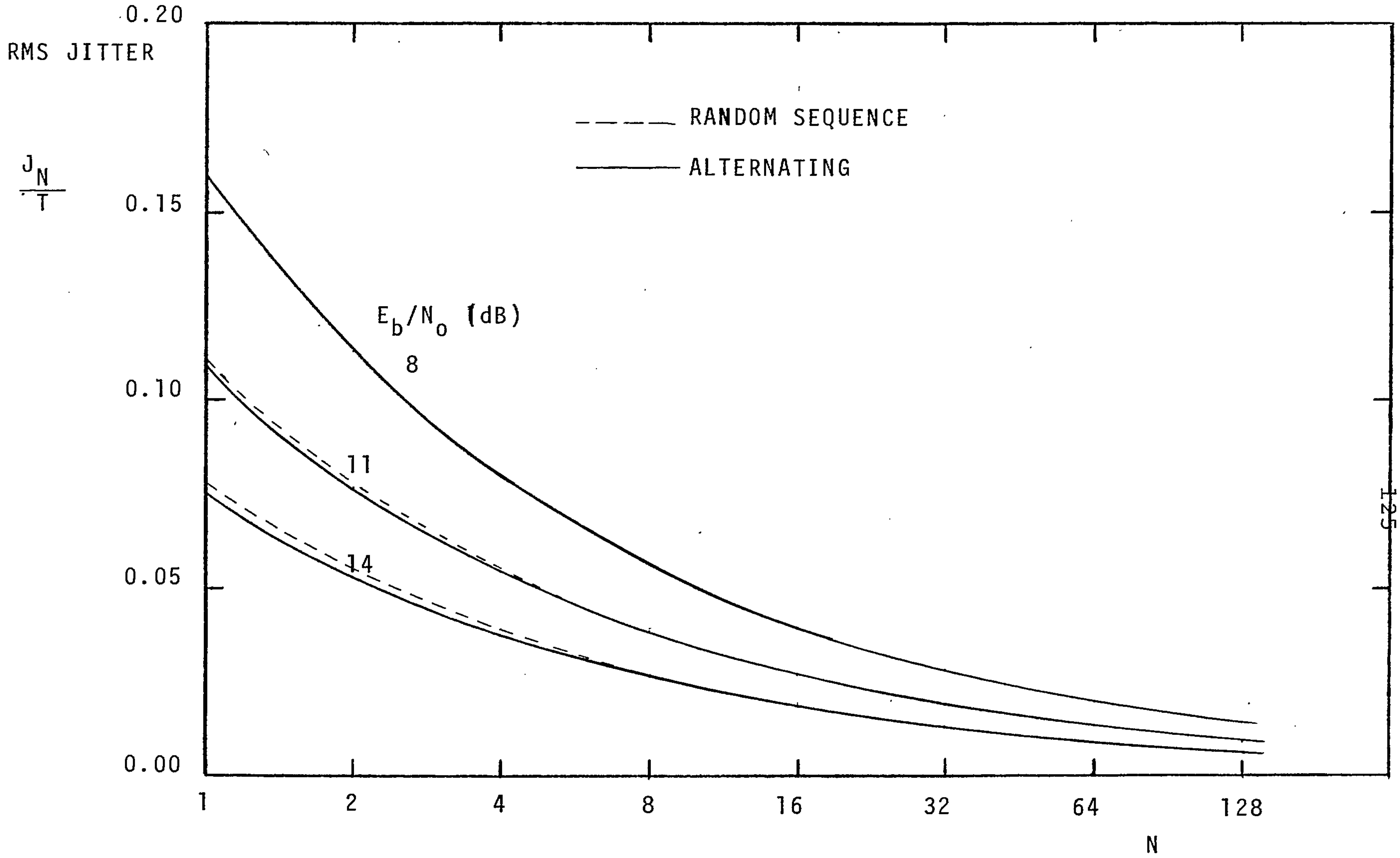

Figure 4.38 Zero Crossing RMS Jitter Averaged Over N Crossings: Rx = 4th Order Butterworth Equ. (BT = 1.1)

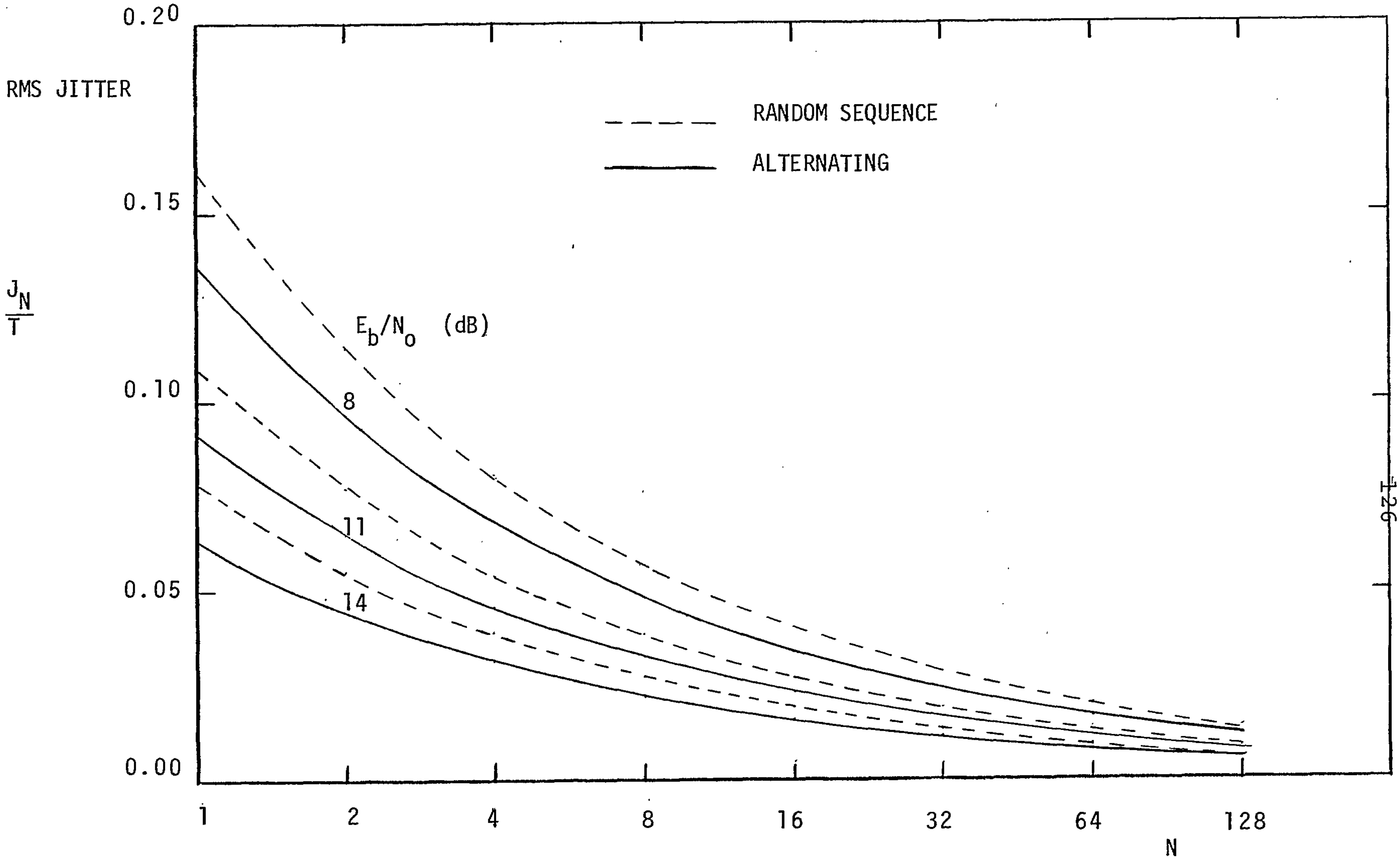

Figure 4.39 Zero Crossing RMS Jitter Averaged Over N Crossings:
Rx = Equalizer to Create 50% Roll-Off Raised Cosine

5.0 INVESTIGATION OF PERFORMANCE WITH EQUALIZATION

In linear PSK systems square-root Nyquist filtering is applied to the transmitter and receiver so that the receiver filter is (1) matched to the receive wave shape and (2) its output does not contain intersymbol interference (ISI) at the sampling instant. A receive filter matched to the MSK spectrum however does not have an ISI-free output when differential detection is performed (see Figure 4.36). The DMSK signal can be equalized to eliminate harmful ISI. Theoretical and simulated performance are determined for just such a receive (Rx) filter, but the penalty is an increased noise power. In the limit as the bit error rate (BER) approaches zero it is determined that the asymptotic degradation of DMSK from CMSK approaches a minimum 1.41 dB.

5.1 Equalization Strategy

We desire a receive filter which yields an output spectrum which does not exhibit severe intersymbol interference (ISI) at the correct sampling times used for comparison in the suboptimal differential detection process following the receive (Rx) filter.

The transmitted signal is given by

$$s(t) = A\cos\left(2\pi f_c t + \phi(t)\right) \tag{5.1}$$

where $\phi(t)$ is the required phase response to give the assumed DMSK signal format. When expressed in OQPSK format, the corresponding transmit pulse is given by

$$g(t) = A\cos\frac{\pi t}{2T} \tag{5.2}$$

The signal amplitude spectrum is given by the Fourier transform of g(t), and is

$$G(f) = \frac{4AT}{\pi} \cdot \frac{\cos 2\pi fT}{1-(4fT)^2} \tag{5.3}$$

A 50% roll-off raised cosine Nyquist spectrum is chosen as the desired resultant spectrum after Rx filtering, as ISI is eliminated and it has the same bandwidth as the mainlobe of the DMSK spectrum. The desired spectrum and corresponding impulse response are given by

$$X(f) = AT, \quad |f| < \frac{1}{4T} \tag{5.4}$$

$$= \frac{AT}{2}\left[1 + \sin 2\pi Tf\right], \quad \frac{1}{4T} < |f| < \frac{3}{4T}$$

$$x(t) = A\,\frac{\sin \pi t/T}{\pi t/T} \cdot \frac{\cos \pi t/2T}{1-(t/T)^2} \tag{5.5}$$

where the amplitude A of the Nyquist pulse x(t) has been chosen to be identical to the amplitude of g(t) at the correct comparison point.

Thus from (5.3) and (5.4) the required Rx filter spectrum is given by

$$R(f) = \frac{X(f)}{G(f)} \tag{5.6}$$

and is tabulated in Table 5.1. The amplitude spectrum of the signal G(f), the desired spectrum X(f), and the required filter R(f), are plotted in Figure 5.1. From this figure we can see that the noise enhancement with the Rx filter of (5.6) will be quite significant in comparison to a filter which is matched to the MSK spectrum, G(f).

BETA	SIGNAL	(DB)
.0000	1.0000	.0000
.0100	1.0004	.0032
.0200	1.0015	.0130
.0300	1.0034	.0292
.0400	1.0060	.0520
.0500	1.0094	.0813
.0600	1.0136	.1171
.0700	1.0185	.1595
.0800	1.0243	.2085
.0900	1.0309	.2641
.1000	1.0383	.3264
.1100	1.0466	.3954
.1200	1.0557	.4711
.1300	1.0658	.5536
.1400	1.0768	.6430
.1500	1.0888	.7392
.1600	1.1018	.8424
.1700	1.1159	.9527
.1800	1.1311	1.0700
.1900	1.1474	1.1946
.2000	1.1650	1.3264
.2100	1.1838	1.4656
.2200	1.2040	1.6122
.2300	1.2255	1.7665
.2400	1.2486	1.9284
.2500	1.2732	2.0982
.2600	1.2983	2.2672
.2700	1.3224	2.4274
.2800	1.3456	2.5765
.2900	1.3679	2.7256
.3000	1.3890	2.8542
.3100	1.4091	2.9788
.3200	1.4280	3.0947
.3300	1.4457	3.2017
.3400	1.4622	3.2999
.3500	1.4773	3.3893
.3600	1.4910	3.4697
.3700	1.5033	3.5409
.3800	1.5141	3.6029
.3900	1.5233	3.6556

BETA	SIGNAL	(DB)
.4000	1.5306	3.6966
.4100	1.5357	3.7317
.4200	1.5398	3.7547
.4300	1.5430	3.7672
.4400	1.5433	3.7688
.4500	1.5415	3.7591
.4600	1.5377	3.7377
.4700	1.5316	3.7036
.4800	1.5236	3.6572
.4900	1.5130	3.5968
.5000	1.5000	3.5218
.5100	1.4845	3.4314
.5200	1.4663	3.3245
.5300	1.4454	3.1998
.5400	1.4217	3.0560
.5500	1.3950	2.8913
.5600	1.3652	2.7036
.5700	1.3322	2.4914
.5800	1.2959	2.2513
.5900	1.2561	1.9804
.6000	1.2127	1.6749
.6100	1.1655	1.3302
.6200	1.1144	.9408
.6300	1.0592	.4995
.6400	.9997	-.0025
.6500	.9358	-.5765
.6600	.8672	-1.2379
.6700	.7937	-2.0069
.6800	.7151	-2.9125
.6900	.6312	-3.9967
.7000	.5417	-5.3251
.7100	.4463	-7.0073
.7200	.3448	-9.2495
.7300	.2368	-12.5133
.7400	.1225	-18.2749

Table 5.1 Filter Required to Genate a 50% Roll-Off Rasied Cosine (BETA = (f-fc)/R)

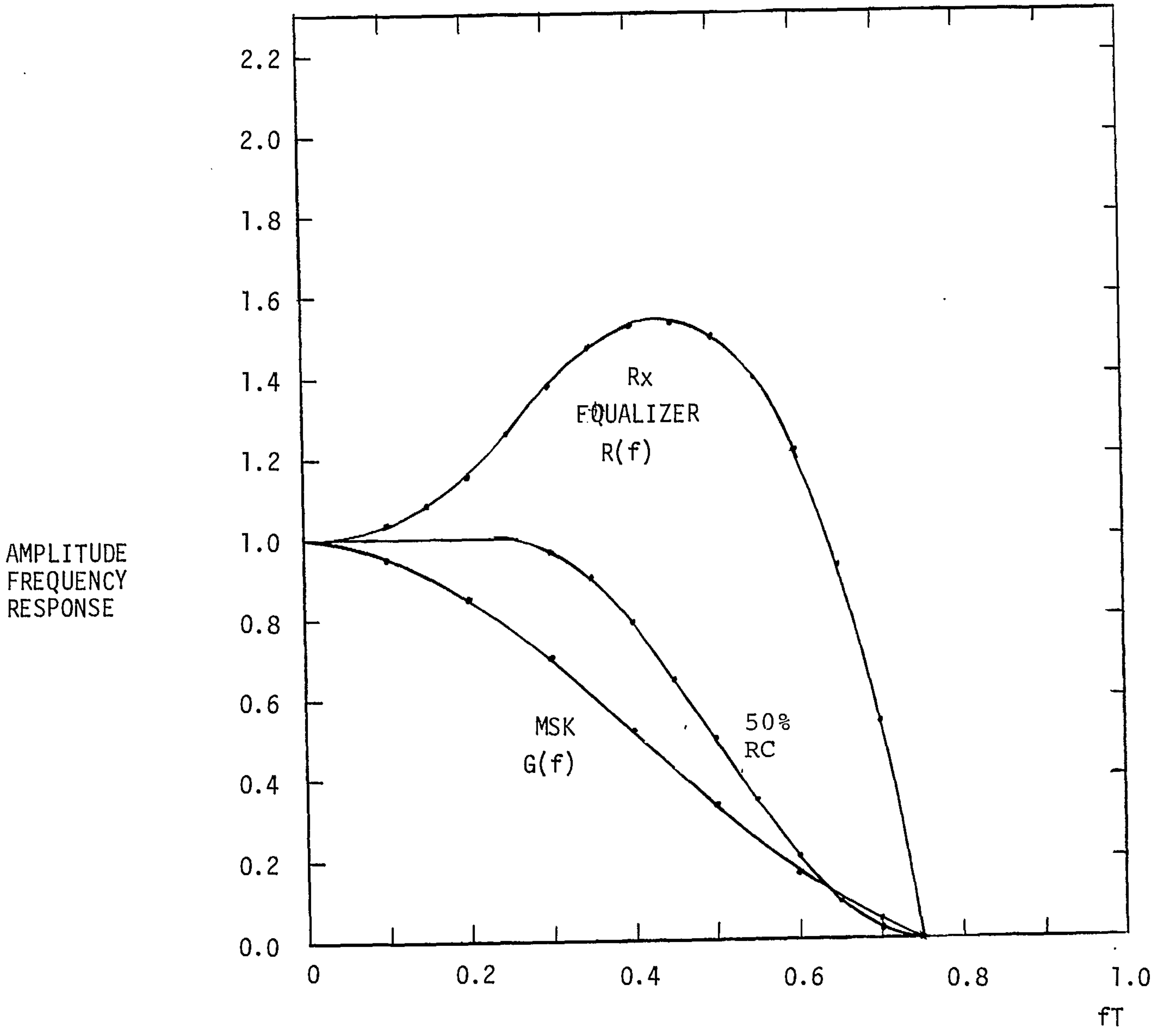

Figure 5.1 Required Filtering To Create 50% Roll-Off Raised Cosine (RC) Signal Spectrum.

5.2 Theoretical And Simulated Performance

From (5.1) the constant signal power is simply

$$P_s = \frac{A^2}{2} \tag{5.7}$$

Given the noise power, $P_n = \sigma^2$, and the assumption of no ISI, it is a well known result [15] that the probability of bit error for the conventional DMSK detector is given by

$$P_e = \frac{1}{2}\exp(-SNR) \tag{5.8}$$

where

$$SNR = \frac{P_s}{P_n} = \frac{A^2}{2\sigma^2} \tag{5.9}$$

The differential detector performs optimally only when the transmitted signal is Nyquist, i.e. when the signal format is such that matched filtering may be used at the receiver and the resultant signal is free of ISI. For this case the instantaneous signal to noise ratio at the desired comparison points is given by $SNR = E_b/N_o$ where E_b is the received energy per bit and N_o is the single sided noise power spectral density. Thus the corresponding probability of bit error is given by

$$P_e = \frac{1}{2}\exp(-E_b/N_o) \tag{5.10}$$

The DMSK signal format does not possess the above desired property and thus must be associated with inferior performance from that of (5.10).

If we use the equalizer defined in (5.6) then ISI is eliminated and the probability of bit error (assuming uncorrelated noise samples) is given by (5.8), where the noise power is given by

$$P_n = \int_{-\infty}^{\infty} |R(f)|^2 \, N_o \, df \tag{5.11}$$

$$= \frac{N_o}{T} (I_1 + I_2) \tag{5.12}$$

where

$$I_1 = 2 \int_{o}^{.25} \left[\frac{\pi}{4} \, \frac{1-(4\gamma)^2}{\cos 2\pi\gamma}\right]^2 d\gamma \tag{5.13}$$

and

$$I_2 = 2 \int_{.25}^{.75} \left[\frac{\pi}{8} \, (1 + \sin 2\pi\gamma) \, \frac{1-(4\gamma)^2}{\cos 2\pi\gamma}\right]^2 d\gamma \tag{5.14}$$

Numerical integration of (5.13) and (5.14) yields

$$I_1 + I_2 = 1.3835 \tag{5.15}$$

Thus the noise power is given by

$$P_n = \sigma^2 = 1.3835 \, \frac{N_o}{T} \tag{5.16}$$

and the probability of bit error by

$$P_e = \frac{1}{2} \exp\left[\frac{-A^2 T}{2N_o 1.3835}\right] \tag{5.17}$$

$$= \frac{1}{2} \exp\left[-.7228 \frac{E_b}{N_o}\right] \tag{5.18}$$

Thus with the assumption of uncorrelated noise samples we conclude that the conventional DMSK detector with the receive filter specified in (5.6) is -10 log .7228 = 1.41 dB worse than the ideal performance specified in (5.10), for which this type of differential detection device is capable. Because the noise correlation will not be zero, actual performance is expected to vary slightly from this result. This will be discussed later.

With SEC performance should be improved, but 1 dB improvements as exhibited for other filters which cause ISI are not to be expected, as the improvement exhibited with SEC increases with the amount of ISI. An empirical relationship relating the bit error rate into (P_i) the SEC device and the resulting output bit error rate (P_o), assuming no ISI, is given by [12]

$$P_o \simeq 0.89\, P_i^{1.06} \tag{5.19}$$

Then from (5.8) the corresponding SNR required to yield BER's of P_i and P_o are

$$SNR_i = -\ln 2P_i \tag{5.20}$$

$$SNR_o = \frac{-1}{1.06} \ln \frac{2P_o}{0.89} \tag{5.21}$$

Thus for the same BER, $P = P_i = P_o$, the improvement in dB with SEC is given by

$$I_{SEC} = 10 \log \frac{SNR_i}{SNR_o} \text{ (dB)} \tag{5.22}$$

$$= 10 \log \frac{1.06 \ln 2P}{\ln 2.247P} \text{ (dB)} \tag{5.23}$$

Using results (5.18) and (5.23), the degradations from ideal CMSK for conventional DMSK and with SEC are tabulated in Table 5.2 for a number of BER's. Also included in this table is the degradation for differentially encoded CMSK. These results are plotted in Figure 5.2 for comparison. As well as these three schemes, ideal differential detection is also shown in Figure 5.2, where performance is given by (5.10), and is 1.41 dB better than conventional DMSK for all BER's.* As can be seen from this figure, for a BER of 10^{-6}, DMSK with SEC is within 1.8 dB of CMSK and within 1.55 dB of coherent detection of differentially encoded CMSK.

Simulated performance for this Rx filter is shown in Figure 5.3 for conventional DMSK and with SEC. Also shown is the performance for ideal CMSK and coherent detection of differentially encoded CMSK. Although simulated performance for conventional DMSK is fairly close to theoretical, a noticeable discrepancy is observed. As stated earlier the theoretical performance is based on the assumption of independent noise samples. If a positive correlation exists between noise samples one bit period apart then actual performance is expected to be better than

*Since the asymptotic degradation for ideal differential detection is 0 dB, the asymptotic degradation for DMSK with the equalizer is 1.41 dB as a result of the fixed noise power enchancement.

	DEGRADATION FROM CMSK (dB)		
		DMSK (Rx = Equalizer)	
BER	DIFF. CMSK	CONVENTIONAL	WITH SEC
10^{-1}	2.05	4.34	3.76
10^{-2}	0.87	3.00	2.61
10^{-3}	0.54	2.56	2.22
10^{-4}	0.40	2.31	2.00
10^{-5}	0.30	2.16	1.86
10^{-6}	0.25	2.07	1.78
0.0	0.0	1.41	1.41

Table 5.2 Theoretical Comparison of 3 Detection Schemes Against Ideal CMSK

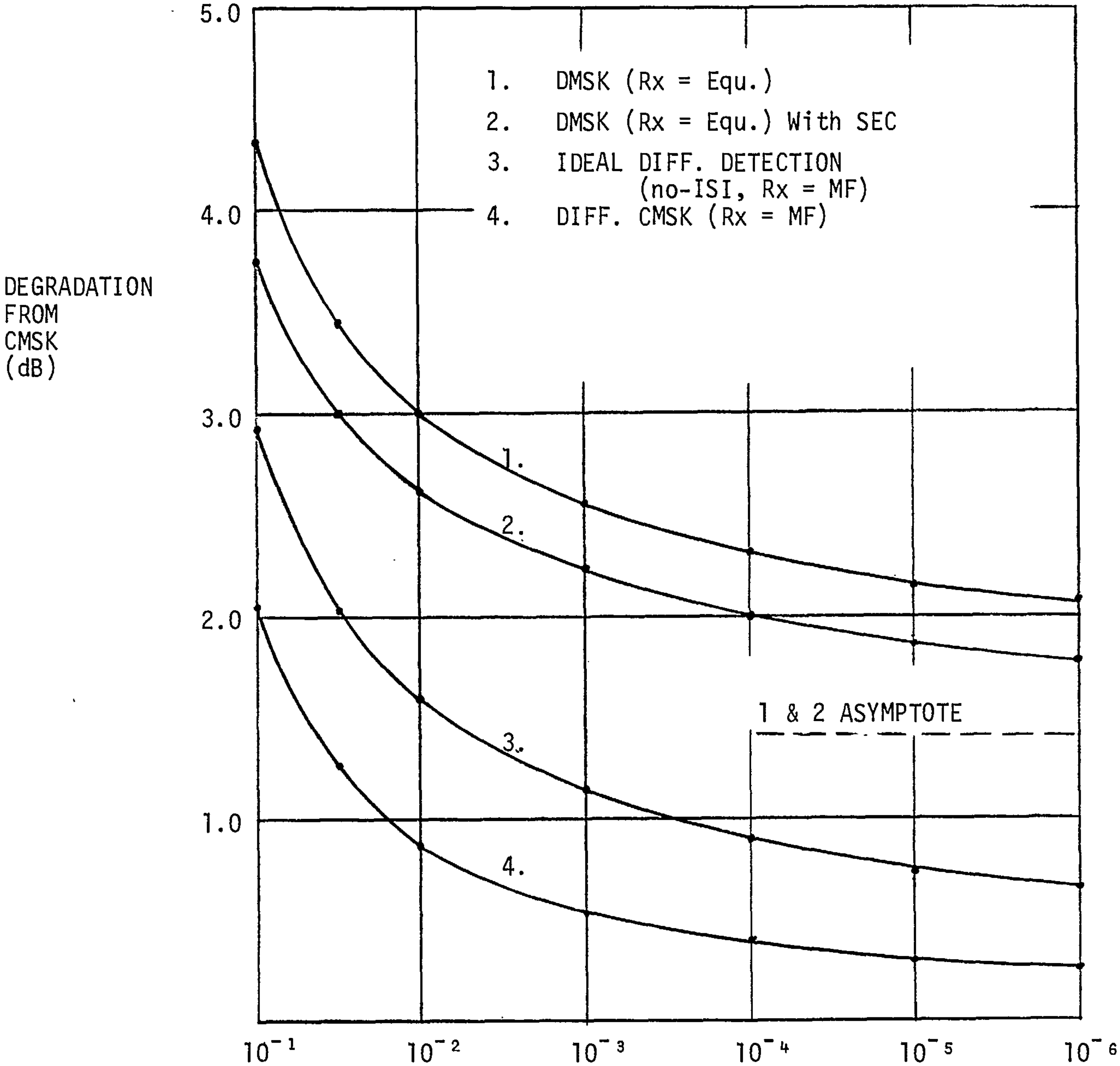

Figure 5.2 Theoretical Comparison Of 4 Detection Schemes Against Ideal CMSK. Note: DIFF.CMSK refers to coherent detection of differentially encoded CMSK.

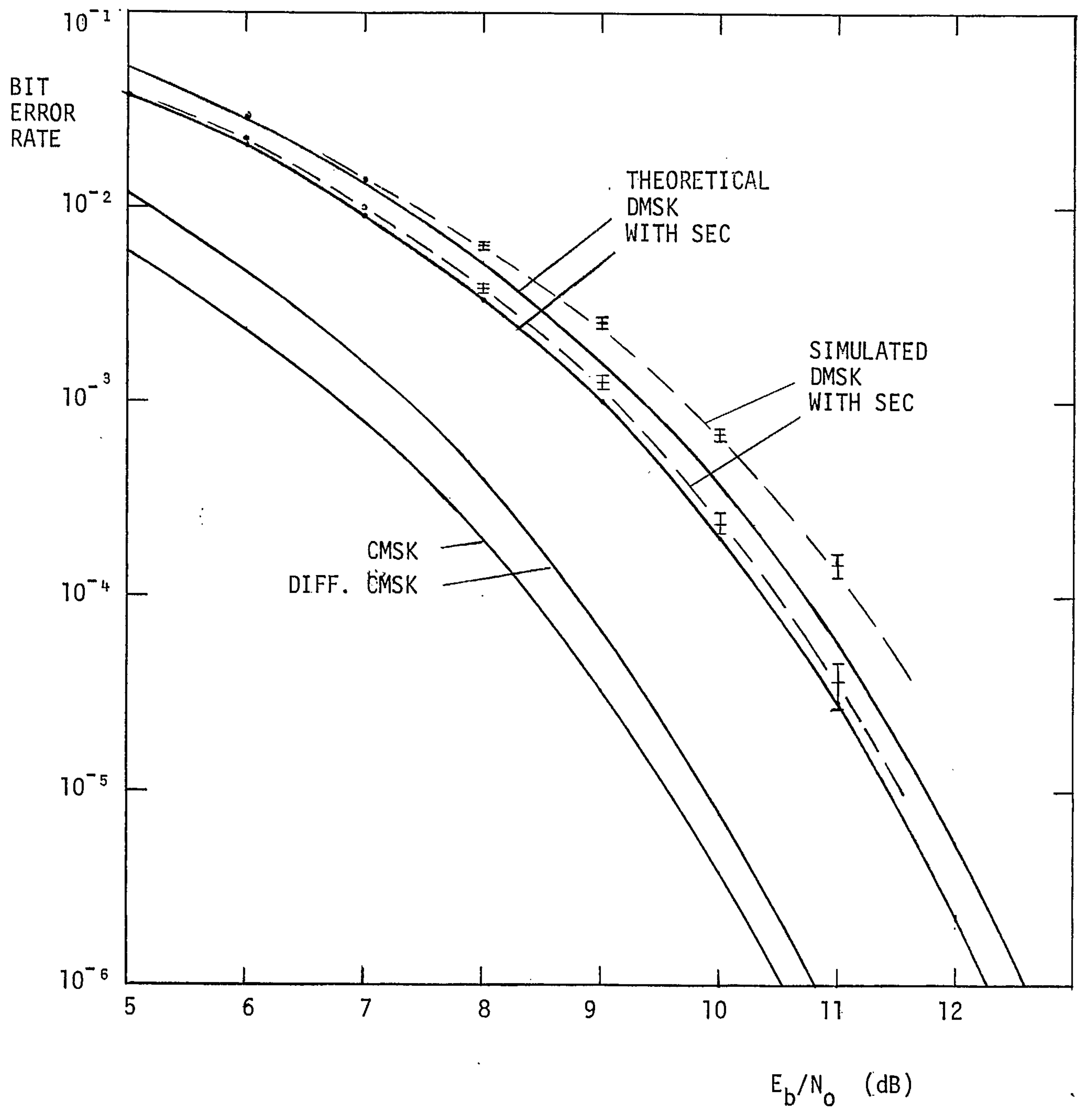

Figure 5.3 Theoretical And Simulated DMSK Performance With Receive Filter Equalization

theoretical for a differential detection device [18]. As shown in Section 5.2.1 below the relevant correlation coefficient for the conventional branch is actually -0.3778, which is far from negligible and is negative, and thus implies that performance is expected to be slightly worse than theoretical. The simulation results bear this out by exhibiting a 0.5 dB degradation from theoretical at a BER of 10^{-4}. Fortunately the SEC device appears to have little difficulty correcting for errors caused by negative noise correlation in the conventional branch. Furthermore, the noise correlation coefficient for the parity bit branch is computed to be 0.1227, which is to the advantage of the SEC device. The overall result is that simulated performance with SEC is almost identical to predicted theoretical performance with SEC.

A computer simulated eye pattern is shown in Figure 5.4. As expected the eye is completely open at the correct sampling time.

5.2.1 Calculation of Noise Correlation

The equivalent baseband autocorrelation of the noise at the output of the R_x filter is given by

$$C(\tau) = F^{-1}[R(f)^2]$$

$$= \int R(f)^2 \, e^{j2\pi f\tau} df \qquad (5.24)$$

where R(f) is the receive filter defined by (5.3), (5.4) and (5.6). The correlation coefficient between noise samples n bit periods apart is thus

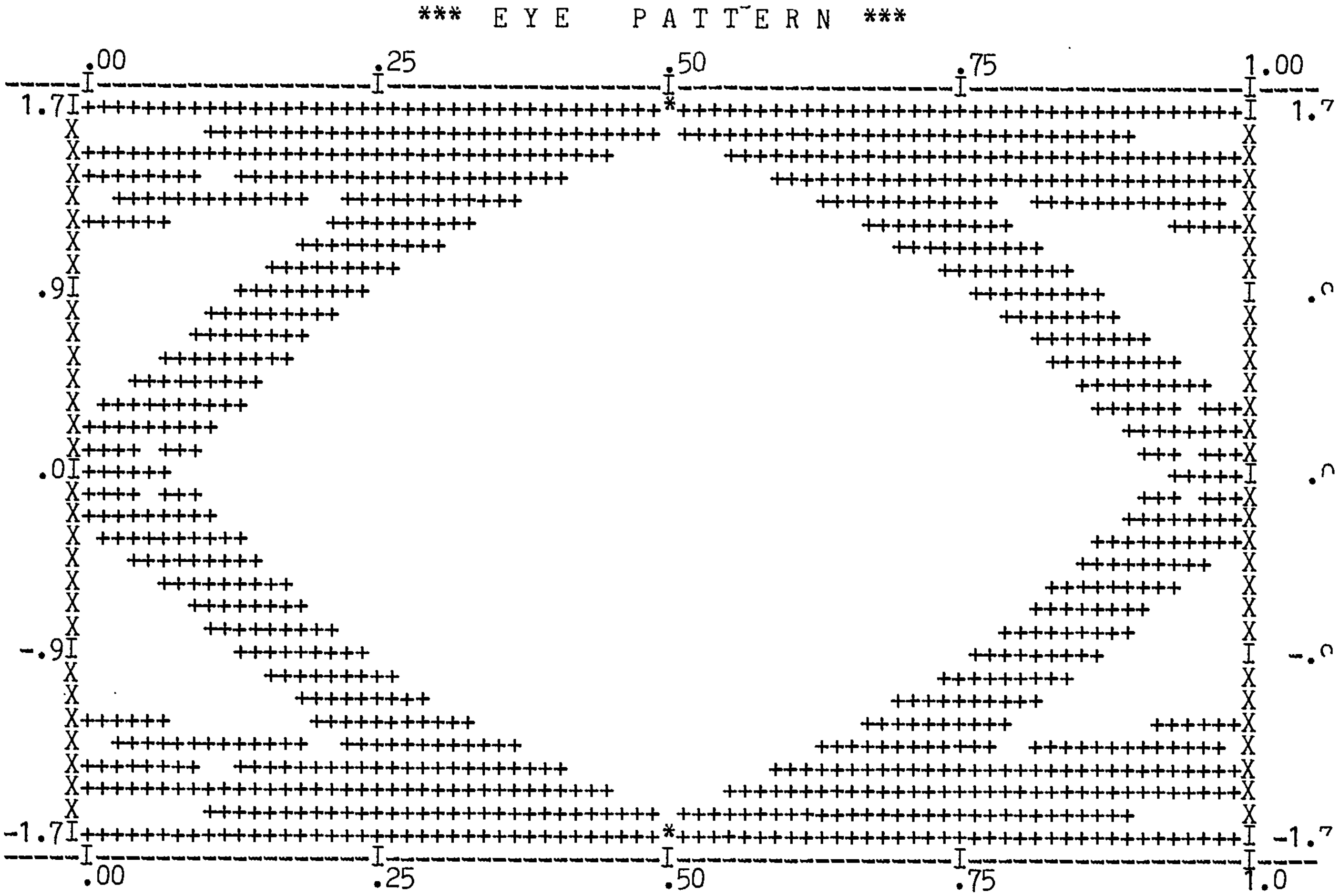

* SAMPLING INSTANT.

FIRST BIT SAMPLED = 1
NUMBER OF BITS PLOTTED = 511
STOP 0

Figure 5.4 Computer Simulated Eye Pattern For Receive Filter Equalization

$$\rho_n = \frac{C(nT)}{C(0)} \tag{5.25}$$

Of interest are ρ_1 and ρ_2 which are directly related to the performance of the conventional and parity bit branches of the detector. Using the symmetric and bandlimited properties of R(f) we can write

$$C(\tau) = 2 \int_{o}^{.75/T} R(f)^2 \cos(2\pi f\tau)\, df \tag{5.26}$$

By numerical integration using Simpson's rule we obtain

$$\rho_1 = -0.3778 \tag{5.27}$$

and

$$\rho_2 = 0.1227 \tag{5.28}$$

5.3 Optimum Filters

Although the receive filter described above gives good performance and is probably close to optimum for BER's approaching zero, it is by no means obvious that this filter is best for a prespecified BER specification. This is especially true with the addition of SEC, because a small amount of ISI (in proportion to the noise power) can always be tolerated with a corresponding reduction in noise power. Thus we desire a filter which is somewhere between the equalizer, R(f), and the matched filter, G(f). One possible approach to finding better filters would be to investigate the family of filters given by

$$R_\gamma(f) = \gamma R(f) + (1-\gamma)\, G(f) \tag{5.29}$$

or

$$R_\gamma(f) = \left[\gamma R(f)^2 + (1-\gamma) G(f)^2\right]^{\frac{1}{2}} \tag{5.30}$$

where γ is a value between 0 and 1 and R(f) and G(f) are as shown in Figure 5.1. When γ equals 0 and 1 we obtain the matched filter and equalizer respectively. In the case of (5.29) we easily see from the linear property of Fourier transforms, that the output is a linear combination of the no-ISI raised cosine pulse x(t), and the matched filter pulse $m(t) = g(t)*g(t)$. Since the ISI is contributed only from the matched filter pulse we can linearly adjust the amount of ISI with the parameter γ, and make a trade-off with the noise power. In the case of (5.30) if we assume G(f) is normalized to give the same amplitude output, then the noise power is easily determined by

$$\begin{aligned} P_n &= \int N_o \left|R_\gamma(f)\right|^2 df \\ &= \gamma \int N_o \left|R(f)\right|^2 df + (1-\gamma) \int N_o \left|G(f)\right|^2 df \\ &= \frac{N_o}{T}\left[\gamma\ 1.3835 + (1-\gamma)\right] \\ &= \frac{N_o}{T}\left[1 + \gamma\ .3835\right] \end{aligned} \tag{5.31}$$

where the result of (5.16) has been used. Thus the noise power is easily set by γ, but the signal power and amount of ISI is not quite as easily determined, except for the two extremes.

For each family of filters, a unique γ must exist which minimizes the required E_b/N_o to obtain a prespecified BER.

5.4 Realizability

Realizability of the filters described above has not been addressed. Certainly the Rx equalizer shown in Figure 5.2 is not easily implemented because ideally it demands finite bandwidth, zero or linear phase response, and significant mid-channel spectrum enhancement. The family of filters described in Section 5.3 may be slightly easier to implement due to the reduced demand for mid-channel enhancement. It is interesting to note that the Gaussian and Butterworth filters investigated in Section 4.2 for the most part lie between the matched filter and the no-ISI equalizer described above. Further, performance with SEC and the 4-th order Butterworth (linear phase) Rx filter with BT product of 1.1 was shown to be within 1.9 dB of CMSK for a BER of 5×10^{-4}. From Figure 5.2 the corresponding degradation for the no-ISI equalizer is approximately 2.2 dB. Thus for this particular BER the Butterworth is 0.3 dB better than the no-ISI equalizer, and may even be close to the optimum filter shape which would be found if the search technique of Section 5.3 were used.

6.0 ISI INVESTIGATION AND ADAPTIVE THRESHOLDING

The DMSK receiver structure, consisting of the conventional and parity bit branches, is shown in Figure 6.1. Normally a zero-threshold device is placed at the output of each demodulator (points A and B). If ISI is present and the previous decision (from either branch) is known, then given this a priori knowledge the optimum threshold level for the current decision is not necessarily zero. The proposed modification is shown in Figure 6.2, where one of these adaptive threshold devices is placed at both points A and B, replacing the single zero-threshold devices. The simple concept is as follows. If the previous decision was positive then (assuming a positive ISI contribution) the next signal level will be biased in the positive direction. This bias may be removed by using a positive threshold device. Similarly for a negative decision. The technique is really nothing more than decision feedback ISI cancelation, assuming only 1 backward ISI contribution.

The optimum threshold level is not as easy to deduce as one might expect, due to the non-linear operation of multiplying 2 noisy signals just prior to the threshold device. In fact, it turns out that the optimum threshold device for the parity bit branch is not even the same as that for the conventional bit branch.

In the following sections the effects of ISI and Noise are investigated, optimum threshold levels are found, and simulated performance with adaptive thresholding is presented.

6.1 Definitions

Since we are only concerned with T spaced samples of the output waveforms, a discrete complex baseband signalling format is assumed. We define $u_e(k)$ and $u_o(k)$ as shown in Figure 6.3, and

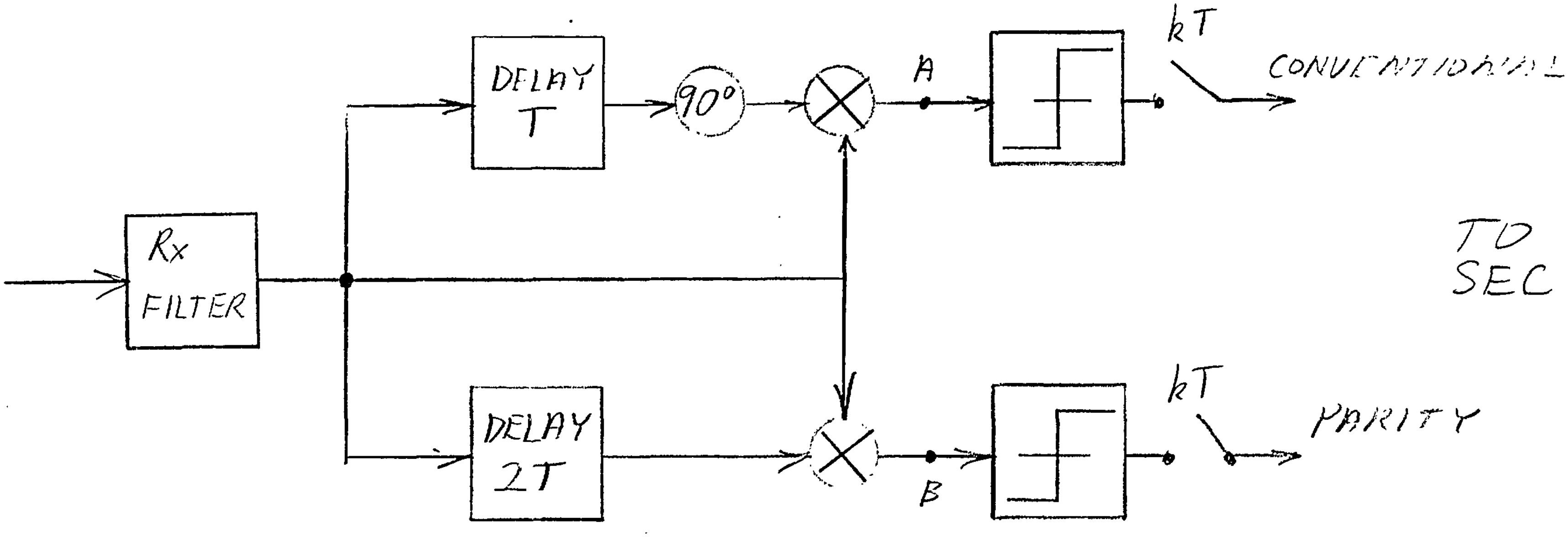

Figure 6.1 Differential Detector For Conventional And Parity Bits

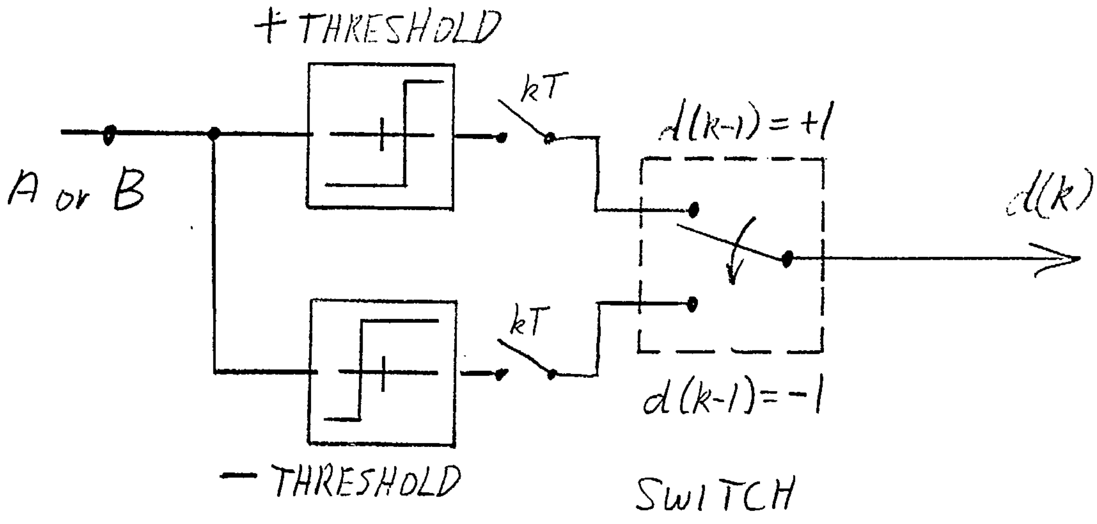

(a) Concept

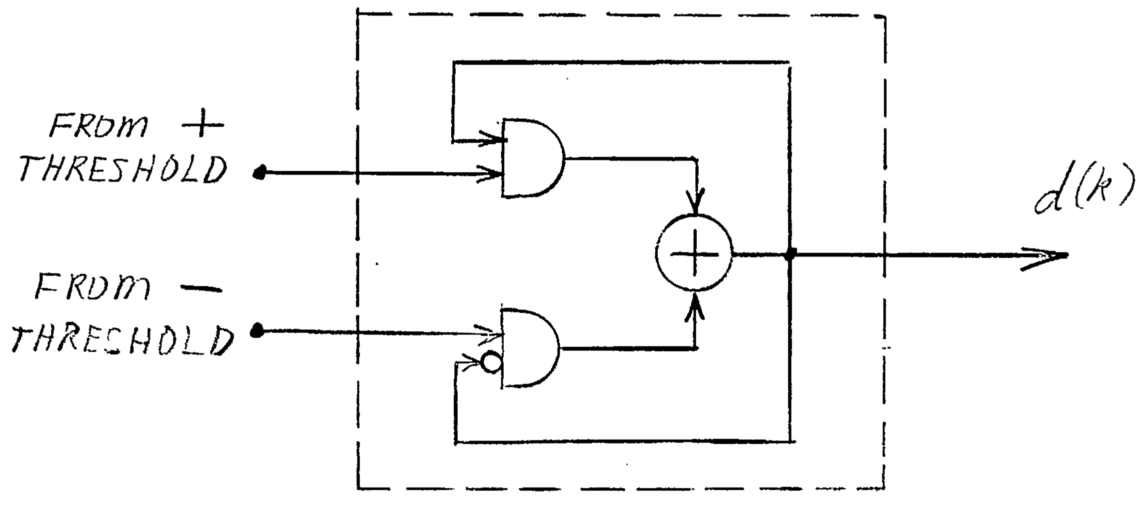

(b) Switch Implementation

Figure 6.2 Adaptive Thresholding

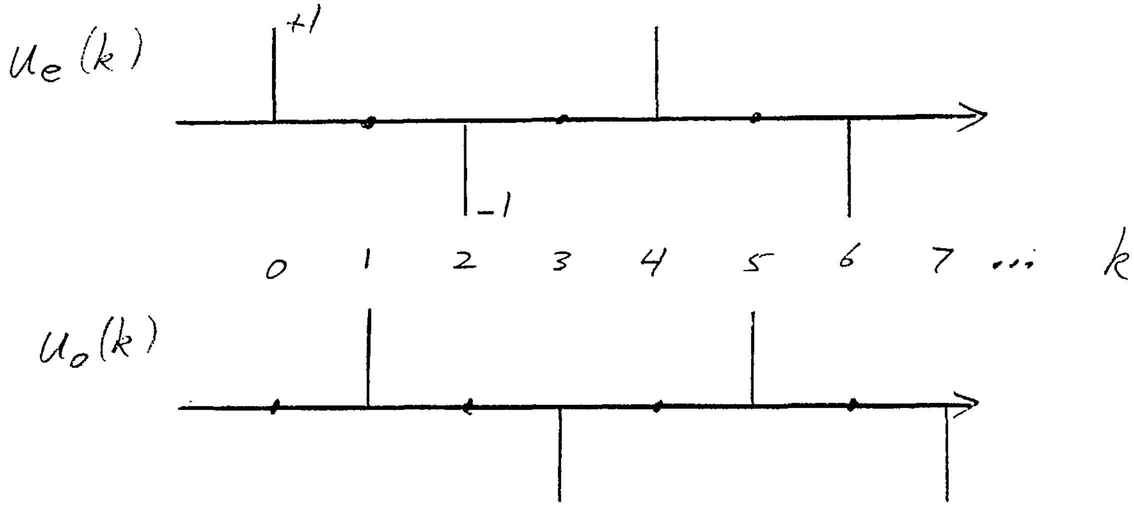

Figure 6.3   Even And Odd Numbered Functions

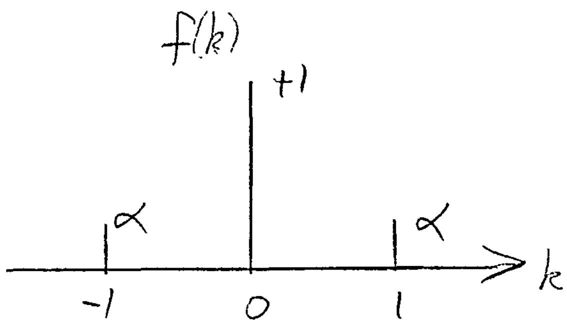

Figure 6.4   Discrete Rx Filter Causing ISI

$$u(k) \triangleq u_e(k) + ju_o(k) \tag{6.1}$$

Useful properties of u(k) are:

$$u(k+1) = ju(k) \tag{6.2}$$

$$u(k-1) = -ju(k) \tag{6.3}$$

$$|u(k)|^2 = u_e(k)^2 + u_o(k)^2 = 1 \tag{6.4}$$

Let the binary data be denoted by a(k) where

$$a(k) = \pm 1 \tag{6.5}$$

The differentially encoded data will be denoted by e(k) where

$$e(k) = -a(k) \cdot e(k-1) \tag{6.6}$$

In keeping with complex envelope notation used in Section 3.0 the transmitted digital signal is given by

$$s(k) = e(k) \cdot u^*(k) \tag{6.7}$$

The received signal (after Rx filtering) is given by

$$r(k) = s(k) * f(k) + n(k) \tag{6.8}$$

where n(k) is a complex noise sequence given by

$$n(k) = n_I(k) + jn_Q(k) \tag{6.9}$$

and $n_I(k)$ and $n_Q(k)$ are assumed independent and Gaussianly distributed with variance σ^2. For notational convenience the noise is defined as being added after the receive filter, with impulse response f(k), which is assumed to introduce the undesired ISI.

The demodulated signal will be denoted as d(k) for both the conventional and parity bit branches, with the context making the usage obvious. The demodulated signals are given by:

Conventional: $d(k) = \text{Re}\left[-jr(k)r^*(k-1)\right]$ (6.10)

Parity: $d(k) = \text{Re}\left[r(k)r^*(k-2)\right]$ (6.11)

The parity of two adjacent information bits is defined as

$$p(k) = -a(k)\cdot a(k-1) = -e(k)\cdot e(k-2)$$

As a quick check, assuming no noise and no ISI the output from the conventional branch, given by (6.10), is

$$\begin{aligned} d(k) &= \text{Re}\left[-js(k)\ s^*(k-1)\right] \\ &= \text{Re}\left[-je(k)u^*(k)e(k-1)\ u(k)(-j)\right] \\ &= -e(k)e(k-1)\left|u(k)\right|^2 \\ &= a(k) \end{aligned} \tag{6.13}$$

which is the expected result.

Similarly, the output from the parity bit branch, given by (6.11), is

$$\begin{aligned} d(k) &= \text{Re}\left[s(k)s^*(k-2)\right] \\ &= \text{Re}\left[e(k)u^*(k)\ e(k-2)\cdot u(k)(-1)\right] \\ &= -e(k)e(k-2)\left|u(k)\right|^2 \\ &= p(k) \end{aligned} \tag{6.14}$$

which is the expected result.

6.2 ISI And No Noise

We assume the Rx filter causes symmetric ISI of amplitude α, as depicted in Figure 6.4. We want to determine the signal contributions due to ISI at the output of each demodulator, thus for this case we assume no noise. From (6.8) the noiseless signal at the output of the Rx filer is given by

$$\begin{aligned} r(k) &= f(k) * s(k) \\ &= \alpha s(k+1)+s(k)+\alpha s(k-1) \\ &= \left[\alpha e(k+1)(-j)+e(k)+\alpha e(k-1)j\right]u^*(k) \end{aligned} \tag{6.15}$$

As shown in Appendix C the output of the conventional branch of the detector is given by

$$d(k) = a(k)\left[1-\alpha^2-\alpha^2 a(k-1)a(k+1)\right] + \alpha^2 a(k-1) + \alpha^2 a(k+1) \tag{6.16}$$

and is tabulated in Table 6.1. Also derived in Appendix C, the output of the parity bit branch is given by

$$d(k) = p(k) + \alpha^2 + \alpha^2 p(k-1) + \alpha^2 p(k+1) + \alpha^2 p(k-1)\ p(k+1) \tag{6.17}$$

and is tabulated in Table 6.2. Note that equation (6.16) is independent of the parity bits, $p(k)$, and that (6.17) is independent of the information bits, $a(k)$. Thus communication between the two branches is not required if adaptive thresholding is to be used.

From Tables 6.1 and 6.2 we can sketch the expected eye patterns for both branches of the receiver. These sketches are shown in Figure 6.5, where straight lines have been used to join up the known signal levels at the correct sampling times. For confirmation, computer generated eye patterns

a(k-1)	a(k)	a(k+1)	d(k)
−	−	−	−1
−	−	+	−1
−	+	−	$+1-4\alpha^2$
−	+	+	+1
+	−	−	−1
+	−	+	$-1+4\alpha^2$
+	+	−	+1
+	+	+	+1

TABLE 6.1 Conventional Branch Output Levels With ISI

p(k-1)	p(k)	p(k+1)	d(k)
−	−	−	−1
−	−	+	−1
−	+	−	1
−	+	+	1
+	−	−	−1
+	−	+	$-1+4\alpha^2$
+	+	−	1
+	+	+	$1+4\alpha^2$

TABLE 6.2 Parity Branch Output Levels With ISI

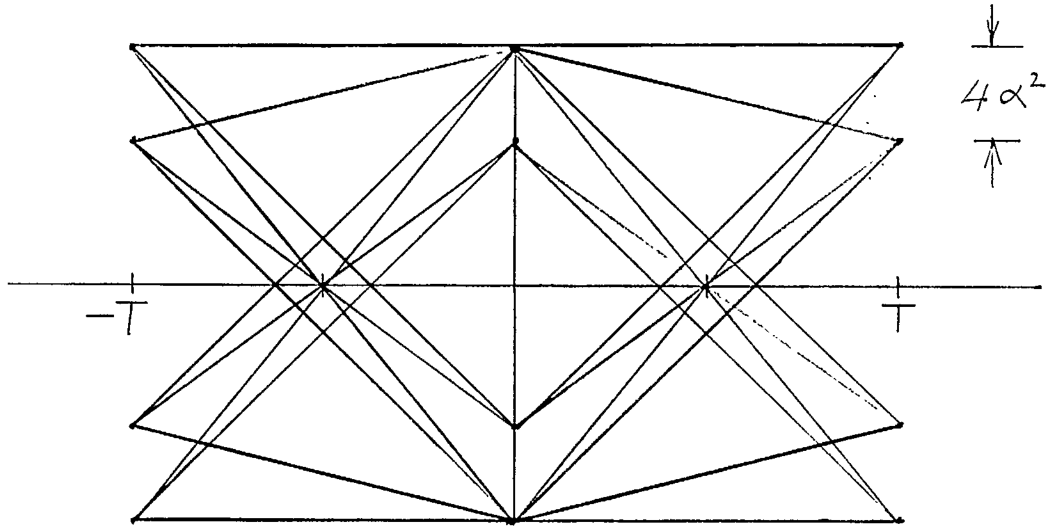

(a) Conventional DMSK Branch

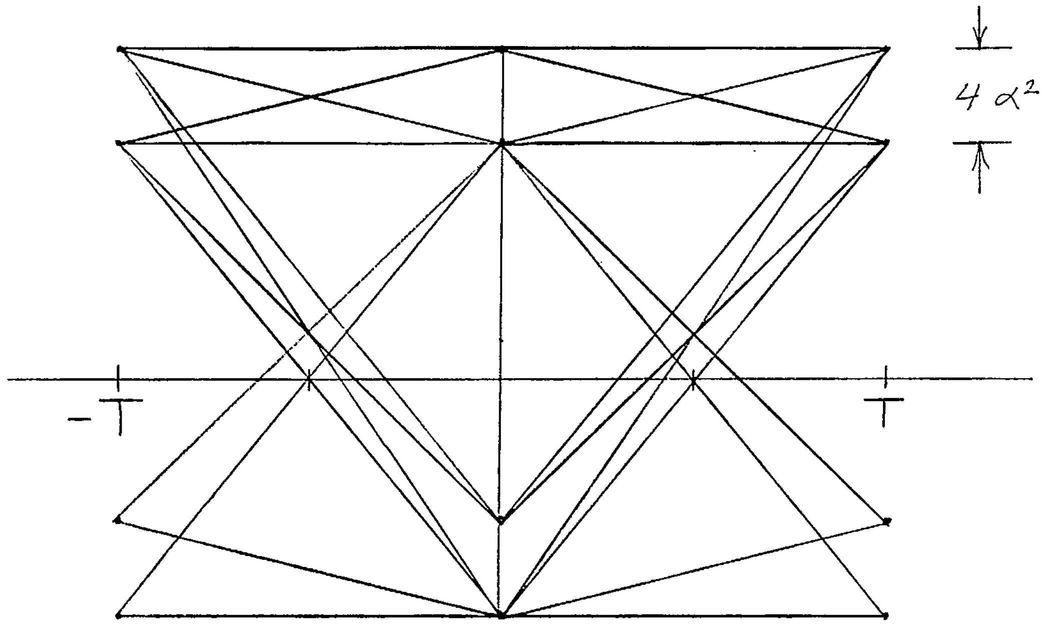

(b) Parity Bit Branch

Figure 6.5 Expected Eye Patterns Based On Mathematical Analysis are shown in Figure 6.6 for a 512 bit PN sequence and matched filtering. When matched filtering is used the ratio of adjacent ISI to the desired signal level is α = .318, which yields a maximum deviation from the desired signal level of

$$4(.318)^2 \times 100 = 40\%$$

From Figure 6.6 we can see that this is indeed the case.

Of interest are the expected signal levels with and without knowing the last bit or decision. If we assume the information and parity bits are independent and equally likely and we do not know the last decision made, then the expected signal levels are given by,

Conventional:

$$E[d(k)] = 0 \tag{6.18}$$

Parity:

$$E[d(k)] = \alpha^2 \tag{6.19}$$

The interesting observation here is that a dc offset exists in the parity branch, which indicates that the optimum threshold level for this branch is not zero even when adaptive thresholding is not used. Of course if no ISI exists then the optimum threshold is zero. If we now assume we know the last information and parity bits, then the expected signal levels are given by,

Conventional:

$$E[d(k) \mid a(k-1)] = \alpha^2 \; a(k-1) \tag{6.20}$$

Parity:

$$E[d(k) \mid p(k-1)] = \alpha^2+\alpha^2 p(k-1) \tag{6.21}$$

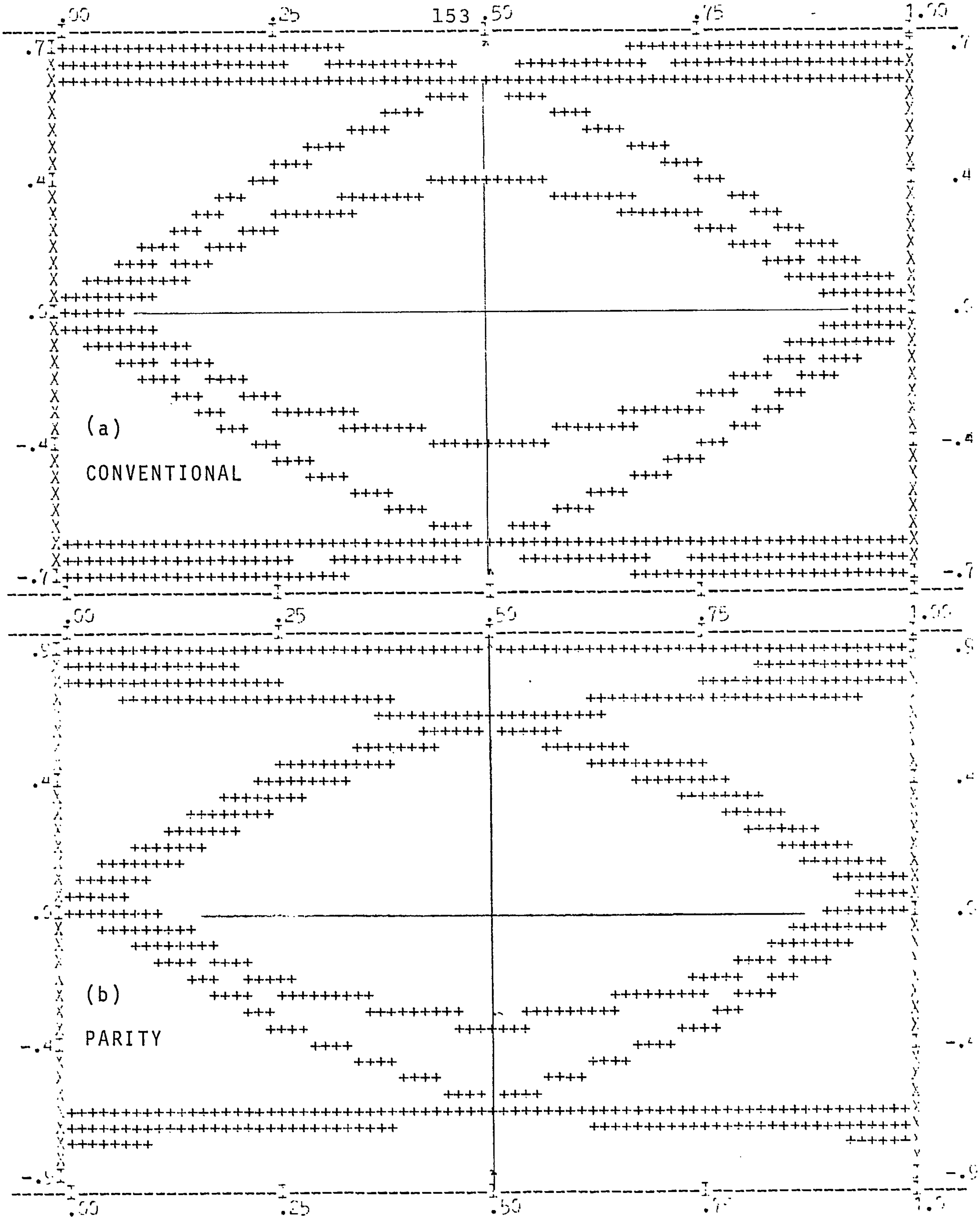

Figure 6.6 Computer Generated Eye Patterns Using A Matched Rx Filter

Thus the expected signal levels are indeed a function of the previous bits, indicating that there may indeed be something to be gained through adaptive thresholding. Equations (6.20) and (6.21) do not however tell us the optimum levels to be used. In order to determine the optimum threshold levels we must first determine the noise characteristics.

6.3 ISI And Noise

We are interested in the characteristics of the noise at the time of thresholding. We will consider the conventional branch first. From (6.8), the filtered received signal with noise is given by

$$r(k) = s_1(k) + n(k) \tag{6.22}$$

where

$$s_1(k) = s(k)*f(k) \tag{6.23}$$

Thus from (6.10) the input to the threshold device is given by

$$\begin{aligned} d(k) &= \mathrm{Re}\left[-jr(k)\cdot r^*(k-1)\right] \\ &= \mathrm{Re}\left[-js_1(k)s_1^*(k-1)-jn(k)s_1^*(k-1)-js_1(k)n^*(k-1)\right. \\ &\quad \left. -jn(k)n^*(k-1)\right] \end{aligned} \tag{6.24}$$

The first term in (6.24) we recognize as the signal input without noise, thus the remaining three terms constitute the noise at the input to the threshold device. If we denote this noise term as $w(k)$, then as shown in Appendix C, the mean and variance of $w(k)$ are given by

$$e\left[w(k)\right] = 0 \tag{6.25}$$

$$V = E[w^2(k)]$$
$$= 2(\sigma^2+\sigma^4) + \alpha^2(4+p(k)+p(k+1))\sigma^2 \qquad (6.26)$$

Similarly, for the parity bit branch the input to the threshold device is given by

$$d(k) = \text{Re}[r(k)r^*(k-2)] \qquad (6.27)$$

$$= \text{Re}[s_1(k)s_1^*(k-2) + n(k)s_1^*(k-2) + s_1(k)n^*(k-2)$$

$$+n(k)n^*(k-2)] \qquad (6.28)$$

where the noise w(k) is given by the last three terms in (6.28) and has mean and variance given by

$$E[w(k)] = 0 \qquad (6.29)$$

$$V = E[w^2(k)]$$

$$= 2(\sigma^2+\sigma^4) + \alpha^2(4+p(k-1) + p(k+1))\sigma^2 \qquad (6.30)$$

From (6.25) and (6.29) we conclude that the noise at the input to the threshold device does not contain a bias for either branch (assuming independent noise samples). From (6.26) and (6.30) we see that the noise power is a function of both the ISI and the parity bits. Taking the expected value of (6.26) and (6.30) with respect to the parity bits, we obtain the average noise power,

$$\overline{V} = 2(\sigma^2 + \sigma^4) + 4\alpha^2\sigma^2 \qquad (6.31)$$

which is the same for both branches. The difference between the actual and the average noise power is tabulated in Tables 6.3 and 6.4 for the conventional and parity bit branches respectively.

With the above noise characteristics determined we now proceed to try and find the optimum threshold levels.

a(k-1)	a(k)	a(k+1)	p(k)	p(k+1)	$\frac{V-\overline{V}}{\alpha^2\sigma^2}=p$
−	−	−	−	−	−2
−	−	+	−	+	0
−	+	−	+	+	2
−	+	+	+	−	0
+	−	−	+	−	0
+	−	+	+	+	2
+	+	−	−	+	0
+	+	+	−	−	−2

TABLE 6.3 Conventional Branch Noise Power Deviations From Average

p(k-1)	p(k)	p(k+1)	$\frac{V-\overline{V}}{\alpha^2\sigma^2} = p$
−	−	−	−2
−	−	+	0
−	+	−	−2
−	+	+	0
+	−	−	0
+	−	+	2
+	+	−	0
+	+	+	2

TABLE 6.4 Parity Branch Noise Power Deviations From Average

6.4 Optimum Threshold Levels

If one looks at the derivations of (6.26) and (6.30) in Appendix C, it is seen that of all the noise components added together to give w(k), only one is not Gaussian distributed. This term is the noise times noise term which has variance $2\sigma^4$. For large signal-to-noise ratios (SNR) the power due to this term becomes very small compared to the other noise contributions. Thus for the purpose of finding threshold levels, a reasonable approximation is that w(k) is Gaussianly distributed with mean zero and variance given by equations (6.26) and (6.30) for the conventional and parity branches of the receiver respectively.

Let the variance of w(k) be given as

$$V(\sigma,p) = 2(\sigma^2+\sigma^4) + \alpha^2(4+p)\sigma^2 \tag{6.32}$$

where p is the parameter which determines the deviation from the average variance and is given by

$$p = \frac{V - \overline{V}}{\alpha^2\sigma^2} \tag{6.33}$$

as given in Tables 6.3 and 6.4, and σ^2 is the variance of the received noise as defined in (6.9).

The probability of a zero-mean Gaussian random variable, with variance b, being greater than level z is given by

$$Q(z,b) = \int_z^\infty \frac{1}{\sqrt{2\pi b}} \exp\left(-\frac{x^2}{2b}\right) dx \tag{6.34}$$

If the level, z, is a function of the threshold, β, then

$$Q'(z,b) \triangleq \frac{dQ(z,b)}{d\beta} \tag{6.35}$$

$$= \frac{dQ(z,b)}{dz} \cdot \frac{dz}{d\beta} \tag{6.36}$$

$$= \frac{-1}{\sqrt{2\pi}} \quad f(z,b) \cdot \frac{dz}{d\beta} \tag{6.37}$$

where

$$f(z,b) = \frac{1}{\sqrt{b}} \quad \exp\left(\frac{-z^2}{2b}\right) \tag{6.38}$$

For the conventional branch, from Tables 6.1 and 6.3 we conclude that the probability of bit error, given $a(k-1) = +1$, is approximately given by

$$\begin{aligned} Pe = {} & \tfrac{1}{4} \cdot Q\,(1 + \beta,\ V(\sigma,\ 0)) \\ & + \tfrac{1}{4} \cdot Q\,(1 - 4\alpha^2 + \beta,\ V\,(\sigma,\ 2)) \\ & + \tfrac{1}{4} \cdot Q\,(1 - \beta,\ V(\sigma,\ 0)) \\ & + \tfrac{1}{4} \cdot Q\,(1 - \beta,\ V(\sigma,\ -2)) \end{aligned} \tag{6.39}$$

To minimize the probability of error with respect to the threshold β we simply differentiate and set equal to zero. From (6.37), the resulting transcendental equation for the optimum threshold, β, is given by

$$\begin{aligned} F_c(\beta) = {} & -f(1+\beta,\ V(\sigma,0)) - f(1-4\alpha^2+\beta,\ V(\sigma,2)) \\ & +f(1-\beta,\ V(\sigma,0)) + f(1-\beta, V(\sigma,-2)) \\ = {} & 0 \end{aligned} \tag{6.40}$$

Due to symmetry we easily conclude that $-\beta$ is the optimum threshold level given $a(k-1) = -1$.

For the parity bit branch the optimum threshold is not the same for both plus and minus values of $p(k-1)$. Similar to the derivation of (6.40), the transcendental equation which defines the optimum threshold, β, for $p(k-1) = +1$, is given by

$$F_p(\beta) = -f(1+\beta,\ V(\sigma,0)) - f(1-4\alpha^2+\beta,\ V(\sigma,2))$$

$$+ f(1-\beta, V(\sigma,0)) + f(1+4\alpha^2-\beta, V(\sigma,2))$$

$$= 0 \tag{6.41}$$

where Tables 6.2 and 6.4 have been used. When $p(k-1) = -1$ it is easily seen that the resulting symmetry forces the optimum threshold level to be given by $\beta=0$.

The optimum threshold levels defined by (6.40) and (6.41) have been computed using a simple binary search technique. Figures 6.7 and 6.8 show the respective resulting optimum threshold levels as a function of the no-ISI signal-to-noise ratio just after Rx filtering, which we define as

$$SNR = -10 \log 2\sigma^2 \quad (dB) \tag{6.42}$$

If the Rx filter has an IF noise bandwidth of B, then $\sigma^2=N_oB$ and

$$SNR = \frac{E_b}{N_o} \cdot \frac{1}{BT} \tag{6.43}$$

Performance with adaptive thresholding is presented in the following section.

6.5 Performance With Adaptive Thresholding

Performance with adaptive thresholding has been simulated for a number of receive (Rx) filters. The Rx filter types which have been investigated are:

a) MSK spectrum shape

b) Gaussian

c) 4-th order Butterworth with linear phase (BW4E)

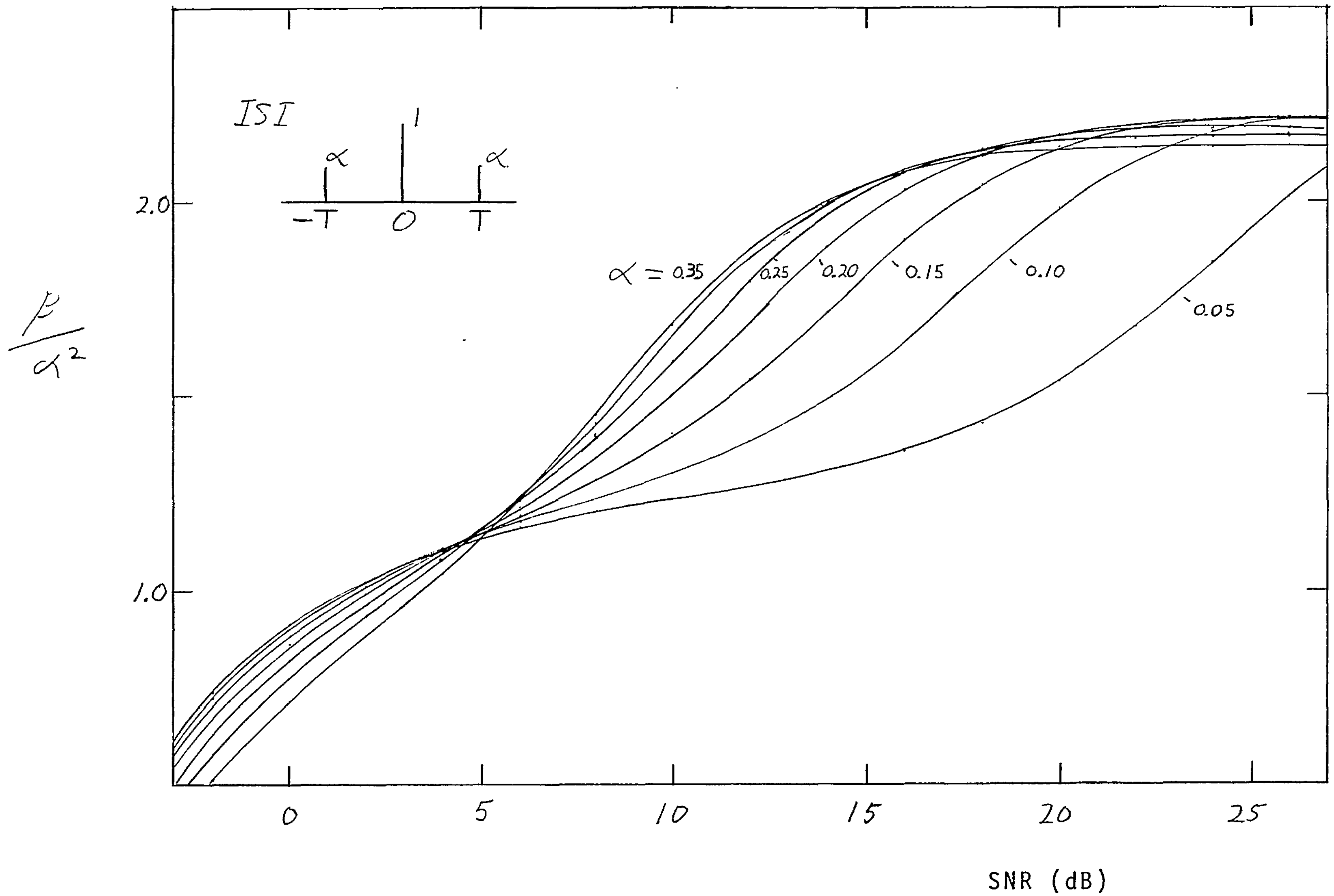

Figure 6.7 Optimum Threshold β For The Conventional Branch And Previous Decision Of Plus One

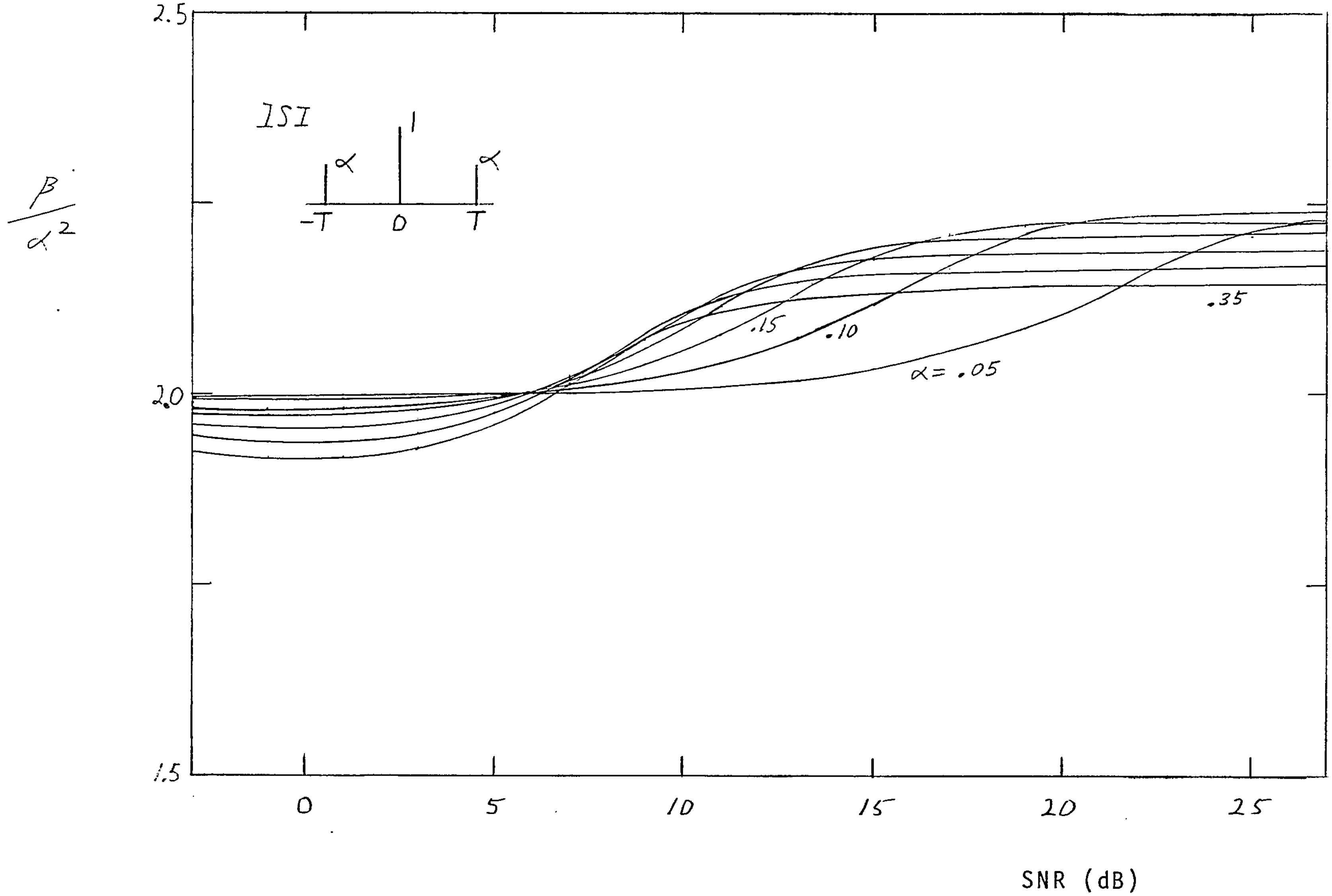

Figure 6.8 Optimum Threshold β For The Parity Branch And Previous Decision Of Plus One

For each filter type the performance was assessed as a function of the BT product, where B is the 3-dB IF filter bandwidth and T is the bit period. The smaller the BT product the larger the intersymbol interference (ISI) and the larger the expected gain with adaptive thresholding.

As a preliminary example the BER performance with and without adaptive thresholding is shown in Figure 6.9 for a matched receive filter, i.e. Rx equals the MSK spectrum shape with a BT product of 0.6. Matched filtering causes severe ISI and thus performance is expected to be fairly poor. As can be seen from this figure, the degradation from CMSK is anticipated to be about 6 dB for conventional DMSK at a BER of $5x10^{-4}$. When adaptive thresholding is introduced in the conventional branch a 2 dB improvement is exhibited, and performance is within 0.5 dB of that obtained with the addition of SEC only. When SEC is included, the addition of adaptive thresholding in both the conventional and parity bit branches realizes a 0.8 dB improvement at a BER of $5x10^{-4}$. This improvement is seen to be increasing steadily for even lower BERs. Expressed as a percentage of the no-ISI signal level, the threshold levels used for this case were plus and minus 15% for the conventional branch, and plus 20% and zero for the parity bit branch.

Plotted in Figure 6.10 is the degradation from ideal CMSK versus the BT product for a BER of $5x10^{-4}$, where the receive filter is the MSK spectrum shape. The results for a BT product of 0.6 are the same as for the matched filter case of Figure 6.9. As the BT product increases the improvement with adaptive thresholding is seen to decrease. This is expected since the ISI will be less severe. Comparing minimum degradations, we see that adaptive thresholding yields approximately a 0.3 dB improvement when used with conventional DMSK, and about a 0.1 dB improvement

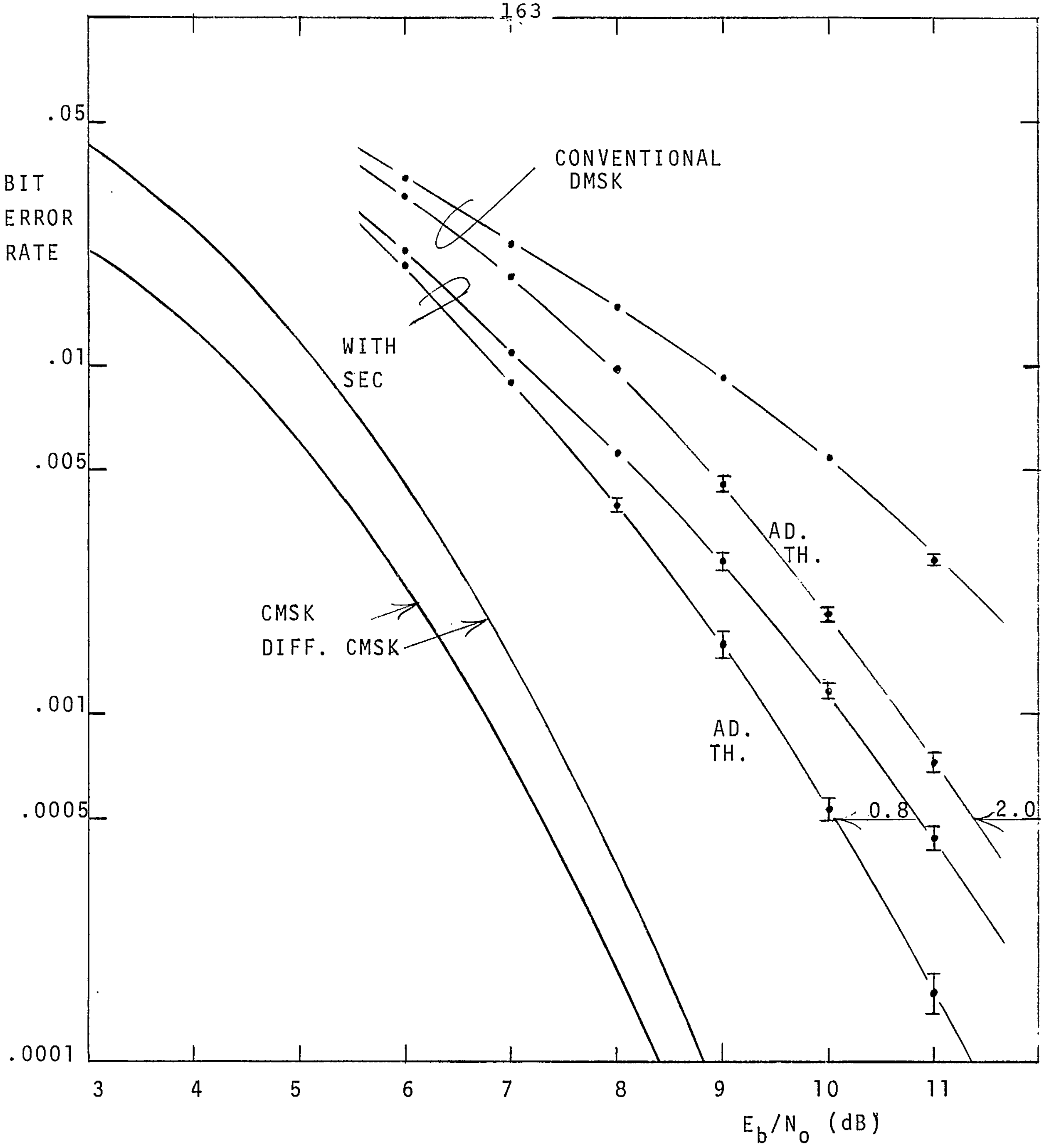

Figure 6.9 Simulated DMSK With And Without Adaptive Thresholding For A Matched Receive Filter

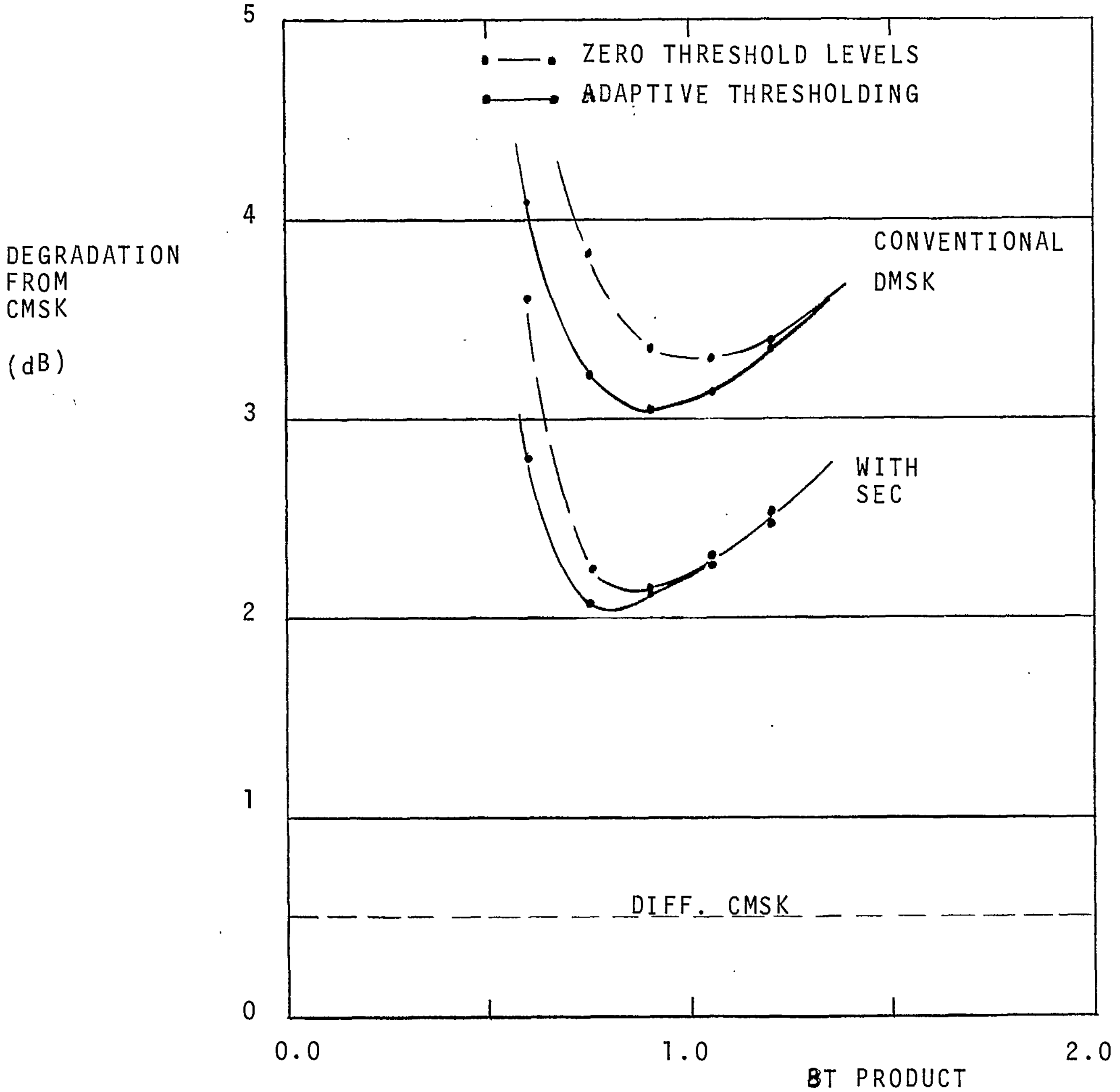

Figure 6.10 Simulated DMSK With Adaptive Thresholding:
Rx = MSK Spectrum Shape
$P_e = 5x10^{-4}$

when SEC is included as well. As expected the optimum BT product with adaptive thresholding is seen to be slightly smaller than the optimum BT product without adaptive thresholding.

The choice of threshold levels used for each of the Rx filters is given in Table 6.5, where α is the magnitude of the adjacent ISI just after Rx filtering. Obviously α is a function of the BT product and decreases as the bandwidth increases.

Plotted in Figure 6.11 is the degradation from ideal CMSK versus the BT product for a Gaussian Rx filter. Comparing minimum degradations, the improvements with adaptive thresholding are approximately 0.2 and 0.1 dB for conventional DMSK and with SEC respectively.

Figure 6.12 contains the results for the 4-th order Butterworth with linear phase. The improvement with adaptive thresholding for the conventional branch is seen to be 0.2 dB, but no improvement is realized when SEC is included. In fact as the BT product decreases, performance with adaptive thresholding becomes slightly worse than that without adaptive thresholding for both schemes. The problem with this filter, as far as adaptive thresholding is concerned, is that it violates the assumption that only adjacent ISI is significant. An investigation prompted by the somewhat unexpected result above uncovered the fact that ISI two bit periods away from the desired sampling instant has a much greater effect on performance than does adjacent ISI, for a given ISI level. This is due to the fact that ISI caused by bits an even number of bit intervals away, is allowed to contribute terms which are proportional to its level, as opposed to the square of its level as for adjacent ISI. For example, if adjacent ISI is of the order of 10%, the ISI two bits away must be much less than 1% if it is to have little additional impact.

	Threshold Level /α^2	
Rx Filter	Conventional	Parity
MSK Shape	1.5	2.0
Gaussian	1.5	2.0
BW4E	1.25	2.0

TABLE 6.5 Threshold Levels Used

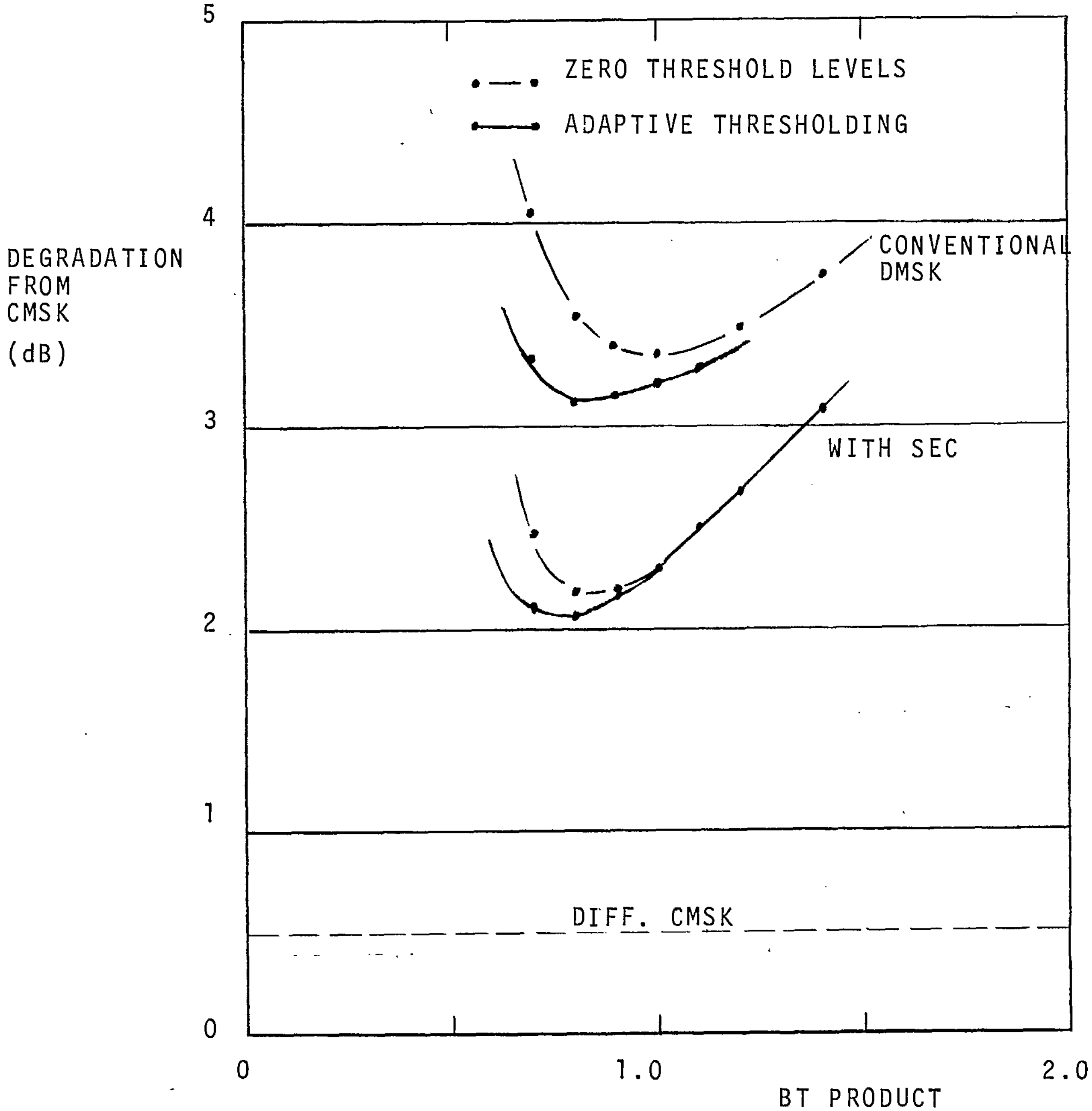

Figure 6.11 Simulated DMSK With Adaptive Thresholding:
Rx = Gaussian
$P_e = 5\times10^{-4}$

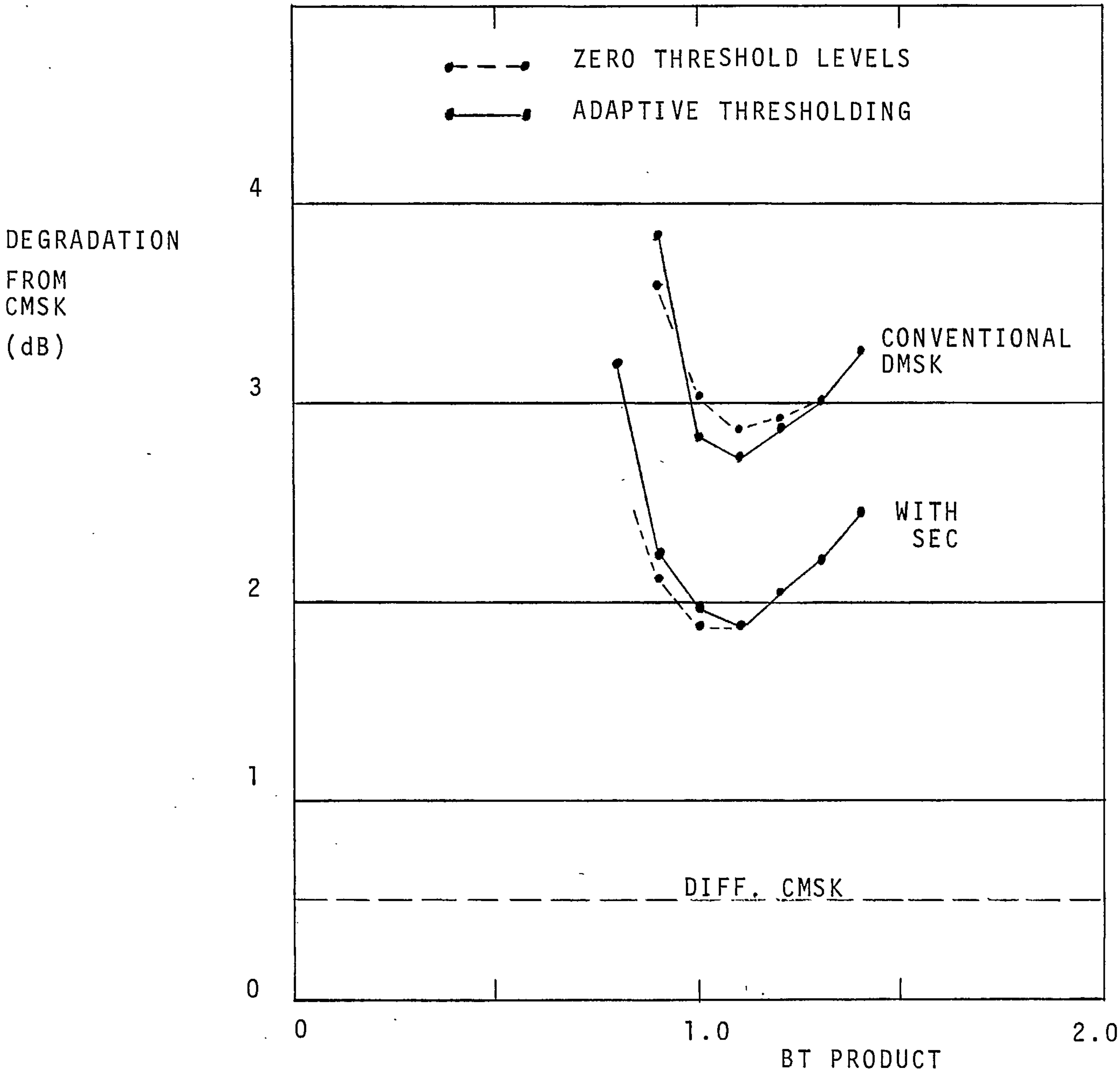

Figure 6.12. Simulated DMSK With Adaptive Thresholding:
Rx = 4th Order Butterworth Equ.
$P_e = 5\times10^{-4}$

This is not the case when a 4th order Butterworth is used with a BT product of about 1.0 or less. It is however a valid assumption for Gaussian or MSK shaped filter spectrums. In fact a true matched filter has a BT product of 0.6 and produces only adjacent ISI.

As can be seen from the three filter types investigated here, the 4-th order Butterworth with linear phase provides the best performance even without exhibiting an improvement with adaptive thresholding when SEC is used, for a BER of 5×10^{-4}.

We conclude then that the advantage provided by adaptive thresholding is a strong function of both the filter type and the bandwidth constraints dictated by the system. For the most part the improvement provided by adaptive thresholding increases as the bandwidth decreases.

6.6 Realizability

From the simple structure presented in Figure 6.2, we can see that at least conceptually adaptive thresholding is very simple to implement. When using this technique an implementation delay is not even required. The only apparent area of concern is the accuracy demanded by the threshold devices. As already mentioned, the threshold levels required when matched filtering is used are on the order of 15 and 20% of the peak pulse value. Certainly these levels would be easily accomodated. More realistic BT products on the order of 1.0 will demand much smaller levels and thus more accuracy. Using the ISI levels measured by the simulation program and the best BT products for each of the three filter types evaluated, Table 6.6 presents the magnitude of the threshold levels required, where the appropriate scaling factor has been taken from Table 6.5. For the Gaussian and MSK shaped Rx filter spectrums the required threshold levels are on the order of 6 to 9%, which is still a reasonable demand for today's technology. The Butterworth filter requires much smaller thresholds.

A more elaborate adaptive thresholding technique could easily be developed to accomodate non-adjacent ISI but the performance margin is thought to be too small.

		Threshold Level (% of Peak Pulse)	
Rx Filter	BT Product	Conventional	Parity
MSK Shape	0.8	6.9%	9.2%
Gaussian	0.8	6.3%	8.4%
BW4E	1.1	2.1%	3.4%

Table 6.6 Magnitude Of Threshold Levels Required For Best BT Product

7.0 MAXIMUM LIKELIHOOD NONCOHERENT MSK BURST CLOCK SYNCHRONIZATION

7.1 Introduction

Although differential detection of MSK eliminates the need for fast carrier acquisition circuitry and a carrier acquisition preamble in burst applications such as TDMA, there is still a need for bit timing recovery (BTR) circuitry and a bit timing acquisition preamble (assuming bit timing coherence is not maintained from burst to burst). We desire the BTR function to be fast and the bit timing preamble to be as short as possible, particularly if the bursts themselves are short (e.g. under 100 bits).

In some applications, such as JTIDS, where short bursts are involved and where the bit E_b/N_o is expected to be low, this BTR task is difficult and conventional approaches, involving non-linear regeneration with an appropriate prefilter [11], may not be suitable. Instead, an approach making more efficient use of available signal energy is required.

If the receiver's bit timing clock does not drift significantly over the period of a burst, then the BTR problem is essentially one of detecting the time of arrival (TOA) of each burst and using this information to reset the phase of the bit timing clock accordingly. Expressed in this fashion, we recognize the similarity of the BTR problem to the radar delay (i.e. range) estimation problem. From radar theory [19, pp.3-8], we know that the matched filter is the optimum filter (in the sense of minimizing TOA error for a given signal and E_b/N_o ratio) for estimating time of arrival in the presence of additive white Gaussian noise (AWGN). Under these same conditions, therefore, resetting the phase of a local bit clock based on a matched filter TOA estimate of an N-bit BTR preamble makes optimum use of the available preamble energy and gives the best (initial) bit timing accuracy.

Now let us digress briefly and consider one of the system implications of conventional bit timing recovery. Conventional BTR circuitry provides bit timing but not an absolute burst timing reference. Typically, the BTR circuit implements a timing correction loop which gradually brings an initially free-running local bit timing clock into synchronism with the bit transitions of the incoming burst. The circuit is designed to achieve the desired steady-state condition by the end of the BTR preamble but cannot indicate when the end of the preamble, and the beginning of the data, actually occur. As a result, conventional TDMA (Time Division Multiple Access) systems usually reserve part of each burst, between the BTR preamble and the burst data, for a "unique word".

A unique word (UW) is a known pattern of (typically) 16 to 32 bits. Given bit timing, the UW is usually detected by a continuous comparison of the received bit pattern with the known UW pattern. A detection is declared when the two patterns match within a programmable number of bit disagreements (to allow for noise). This detection then provides a single unambiguous timing mark from which absolute burst timing (burst sync) may be derived.

By designating one or more bursts in the TDMA frame as reference bursts, and by giving them distinct UWs, a UW detector can also be applied to give absolute frame time (frame sync), and thereby provide the means for identifying bursts in the frame by their frame position (i.e. frame "address").

Figure 7.1 provides a summary of these ideas.

Now returning to the matched filter BTR approach, we see that it can combine the ideas of bit timing recovery and unique word detection. Since the entire BTR preamble is coherently matched filtered, a properly chosen preamble pattern will give a single unambiguous timing mark from which both bit timing and burst timing may be simultaneously derived. Thus, the matched filter approach is doubly advantageous since, for a given E_b/N_o,

(i) it minimizes the number of preamble bits needed for a given bit timing accuracy, and

(ii) it eliminates the overhead of a separate bit pattern for burst synchronization.

With both bit timing and burst sync provided by the BTR preamble, frame sync then requires only one overhead bit for one reference burst, or two overhead bits for up to three reference bursts. From a total system perspective, therefore, the matched filter BTR approach is exceptionally efficient in its use of signal energy and is a clear contender for TDMA systems where timing coherence is not maintained from burst to burst, and where short burst lengths are required, especially if low E_b/N_o is also expected.

Here, we are interested in establishing the performance, and outlining the implementation, of a burst TOA estimator based on matched filter detecting an N-bit BTR preamble. Specifically, in following sections we

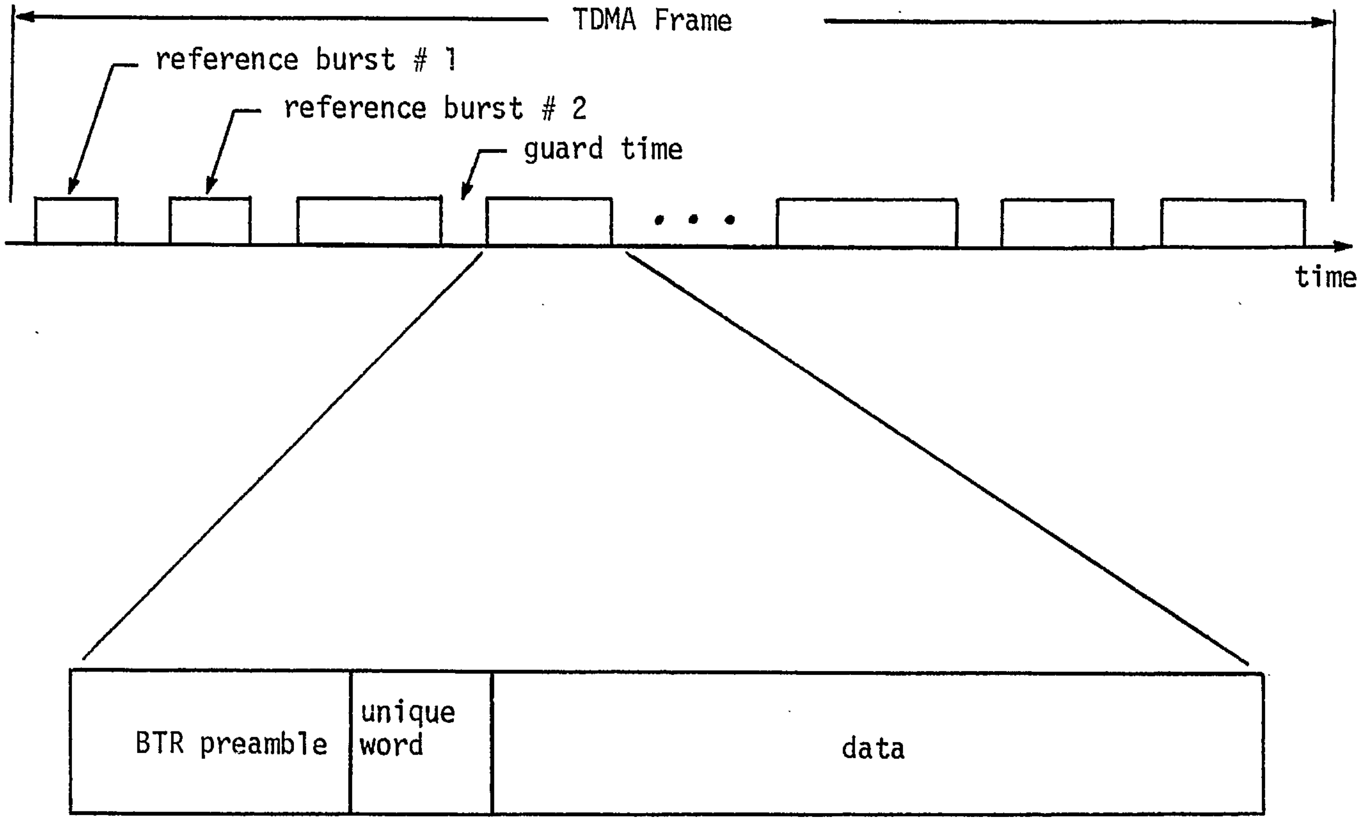

Figure 7.1 Typical Frame and Burst Structure for a Conventional TDMA System.

(i) provide an overview of the matched filter approach in greater detail and state our assumptions,

(ii) describe the performance of the method in terms of TOA accuracy and the probability of not correctly acquiring, and

(iii) investigate briefly alternate implementation structures, technologies, and corresponding technical risks.

Analytical details are contained in Appendix D.

7.2 Overview Of The Matched Filter Synchronization Approach

7.2.1 Review of Radar Fundamentals

In the classical radar range estimation problem the time of arrival of a "known" signal in additive white Gaussian noise (AWGN) must be determined. By a known signal is usually meant a signal with known modulation but unknown Doppler frequency offset and phase. In most situations an estimate of phase cannot be derived so the TOA estimate must be based on the envelope of the received signal alone. Let the complex envelope of such a received waveform be given as follows

$$\tilde{r}(t) = \sqrt{E}\,\tilde{s}(t-\tau_a)e^{j\omega_d t} + \tilde{n}(t)\ , \quad -\infty \leq t \leq \infty \qquad (7.1)$$

where $\tilde{s}(t)$ is a waveform of unit energy, E is the energy of the received signal, τ_a is the true TOA, ω_d is the true

Doppler offset*, and $\tilde{n}(t)$ is complex narrowband noise with two-sided spectral density $N_o/2$. It then follows from standard analysis [20] that the relevant likelihood function is

$$\ln\Lambda_1(\tau_a,\omega_d) = \frac{1}{N_o}\left(\frac{E}{N_o+E}\right)\cdot\left|\tilde{L}(\tau_a,\omega_d)\right|^2 \qquad (7.2)$$

where

$$\tilde{L}(\tau_a,\omega_d) = \int_{-\infty}^{\infty} \tilde{r}(t)\ \tilde{s}^*(t-\tau_a)e^{-j\omega_d t}\,dt \qquad (7.3)$$

The factor involving E and N_o is only important for the computation of the Cramer-Rao bound (which we discuss in Section 7.3), so suppressing it for now, the function to be computed becomes

$$\ln\Lambda(\tau_a,\omega_d) = \left|\tilde{L}(\tau_a,\omega_d)\right|^2 \qquad (7.4)$$

Thus, the maximum likelihood estimator of τ becomes a matched filter followed by a square-law envelope detector and peak detector, as illustrated in Figure 7.2.

*Note that we have introduced a simplification here by ignoring the compression or stretching of the time scale of the complex envelope. In actuality we should have written $\tilde{s}(t-\tau_a)$ as

$$\tilde{s}(t-\tau_a + \frac{\omega_d}{\omega_c}\,t)$$

where ω_c is the carrier frequency. Our assumption is valid providing the time bandwidth product of s(t) is much less than ω_c/ω_d, which is normally the case.

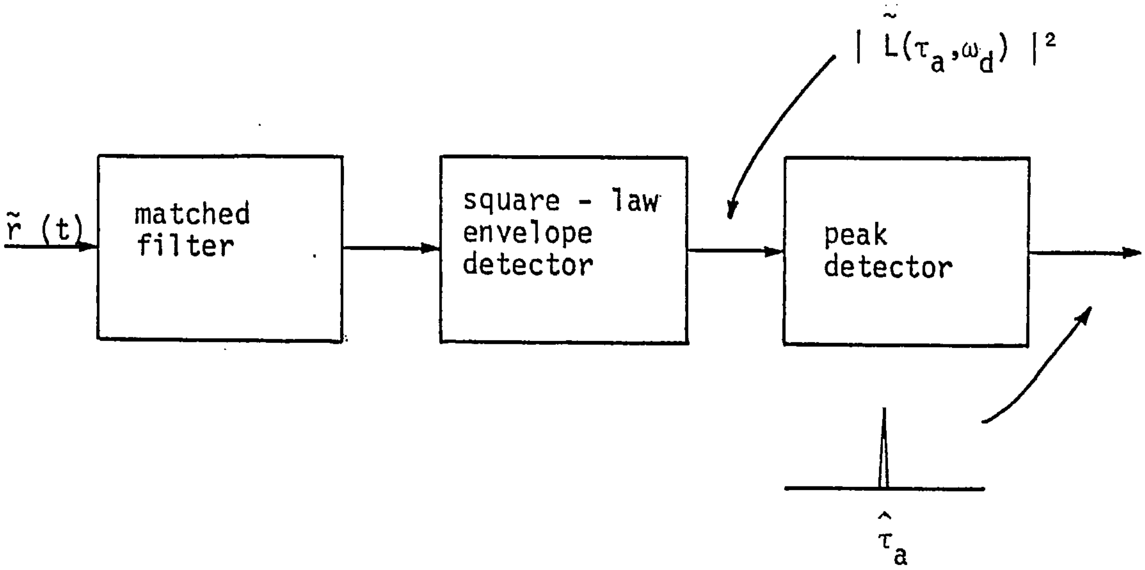

Figure 7.2 Maximum Liklihood Estimator of τ_a

The likelihood function of equation (7.4) also provides a useful and frequently encountered design tool: the ambiguity function. Specifically, if τ and ω are the errors in the estimates of τ_a and ω_d, then neglecting noise, the ambiguity function is defined as

$$\theta(\tau,\omega) = \left|\tilde{L}(\tau,\omega)/\tilde{L}(0,0)\right|^2 \tag{7.5}$$

A plot of $\theta(\tau,\omega)$ is called an ambiguity diagram and may be used to assess the properties of $\tilde{s}(t)$ as regards range/Doppler estimation accuracy and ambiguity. For example, a plot of $\theta^{\frac{1}{2}}(\tau,\omega)$ for a rectangular pulse of duration T is given in Figure 7.3. A sharper peak at $\theta(0,0)$ implies higher achievable range/Doppler estimation accuracy, or equivalently, a greater sensitivity of the matched filter to time and Doppler offset. Peaks of significant height other than the one at $\theta(0,0)$ imply ambiguity and/or sites having particular sensitivity to false alarms. We shall make reference to the ambiguity function in Section 7.3 and Appendix D where performance is calculated.

7.2.2 Application of Maximum Likelihood Time of Arrival Estimation to Sychronization

Applying the theory of the previous section immediately leads to the BTR circuit structure of Figure 7.4. Briefly,

(i) The key elements of the circuit are a bandpass filter matched to the BTR preamble followed by a square-law envelope detector. Equivalently, this could be implemented by a pair of baseband matched filters whose outputs are square-law combined.

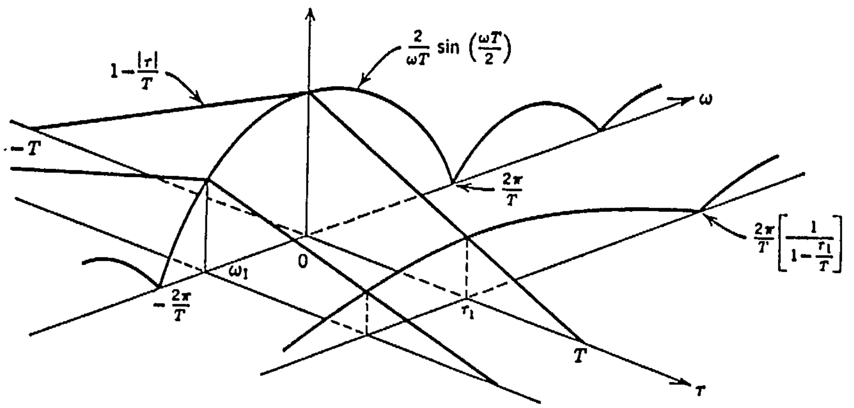

Figure 7.3 Plot of $\theta^{\frac{1}{2}}(\tau,\omega)$ for a Rectangular Pulse [20]

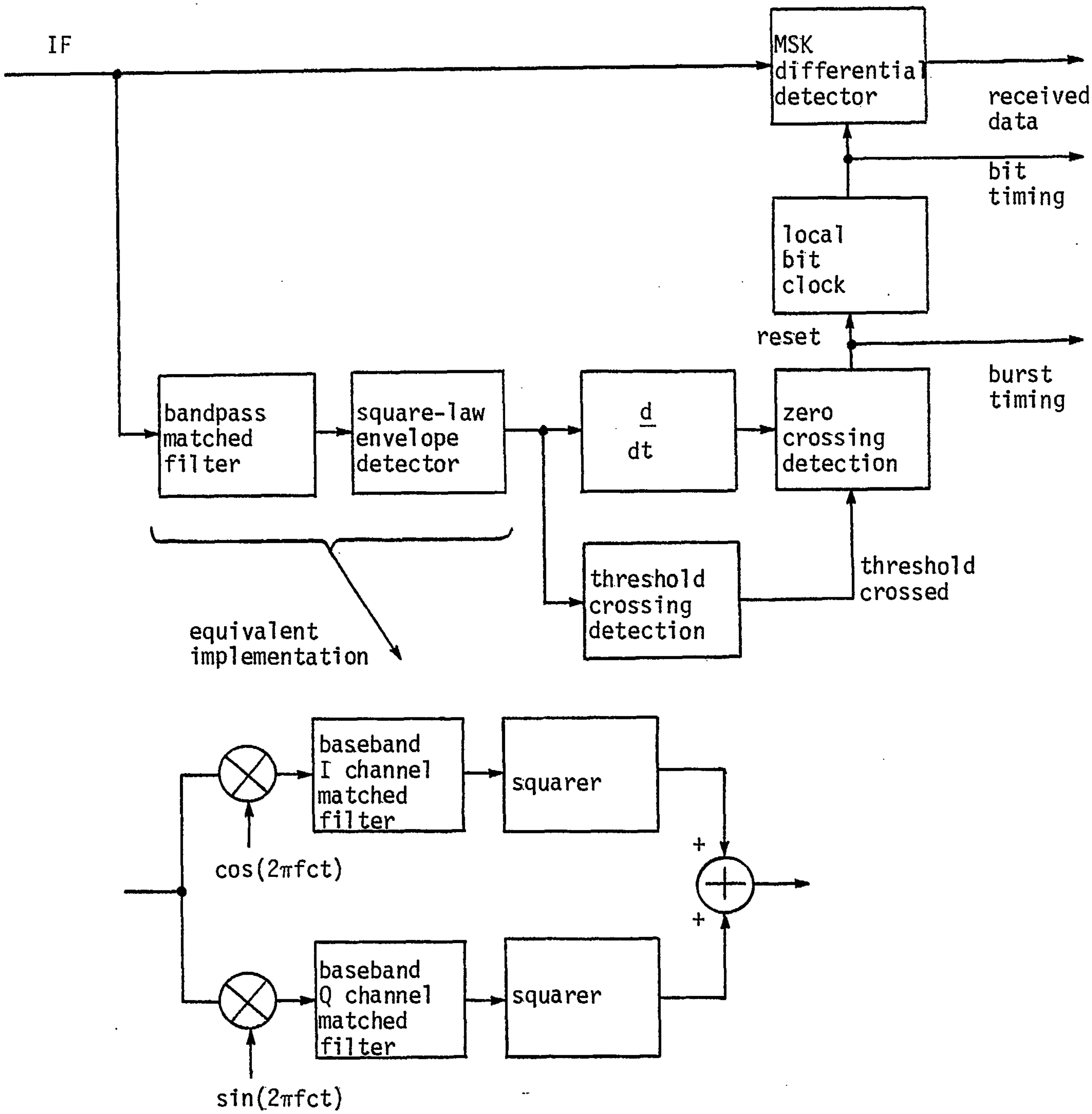

Figure 7.4 BTR Circuit Structure

(ii) The output of the above circuitry is the ambiguity function corrupted with noise and the peak of this output defines the maximum likelihood estimate of τ_a. The most convenient means to detect the peak is to differentiate the signal and detect the zero crossing.

(iii) However, once the matched filtered signal envelope is differentiated, the sense of signal magnitude is lost, making the above circuit highly prone to false alarms. To circumvent this difficulty we subject the matched filtered signal to a threshold to distinguish the central peak of the ambiguity function from preceding spurii. We accept only the zero crossing immediately following* the crossing of the threshold (from below).

(iv) The accepted zero crossing detection then gives absolute burst timing (burst sync) which is also used to reset the phase of the local bit clock and thereby provide bit timing.

Note that in Figure 7.4 the BTR function precedes, and is completely independent of, whatever circuit performs the data detection function. An alternate approach (as described in [21]) is to match filter and peak detect the baseband output of a differential data detection circuit. This latter approach avoids the need for envelope detection and dual baseband filters (both minor advantages), and to a

*Accepting only the first zero crossing is the most likely practical implementation but is very slightly suboptimal. The optimal implementation would be to record all zero crossings between the times the signal crossed the threshold from below and from above, and to accept the zero crossing associated with the greatest signal magnitude. Unless the matched filter signal to noise ratio is "low" (which will give poor TOA accuracy anyway), the performance degradation incurred should be negligible.

certain degree takes advantage of phase coherency (in a suboptimal noisy differential sense), thus giving it the potential to be slightly better than the non-coherent envelope approach. It is however not optimal because the data detection circuitry causes the noise entering the preamble matched filter (PMF) to be non-white and non-Gaussian. Because of this alternate approach's sensitivity to data detector design, and the analytical intractibility of non-white/non-Gaussian noise, we do not consider it further in this study.

Another suboptimal approach is to employ the circuit of Figure 7.4 but dispense with the peak detector and take timing directly from the threshold crossing. In this case the threshold would have to be set sufficiently high to give the desired timing accuracy. Unfortunately, high thresholds also result in lowered probabilities of detection (i.e. a greater chance of losing data), and it might not be possible to simultaneously achieve a required timing accuracy and probability of detection. Dostert and Pandit [22] have experimentally compared the circuit TOA accuracy performance with and without the peak detector for a PSK direct sequence spread spectrum communications application. As might be anticipated, the actual input signal level required for the timing circuit with differentiation to achieve a specified timing variance was found to be less than that of a timing circuit without differentiation by about 3 dB (since the ambiguity function central peak is less sharp, the results for MSK could be expected to show a greater difference in performance). Unfortunately, Dostert and Pandit have not quoted the rate at which detections were missed in their experiment.

For the purposes of this study we restrict ourselves to the optimal noncoherent implementation of Figure 7.4. Our baseline signal is assumed to be a 5 Mbps MSK burst waveform. The preamble portion of each burst p(t) is taken to consist of N bits, each of duration T seconds. Preceding the preamble is AWGN only, while following the preamble is MSK data. We assume that the receiver has achieved frame synchronization* so that each burst is known to have an arrival time bounded by a window of duration WT (W a positive integer). The displacement (time of arrival) of the first data bit from the start of the window is τ_a, and the probability density of τ_a is uniform over WT (the maximum likelihood case). Figure 7.5 illustrates these assumptions.

7.3 Estimate Of Performance

Three performance measures are generally of interest for bit or burst synchronizers, namely

(a) time to acquire (T_{acq}),

(b) timing jitter or TOA accuracy (σ_τ), and

(c) the probability (P_{NCA}) of not correctly acquiring (i.e. of losing an entire burst of data).

For the matched filter BTR technique, the time to acquire is merely the preamble duration (i.e. T_{acq} = NT). The other two performance measures are somewhat more complex to compute and are the subject of this section. Our interest here will be in estimating ultimate performance, i.e. performance when the only source of degradation is additive white Gaussian noise.

*Without frame synchronization a false detection would occur whenever the data within any burst randomly matched the BTR preamble pattern. Acquiring frame synchronization involves distinguishing between false occurences of the BTR pattern in data and the true BTR preambles. If the data changes randomly this can be achieved simply by observing which detections occur consistently (due to the preambles) and which occur sporadically (due to the data).

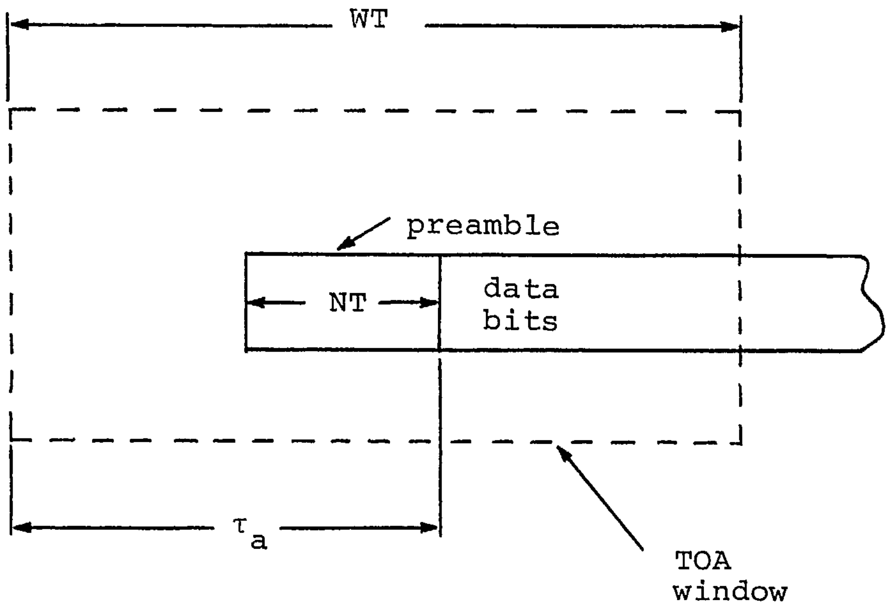

Figure 7.5 Frame Structure

7.3.1 Time Of Arrival Accuracy

The Cramer-Rao lower bound may be used as an estimate of TOA accuracy. In Section D.2 of Appendix D we have computed this bound for the case of an N-bit MSK preamble. Basically, the calculation requires us to compute the effective (Gabor) bandwidth of the preamble, or equivalently, the second derivative at the origin of the preamble ambiguity function. The result we find is as follows

$$\left(\frac{\sigma_\tau}{T}\right)^2 \geq \left[\frac{NE_b}{N_o}\left(\frac{NE_b}{NE_b+N_o}\right)\right]^{-1}\left[\frac{\pi^2}{2}\left(1-r_1^2\right)\right]^{-1} \tag{7.6}$$

where σ_τ^2 is the TOA error variance and r_1 is the first autocorrelation sidelobe of the preamble code (with the autocorrelation peak normalized to unity):

$$r_1 = \frac{1}{N}\sum_{k=0}^{N-1} a_k\, a_{k+1} \qquad \begin{array}{l}(a_0,\, a_1, \ldots, a_{N-1}) \text{ is the} \\ \text{preamble code}\end{array} \tag{7.7}$$

In Figure 7.6 we have plotted equation (7.6) for the case a of a single MSK pulse ($N=1$, $r_1=0$) and for all known Barker codes (see Table 7.1). We have also plotted the experimentally measured result of Campbell and Nowland [21], which corresponds to the approach of matched filtering the data detection circuit baseband output.

As one would expect, higher values of E_b/N_o or N result in less timing jitter. The measured result quoted by Campbell and Nowland suggests that practical implementations quite close to the bound may be achieved (from the figure we see that their result is within 1 dB of the bound).

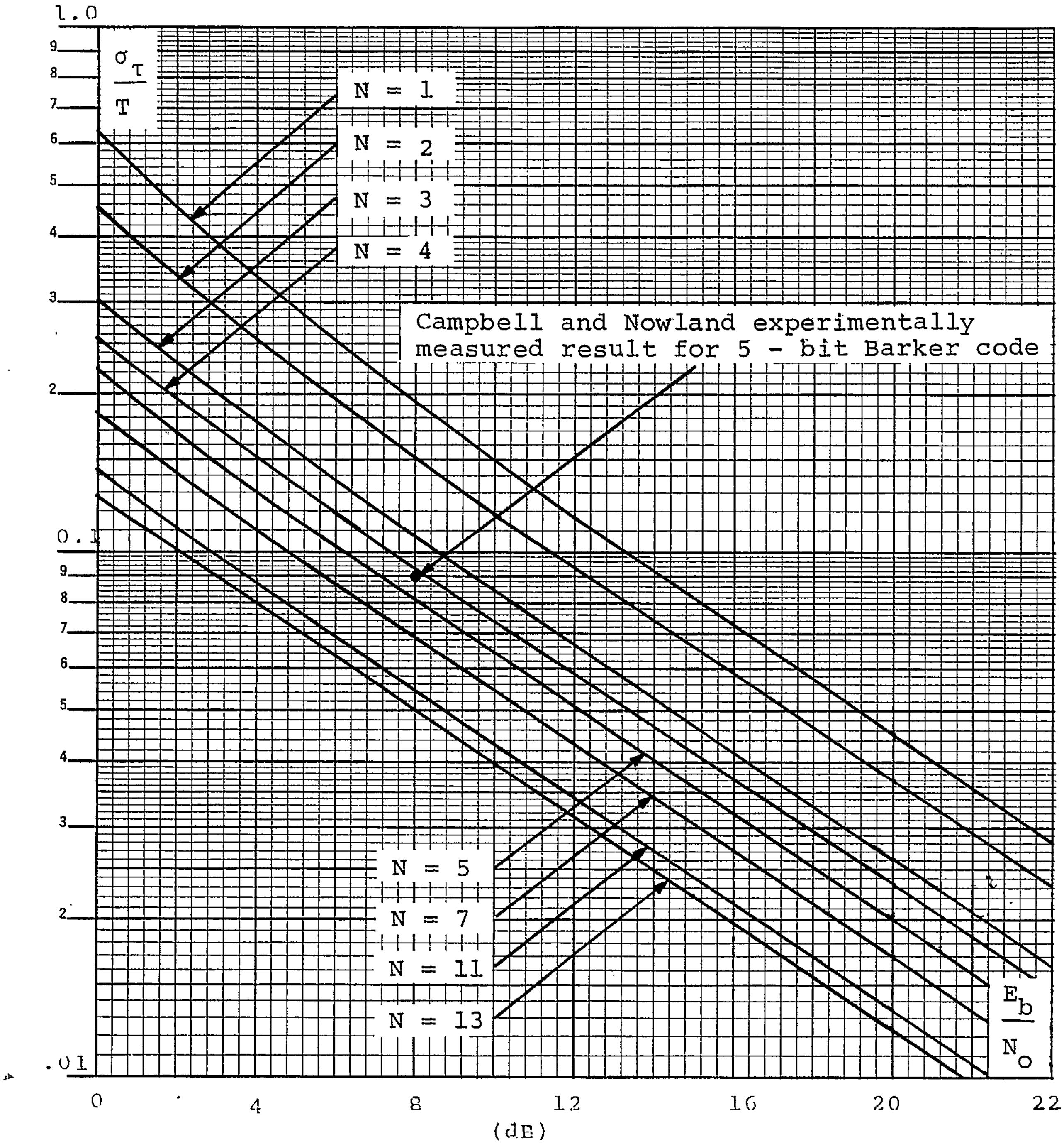

Figure 7.6 Cramer-Rao Lower Bound for TOA Accuracy Computed for a Single MSK Pulse (N = 1) and All Known Barker Codes

Note that result quoted by Campbell and Nowland [21] is for a filter matched to the data detection circuit output.

Code Length	Code Elements	First Sidelobe Nr_1
2	+- , ++	-1, +1
3	++-	0
4	++-+, +++-	-1, +1
5	+++-+	0
7	+++--+-	0
11	+++---+--+-	0
13	+++++--++-+-+	0

Table 7.1 Known Barker Codes and the Values of Their First Sidelobes

7.3.2 Probability Of Not Correctly Acquiring

The timing jitter result of the previous section assumes that the main lobe of the matched filter output has been correctly identified by the threshold circuit (see Figure 7.4). If this is not the case, acquisition cannot take place correctly and the entire burst of data will be lost. This can happen in two ways:

(a) the threshold may be crossed prematurely (false alarm), or

(b) the true correlation peak may be missed (miss).

If we denote the probabilities of not correctly acquiring, false alarm, and miss by P_{NCA}, P_{FA}, and P_M, respectively, then we find

$$P_{NCA} = P_{FA} + P_M\,(1-P_{FA}) \simeq P_{FA} + P_M \qquad (7.8)$$

Assuming the preamble code and E_b/N_o are fixed (by timing jitter requirements), our objective is to set the normalized threshold level γ ($0<\gamma<1$, where $\gamma=1$ corresponds to the peak value of the ambiguity function) to minimize P_{NCA}. In radar this minimization criterion is referred to as the Ideal Observer [23].

A calculation of P_{NCA} is presented in Section D.3 of Appendix D. There are four steps:

(a) first the rate of false alarms (crossings of the threshold from below) is derived,

(b) then the false alarm rate is shown to be dominated by false alarms occurring at secondary maxima of the ambiguity function, and this insight is used to convert false alarm rate into false alarm probability,

(c) next the probability of detection P_D, and hence the probability of miss ($P_M = 1-P_D$), is derived, and

(d) finally P_{FA} and P_M are combined according to (7.8) to give P_{NCA}.

In Figure 7.7 the variation of P_{NCA} with γ is plotted for E_b/N_o = 10 dB and the 13-bit Barker code. The optimum threshold is seen to be $\gamma_{opt} = 0.6$. Note that P_{NCA} is extremely sensitive to γ. A 10% error in γ results in nearly a three orders of magnitude change in P_{NCA}. Note also that the minimum value of P_{NCA} is nearly 10^{-24} for this case, meaning that the bit synchronizer is very reliable if γ is properly set.

In Figures 7.8 and 7.9 the variation of γ_{opt} and P_{NCA}^{min} with E_b/N_o is plotted for all Barker codes of length greater than 2*. We see that γ_{opt} is fairly stable as E_b/N_o is increased, the rate of decrease being quite precipitous for the longer codes.

7.4 Implementation Considerations

Most of the block diagram circuit structure of Figure 7.4 represents fairly standard equipment with correspondingly low technical risk (e.g. differentiator, zero and threshold crossing detectors, etc.). The only non-standard element is the preamble matched filter. The implementation of this element is what we concentrate upon in this section.

As indicated by Figure 7.4, the preamble matched filter may be implemented at IF or baseband. For a 5 Mbps data rate, surface acoustic wave (SAW) devices are appropriate at IF, while charge-coupled devices (CCDs) are appropriate at baseband.

*Plots for the length 2 Barker codes could not be produced because γ_{opt} was too close to 1 for the various approximations used in the calculations to remain valid.

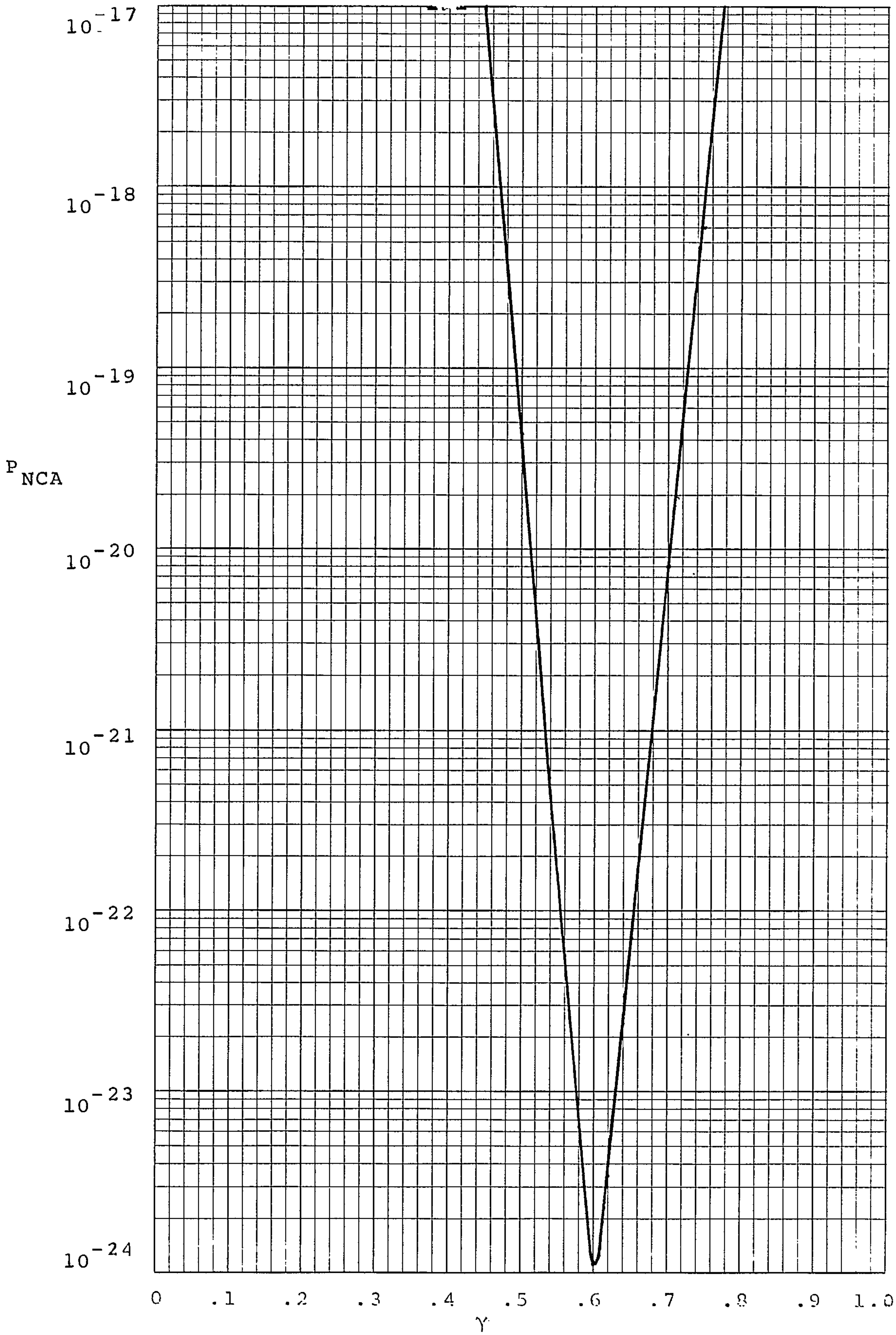

Figure 7.7 P_{NCA} Versus γ for $E_b/N_o = 10$ and the 13-bit Barker Code

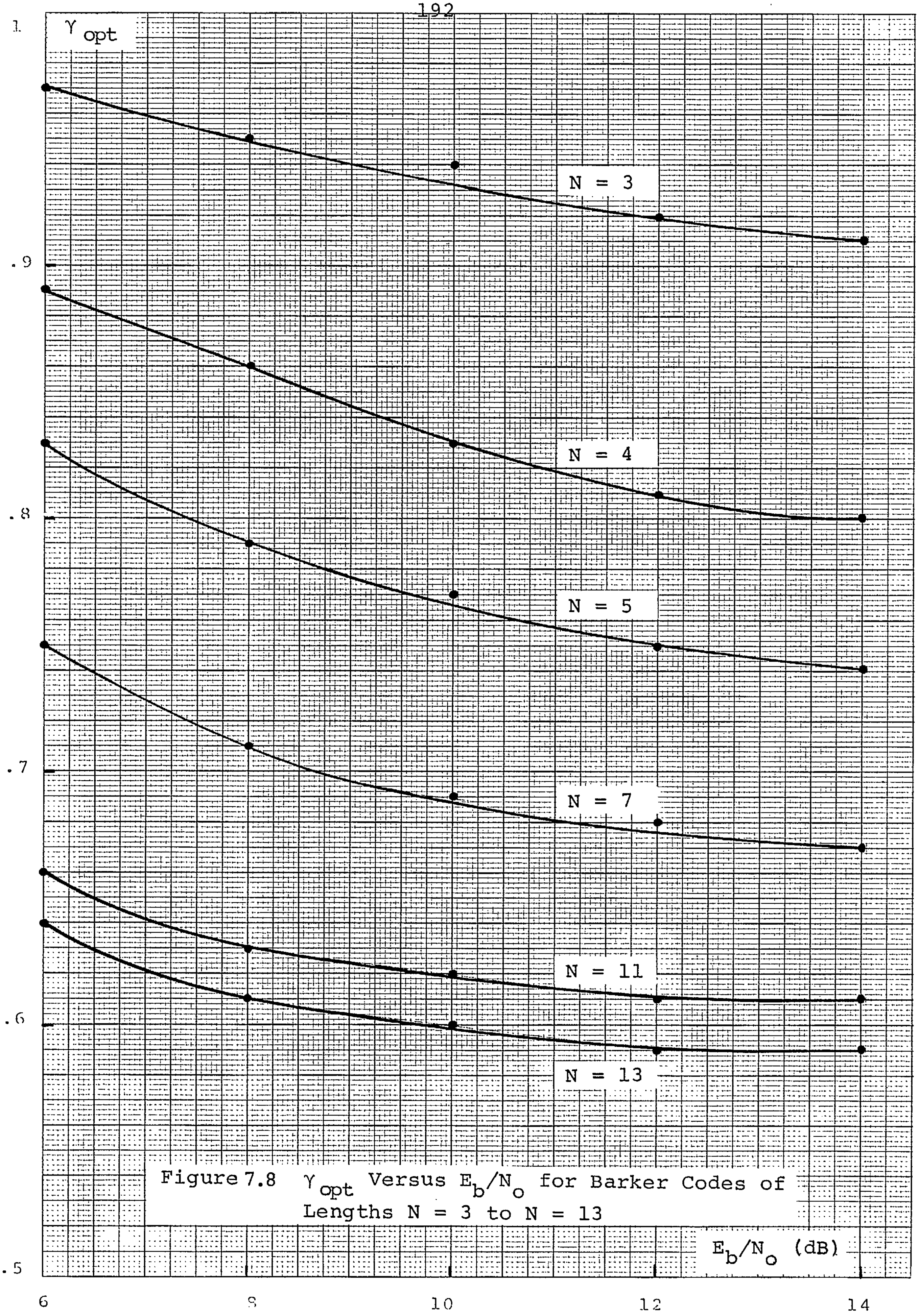

Figure 7.8 γ_{opt} Versus E_b/N_o for Barker Codes of Lengths N = 3 to N = 13

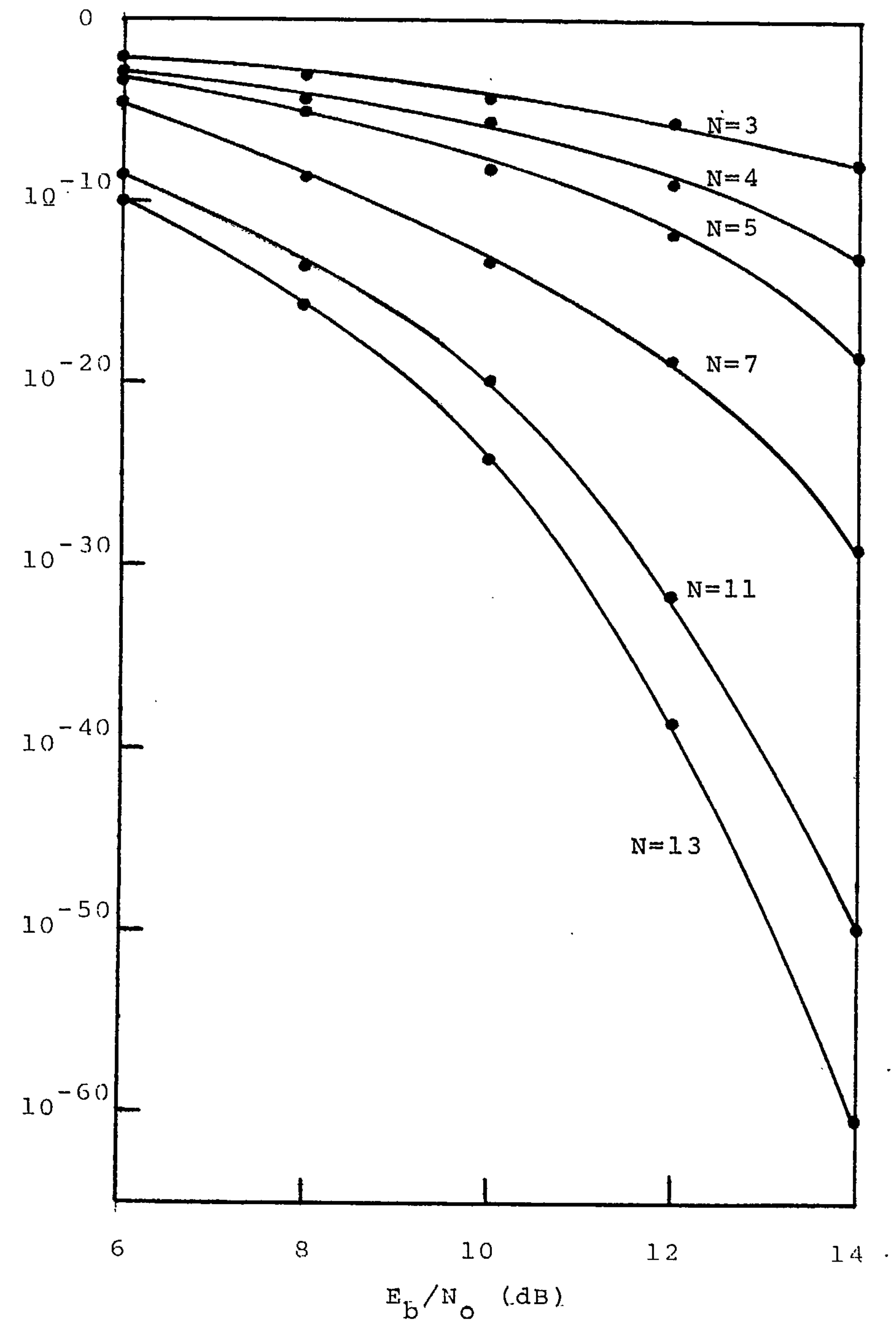

Figure 7.9 P_{NCA}^{min} Versus E_b/N_o for Barker Codes of Length N=3 to N=13

7.4.1 Bandpass Matched Filtering with SAWs

The JTIDS IF frequency of 70 MHz is well suited to the implementation of matched filters with SAW devices. At the present time, the design of SAW filters is at the point where insertion losses as low as a few decibels, processing times of tens of microseconds, and a centre frequency which ranges from 10 MHz to a few gigahertz have been achieved [24]. A filter matched to a 13-bit Barker code and 5 Mbps data rate requires a processing time of 2.6 μs, well within the range of SAW technology. Recently, a 64-tap programmable delay line (with associated electronics) built by the Hazeltine Corp. has been reported [24]. It is designed to operate with either 5 Mbps PSK or MSK, and some of its specifications are tabulated in Table 7.2.

7.4.2 Baseband Matched Filtering With CCDs

An alternative implementation is to use CCDs as part of a baseband I-Q structure. In this case two CCDs are needed - one each for the I and Q channels. If we take the bandwidth of the MSK signal to be the width of its main lobe, then the single-sided bandwidth of a 5 Mbps signal is 3.75 MHz. The minimum (complex) sampling rate is then 7.5 MHz. At the present state of technology, 5 MHz sampling rate CCD devices are readily available. Using these devices in pairs will provide a 10 MHz sampling rate (which allows some margin for anti-aliasing filtering). For instance, the Reticon TAD-32A Tapped Analog Delay Line [25] is a 32 stage device which may be fitted with external resistors to form the tap weight function, and which is capable of sampling rates from 1 kHz to 5 MHz and dynamic ranges greater than 60 dB. Higher sampling rate CCDs are also purportedly under development [26].

Number of taps	64
Tap spacing/code rate	0.2 μs/5 Mbit/second
Center frequency	75 MHz
MSK spectral bandwidth	3.1 MHz
Sidelobe level	Within 2 dB of theoretical
Processing gain	Within 1 dB of theoretical
Insertion loss	45 dB
Noise output	-005 dBm
Programming time	8 μs

Table 7.2 Summary of Hazeltine Programmable Matched Filter Specifications [24]

8.0 SUMMARY AND RECOMMENDATIONS

The purpose of this study was to identify the essential components of a differential minimum shift keyed (DMSK) demodulator, and to determine its bit error rate (BER) performance subject to a number of distortions and interfering factors. Thus, this study provides a basis for determining modem specifications for a specific communications application.

In determining the BER performance of the DMSK demodulator, both theoretical analysis and computer simulation were used. Theoretical performance predictions correspond to simplified system configurations or performance bounds (depending on the assumptions made), and are thus used for benchmarking purposes. Determining the theoretical performance for realistic cases quickly becomes a formidable task, especially when distortion mechanisms (either in the channel or the receiver) or non-linearities such as the single error correction circuit and hard limiters, are introduced. For these reasons the bulk of the BER performance evaluation was performed through computer simulation, where the generation of noise samples is used, as opposed to other techniques which involve a combination of simulation and analysis. Because of the lengthy computation times required by this approach, E_b/N_o degradations were determined for BER's on the order of 10^{-4} or higher. Lower rates would have required extremely long computation times. However it is expected that this error rate is in the range of interest for many applications.

While it is expected that the best selection of component parameters (e.g. filter) and the corresponding performance will vary to some degree depending upon the error rate, the results produced in this study should identify the preferred class, order, and the approximate BT products required of filters to be used, as well as the allowable range of values for degrading factors in specific applications.

Preliminary theoretical analysis was performed in Section 2.0. The purpose of this section was to describe the MSK signal format, DMSK detection, and to establish the theoretical BER performance bounds which were used as bench marks for comparison with the BER's obtained in the sections which followed. In Section 3.0 the simulation models were presented. The simulation performance results were presented in Section 4.0 and an abbreviated summary will be presented in this section. In Section 5.0 an investigation of performance with equalization to remove intersymbol interference (ISI) was presented. In Section 6.0 the ISI associated with common filter shapes was investigated and a simple adaptive thresholding technique, for the purposes of partial ISI cancellation was described. Presented in Section 7.0 was the maximum likelihood non-coherent approach to MSK burst clock synchronization.

8.1 Demodulator Structure

A description of the DMSK signal and its detection was given in Section 2.1. The DMSK detector and single error correction (SEC) circuit investigated are shown in Figure 2.2. A DMSK demodulator is quite simple, requiring the multiplication of the received signal by a delayed version of itself. Carrier recovery is not required; thus, acquisition time only depends on bit timing recovery (BTR), making it a very attractive detection scheme in short burst applications such as is sometimes found in time division multiple access (TDMA) and possibly digital mobile radio. Furthermore, its simplicity relative to a coherent demodulator make it an attractive candidate for regenerative satellites.

The basic components of the DMSK detector are*:

(1) IF receive (Rx) filter,

(2) IF signal delay elements (T-delay element required for the conventional branch, and 2T-delay element required for the parity bit branch used by the SEC circuit),

(3) IF phase adjusters (both branches)

(4) demodulators (IF mixer, i.e. multiplier, both branches)

(5) post-demodulation filters (both branches)

(6) BTR circuit

(7) decision threshold devices (both branches)

(8) samplers (data rate)

(9) SEC circuit

Other components required but not directly addressed in this study are automatic gain control (AGC), and automatic frequency control (AFC). The effects of frequency offset are studied, so that AFC requirements can be determined.

8.2 Distortion and Interfering Factors Investigated

Filtering as it relates ultimately to error rate performance is a major concern. In Section 4.2 the BER performance of various DMSK filters was evaluated. The desired result was a transmit/receive/post-demodulation

---

*A baseband detector is possible. The IF detector was selected because it is simpler, and provides the same performance.

filter combination which yields the best BER performance. The best BER performance found is given in the next section. The sensitivity evaluation of Section 4.4 presented the degradations in performance associated with the following:

(a) Bit timing errors,

(b) Threshold errors,

(c) Delay errors,

(d) Phase shift errors,

(e) Carrier frequency offset, and

(f) Non-constant group delay.

Sections 4.5 to 4.8 presented the BER performance related to:

(a) Hard limiters in the demodulator,

(b) Multipath (one additional path),

(c) Jamming, and

(d) Doppler.

These results are summarized in the next section.

8.3 BER Performance

The BER performance of the DMSK detector, for various transmit/receive/post-demodulation filter combinations was determined. The primary objective was to find the filter combination which requires the least amount of energy per bit for a specific value of BER. An assumed constraint, however, was that the transmit filtering was not allowed to degrade the DMSK signal format, i.e. severe filtering at the transmitter would destroy the constant envelope characteristic and introduce significant ISI.

Performance was obtained for the following 6 filter types:

(i) Ideal Gaussian

(ii) 2-nd order Butterworth (BW2)

(iii) 2-nd order Butterworth equalized (BW2 Equ.)

(iv) 4-th order Butterworth (BW4)

(v) 4-th order Butterworth equalized (BW4 Equ.)

(vi) Ideal rectangular bandpass

The variable parameter was taken to be the BT product, where B stands for the 3-dB double sided bandwidth and T is the bit period, equal to the reciprocal of the data rate. Equalized filters refer to an ideal zero or linear phase response. For each filter type the objective was to obtain the BT product which resulted in the smallest degradation (in dB) from coherent detection of MSK (CMSK), for the specified BER.

Assuming no transmit filtering and an ideal low-pass post-demodulation filter (assumed to remove only unwanted second harmonics), the best receive filter (also best filter combination) was found to be a fourth-order Butterworth with ideal linear phase (BW4 Equ.) and BT product of 1.1. The degradations from CMSK, for a BER of 5×10^{-4}, were determined to be 2.9 and 1.9 dB for conventional DMSK and with SEC respectively. The six filters investigated and their corresponding minimum degradations from CMSK, at a BER of 5×10^{-4}, are listed in Table 8.1, (in order of increasing degradation).

The improvement provided by the SEC circuit was about 1.0 dB for all filters, at this BER. The sensitivity to the BT product tended to be greatest for those filters exhibiting the smallest minimum degradations (see Figures 4.3 to 4.8).

When non-ideal post-demodulation filtering was used, it was found that the degradation increased as the BT product of the post-demodulation filter decreased. The best performance is thus given by an ideal low-pass filter which is assumed to remove only the unwanted harmonics without further distorting the baseband signal. Similarly, any bandwidth constraint at the transmitter also imposed a further degradation. As an example, for the best receive filter found above, and a BW4 Equ. transmit filter with BT product of 1.5 (width of the main lobe), the additional degradation (with SEC circuit included) was found to be approximately 0.3 dB (see Figure 4.11).

From Table 8.1, the penalty associated with not having an ideal linear phase (i.e. unequalized fourth-order Butterworth) is seen to be only 2.0 - 1.9 = 0.1 dB (with SEC). For the 5×10^{-4} BER considered, this penalty is

Receive Filter Type	Degradation From CMSK (dB)* (with SEC)
BW4 Equ.	1.90
BW4	2.00
Ideal Bandpass	2.10
Gaussian	2.20
BW2 Equ.	2.25
BW2	2.35

*The computed theoretical standard deviation on all degradations is approximately 0.15 dB.

Table 8.1: Minimum Degradation from Ideal CMSK for DMSK with SEC at a BER of 5×10^{-4}

not severe, and thus performance is still good for a simple fourth-order Butterworth receive filter. The sensitivity and thus the degradation due to a non-linear phase is expected to increase for lower BER's.

Using the best resulting filter combination described above, Table 8.2 lists example individual distortions and interfering factors and the corresponding degradations imposed. Each distortion value related to modem design corresponds to a degradation of approximately 0.1 dB (with SEC). We can see that bit timing must be very accurate (within 2.5%) to allow a 0.1 dB degradation. Threshold levels of 5% should be easily accommodated.

Without phase adjusters the delay elements would have to be accurate to within 0.1% to allow only a 0.1 dB degradation. With constant phase adjusters, the 0.1% accuracy only applies to the stability of the delay elements. The actual accuracy requirements then, need only be of the same order as the bit timing, namely 2.5% for a degradation on the order of 0.1%. If automatic phase adjusters were used (i.e. not fixed), then the stability requirement for the delay elements could be relaxed as well. The corresponding phase error requirements for the phase adjusters would be on the order of 5 degrees* for a 0.1 dB degradation. As can be seen if a phase error of 20° exists only in the conventional branch, the degradation is still only 0.1 dB, due to the SEC circuit's ability to correct single errors.

*The phase error for the conventional branch is given by $\phi=\omega_c T d_e$, where d_e is the delay error. For f_c=70 MHz, R=1/T = 5 Mbps, and d_e = 0.1%, the phase error is $\phi=2\pi \times 14 \times .001=5°$. For the parity bit branch the phase error is twice this value, namely 10°.

#	Type of Perturbation	Extent	Degradation (dB) (with SEC)
Distortions			
1	Bit timing error	2.5% of bit period	0.1
2	Threshold level error	5% of peak signal level	0.1
3	Delay elements	0.1% delay error (f_c = 70 MHz, R = 5 Mbps)	0.1
4	Phase shift error (conventional branch only)	20 degrees	0.1
5	Carrier frequency offset	50 kHz (f_c = 70 MHz, R = 5 Mbps)	0.1
6	Non-constant group delay (linear group delay error only)	36° phase error at f = R(bit rate)	0.1
Interference			
1	Multipath (one interfering path)	C/I = 15 dB	0.7 dB
2	Jamming (in band tone)	C/I = 15 dB	0.5 dB

Table 8.2: Example Distortion and Interference Factors and Corresponding Degradations.

The degradation associated with a carrier frequency offset is due to two effects; namely (1) a phase error caused by a deviation in the $\omega_c T$ product, and (2) non-symmetric IF receive filtering. From Table 8.2, a 50 kHz frequency offset (nominal f_c = 70 MHz) results in a 0.1 dB degradation. It was shown in Section 4.8 that Doppler is expected to be insignificant for carrier frequencies as high as 1.0 GHz.

For a non-constant group delay (linear group delay error considered only, i.e. parabolic phase error) the degradation is 0.1 dB for a phase error of 36° at $|f-f_c|=R$, where R is the bit rate.

It was shown in Section 4.5 that hard limiters in any branch of the detector (after the receive filter) do not impose a further degradation. Thus the pure product law in the basic system model can be approximated by a simple switched mixer without introducing a further degradation.

The BER monitoring capability of certain SEC circuit state variables was described in Section 4.9.

8.4 Improving Performance

8.4.1 Performance With Equalization

The DMSK signal can be equalized to eliminate harmful ISI. Theoretical and simulated performance were both presented in Section 5.0. If the predetection filter acts as an equalizer and produces a 50% roll-off raised cosine Nyquist spectrum with overall width equal to the width of the main lobe of the MSK spectrum, theoretical and simulated results indicate an asymptotic 1.41 dB degradation from CMSK for large E_b/N_o. For a BER of 10^{-6} the degradation from CMSK is 2.1 dB (without SEC). This represents an improvement of 1.9 dB compared with previously published theoretical results for Gaussian filters [16]. With SEC an additional 0.3 dB improvement is realized.

Optimum Filters

Although the receive filter described above gives good performance and is probably close to optimum for BER's approaching zero, it is by no means obvious that this filter is best for a prespecified BER specification. This is especially true with the addition of SEC, because a small amount of ISI (in proportion to the noise power) can always be tolerated with a corresponding reduction in noise power. Thus we desire a filter which is somewhere between the equalizer and the matched filter.

It is interesting to note that the Gaussian and Butterworth filters investigated in Section 4.2 for the most part lie between the matched filter and the no-ISI equalizer described above. Further, performance with SEC and the 4-the order Butterworth (linear phase) Rx filter with BT product of 1.1 was shown to be within 1.9 dB of CMSK for a BER of 5 x 10^{-4}. From Figure 5.2 the corresponding degradation for the no-ISI equalizer (described above) is approximately 2.2 dB. Thus for this particular BER the Butterworth is 0.3 dB better than the no-ISI equalizer, and may even be close to the optimum filter shape which would be found if the search technique suggested in Section 5.3 were used.

8.4.2 Adaptive Thresholding

An adaptive thresholding technique was described in Section 6.0. The simple concept is as follows. If the previous decision is positive then (assuming a positive ISI contribution) the next signal level will be biassed in the positive direction. This bias may be removed by using a positive threshold device. Similarly for a negative decision. The technique is really nothing more than decision feedback ISI cancellation (conceptually), assuming only one backward ISI contribution.

The minimum improvements with adaptive thresholding were greatest for Gaussian and MSK shaped receive filters, yielding approximtely 0.3 dB and 0.1 dB improvements for conventional DMSK and with SEC respectively. For the 4-th order Butterworth (linear phase) and SEC included, an improvement with adaptive thresholding was not obtained (see Section 6.5). Overall performance was still best for this filter.

The advantage provided by adaptive thresholding is a strong function of both the filter type and the bandwidth constraints dictated by the system. For the most part the improvement provided by adaptive thresholding increases as the bandwidth decreases.

8.5 Bit Timing Recovery

Two bit timing recovery (BTR) strategies were investigated. A simple baseband zero crossing detection strategy was described and simulation results presented in Section 4.11. Presented in Section 7.0 was the maximum likelihood non-coherent approach to MSK burst clock synchronization. The zero crossing technique turned out to be slightly more accurate* as far as obtaining a correct clock phase is concerned, but the matched filter approach (Section 7.0) has the added benefit that absolute frame reference is also simultaneously obtained without an additional unique word requirement. An alternate approach [21] is to match filter and peak detect the baseband output from a DMSK detector. This approach avoids the need for envelope detection and dual baseband filters, and to a certain degree takes advantage of phase coherency*. It is however not optimal because the data detection circuitry causes the noise entering the preamble matched filter to be non-white and non-Gaussian. The RMS jitter values determined for each of these three techniques, for E_b/N_o of 8 dB and a 5 bit preamble, are:

Technique	RMS Jitter/T
zero crossing detector	7%
noncoherent matched filtering	8%
baseband detector output matched filtering	9% [21]

*Techniques which use the baseband output of the detector have the potential for being better than the noncoherent matched filter approach because to a certain degree these baseband techniques take advantage of phase coherency (in a suboptimal noisy differential sense).

Doubling the preamble length corresponds to approximately a $1/\sqrt{2}$ factor reduction in RMS jitter for all schemes. Thus, for an E_b/N_o of 11 dB (3 dB more energy per bit), a 20 bit preamble (5 doubled twice) and non coherent matched filtering the RMS jitter should be reduced to about $8/\sqrt{2}^3$ = 2.8%.

8.6 Degradation Budget For Implementation

Assuming differentially encoded MSK, a degradation budget for the DMSK modem is given in Table 8.3 (for a BER of 5 x 10^{-4}). The fundamental degradation determined for DMSK as compared to ideal coherent detection is 1.4 dB*. Other expected degradations are as indicated. The total degradation budget is determined to be about 2.3 dB (assuming degradations are additive). If transmit filtering could be kept to a minimum (or eliminated), then the total degradation budget is reduced to just 2 dB. This is felt to be a very good implementation margin considering the simplicity and acquisition advantages of the DMSK detector.

8.7 Conclusions And Recommendations

This study has shown that the E_b/N_o required to achieve a BER of 10^{-4} is 1.4 dB worse than that required theoretically for coherent detection of differentially encoded MSK. This is possible with a fairly trivial single error correction circuit that does not require the transmission of redundant bits. For a linear channel where the MSK main lobe is passed relatively undistorted, an implementation margin of approximately 0.8 dB results in a total degradation from the theoretical MSK case of 2.2 dB.

*The degradation from CMSK was determined to be 1.9 dB, and differential encoding imposes a 0.5 dB penalty. Thus the resulting degradation for DMSK compared to ideal coherent detection of differently encoded MSK is 1.9 - 0.5 = 1.4 dB, at a BER of 5 x 10^{-4}.

	Source	Degradation (dB)
1.	Differential Detection with Rx = BW4 Equ. and SEC circuit	1.4
2.	Distortions (reference Table 8.2)	0.5
3.	Non-ideal Rx phase (reference Table 8.1)	0.1
4.	Tx filtering (BT = 1.5)	0.3
5.	Post-Demod filtering	~0
6.	Hard Limiters	~0
	Total	2.3 dB

Table 8.3: DMSK Degradation Budget Compared to Ideal Coherent Detection of Differentially Encoded MSK ($BER = 5 \times 10^{-4}$)

This is on the order of 0.7 dB worse than that expected for a coherent modem implementation. While an E_b/N_o penalty is incurred, DMSK has the advantage that because a carrier recovery circuit is not required, signal acquisiton is faster and thus DMSK is well-suited to burst applications. Furthermore, a simpler circuit implies a less costly and more reliable implementation (this would be an important consideration for regenerative satellite receiver design).

The decision to proceed with a hardware development should be based upon a comparison of the proposed modulation with other known techniques using such criteria as economics and performance as bases.

The advantages of differential detection have been reviewed. Such a detection scheme is equally applicable to both 2- and 4-phase PSK and in these cases demodulator complexity is of the same order as that for DMSK. Prior to proceeding with a hardware development it would appear that a comparison of the performances of the three modulations with differential detection is required. Only when the relative merits are clarified should one technique be selected for development.

No major risk areas have been identified. However, some improvement in BER performance is possible with respect to filter selection.

REFERENCES

[1] J. Rubin, "Distributed Time Division Multiple Access (DTDMA) An Advanced Communication Technique With Application to C^3 And Integrated CNI," NTC'77, pp. 35:6-1 to 35:6-5.

[2] Advisory Group for Aerospace Research And Development, AGARDograph No. 245, "Principles and Operational Aspects of Precision Position Determination Systems", Dr. C. T. Leondes ed., Part III, July 1979.

[3] W. J. Schoppe, "The Navy's Use of Digital Radio", IEEE Trans. Commun., Vol. COM-27, No. 12, December 1979.

[4] R. de Buda, "Coherent Demodulation of Frequency-Shift Keying with Low Deviation Ratio", IEEE Trans. Commun. (concise paper), Vol. COM-20, pp. 429-435, June 1972.

[5] M. L. Doelz et al, "Minimum-Shift Data Communication System", U.S. Patent Number 2 977 417, March 1961.

[6] W. M. Hutchinson et al, "Data Demodulator Apparatus", U.S. Patent Number 3 743 755, July 1973.

[7] S. A. Gronemeyer and A. L. McBride, "MSK and Offset QPSK Modulation", IEEE Trans. Commun., VOL. COM-24, No. 8, August 1976.

[8] H. R. Mathwich, J. F. Balcewicz, M. Hecht, "The effect of tandem band and amplitude limiting on tke E_b/N_o performance of minimum (frequency) shift keying (MSK)", IEEE Trans. Commun., vol. COM-22, October 1974.

[9] H. C. Chan, D. P. Taylor, S. S. Haykin, "A comparative study of digital modulation techniques for single-carrier satellite communications", presented at the 3rd Int. Conf. Digital Satellite Communications, Kyoto, Japan, November 1975, Paper B2.

[10] R. Matyas, S. Sunter, C. Jagger, P. Jeans, "An LSI FFSK (MSK) Modem", Proc. NTC '81, New Orleans, November 30 - December 4.

[11] F. M. Gardner, "Carrier and Clock Synchronization for TDMA Digital Communication", European Space Research Organization, ESTEC Report 744976, Noordwijk, Netherlands; June 1974.

[12] T. Masamura, S. Samejima, Y. Morihiro, H. Fuketa, "Differential Detection of MSK with Nonredundant Error Correction", IEEE Trans. Comm., VOL. COM-27, June 1979, pp. 912-917.

[13] P. F. K. Chow. D. H. S. ko "Improving DCPSK transmission by means of error control", IEEE Trans. Commun., vol. COM-19, p.715, October 1971.

[14] J. Wozencraft, I. Jacobs, Principles of Communication Engineering, New York: Wiley, 1965.

[15] W. Bennett, J. Salz, "Binary Data Transmission by FM over a Real Channel", BSTJ, September 1963, pp. 2387-2426.

[16] H. Suzuki, "Optimum Gaussian Filter for Differential Detection of MSK", IEEE Trans. Commun, June 1981.

[17] Papoulis, Probability, Random Variables, and Stochastic Processes, McGraw Hill, 1965, pp. 158.

[18] R. Anderson, W. Bennett, J. Davey, J. Salz, "Differential Detection of Binary FM", BSTJ, January 1965, pp. 111 - 145.

[19] M.I. Skolnik, ed., Radar Handbook, McGraw-Hill, New York, 1970.

[20] H.L. Van Trees, Detection, Estimation, and Modulation Theory; part III (Radar-Sonar Signal Processing and Gaussian Signals in Noise), Wiley, New York, 1971, Chapter 10.

[21] R.J. Campbell and W.L. Nowland, private communication.

[22] K. Dostert and M. Pandit, "Performance of a SAW Tapped Delay Line in an Improved Synchronizing Circuit", IEEE Trans. Commun., vol. COM-30, no. 1, (January 1982), pp. 219 - 222.

[23] M. I. Skolnik, Introduction to Radar Systems, 2nd Ed., McGraw-Hill, New York, 1980, p. 380.

[24] L. B. Milstein and P. K. Das, "Surface Acoustic Wave Dervices", IEEE Commun. Mag., vol. 17, no. 5, (September 1979), pp. 25-33.

[25] EG&G Reticon, Product Summary: Discrete Time Analog Signal Processing Devices, 345 Potrero Ave., Sunnyvale, California, 94086.

[26] Fairchild Camera and Instrument Corp., CCD361 Objective Performance, courtesy of Dr. Richard Miller, Fairchild Advanced Research and Development Laboratory, 4001 Miranda Ave., Palo Alto, California, 94304.

[27] S. Pasupathy, "Minimum Shift Keying: A Spectrally Efficient Modulation", IEEE Commun. Mag., vol. 17, no. 4 (July 1979), pp. 14-22.

[28] L.E. Franks, "Carrier and Bit Synchronization in Data Communication - A Tutorial Review", IEEE Trans. Commun., vol. COM-28, no. 8, (August 1980), pp 1107-1121.

[29] F. Amoroso and J.A. Kivett, "Simplified MSK Signalling Technique", IEEE Trans. Commun., vol. COM-25, no. 4, (April 1977), pp. 433-441.

[30] J.V. DiFranco and W.L. Rubin, Radar Detection, Prentice-Hall, Englewood Cliffs, 1967, Appendix B.

[31] S.O. Rice, "Mathematical Analysis of Random Noise", B.S.T.J. Vol. 23, pp 282-332, (July 1944); and vol. 24, pp. 46-156, (January 1945).

[32] M. Schwartz et. al., Communication Systems and Techniques, McGraw-Hill, New York, 1966, Appendix A.